

TA97

Microwave Electronics



**INVESTIGATIONS ON BROADBAND PLANAR
MONOPOLE ANTENNAS WITH TRUNCATED
GROUND PLANE**

A thesis submitted by

SUMA M.N

in partial fulfillment of the requirements for the degree of

DOCTOR OF PHILOSOPHY

Under the guidance of

Prof. P. MOHANAN



**DEPARTMENT OF ELECTRONICS
FACULTY OF TECHNOLOGY
COCHIN UNIVERSITY OF SCIENCE AND TECHNOLOGY
COCHIN-22, INDIA
January 2008**



Department of Electronics
Cochin University of Science and Technology,
Kochi – 682 022

Date: 14th January 2008

Dr. P. Mohanan
(Supervising Teacher)
Professor
Department of Electronics
Cochin University of Science and Technology

Certificate

This is to certify that this thesis entitled “**INVESTIGATIONS ON BROADBAND PLANAR MONOPOLE ANTENNAS WITH TRUNCATED GROUND PLANE**” is a bonafide record of the research work carried out by Ms. Suma M.N under my supervision in the Department of Electronics, Cochin University of Science and Technology. The results embodied in this thesis or parts of it have not been presented for any other degree.


Dr. P. Mohanan

DECLARATION

I hereby declare that the work presented in this thesis entitled “INVESTIGATIONS ON BROADBAND PLANAR MONOPOLE ANTENNAS WITH TRUNCATED GROUND PLANE” is a bonafide record of the research work done by me under the supervision of Dr. P. Mohanan, Professor, Department of Electronics, Cochin University of Science and Technology, India and that no part thereof has been presented for the award of any other degree.

Cochin-22
14th January 2008

Suma M.N

Suma M.N
Research Scholar
Department of Electronics
Cochin University of Science and Technology

Acknowledgement

The thesis dissertation marks the end of a long and eventful journey for which I am indebted to many people who have greatly inspired and supported me all along the way.

I remember with gratitude.....

My supervising guide, Dr. Mohanan Pezholil, Professor, Department of Electronics, Cochin University of Science and Technology, for his guidance, encouragement and the timely care he rendered me during my research period. The opportunities and exposure that he offered during the course of my research is invaluable to me. His profound viewpoints and extraordinary motivation enlightened me to shape my traits and career.

Dr. K.G. Nair, Director, Centre for Science in Society, Cochin University of Science and Technology and former Head, Department of Electronics, Cochin University of Science and Technology for transferring new informations through his precious advices and suggestions.

Prof. K. Vasudevan, Head of the Department of Electronics for his constant encouragement and concern, and for extending the enormous facilities of Department of Electronics for my research. I also wish to thank him for his valuable suggestions in my thesis.

Dr. C. K. Aanandan, Reader, Department of Electronics, Cochin University of Science and Technology for his well-timed care in my research, valuable suggestions and constant encouragements to improve my work.

Prof. K. G. Balakrishnan, former Head, Department of Electronics, Prof. K. T Mathew and Prof. P.R.S Pillai, of Department of Electronics, for their whole hearted support, constant encouragement and valuable suggestions.

Dr. Tessamma Thomas, Mr. James Kurien, Mrs. M.H. Supriya, and all other faculty members of Department of Electronics for the help and assistance extended to me.

Dr.M.T Sebastain, Scientist Regional Research Laboratory (RRL), Trivandrum for his generous support and worthy discussions.

Dr. H Sreemoolanadhan, Scientist-E, Advanced Materials and Cermaic division, Vikram Sarabhai Space Centre, Trivandrum , Dr. Ratheesh, Scientist, C-MET and Dr.P.V Bijumon, Post Doctoral Fellow, Canada for the worthy discussions on materials and dielectric resonators.

Mr. Siby Mathew and Prof. Ramanathan, Sacred Heart College, Thevara for their inspiring words which directed me towards research.

Dr. Binu Paul and Dr. Mridula S, School of Engineering, CUSAT, for their fruitful and valid discussions and suggestions to improve this thesis.

Mr. Rohith K Raj for the advice and willingness to share his bright thoughts with me, which was very fruitful for shaping up my ideas and research.

Mr. Manoj Joseph for his friendship, encouragement and fruitful discussions.

Mr. Deepu V for his supreme emotional support and care that helped me get through the difficult times.

Mrs. Sreedevi K. Menon, Dr. Lethakumary B, M.G. Universtiy, Kottayam, Mr. K. Francis Jacob, Mrs. Shameena , and Ms. Bybi P.C, for their whole hearted support, helps and above all the association with me.

Mr. Anupam R. Chandran, Post Doctoral Fellow, Belfast University and Mr. Shynu S.V, Post Doctoral fellow, Dublin institute of Technology, for their valuable help, fruitful discussions and constant encouragement.

My friends at Centre for Research in Electromagnetics and Antennas, Centre for Ocean Electronics (CUCENTOL), Microwave Tomography and Material Research Laboratory (MTMR) and Audio and Image Research Lab (AIRL) CUSAT for their encouragement and help rendered to me.

My friends Anju and Sheena for their support, prayer and care extended during the hardest time. I appreciate the shoulder to lean on.

Council of Scientific and Industrial Research (CSIR), Govt. of India for financial assistance in the form of Senior Research Fellowship (SRF).

Kerala State Council for Science Technology and Environment (KSCSTE), Govt. of Kerala and Cochin University of Science and Technology for financial assistance at the earlier stages in the form of JRF.

All non-teaching staffs of Department of Electronics for their amicable relation, sincere cooperation and valuable helps.

Raji chechi and Sreenanna, for their unparalleled way of incentive, concern. Understanding, love and encouragement.

My dear sister Manju for being a powerful source of inspiration and support.

My Family, for being there always as incredible pillar of support. My parents each of them had their own special way to make my life great, Amma being my best friend and Appa being the source of courage to face even the hardest situation. I am really proud about the deep love, care and their seamless effort, which gave me the courage to persevere.

Almighty God for always being there to guide me through thick and thin.

Suma M.N

PREFACE

With the rapid growth of modern wireless communication systems there are ever growing demands for compact, lightweight, multifunction and multiband antenna. At the same time, most of the wireless gadgets adapt prevalently the internal antenna structure also. Planar antenna technology is growing in fast pace to meet the miniaturization demands of modern wireless technology. Planar antennas such as Microstrip antenna and printed antennas have the attractive features like low profile, small size and conformability to mounting the hosts are promising candidates for satisfying the design considerations of antenna engineers. Compact and broadband design of planar antenna is an area always attracted the researchers and engineers in the present scenario. Very recently planar monopole started elating the Antenna designers as low profile concealable antennas. For planar monopole antennas excited by microstrip line ground plane dimensions play a crucial role in determining the resonance and radiation characteristics. Ground plane truncation will modify the antenna characteristics considerably.

The main objectives covered in the thesis are:

- Investigations of the ground plane dimensions on the performance of planar strip monopole antennas.
- Optimum design of the ground plane dimensions leading to dwindling the antenna size.
- Design of an extremely wide band planar strip monopole antenna effectively utilizing the truncated ground plane concept.
- Investigations on the folding the strip monopole for size reduction.
- Investigations to overcome the bandwidth degradation occurred due to folding.

- Design of novel compact broadband planar monopole antenna with dual band features.

All the above objectives are explained theoretically and verified experimentally. Simple equations are provided to design an antenna with such characteristics. The design equations are verified by designing different antennas for different applications.

CONTENTS

Chapter 1

Introduction.....	01 - 39
1.1 Wireless...A Glimpse through evolution	02
1.2 Modern wireless communication systems and antennas	03
1.3 Overview of antenna research	06
1.4 Antenna design challenges in modern wireless communication systems	09
1.5 Itinerary towards planar antennas	12
1.6 Review of State of art in planar antenna design	14
1.6.1 Microstrip antenna	15
1.6.2 Planar Inverted F Antennas	18
1.6.3 Planar monopoles and printed dipoles	19
1.7 Printed monopoles: A brief overview	21
1.7.1 Excitation techniques	21
1.7.2 Dual band and multiband designs	23
1.7.3 Broad banding techniques: UWB monopoles	24
1.7.4 Multiband technique: Fractal monopoles	25
1.8 Motivation of present Research	25
1.9 Thesis Organization	28
1.10 References	30

Chapter 2

Techniques for analysis and characterization of the antennas	41 - 103
2.1 Background of theoretical analysis	42
2.2 Computational Electromagnetics for antenna field problems	43
2.3 Numerical investigations : Finite Difference Time Domain	52
2.3.1 Fundamental concepts of FDTD	53
2.3.2 Implementation	55
2.3.3 Boundary conditions	59
2.3.3.1 First order Mur's ABC	62
2.3.3.2 Bergner's PML ABC	64
2.3.4 Numerical dispersion and stability criteria	76
2.3.5 Luebbers feed model for fast FDTD convergence	77
2.3.5.1 Resistive source model	78
2.3.5.2 Staircase transition for microstrip line feed	80

2.3.6	Excitation source modeling.	80
2.3.7	Flowchart of Yee algorithm	83
2.4	Antenna characteristics using FDTD	84
2.4.1	Reflection characteristics	84
2.4.1.1	Return loss, Resonant frequency and 2:1 VSWR Band width	84
2.4.2	Radiation characteristics	85
2.4.2.1	Principal plane radiation patterns	86
2.4.2.2	Antenna gain	89
2.4.2.3	Efficiency	89
2.5	Experimental analysis	91
2.5.1	Antenna fabrication: photolithography technique	91
2.5.2	Experimental setup	92
2.5.2.1	HP 8510C Vector Network analyzer (VNA)	92
2.5.2.2	E8362B programmable Network Analyzer (PNA)	94
2.5.2.3	Automated turn table assembly for far field measurement	94
2.5.2.4	CREMA Soft: Automated antenna measurement	94
2.6	Simulation studies	97
2.6.1	IE3D Electromagnetic simulator	97
2.6.2	HFSS: 3D Electromagnetic simulator	98
2.7	References	99

Chapter 3

Theoretical and Experimental analysis of Printed strip monopole antenna.....	105 -171	
3.1	Introduction	106
3.2	Microstrip fed printed strip monopole antenna	107
3.3	Resonance and radiation in microstrip fed printed strip monopole	109
3.3.1	Resonance phenomenon	110
3.3.2	Radiation characteristics	114
3.3.2.1	3D radiation patterns	116
3.3.2.2	Gain and efficiency	117
3.3.3	Truncated Ground plane effects on antenna characteristics	118
3.3.3.1	Effect of ground plane width W_g	119
3.3.3.2	Effect of ground plane length L_g	126

3.3.4	Broadband printed strip monopole	130
3.3.5	Parametric analysis	145
3.3.5.1	Effect of monopole length L_m	145
3.3.5.2	Effect of monopole width W_m	147
3.3.5.3	Effect of dielectric constant of substrate	151
3.3.5.4	Effect of substrate height	153
3.3.6	Compact printed strip monopole antenna with optimum ground plane dimensions	155
3.3.7	Design procedure	164
3.3.7.1	Design procedure for wideband performance	164
3.3.7.2	Design procedure for Compact antenna	164
3.3.8	Printed monopole designs in modern communication bands	165
3.4	Comparison of printed strip monopole with standard planar antennas	169
3.5	Summarized conjecture at a glance	170
3.6	Conclusions	171

Chapter 4

Double folded strip monopole antenna for dual band applications 173 - 221

4.1	Reactive loading for antenna miniaturization: an overview	174
4.2	FDTD analysis of Folded strip monopole antenna (FSMA) for size reduction	175
4.2.1	Resonant modes in folded monopole antenna	180
4.2.2	Effect of folding on antenna characteristics	182
4.2.2.1	Return loss characteristics	183
4.2.2.2	Far field radiation pattern	184
4.2.2.3	Gain and efficiency	186
4.2.2.4	Cross polar levels	187
4.3	Parametric analysis of folded monopole antenna	188
4.3.1	Effect of loading location L_1	188
4.3.2	Effect of spacing between parallel strip and monopole arm, L_2	191
4.3.3	Effect of loaded parallel strip, L_3	194
4.3.4	Effect of Dielectric constant of substrate, ϵ_r	195
4.3.5	Effect of substrate height, h	197
4.4	Design procedure for a compact folded monopole antenna	199
4.5	Antenna designs in various wireless communication standards	200

4.6	FDTD analysis of Double Folded strip monopole antenna (DFSMA) for dual band operation.	202
4.6.1	Resonance and radiation phenomenon in DFSMA	203
4.6.2	Double Folding for dual frequency: A case study	209
	4.6.2.1 Effect of mutual coupling of arms	209
	4.6.2.2 Effect of arm 2 on first resonance	211
	4.6.2.3 Effect of arm 1 on second resonance	212
4.6.3	Parametric analysis of double folded monopole antenna	216
	4.6.3.1 Effect of folded arm1	217
	4.6.3.2 Effect of folded arm2	219
	4.6.3.3 Effect of strip width 'w'	222
	4.6.3.4 Effect of dielectric constant of substrate	222
	4.6.3.5 Effect of substrate height	223
4.5	Design procedure for compact dual band planar antenna	224
4.6	Dual band designs in modern wireless communication bands	226
4.7	Printed strip monopole designs in a nut shell	229
4.8	Conclusions.	229

Chapter 5

Conclusion and Future perspective 223 - 240

5.1	Thesis highlights and Key contributions	234
5.2	Inferences from wideband printed strip monopole antenna	235
5.3	Conjecture from optimum ground plane compact printed strip monopole antenna	236
5.4	Features of folded strip monopole antenna	237
5.5	Salient features of double folded printed strip monopole antenna	238
5.6	Suggestions for future work	239

Appendix A:	A Wide band Hybrid Printed Monopole/Rectangular Patch Antenna	241 - 249
--------------------	--	------------------

Appendix B:	A Compact Hybrid CPW Fed Planar Monopole/Dielectric Resonator Antenna	251 - 259
--------------------	--	------------------

Publications relevant to thesis

List of Publications

Resume of the Author

INTRODUCTION

“The IEEE embraced the new field of wireless and radio, which became the fertile field of electronics and later the computer age. But the antennas and propagation will always retain their identity, being immune to miniaturization or digitization.”

-Harold A. Wheeler

The electronic industry has historically dwindled the physical dimensions of their product to cater the needs of the modern people. In the age of wireless products the drive to miniaturization continues beyond our imagination. Antennas, the eyes and ears to the world, are critical devices that limit the miniaturization of wireless communication standards. The new and vibrant world of printed antennas was initially driven by the pursuit for the need of low profile compact antennas to meet the miniaturization requirement of modern wireless technology innovations. This rapid boom of wireless communication is invigorating the researchers to discover new dimensions in the printed antenna field.

The chapter serves to explore the historical advancements in the printed antenna technology. Literature overview of the state of art technologies is followed by the state of affairs that motivated the present investigations. The chapter concludes with a description of the organization of subsequent sections.

1.1 Wireless....A Glimpse through evolution

The field of microwave technology is based on the rich history dating back to 19th century with the fundamental discoveries in Electromagnetics by the giants - Michael Faraday, James Clerk Maxwell, Lord Rayleigh, Heinrich Hertz and J.C Bose. Subsequent researchers were fortunate to have a very strong and elegant foundation, especially that established by Maxwell through his magical mathematical touch on classical laws with his famous equations. The primary efforts of these scientists were directed towards the generation, guidance, detection and control of electromagnetic waves.

The monumental discoveries of electrical communication was initiated by Samuel F.B Morse in 1844 with his first demonstration of electrical communication over a substantial distance with dot-dash message through a single wire between Baltimore and Washington DC, using earth as return path. In 1876 Alexander Graham Bell received patent for telephone. The elegant unified theory of Electricity and Magnetism by James Clark Maxwell in his classic theoretical work in 1864 [1] rejuvenated Heinrich Rudolf Hertz to demonstrate electric wave communication in 1886. After a decade, in 1896 Guglielmo Marconi startled the world by demonstrating the radio system with a big antenna and a ground system [2] for longer wavelength transmission. The generation and use of millimeter wave for communication, development of microwave devices and horn antennas, revolutionary work of the Great Indian Scientist Jagdish Chandra Bose[3] and experiments by the other successors of Hertz inspired Marconi to succeed in Transatlantic communication over 1700 miles [4]. Over the past century research in wireless communication has witnessed remarkable revolution. The modern wireless technology allows simultaneous transmission of multiple channels of television, radio, video and audio to a range of multi-media devices including mobile phones, PDAs, PCs

and other handheld devices. The great visions of early pioneers of radio science are thus being established through converging technologies. Meanwhile, antenna - the vital part of wireless gadgets has endured renovation from a simple metallic rod to ceramic chip, reconfigurable, active and complicated smart antenna.

1.2 Modern wireless communication systems and antennas

The desire for mobility and communication is deeply ingrained in human nature. The need to develop an efficient public mobile communication system has been driving a lot of researchers. Guglielmo Marconi gained a patent for his wireless telegraph in 1909[5]. Since then, mobile communication has immensely grown from its infant stages where it was mainly used for navigation, to maturity by the end of the twentieth century, where it offers much more than just voice communication. The 1G analog systems of 1980's evolved into 2G digital technology in the 90's and to third generation of mobile communication which includes wireless multimedia services. The 2G systems designed in the 1980's was still used mainly for voice applications but were based on digital technology, including digital signal processing techniques. These 2G systems provided circuit- switched data communication services at a low speed. The competitive rush to design and implement digital systems led again to a variety of standards such as GSM (global system mobile), TDMA (time division multiple access) PDC (personal digital cellular) and CDMA (code division multiple access). These systems operate nationwide or worldwide and are today's mainstream systems, although the data rate for users in these systems is very limited. The 3G mobile system evolved in 2002's eliminating previous incompatibilities and became a truly global system. The approaching 4G (fourth generation) mobile communication systems are projected to solve the still-remaining problems of 3G systems and to provide a wide variety of

new services, from high-quality voice to high-definition video to high-data-rate wireless channels. New technologies have now been developed that enable users to watch streamed television-like services on their mobile telephone. A short history of wireless technology is presented in Table 1.1. An overview of the frequency band allocated for modern wireless communication standards are summarized in Table 1.2

Table 1.1 Short history of wireless technology

TECHNOLOGY	1G	2G	2.5G	3G	4G
Year	1984	1991	1999	2002	?
Standards	AMPS, TACS,NMT etc	DAMPS, GSM 900 CDMA, TDMA	GPRS, EDGE	WCDMA, CDMA 2000, TD-CDMA	Single standard
Service	Analog voice	Digital voice and short messages	High capacity packetized data	High capacity broadband data.	High capacity, completely IP oriented multimedia data.
Access technique	FDMA	TDMA, CDMA	TDMA, CDMA	CDMA	CDMA?
Data bandwidths	1.9Kbps	14.4Kbps	384Kbps	2Mbps	200Mbps

Table 1.2 frequency spectrum allotted for wireless communication

Wireless Communication Service		Allotted Frequency Band	Commonly Used Antenna
GPS 1575 GPS 1400	Global Positioning System	1565-1585 MHz 1227-1575 MHz	Microstrip patch or bifilar helix
GSM 900	Global system for mobile communication	890-960 MHz	Dipoles or patch array in base stations Monopoles, sleeve dipoles and patch in mobile handsets
DCS 1800	Digital communication system	1710-1880 MHz	
PCS 1900	Personal Communication System	1850-1990 MHz	
UMTS 2000	Universal Mobile Telecommunications Systems	1920-2170 MHz	
3G IMT-2000	International Mobile Telecommunications-2000	1885-2200 MHz	
ISM 2.4 ISM 5.2 ISM 5.8	Industrial, scientific, medical	2400-2484 MHz 5150-5350 MHz 5725-5825 MHz	
RFID	Radio frequency Identification systems	30 MHz to 2.4 GHz	Loops, folded-F, patch and monopole
DVB-H	Digital video Broadcasting on handheld devices	470-890 MHz	Compact printed antennas
UWB	Ultra wide band	3.1 -10.6 GHz	Printed dipoles or monopoles

1.3 Overview of antenna research

Since Marconi's first experiments with transmitting electromagnetic waves in 1901, antennas have found several important applications over the entire radio frequency range. Antennas enjoy a very large range of applications, in both military and commercial sectors. The most well known applications of antennas to the average person are those associated with radio, TV, and communication systems. Today, antennas find extensive use in biomedicine, radar, remote sensing, astronomy, navigation, RF identification, controlling space vehicles, collision avoidance, air traffic control, Global Positioning System, pagers, wireless telephone, and Wireless Local-Area Networks (WLANs). An antenna is used to either transmit or receive electromagnetic waves and it serves as a transducer for converting guided waves into free-space waves in the transmitting mode or vice versa in the receiving mode. All antennas operate on the same basic principles of electromagnetic theory formulated by James Clerk Maxwell. Modern antennas or antenna systems require careful design and a thorough understanding of the radiation mechanism involved. Selection of the type of antenna to be used is determined by electrical and mechanical constraints and operating costs. The electrical parameters of the antenna include the frequency of operation, gain, polarization, radiation pattern, and impedance. The mechanical parameters of importance include the size, weight, reliability, and manufacturing process. In addition, the environment under which the antenna is to be used also must be considered, including the effects of temperature, rain, wind and the antenna platform. Antennas are protected from the environment by the use of radomes whose presence is also taken into account while designing the antenna.

'Wire antennas'- the first type of antennas are the most familiar to the common man. These antennas can be linear or in the form of closed loops. Loop antennas can have several different shapes such as circular, square, or rectangular.

Electrically small loops are those whose overall wire extent is less than one-tenth of a wavelength. Electrically large loops have circumferences that are of the order of a wavelength. An electrically small circular or square loop antenna can be treated as an infinitesimal magnetic dipole with its axis perpendicular to the plane of the loop. Various configurations of polygonal loop antennas have been investigated [6-7]. Dipole and loop antennas find applications in the low– medium-frequency ranges. They have wide beam widths, and their behavior is greatly affected by nearby obstacles or structures. These antennas are often placed over a ground plane. The spacing above the ground plane can effectively modify the radiation pattern and directivity [8].

In the year 1926 Yagi–Uda antenna “the most prevalent and recognizable antennas in existence” was introduced [9] and is commonly used for television reception. It has several desirable characteristics that include low cost, low weight, simple assembly and radiation qualities adequate for many applications. This classical work is still a potential candidate as the home TV antenna.

Since World War II, the reflector antennas gained prominence for their use with radar systems, and played an important role in the field of communications. Reflector antennas have a variety of geometrical shapes and require careful design and a full characterization of the feed system (the system that illuminate the reflector surface with electromagnetic fields). Silver the ‘Author of Antenna Bible’ [10] presented the technique for analysis based on aperture theory and physical optics. Other methods such as the geometric theory of diffraction (GTD) and Fast Fourier transform (FFT) along with various optimization techniques [11] are now used for a more accurate design of these antennas. World War II was the flourishing period in antenna research and new innovation in this period were aperture type antennas such as open ended waveguides, horns, lens antennas etc. They are useful for a variety of airborne, ground-based, space, and missile

applications in the microwave frequency bands. V.H Ramsey in 1950 revolutionized the antenna world by the concept of frequency independent antennas, extending antenna bandwidths by greater than 40% [12]. Ideally, an antenna will be frequency-independent if its shape is specified only in terms of angles. Examples of this type include Log periodic and Archimedean spiral antennas.

The concept of microstrip radiators was first proposed by Deschamps [13] in 1953. However, 20 years passed before practical antennas were fabricated and these classes of antennas received attention and research in this direction was accelerated during the 1970's. These antennas are lightweight, easy to manufacture using printed-circuit techniques, and compatible with MMICs (Monolithic Microwave Integrated Circuits). An additional attractive property of these antennas is that they are low-profile and can be mounted on surfaces and referred to as conformal antennas. However, the inherent narrow bandwidth of these antennas limits their usage in many applications.

Recently printed antennas have received much attention due their low profile and omnidirectional radiation characteristics. The rapid growth of Ultra Wide Band communication [14] demands ultra wide band antennas to accommodate the large frequency spectrum of ultra short pulse used for this communication. There is a growing demand for small and low cost UWB antennas that can provide satisfactory performances in both frequency domain and time domain.

Around 1940, the Researchers began to consider the problem of electrically small antennas for wireless broadcasting and detection. Pioneering works by Chu [15] and Wheeler [16] formed a basis for the design of electrically small antennas. Antennas that are electrically small, efficient and have significant bandwidth would fill many needs if antenna engineers could reconcile these usually contradictory requirements. This is especially true recently with increased uses of wireless

technologies for communications and sensor networks. As the demand for wireless equipment grows and sizes of the devices shrink; electrically small and low-profile antenna designs become more attractive despite their inherent inefficiencies. Manufacturers demand antennas that are as unobtrusive as the equipment they produce. It is the challenge of the modern day antenna engineer to design high performance, compact, unobtrusive antennas for integration into hand-held radio units.

Converging technologies demands compact sub wavelength antenna to meet the miniaturization requirements. Recently, sub wavelength resonant structures are obtained by introducing metamaterial in antennas. A metamaterial medium is introduced in antennas to obtain electrically small antenna element with good efficiency [17].

Very recently, the addition of more and more features in each new generation communication systems demands universal antennas. A universal antenna should support five cellular bands (GSM850/900/1800/1900 + 3G), Wireless LAN, Bluetooth, Digital TV (DVB-H), FM radio and GPS. In the next few years, several new wireless systems such as RF-ID, UWB, WiMAX etc. will probably also be integrated to the terminal.

1.4 Antenna design challenges in modern wireless communication systems

Modern telecommunication systems require antennas with wider bandwidths and smaller dimensions than conventionally possible. The prime considerations for mobile phone antenna design are low cost, light weight, small size, robustness, flexibility and ease of mass production. The fundamental limitations of electrically small antennas are in terms of impedance bandwidth, gain and radiation efficiency. In addition to these fundamental restrictions imposed by physics, a terminal antenna designer also has to respect limits that

come from practical considerations. Antenna design challenges are briefly outlined in this section.

Theoretical limitations:

Several of antenna design principles may have to be modified while dealing with miniature antennas. By convention, a small antenna is defined as one occupying a fraction (typically $< 1/6$) of the wavelength [18]. The primary concern in their design is in the impedance matching. This is better explained in the context of dipole antennas. As the length of a dipole antenna is reduced the real part of its input impedance approaches zero, while the imaginary part tends to be an extremely large negative number. This causes major reflections at the input terminal as the transmission line connected to it generally has standard characteristic impedance (50Ω). The reactive part of the impedance is contributed by the induction fields in the near-zone of the antenna [19]. The resistive part on the other hand may be attributed to various loss mechanisms present in and around the antenna, including the radiation “loss”. Losses due to the finite conductivity of the antenna structure, and that due to currents induced on nearby structures including ground contribute to the antenna input resistance. It is often preferred to operate an antenna around its resonance to obtain proper impedance match with the transmission line. There are several artificial ways of obtaining similar input characteristics without actually making the dipole $\lambda/4$ long. One method is to use reactive elements at the input that cancel out the reactance of the antenna. However, this approach often limits the bandwidth of operation of the antenna. Another method is to extend the length of the dipole, without actually making it longer. Meandered and zigzag lines are examples of this approach. Bends and corners introduced by this modification add to the inductance of the line, but do not significantly impact the real part of impedance.

*Practical limitations:
Available Volume:*

Wireless gadgets are constantly getting smaller. The latest trend in terminal design is therefore ultra-thin phones, leading to very small heights above ground plane available to the antenna elements. This has a huge impact on patch type of antennas (such as the popular Planar Inverted F Antenna (PIFA)) as the achievable bandwidth and radiation efficiency is proportional to its height [20].

Ground plane effects:

The metallized layer of the PCB, together with other metallized parts of the chassis, functions as a ground plane for the various subcomponents in the terminal. The characteristics of small internal (e.g. PIFA) antennas mounted on handheld terminals are very different compared to that when placed on an infinite ground plane, and depends on both the antenna position on the terminal chassis and the dimensions of the chassis (the length in particular). This is due to the existence of radiating surface currents on the terminal ground plane induced by the antenna element. While the typical bandwidth of a patch type antenna on an infinite ground plane is in the 1-3 percent range (depending mainly on the height above ground), more than 10% is regularly achieved in standard size terminals. Currents are induced in the edges of the ground plane which are in phase with the currents in the radiating sections. Hence ground plane dimension contributes to the overall performance of the antenna. Ground plane truncation affects the antenna characteristics significantly.

Current consumption/Linearity:

Active antennas integrated together with the radiating element, consumes DC current thus reducing battery life time. This has so far limited widespread deployment in commercial wireless gadgets. A more practical problem is that the active devices in many cases (such as switches) needs control voltages, implying that the antenna cannot be designed independently from the front-end module.

1.5 Itinerary towards planar antennas

The recent trend in miniaturization of wireless gadgets fuelled the evolution of planar antenna technology. It is worth noting that many of the planar antennas can be viewed as the modifications of conventional antennas. Broad band planar metal plate monopoles are fabricated by transforming a conventional monopole. Further miniaturization can be achieved by printing the monopole on a dielectric substrate. Transition of wire monopole to printed antenna is shown in Fig.1.1

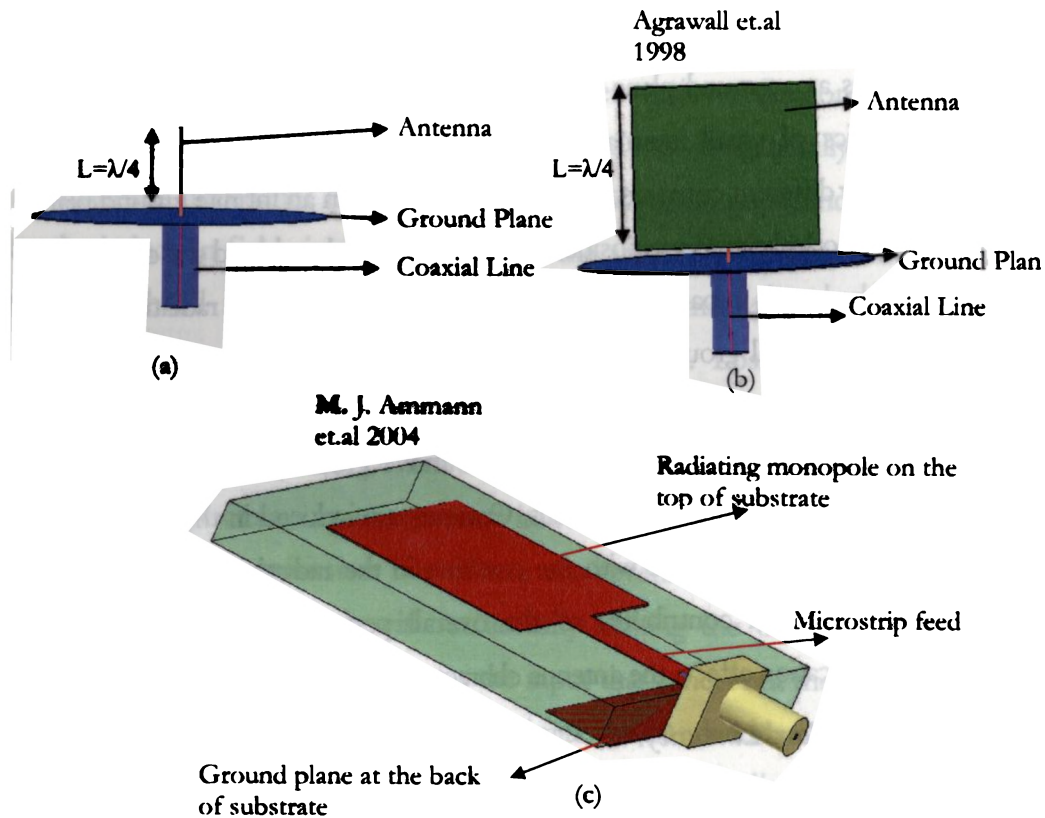


Fig.1.1 Transition of simple wire antenna to broad band printed antenna
 (a) wire monopole above a conducting ground plane
 (b) broad band planar monopole above conducting ground plane
 (c) Microstrip fed printed monopole with truncated ground plane

A broad band frequency independent biconical antenna is transformed to printed quasi dipole elliptical antenna which can yield broad band operation. The conical dipole yields ultra wide band characteristics due to the wide transition angle of the conical arm of the dipole. Similar characteristics are obtained when an elliptical dipole is printed on PCB substrate. Fig 1.2 shows the transition of biconical antenna to printed antenna. The conformal nature of printed antennas attracted the researchers to transform conventional antennas such as slot, log periodic, spiral, vivaldi antenna to their printed form.

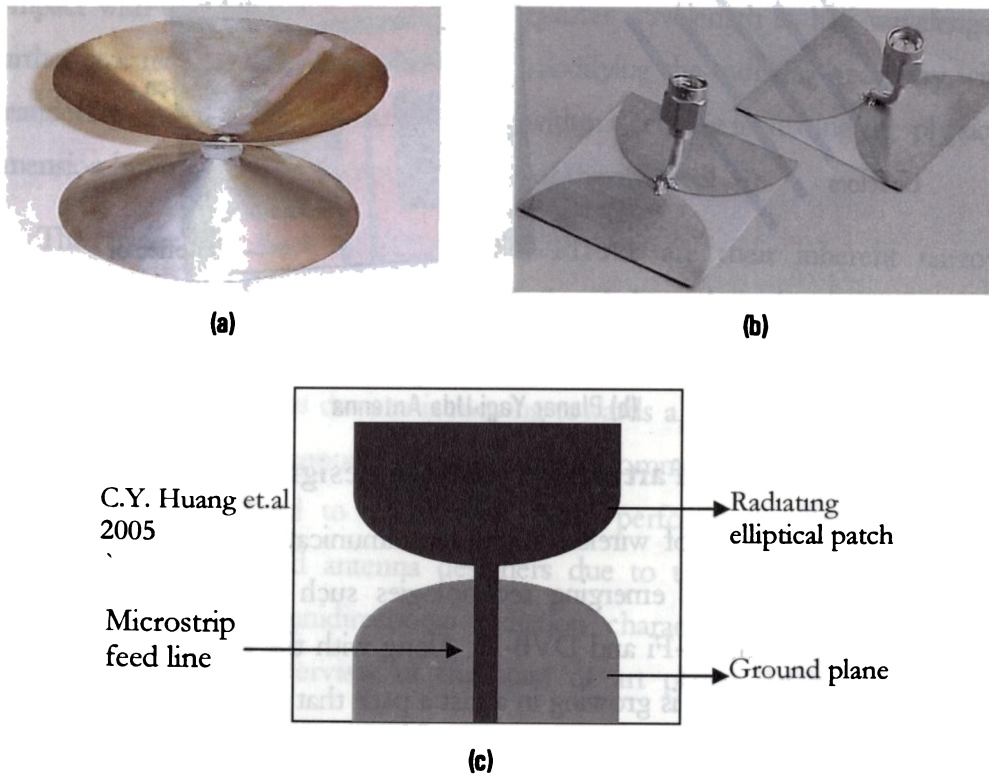
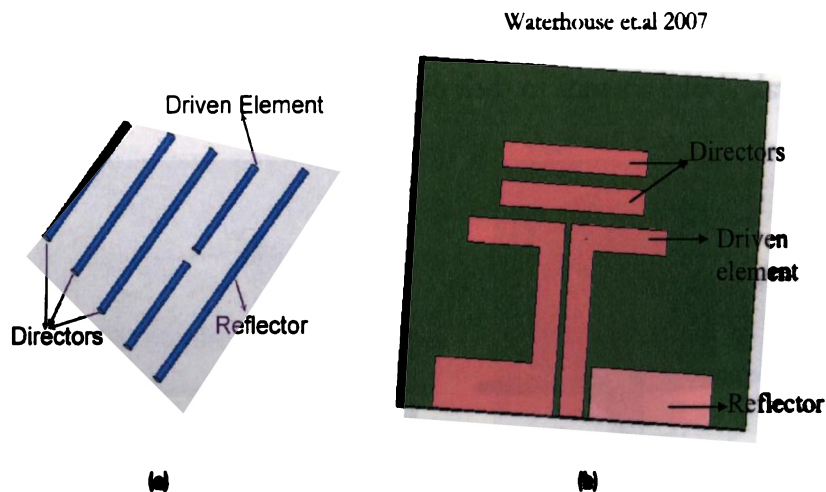


Fig1.2 Transition of biconical antenna to printed broad band antenna

- (a) Biconical antenna
- (b) Planar elliptical dipole antenna
- (c) Printed elliptical dipole antenna

A transition of conventional Yagi-Uda antenna to its planar form has received renewed interest recently due to its suitability for a wide range of application such as wireless communication systems, power combining, phased arrays, active arrays as well as millimeter-wave imaging arrays.

The conventional home TV antenna and its printed form are presented in Fig 1.3



**Fig 1.3 (a) Conventional Yagi-Uda Antenna
(b) Planar Yagi-Uda Antenna**

1.6 Review of State of art planar antenna design

The fast expansion of wireless mobile communication is remarkable during the past few years with emerging technologies such as Wireless Local Area networks, Blue tooth, Wi-Fi and DVB-H. Along with the emerging technologies the trend of compactness is growing in a fast a pace that the antenna designers are constrained for designing compact antennas suitable for integration in wireless gadgets without compromising the performance characteristics. The planar antenna has grown with the wireless mobile communication. An efficient antenna will improve transmission, reception, power consumption and should congregate with the multiband or broadband demands of future mobile communication systems with compact dimensions.

Antennas used for early handheld applications were monopole or whip antennas [21]. The quarter wavelength whip or antennas are popular due to its simple geometry and nearly omnidirectional radiation characteristics. But these external antennas have remained relatively large compared to the handset and protrude from the mobile device in an awkward way which increased the demand of planar antennas within the housing of mobile phones.

Planar Inverted F Antennas (PIFA's) and microstrip antennas are the trend setters in handheld device application due to their low profile. These antennas are compact with the dimension ranging from quarter wavelength to half wavelength. Further size reduction can be achieved by modifying the radiating geometry with meandering or reactively loading with slots without actually increasing the physical dimension but increasing the electrical length of the antenna.

The major drawback of MSA's and PIFA's are their inherent narrow bandwidth. Advanced designs such as stacked and shorted patches [22-23] ensure the wideband performance. In addition to wide band performance, the market trends of personal wireless devices is moving towards a universal system that can be used anywhere and supports various wireless communication standards. This demands the multi band to Ultra Wide Band performance. Recently planar monopoles have attracted antenna designers due to their advantages like low profile, light weight, omnidirectional radiation characteristics and broadband performance. A brief overview of the state of art planar antenna designs is summarized in the following sections.

1.6.1 Microstrip antenna

Microstrip circuitry consists of a metal strip or patch on a dielectric substrate backed by a metal ground plane. Microstrip antennas are finding increasing popularity owing to their advantages in size, cost, low profile, ease of fabrication and conformity to the supporting structure. By using simple photolithographic

masking and etching techniques it is possible to fabricate a wide variety of microstrip circuits including antenna arrays, feeding networks and active devices such that preamplifiers or distributed transmitters can be conveniently placed next to the antenna elements. In addition, diode phase shifter circuits can also be etched on the same substrate to form single-board phased arrays. Typical geometry of microstrip antenna is depicted in Fig.1.4

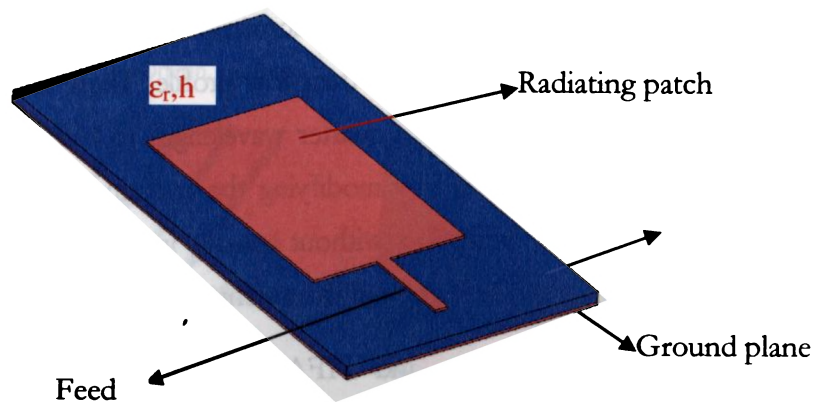


Fig 1.4. The basic Microstrip antenna geometry

The patch conductors, normally copper or gold, can assume virtually any shape but regular shapes are generally used for simplified analysis and performance prediction. Ideally the dielectric constant ϵ_r of the substrate should be low to enhance the fringing field that accounts for the radiation. However, other performance requirements dictate the use of high dielectric constant but on the cost of narrow bandwidth and low efficiency due to the high Q of the resonator. Flexible substrates can be used for the conformal wrap around antennas. The major advantages of these antennas are [24]

- Light weight, low volume, thin profile configuration which easily conforms to the surface of wireless gadgets.

- Low fabrication cost; readily amenable to mass production.
- Suitable for integration with Monolithic Microwave Integrated Circuits (MMICs).
- Compatible for producing linear and circular polarization with broadside radiation.
- Feed lines and matching circuits can be simultaneously fabricated with antenna structure.
- Dual frequency or multi frequency operation can be possible with geometry modifications.

However microstrip antennas have some inherent disadvantages which limit the use in many wireless applications. These demerits include

- Narrow band width and low gain.
- Uni polar radiation; microstrip antennas radiate into half space.
- Lower power handling capacity and poor end fire radiation.
- Excitation of surface waves when thick substrates are used.

Research in microstrip antenna design has progressed in such a way that there are many ways to minimize the effect of these limitations. Bandwidth can be increased to more than 60% by employing different techniques such as stacking parasitic radiators or reducing the Q of the microstrip radiators by employing thick air or foam substrates. Considerable amount of literature has appeared on the broad banding aspect of microstrip antennas [25-28]. Theoretical approaches are proposed for predicting the far field characteristics [29]. To obtain an enhanced antenna gain, methods involving the loading a high-permittivity dielectric superstrate [30, 39] or an amplifier-type active circuitry [40, 41] to a compact microstrip antenna have been demonstrated. By meandering the surface current paths on the radiating patch, the half wavelength length antennas can be made electrically large and the fundamental resonant frequency [42, 43–46] be lowered. Surface wave associated limitations such as

poor efficiency, increased mutual coupling, reduced gain and radiation pattern degradation can be overcome by the use of photonic band gap structures [47].

1.6.2 Planar Inverted F Antennas

Planar Inverted-F antennas (PIFA's) [48] have been very attractive for application as internal antennas in wireless communication devices such as mobile handsets, Personal Digital Assistants (PDAs), PDA phones, notebook computers, and so on. Planar inverted-F antennas (PIFA's) have been shown to be promising candidates for these applications because of their compact size, low profile, light weight, and the advantage of less backward radiation toward the user. A PIFA is in general achieved by short circuiting its radiating path or wire to antenna's ground plane with a shorting pin. PIFA can resonate at a smaller antenna size as compared to conventional antenna. Fig 1.5 shows a typical configuration of PIFA mounted on the top portion of the circuit board of a practical mobile phone.

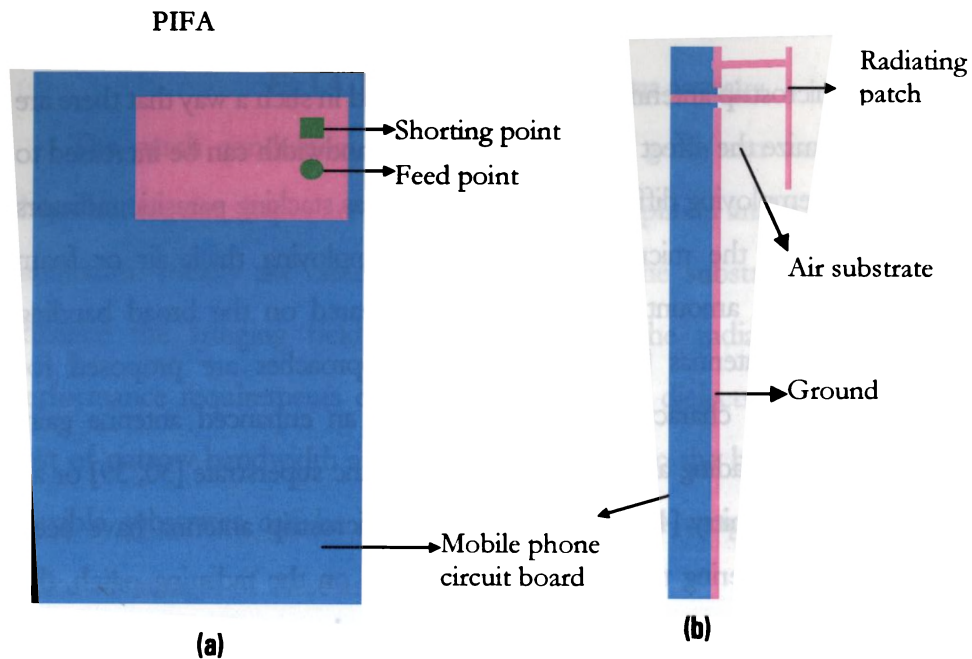


Fig. 1.5 Geometry of typical PIFA antenna (a) Top view (b) Side view

The PIFA designs usually occupy a compact volume and can be integrated within the mobile housing, leading to internal mobile phone antenna. These internal antennas can avoid the damages such as breaking compared with the conventional protruded whip or monopole antennas used for handheld applications. Compared to the whip antennas, these PIFA's have the advantage of relatively smaller backward radiation towards the mobile phone user. This suggests that electromagnetic energy absorption by the user's head can be reduced. These advantages led to many novel PIFA designs, most of them capable of dual or multiband operation to be applied in the mobile phones in the market. A variety of designs for dual-band PIFA's used in mobile handsets can be found in the literature [49– 54].

1.6.3 Planar monopoles and printed dipoles

Conventional monopoles usually protrude from the mobile phone housing apparently increasing the total length of the mobile phones and tending to break off easily. To overcome dimensional constraints and narrow bandwidth, several novel monopole designs with much reduced height have been developed very recently. So far, the most common techniques used to broaden the bandwidths of simple monopole or dipole antennas have been the employment of thick or loaded wire antennas. The typical designs include conical or skeletal-conical and various top-hat or dielectric loading monopoles. Also, planar elements were suggested to replace the wire elements for increasing impedance bandwidths [55 –63]. These kinds of low profile planar monopoles are very useful to integrate within the mobile housing and can be used as built in internal antenna. For example, in 1952 the triangular planar sheet monopoles were introduced as the geometrical approximations of the broadband solid- or shell-conical monopoles, covering the UHF TV channels ranging from 480–900 MHz [55]. A circular planar monopole was presented for the design of an 8:1 impedance bandwidth [56]. Recently, monopoles with

elliptical, square (rectangular), bow-tie, diamond, and trapezoidal sheets, have been designed and investigated [57-63]. Geometry of square planar monopole and other possible geometries are shown in Fig 1.6.

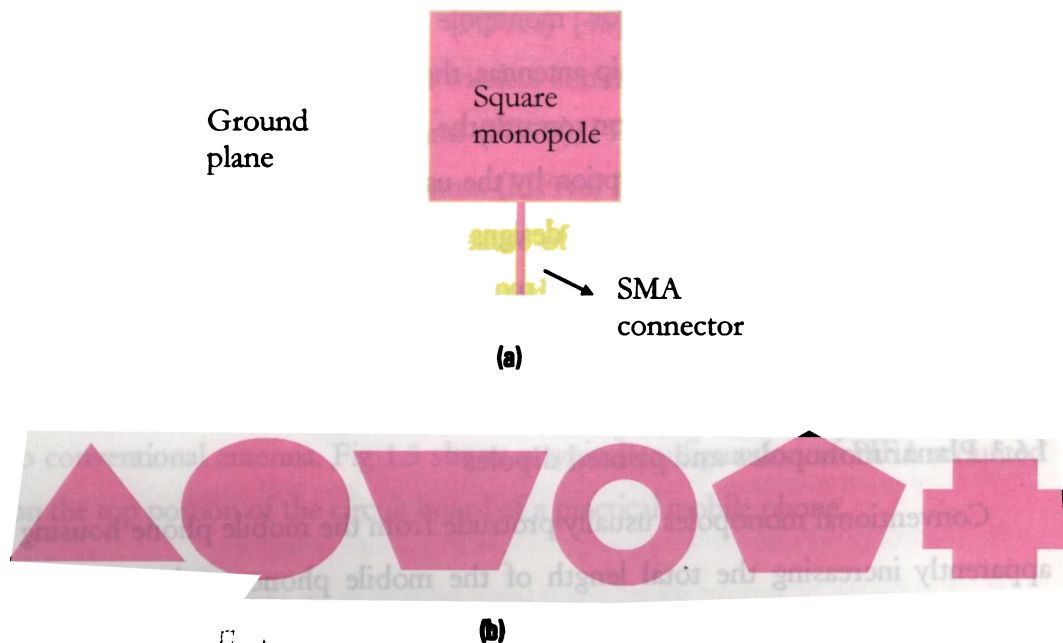


**Fig 1.6: (a). Square planar monopole for broadband operation
 (b) Other possible monopole structures**

Dipole antennas are extensively used in variety of applications such as being the basic units of phased-array antennas and the feeding sources of aperture antennas [64-66]. Compared with traditional wire antennas, printed dipole antennas have extra advantages including planar structure, small volume, light weight and low cost, which are significantly suitable for applications sensitive to the receiver sizes. Recently, various types of printed dipole antennas have been studied [67-69] to comply with the compact high performance broad band/multiband requirements. With the use of parasitic elements printed dipoles can be effectively used for multiband operations [70]. Geometry of a typical microstrip fed printed dipole antenna is depicted in Fig 1.7.

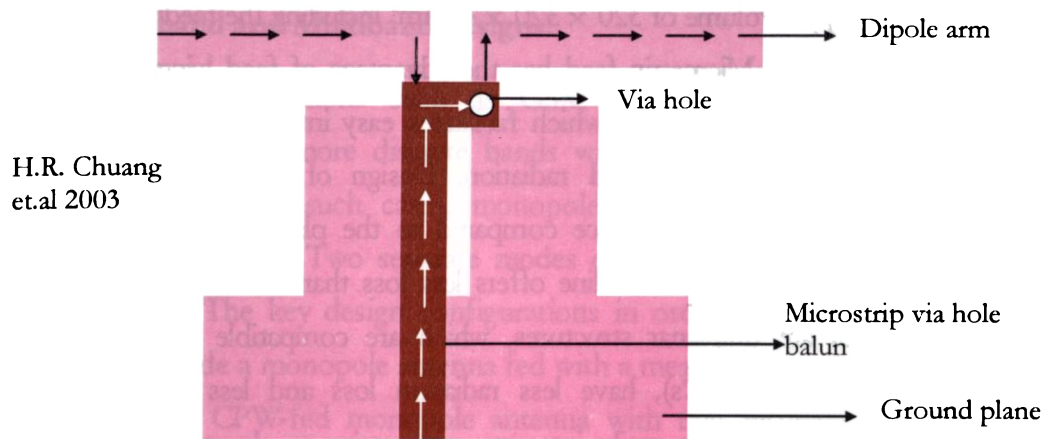


Fig 1.7 Geometry of a typical printed dipole antenna

1.7 Printed monopoles: A brief overview

Planar monopole antenna has a considerably larger bandwidth, and has made monopole more attractive for wireless communication applications. But the ground plane size and orientation of the radiator can place physical limitations on the use of such antennas. Recently there has been a move towards printed type monopole antennas with ground plane printed on a substrate parallel to the radiator. This has made the antenna low in profile, low in volume, ease of fabrication and suitable integration into circuit board as terminal antenna.

1.7.1 Excitation techniques

There are various configurations that can be used to feed the printed monopole antennas as shown in Fig.1.8. Selection of appropriate feed is a crucial factor in application point of view. Earlier printed monopole designs used coaxial probe feed in which radiating geometry is printed on the substrate and inner conductor of the coaxial connector is connected to the radiating monopole and the outer conductor is grounded. But the practical applications of these broadband monopoles are limited as the radiating structure is perpendicular to the ground plane which increases the complexity of the system as the entire system is not planar. Moreover, these 3D

monopoles occupy a volume of $320 \times 320 \times 40\text{mm}^3$ including the feed structure and ground plane [71-73]. Microstrip feed has the advantage of feed lying in the same plane of the radiating monopole, which facilitates easy integration with RF circuit boards but, creates spurious feed radiation. Design of microstrip fed printed monopoles yield better performance compared to the planar monopoles [74-76]. Coplanar Waveguide transmission line offers less loss than microstrip transmission line. CPW lines are uniplanar structures, which are compatible with Microwave Integrated Circuits (MMICs), have less radiation loss and less dispersion than microstrip line, and can be easily integrate with series or shunt lumped passive elements without any need of via hole as in the case of microstrip technology. CPW fed monopoles are increasingly popular for dual band broadband operations [77-78]. Recently uniplanar feeding techniques such as asymmetric coplanar strip line and slot lines are easily spreading the attention of antenna designers [79-80].

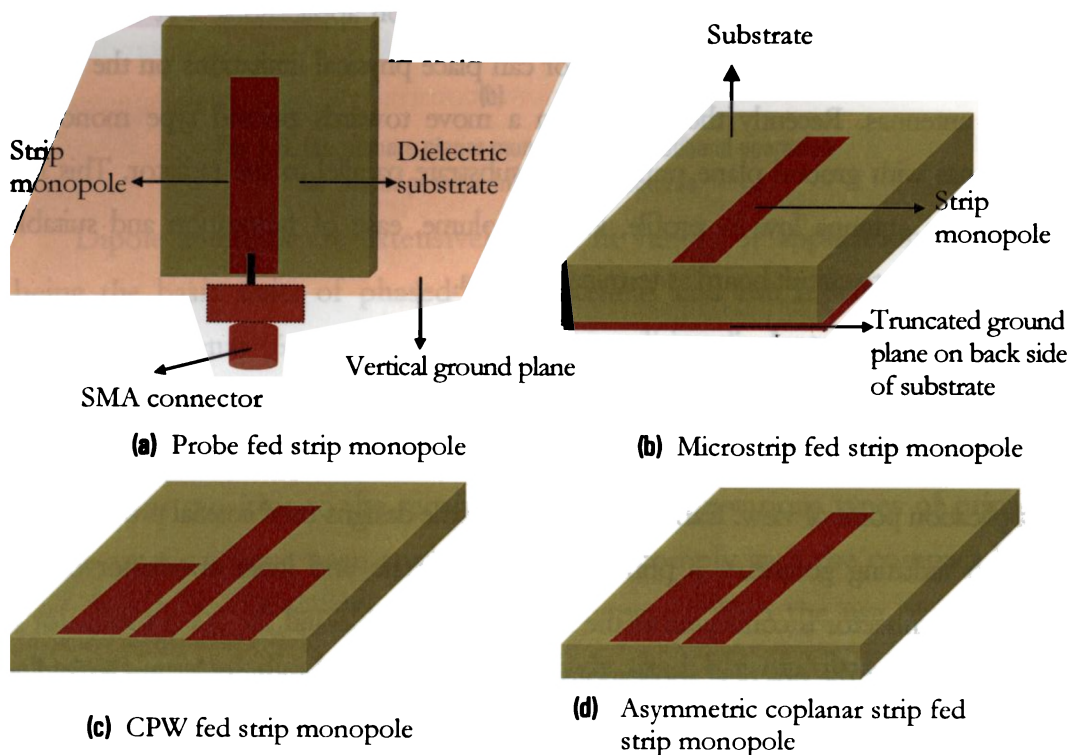


Fig 1.8 Various excitation techniques for printed monopole antennas

1.7.2 Dual band and Multiband designs:

In many applications such as GSM 900/1800, WLAN 2.4/5.2GHz operation in two or more discrete bands with an arbitrary separation of the bands is desired. In such cases, monopole antenna suitable for multiband operation is essential. Two separate modes can be excited with two different current paths. The key design configurations in order to meet this dual-band operation include a monopole antenna fed with a meandered coplanar waveguide (CPW) [81], a CPW-fed monopole antenna with two resonant paths [82], a CPW-fed tapered bent folded monopole antenna [83], a microstrip-fed double-T monopole antenna [84], a meander-line monopole antenna with a backed microstrip line [85], a C-shaped monopole antenna with a shorted parasitic element [86], Y shaped monopole antenna with CPW feed [87], triangular monopole antenna with trapezoidal slit [88] etc.

1.7.3 Broad banding techniques: UWB monopoles

The emerging ultra wide-band (UWB) radio is the technology of transmitting and receiving short, information encoded electromagnetic impulses [89-90]. Ultra wide-Band (UWB) technology is one of the most promising solutions for future communication systems due to its high-speed data rate and excellent immunity to multipath interference. According to the Federal Communications Commission (FCC), the frequency band of the UWB should be between 3.1 and 10.6 GHz. To achieve the high data rate UWB antenna should radiate short pulse with duration of 0.3ns without time ranging. Some of the critical requirements in UWB antenna design are: ultra wide bandwidth, directional or omni-directional radiation patterns, constant gain and group delay over the entire band, high radiation efficiency and low profile. Before the decade 1990's, all the proposed UWB antennas were based on general volumetric structures, such as spheroidal antenna, biconical antenna,

coaxial horn element, omni-directional and directional coaxial horn antenna, conical horn antenna, rectangular horn antenna, ellipsoidal monopole and dipole antenna, etc [91]. Today the state of the art of UWB antennas focuses on the microstrip, slot and planar and printed monopole antennas. Microstrip fed or CPW fed planar monopoles are recently used for Ultra Wide Band applications [92-96]. To improve the impedance bandwidth for UWB applications, several bandwidth enhancement techniques have been reported, such as the use of an asymmetrical feed arrangement [97], adjusting the gap between radiating element and ground plane [98], a double feed [99], a beveling radiating element [100], a beveling ground pattern [101], and so on. Recently structural modifications are employed to excite multi current paths which can lead to Ultra Wide Band performance [102-104].

1.7.4 Multiband technique: Fractal monopoles

In recent years, the fractal technology is often used to realize the multi frequency feature and miniaturize antenna because of its self-similarity property and space filling property. Self-similar objects look “roughly” the same at any scale. Thus, in an antenna with fractal shape, similar surface current distributions are obtained for different frequencies, and multiband behavior is provided [105]. The space filling property, which is able to add more electrical length in less volume, can be utilized to miniaturize antennas [106]. Traditional fractals such as Koch curves, Sierpinski triangles, and Minkowski fractals, etc, have been used to design compact antennas for multiband , broadband operation or even ultra wide band operation [107- 116]. Various fractals geometries commonly used for printed monopole antenna design are shown in Fig. 1.9.

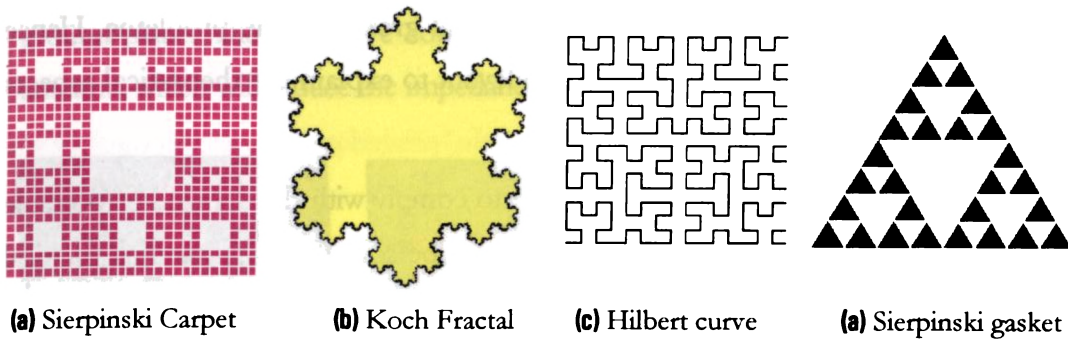


Fig 1.9 various configurations of fractal geometries suitable as monopole structures

1.8 Motivation of present research

Printed monopole antennas are promising candidates for modern wireless communication systems due to their low profile, light weight and nearly omnidirectional characteristics. The State of art technologies portraits the demand of monopole antennas with simple strip structure to complicated fractal geometries. Whatever is the geometry of the printed monopole the radiating geometry is printed on a substrate and ground plane is printed parallel to the radiating structure. Ground plane is a crucial factor for these printed monopoles. The antenna performance significantly varies for infinite to finite ground plane transition. When the ground plane is truncated, the current distribution on the ground plane at the radiating frequency becomes more significant. This influences the radiation characteristics of the antenna to a great extent. Unfortunately antenna designers often choose the ground plane dimension in an adhoc manner driven by the convenience rather than through examination of electrical limitations. Even though the printed technology is fully matured, the dependence of ground plane on the antenna characteristics is often least considered by the researchers and designers. This state of affairs inspired for detailed investigations on the ground plane effects of simple strip monopole. Numerical analysis using Finite Difference Time Domain (FDTD)

method gives a physical insight to the actual ground plane problems. Hence numerical analysis based on FDTD is relevant to explain the theoretical aspects of the antenna characteristics.

Miniaturization of printed monopole to comply with the demand of portable wireless systems is another important issue to be solved. When antenna physical size is reduced considerably, the bandwidth and radiation efficiency is degraded. In conventional wire monopole antennas size reduction can be achieved by techniques such as reactive loading (for example, inductance loaded whip antennas) or folding the monopole element. Some of these size reduction techniques are shown in Fig. 1.10.

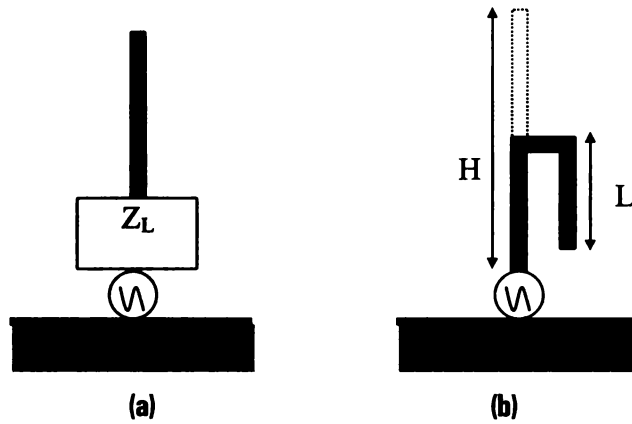


Fig.1.10. Reducing the size of wire monopole antennas

- (a) Reactance loaded monopole antenna**
- (b) Parallel line loaded monopole antenna**

Folding the element length is a widely accepted method in monopole antenna designs. Consider the case of a simple straight printed monopole element excited with a microstrip line, shown in Fig 1.11 (a). When it is folded as shown in Fig 1.11 (b) to achieve considerable size reduction, there will be serious impact on the impedance bandwidth characteristics. The bandwidth of the antenna is degraded due to the strong coupling of the horizontal portion of the folded strip with the

ground plane. The capacitive coupling will introduce large reactance part in the antenna, which will reduce the impedance matching and obviously the bandwidth.

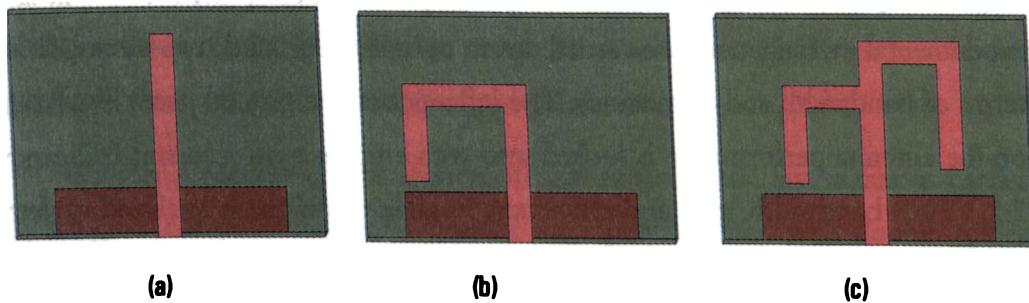


Fig 1.11 An evolution to the dual band planar branched monopole antenna
(a) printed strip monopole antenna
(b) single folded strip monopole antenna
(c) Double folded printed strip monopole antenna

The key idea behind the work presented in this thesis is that by judiciously placing another folded strip on the microstrip fed folded monopole element the bandwidth can be enhanced for the fundamental resonance and a new resonance at a higher frequency can be excited with good bandwidth and radiation characteristics. The modified geometry of double folded monopole with two different resonant lengths thus offers dual band operation. The double folded monopole geometry thus derived is shown in Fig 1.11 (c).

The position of the new element is very critical to achieve the desired performance. The new branch thus introduced offers inductive reactance to the system over a wide frequency in the first band, to cancel the capacitive reactance introduced in the system due to the coupling. The compact dual band monopole antenna thus obtained meets almost all criteria required to use in modern wireless gadget applications as an internal antenna. The optimized ground plane required for the antenna is very small. The novel antenna designed using the above concept is termed as 'double folded monopole'.

1.9 Thesis Organization

The main objectives of the research work are the investigations on the effect of ground plane on the characteristics of the printed monopole. Numerical and experimental investigations are carried out to optimize a printed strip monopole in terms of bandwidth and dimensions. The influence of the ground plane dimension on the antenna performance is looked into with emphasis on resonant frequency, 2:1 VSWR bandwidth, gain and efficiency. Folding technique is analyzed in detail for size reduction and double arm loaded printed strip monopole is proposed for dual band performance. Parametric analysis of the antenna is performed using the powerful Finite Difference Time Domain method. The FDTD analysis provides an insight into the spatial and temporal field behavior of the antenna geometry and also helps to predict the antenna performance characteristics. From exhaustive numerical and experimental studies simple design formulation are presented in the thesis.

Investigations on loading the printed strip monopoles with parasitic radiator such as dielectric resonators and patches are potential techniques analyzed for gain and bandwidth enhancement.

A brief overview of planar antennas and printed monopoles are presented in chapter 1. The rest of the thesis is organized into five chapters as follows.

Chapter 2 highlights the numerical techniques used for the analysis of the antenna with due emphasis on Finite Difference Time Domain method. The fundamental and mathematical concept behind the FDTD method is elaborated. A brief outline of the Perfectly matched layer (PML) boundary and techniques to extract antenna reflection and radiation parameters are discussed. A description of techniques used for the experimental and simulation study is also presented.

The results of theoretical and experimental investigations on ground plane effects of printed strip monopoles are illustrated in chapter 3. The radiation and reflection characteristics predicted using FDTD is compared with experimental and simulation results. The Chapter is concluded with a simple design formulation predicted from the numerical analysis.

Chapter 4 focuses on the theoretical and experimental investigations carried to design a compact dual band printed monopole antenna with double folded arms. Parametric analysis and empirical design equations along with the designs suitable for modern wireless communication bands are presented.

A summary of the conclusions drawn from the research work is presented in Chapter 5. Some directions for future work in this area are also suggested.

The experience obtained from numerical and experimental investigations on the printed monopoles are applied in for some further research in this direction.

The results of theoretical and experimental investigations carried out to enhance the bandwidth and radiation properties of the antenna with parasitic resonators are presented in the appendix part of the thesis. Thus a hybrid antenna technology with different radiators of similar radiation characteristics is the subject outlined in the Appendixes.

Appendix I and II describes two such designs. Appendix I illustrate the design of planar strip monopole antenna loaded with rectangular patch. Appendix II presents a uniplanar CPW fed planar monopole antenna loaded with ceramic dielectric resonator for broadband applications.

1.10 References

- [1] J.C Maxwell, "*A Treatise on Electricity and Magnetism*". London, England: Oxford University Press, 1873, 1904.
- [2] W.J.G Beynon, "Marconi, radio waves and the ionosphere", *radio science*, vol.10, no.7, pp 657-664, July 1975.
- [3] Tapan K. Sarkar and Dipak L. Sengupta., "An Appreciation of J. C. Bose's Pioneering Work in Millimeter Waves" *IEEE Antennas and Propagation Magazine*, Vol. 39, No. 5, October 1997.pp.55-63.
- [4] John D. Kraus, "Antennas since Hertz and Marconi", *IEEE Trans. Antennas and Propagat.* vol.33, no.2, pp 131-136, February 1985.
- [5] Andy D. Kucar, "Mobile radio: An overview", *IEEE communications magazine*, pp 72-85, November 1991.
- [6] T. A. Mulligan, "*Modern Antenna Design*", McGraw-Hill, New York, 1985.
- [7] T. Tsukiji and S. Tou, "On polygonal loop antennas", *IEEE Trans. Antennas and Propagat.* AP-28(4):571-575, July 1980.
- [8] J. D. Kraus, "*Antennas*", McGraw-Hill, New York, 1950, 1988.
- [9] S. Uda, "Wireless Beam of short electric waves", *J. IEE (Japan)*, pp. 273-282, March 1926 and pp. 1209-1219, Nov. 1927.
- [10] S. Silver, "*Microwave Antenna Theory and Design*", MIT Radiation Lab. Series, Vol. 12. McGraw-Hill, New York, 1949.
- [11] P. J. Wood, "*Reflector Analysis and Design*", Peter Peregrinus, London, 1980.
- [12] V. H. Rumsey, "*Frequency Independent Antennas*", Academic Press, New York, 1966.
- [13] Deschamps G. A , "*Microstrip Microwave Antennas*", 3rd USAF symposium on Antennas, 1953.
- [14] FCC, First Report and Order 02-48. February 2002.

- [15] Chu, L. J. "Physical Limitations of Omni-Directional Antennas". *Journal of Applied Physics*, v. 19, Dec. 1948, pp. 1163-1175.
- [16] Wheeler, H. A. "Fundamental Limitations on Small Antennas". *Proceedings of the IRE*, v. 35, Dec. 1947, pp. 1479 - 1484.
- [17] Richard W. Ziolkowski and Aycan Erentok, "Metamaterial-Based Efficient Electrically Small Antennas", *IEEE Transactions on Antennas and Propagation*, Vol. 54, No. 7, July 2006, pp. 2113-2130.
- [18] H.A. Wheeler, "Small Antennas," *IEEE Trans. Ant. Propagat*, vol. AP-23, pp. 462- 469, 1975.
- [19] R.E. Collin and F.J. Zucker, "Antenna Theory", Pt. 1, New York: McGraw-Hill, 1969.
- [20] K.-L. Wong, "Planar Antennas for Wireless Communications", Wiley, 2003.
- [21] L. Setian, "Practical Communication Antennas with Wireless Applications", Prentice Hall PTR, New Jersey: 1998.
- [22] J. Ollikainen, M.Fisher and P.Vainikainen, " Thin dual resonant stacked shorted patch antenna for mobile communication," *Electron.Lett.* vol.35,pp 437-438, March 18 ,1999.
- [23] G.Y Lee, T.W Chiou and K.L Wong, " Broadband stacked shorted patch antenna for mobile communication handsets," in *Proc. 2001 Asia-Pacific Microwave Conf.* pp 232-235.
- [24] Ramesh Garg, Prakash Bhartia, Inder Bahl and Apisak ittipiboon, "Microstrip Antenna Design Handbook" Artech House,Boston.
- [25] Pozar D.M., "A review of bandwidth Enhancement techniques for microstrip antennas," in *Microstrip antennas, The Analysis and Design of Microstrip Antennas and Arrays*, IEEE press, New York, 1995 pp 157-166.
- [26] Sanchez-Hernandez D, and I.D Robertson, "A survey of Broadband Microstrip Patch Antennas," *Microwave Journal*, September 1996, pp 60-84.
- [27] Zurcher, J.F and F.E Gardiol, "Broadband Patch Antennas", Artech House, Norwood, MA, 1995.
- [28] Debatosh Guha and Yahia M. M. Antar, "Circular Microstrip Patch Loaded With Balanced Shorting Pins for Improved Bandwidth". *IEEE Antennas and Wireless Propagation Letters*, Vol. 5, 2006.Pp 217-219.

- [29] A.K Bhattacharjee, S.R Bhadra Chaudhuri, D.R Poddar and S.K Chowdhury "Equivalence of radiation properties of Square and Circular Microstrip Patch Antennas" *IEEE Transactions on Antennas and Propagation*, Vol.38, No.10, October 1990, pp1710-1711.
- [30] C.Y. Huang, J.Y.Wu, and K. L.Wong, "High-gain compact circularly polarized microstrip antenna," *Electron. Lett.* **34**, 712–713, April 16, 1998.
- [31] J. H. Lu, C. L. Tang, and K. L.Wong, "Single-feed slotted equilateral-triangular microstrip antenna for circular polarization," *IEEE Trans. Antennas Propagat.* **47**, 1174–1178, July 1999.
- [32] J. H. Lu and K. L.Wong, "Single-feed circularly-polarized equilateral-triangular microstrip antenna with a tuning stub," *IEEE Trans. Antennas Propagat.* **48**, 1869–1872, Dec. 2000.
- [33] W. S. Chen, C. K. Wu, and K. L. Wong, "Novel compact circularly polarized square microstrip antenna," *IEEE Trans. Antennas Propagat.* **49**, 340–342, March 2001.
- [34] K. P. Yang, K. L.Wong, and J. H. Lu, "Compact circularly-polarized equilateral-triangular microstrip antenna with Y-shaped slot," *Microwave Opt. Technol. Lett.* **20**, 31–34, Jan. 5, 1999.
- [35] W. S. Chen, C. K.Wu, and K. L.Wong, "Compact circularly polarized circular microstrip antenna with cross slot and peripheral cuts," *Electron. Lett.* **34**, 1040–1041, May 28, 1998.
- [36] W. S. Chen, C. K. Wu, and K. L. Wong, "Single-feed square-ring microstrip antenna with truncated corners for compact circular polarization operation," *Electron. Lett.* **34**, 1045–1047, May 28, 1998.
- [37] K. L. Wong and M. H. Chen, "Slot-coupled small circularly polarized microstrip antenna with modified cross-slot and bent tuning-stub," *Electron. Lett.* **34**, 1542–1543, Aug. 6, 1998.
- [38] W. S. Chen, K. L. Wong, and C. K. Wu, "Inset microstripline-fed circularly polarized microstrip antennas," *IEEE Trans. Antennas Propagat.* **48**, 1253–1254, Aug. 2000.
- [39] C. Y. Huang, J. Y. Wu, C. F. Yang, and K. L. Wong, "Gain-enhanced compact broadband microstrip antenna," *Electron. Lett.* **34**, 138–139, Jan. 22, 1998.
- [40] B. Robert, T. Razban, and A. Papiernik, "Compact amplifier integration in square patch antenna," *Electron. Lett.* **28**, 1808–1810, Sept. 10, 1992.

- [41] M. C. Pan and K. L. Wong, "A broadband active equilateral-triangular microstrip antenna," *Microwave Opt. Technol. Lett.* **22**, 387–389, Sept. 20, 1999.
- [42] S. Dey and R. Mittra, "Compact microstrip patch antenna," *Microwave Opt. Technol. Lett.* **13**, 12–14, Sept. 1996.
- [43] K. L. Wong, C. L. Tang, and H. T. Chen, "A compact meandered circular microstrip antenna with a shorting pin," *Microwave Opt. Technol. Lett.* **15**, 147–149, June 20, 1997.
- [44] C. K. Wu, K. L. Wong, and W. S. Chen, "Slot-coupled meandered microstrip antenna for compact dual-frequency operation," *Electron. Lett.* **34**, 1047–1048, May 28, 1998.
- [45] J. H. Lu and K. L. Wong, "Slot-loaded, meandered rectangular microstrip antenna with compact dual-frequency operation," *Electron. Lett.* **34**, 1048–1050, May 28, 1998.
- [46] J. George, M. Deepukumar, C. K. Aanandan, P. Mohanan, and K. G. Nair, "New compact microstrip antenna," *Electron. Lett.* **32**, 508–509, March 14, 1996.
- [47] Qian Y., et al. "Microstrip patch Antenna using Novel Photonic Band Gap Structures", *Microwave Journal*, vol.42, Jan 1999, pp 66-76.
- [48] T. Taga and K. Tsunekawa, "Performance analysis of a built-in planar inverted-F antenna for 800MHz hand portable radio units," *IEEE J. Selected Areas in Communication*, vol.5, pp 921-929, 1987.
- [49] Z. D. Liu, P. S. Hall, and D. Wake, "Dual-frequency planar inverted-F antenna". *IEEE Trans Antennas Propagat AP-45* (1997), 1451–1458.
- [50] C. R. Rowell and R. D. Murch, "A compact PIFA suitable for dual-frequency 900/1800-MHz operation", *IEEE Trans Antennas Propagat. AP-46* (1998), 596–598.
- [51] P. Salonen, M. Keskilampi, and M. Kivikoski, "New slot configurations for dual-band planar inverted-F antenna", *Microwave Opt Technol Lett* **28** (2001), 293–298.
- [52] M. Martínez-Vázquez, M. Geissier, D. Heberling, A. Martínez-González, and D. Sánchez-Hernández, "Compact dual-band antenna for mobile handsets", *Microwave Opt Technol Lett* **32** (2002), 87–88.

- [53] F.R. Hsiao, H.T. Chen, T.W. Chiou, G.Y. Lee, and K.L. Wong, "A dual-band planar inverted-F patch antenna with a branch-line slit", *Microwave Opt Technol Lett* 32 (2002), 310–312.
- [54] C.W. Chiu and F.L. Lin, "Compact dual-band PIFA with multiresonators", *Electron Lett* 38 (2002), 538–540.
- [55] G.H. Brown and O.M. Woodward, Jr., "Experimentally determined radiation characteristics of conical and triangular antennas", *RCA Rev* 13 (1952), 425–452.
- [56] S. Honda, M. Ito, H. Seki, and Y. Jinbo, "A disk monopole antenna with 1:8 impedance bandwidth and omnidirectional radiation pattern", *ISAP '92, Sapporo, Japan*, (1992), 1145–1148.
- [57] N.P. Agrawal, G. Kumar, and K.P. Ray, "Wide-band planar monopole antenna", *IEEE Trans Antennas Propagat* AP-46 (1998), 294–295.
- [58] M.J. Ammann, "Square planar monopole antenna", *National Conf Antennas Propagat, York, England* (1999), 37–40.
- [59] Z.N. Chen, "Impedance characteristics of planar bow-tie-like monopole antennas", *Electron Lett* 36 (2000), 1100–1101.
- [60] Z.N. Chen, "Experimental on input impedance of tilted planar monopole antennas", *Microwave Opt Technol Lett* 26 (2000), 202–204.
- [61] Z.N. Chen and M.Y.W. Chia, "Impedance characteristics of trapezoidal planar monopole antenna", *Microwave Opt Technol Lett* 27 (2000), 120–122.
- [62] J.A. Evans and M.J. Ammann, "Planar trapezoidal and pentagonal monopoles with impedance bandwidths in excess of 10:1", *IEEE Int Symposium on Antennas and Propagat, Orlando, USA*, (1999), 1558–1561.
- [63] M.J. Ammann, "Impedance bandwidth of the square planar monopole", *Microwave and Opt Technol Lett* 24 (2000), 185–187.
- [64] Mitilineos, S. A., S. C. A. Thomopoulos, and C. N. Capsalis, "Genetic design of dual-band, switched-beam dipole arrays, with elements failure correction, retaining constant excitation coefficients," *Journal of Electromagnetic Waves and Applications*, Vol. 20, No. 14, 1925–1942, 2006.

- [65] Lei, J., et al., "An omnidirectional printed dipole array antenna with shaped radiation pattern in the elevation plane," *Journal of Electromagnetic Waves and Applications*, Vol. 20, No. 14, 1955–1966, 2006.
- [66] Ayestaran, R. G., J. Laviada, and F. Las-Heras, "Synthesis of passive-dipole arrays with a genetic-neural hybrid method," *Journal of Electromagnetic Waves and Applications*, Vol. 20, No. 15, 2123–2135, 2006.
- [67] G.Y. Chen and J.S. Sun, "A printed dipole antenna with microstrip tapered balun", *Microwave Opt Technol Lett* 40 (2004), 344–346.
- [68] T. Vasiliadis, E. Vaitopoulos, and G. Sergiadis, "A wideband printed dipole antenna with optimized tapered feeding balun for ISM, and FW bands", *Microwave Opt Technol Lett* 43 (2004), 437–441.
- [69] K. Chang, H. Kim, and Y. Yoon, "A triple-band printed dipole antenna using parasitic elements", *Microwave Opt Technol Lett* 47 (2005), 221–223
- [70] Jean-Marie Floc'h and Hatem Rmili., " Design Of Multiband Printed Dipole Antennas Using Parasitic Elements", *Microwave And Optical Technology Letters* , Vol. 48, No. 8, August 2006
- [71] Chen, Z. N. "Broadband planar monopole antenna," *IEE Proc. Microw. Antennas Propag.* Vol. 147, no.6, 2000, pp.526–528.
- [72] Chen, Z. N., Ammann, M. J., Chia, M. Y. W. and See, T. S. P. "Circular annular planar monopole with EM coupling," *IEE Proc. Microw. Antennas Propag.* vol 150, no.4,pp. 269–273, 2000.
- [73] Chen, Z. N. and Chia, M. Y. W. "Impedance characteristics of EMC triangular monopoles," *IEE Electronics letters*, vol.37, no.21, pp. 1271–1272, 2001.
- [74] J. Liang, C. C. Chiau, X. Chen, and C. G. Parini, "Analysis and design of UWB disc monopole antennas," in *Proc. Inst. Elect. Eng. Seminar on Ultra Wideband Communications Technologies and System Design*, Queen Mary, University of London, U.K., Jul. 2004, pp. 103–106.

- [75] J. Liang, C. C. Chiau, X. Chen, and C. G. Parini "Printed circular disc monopole antenna for ultra wideband applications," *Electron. Lett.*, vol. 40, no. 20, Sep. 2004.
- [76] J. Liang, C. C. Chiau, X. Chen, and C. G. Parini "Study of a Printed Circular Disc Monopole Antenna for UWB Systems", *IEEE Transactions On Antennas And Propagation*, Vol. 53, No. 11, November 2005, pp 3500-3504.
- [77] Chen, H.D., and Chen, H.T.: 'A CPW-fed dual-frequency monopole antenna', *IEEE Trans. Antennas Propag.*, 52, (4), pp. 978–982.
- [78] Lee, S.H., Park, J.K., and Lee, J.N.: 'A novel CPW-fed ultra-wideband antenna design', *Microw. Opt. Technol. Lett.*, 2005, 44, (5), pp. 393–396.
- [79] Deepu V, Rohith K. Raj, Manoj Joseph, Suma M.N and P. Mohanan "Compact Asymmetric Coplanar Strip Fed Monopole Antenna for Multiband Applications", *IEEE Transactions on Antennas and Propagations*. Vol. 55, No. 8, August 2007.
- [80] Deepu V, Rohith K. Raj, Manoj Joseph, Suma M.N and P. Mohanan, "A Compact uniplanar antenna for WLAN applications". *IEE Electronics Letters.*, Volume 43, Issue 2, January 18 2007 Page(s):70 – 72
- [81] W. C. Liu and W. R. Chen, "CPW-fed compact meandered patch antenna for dual-band operation," *Electron. Lett.*, vol. 40, no. 18, pp. 1094–1095, Sep. 2004.
- [82] T. H. Kim and D. C. Park, "CPW-fed compact monopole antenna for dual-band WLAN applications," *Electron. Lett.*, vol. 41, no. 6, pp. 292–293, Mar. 2005.
- [83] Y.-D. Lin and P.-L. Chi, "Tapered bent folded monopole for dual-band wireless local area network (WLAN) systems," *IEEE Antennas and Wireless Propag. Lett.*, vol. 4, pp. 355–357, 2005.
- [84] Y.-L. Kuo and K.-L. Wong, "Printed double-T monopole antenna for 2.4/5.2 GHz dual-band WLAN operations," *IEEE Trans. Antennas Propag.*, vol. 51, no. 9, pp. 2187–2192, Sep. 2003.
- [85] S. H. Choi, J. K. Park, S. K. Kim, and H. Y. S. Kim, "Design of dualband antenna for the ISM band using a backed microstrip line," *Microw. Opt. Technol. Lett.*, vol. 41, no. 6, pp. 457–460, Jun. 2004.
- [86] C.-Y. Huang and P.-Y. Chiu, "Dual-band monopole antenna with shorted parasitic element," *Electron. Lett.*, vol. 41, no. 21, pp. 1154–1155, Oct. 2005.

- [87] W.-C. Liu and C.-M. Wu. "Dual-band CPW-fed Y-shaped monopole antenna for PCS/WLAN application", *Electronics Letters* 31st March 2005 Vol. 41 No. 7. pp 390-391.
- [88] H.-M. Chen., "Microstrip-fed dual-frequency printed triangular monopole". *Electronics Letters* 20th June 2002 Vol. 38, No.13. PP.619-620.
- [89] K. Siwiak and L. L. Huckabee, "UWB radio physical layer for WPAN standards," in Proc. 5th Meeting Wireless World Research Forum, Tempe, AZ, Mar. 7–8, 2002.
- [90] S. Roy, J. R. Foerster, V. S. Somayazulu, and D. G. Leeper, "Ultra wideband radio design: The promise of high-speed, short-range wireless connectivity," *Proc. IEEE*, vol. 92, no. 2, pp. 295–311, Feb. 2004.
- [91] H. Schantz, "A Brief History of UWB Antennas". *Aerospace and Electronic Systems Magazine*, IEEE Volume 19, Issue 4, April 2004, pp.22-26.
- [92] Y. Kim and D.-H. Kwon, "CPW-fed planar ultra wideband antenna having a frequency band notch function", *Electronics Letters*, vol. 40, no. 7, pp. 403-405, April 2004.
- [93] Wei Wang, S. S. Zhong and Sheng-Bing Chen, "A Novel Wideband Coplanar-Fed Monopole Antenna", *Microwave and Optical Technology Letters*, vol. 43, no. 1, pp. 50-52, October 5 2004.
- [94] Seong-Youp Suh, W.Shutzman, W.Davis, A.Waltho and J.Schiffer, "A novel CPW-fed Disc Antenna", *IEEE Antennas and Propagation Society Symposium*, vol. 3, pp. 2919 - 2922, June 20-25, 2004.
- [95] Tacyoung Yang and Davis, W.A, "Planar half-disk antenna structures for UWB communications", *IEEE Antennas and Propagation Society Symposium*, vol. 3, pp. 2508 - 2511, June 20-25, 2004.
- [96] Hyungkuk Yoon, Hyunrak Kim, Kihun Chang, Young Joong Yoon and Young- Hwan Kim, "A study on the UWB antenna with band-rejection characteristic", *IEEE Antennas and Propagation Society Symposium*, vol. 2, pp. 1784 - 1787, June 20-25, 2004.
- [97] Ammann, M.J., and Chen, Z.N.: 'An asymmetrical feed arrangement for improved impedance bandwidth of planar monopole antennas', *Microw. Opt. Technol. Lett.*, 2004, 40, pp. 156–158.

-
- [98] Floc'h, J.M., and Desclos, L.: "Surface-mounted monopole antenna", *Microw. Opt. Technol. Lett.*, 1997, 16, pp. 349–352.
- [99] Antonino-Daviu, E., Cabedo-Fabres, M., Ferrando-Bataller, M., and Valero-Nogueira, A.: "Wideband double-fed planar monopole antennas", *Electron Lett.*, 2003, 39, pp. 1635–1636.
- [100] Ammann, M.J., and Chen, Z.N.: "Wideband monopole antennas for multi-band wireless systems", *IEEE Antennas Propag. Mag.*, 2003, 45, pp. 146–150.
- [101] Wang, W., Zhong, S.S., and Chen, S.B.: "A novel wideband coplanar-fed monopole antenna", *Microw. Opt. Technol. Lett.*, 2004, 43, pp. 50–52.
- [102] W. S. Lee, D. Z. Kim, K. J. Kim, and J. W. Yu, "Wideband Planar Monopole Antennas with Dual Band-Notched Characteristics," *IEEE Trans. Microw. Theory Tech.*, vol.54, no.6, pp2800-2806, June 2006.
- [103] D. C. Chang, M. Y. Lin, and C. H. Lin, "A CPW-fed U type Monopole Antenna for UWB Applications," in *Proc. IEEE Antennas and Propagat. Soc. Int. Symp.*, vol.5A, pp512-515, July 2005.
- [104] K. F. Jacob, M. N. Suma, R. K. Raj, M. Joseph and P. Mohanan, "Planar Branched Monopole Antenna for UWB Applications," *Microw. Opt. Technol. Letts.*, vol.49, no.1, pp45-47, Jan. 2007
- [105] J. Guterman, A.A. Moreira, and C. Peixeiro, "Microstrip fractal antennas for multistandard terminals", *IEEE Antennas Wireless Propag Lett* 3 (2004), 351–354.
- [106] J.P. Gianviffwb and Y. Rahmat-Samii, "Fractal antennas: A novel antenna miniaturization technique, and applications", *Antennas Propag. Mag* 44 (2002), 20–36.
- [107] Min Ding, Ronghong Jin, Junping Geng, and Qi Wu., " Design Of A Cpw-Fed Ultrawideband Fractal Antenna", *Microwave And Optical Technology Letters* , Vol. 49, No. 1, January 2007
- [108] Fractal Antenna System Inc., Fort Lauderdale, FL [Online]. Available: www.fractenna.com
- [109] C. Puente, J. Romeu, and R. Pous., "Small but long Koch fractal monopole," *Electron. Lett.*, vol. 34, no. 1, pp. 9–10, 1998.

- [110] C. Puente, J. Romeu, and R. Pous, "On the behavior of the Sierpinski multiband fractal antenna," *IEEE Trans. Antennas Propag.*, vol. 46, no. 4, pp. 517–524, Apr. 1998.
- [111] H. A. Ghali and T. A. Moselhy, "Broad-band and circularly polarized space-filling-based slot antenna," *IEEE Trans. Microw. Theory Tech.*, vol. 53, no. 6, pp. 1946–1950, Jun. 2005.
- [112] K.J. Vinoy, K.A. Jose, V.K. Varadan, and V.V. Varadan, "Hilbert curve fractal antenna: A small resonant antenna for VHF/UHF applications," *Microwave & Opt. Technol. Lett.*, vol. 29, pp. 2 15-2 19, 2000.
- [113] K.J. Vinoy, K.A. Jose, V.K. Varadan, and V.V. Varadan, "Resonant frequency of Hilbert curve fractal antennas," In: *IEEE- AP-S International Symposium*, Boston, July 8-13. 2001 Digest vol. 111, pp. 648-651, 2001.
- [114] K. J. Vinoy, "Fractal shaped antenna elements for wide- and multi-band wireless applications," Ph.D. dissertation, Pennsylvania State Univ., University Park, 2002.
- [115] K. J. Vinoy, Jose K. Abraham, and Vijay K. Varadan, "On the Relationship Between Fractal Dimension and the Performance of Multi-Resonant Dipole Antennas Using Koch Curves" *IEEE Transactions On Antennas And Propagation*, Vol. 51, No. 9, September 2003.pp 2296-2303.
- [116] P. W. Tang and P. F. Wahid "Hexagonal Fractal Multiband Antenna", *IEEE Antennas and Wireless Propagation Letters*, Vol. 3, 2004.pp.111-112.

TECHNIQUES FOR ANALYSIS AND CHARACTERIZATION OF THE ANTENNAS

"Maxwell's equations provide the physics of Electromagnetic wave phenomenon from DC to light and their accurate modeling is essential to understand high speed effects having wave-transport behavior."

-Allen Taflove

The application of Computational Electromagnetics techniques to antenna problems provides a powerful and increasingly popular means to explore critical antenna design issues. The chapter explores a brief overview of the computation Electromagnetics techniques for antenna problems. The Finite Difference Time Domain technique, the method adopted for theoretical analysis in this thesis is elaborately portrayed. The chapter focuses on the fundamental mathematical concepts of FDTD and the theoretical aspects for foretelling the antenna reflection and radiation characteristics. A brief description of basic facilities used for fabrication, experimental characterization and simulation studies of the antenna is outlined in the concluding section.

2.1 Background of theoretical analysis

The art of computation of electromagnetic (EM) problems has grown exponentially during the last three decades due to the availability of powerful computer resources. Scientists and engineers use different techniques for solving field problems. Most common techniques are either analytical or numerical. Exact analytical solutions are always the preferred method to a given problem, if possible. However, for most of the electromagnetic problems, exact solutions are more complicated and we have to depend on numerical solutions. Application of these methods is not limited to EM problems; they find applications in other fields like fluid dynamics, heat transfer, acoustics etc [1]. Until the 1940s, most EM problems were solved using the methods of separation of variables and integral equation solutions. Since these techniques require large experience and effort for defining complex geometries only a narrow range of practical problems were investigated. Numerical solution of EM problems started in the mid-1960s with the availability of modern high-speed digital computers. Since then, considerable effort has been spent on solving practical, complex EM-related problems for which closed form analytical solutions are either intractable or do not exist. The numerical approach has the advantage of allowing the actual work to be carried out by operators without the knowledge of higher mathematics or physics. Modeling of engineering system involving electromagnetic wave interactions is based on frequency domain techniques such as asymptotic methods [2-3] and integral equation method [4-5] or time domain techniques such as Finite Difference Time Domain method. Frequency domain numerical solutions are achieved by approximating the relevant differential or integral equations and solving large matrix equations. Differential equation solutions such as Finite difference (FDM) and finite Element (FEM) methods are the easiest techniques to implement but result in large sparse matrices. Integral equation solutions employing Method of Moments (MOM) involves more detailed mathematical

formulation and for complex problem can lead to complex matrices. Time domain numerical solution has gained attention as modeling technique and solution to the problem can be obtained either Fourier transforming the frequency domain results or directly implementing finite difference time stepping algorithm. Application of these techniques to antenna analysis yields design flexibility and a physical insight to the actual radiation phenomenon and operating principles that could help the design and its enhancement.

2.2 Computational Electromagnetics for antenna field problems

The objectives of antenna analysis are to predict the radiation characteristics such as radiation pattern, gain, polarization as well as near field characteristics such as input impedance, impedance bandwidth, efficiency and mutual coupling. The analysis of printed antennas is complicated due to the presence homogenous boundary condition and wide variety of substrates, patch geometry and feeding techniques. Elaborate techniques have been proposed and used for extracting antenna characteristics. Analytical techniques are based on simplifying assumptions and these techniques maintain simplicity at the expense of accuracy. Full wave technique gained increased attention due to their rigor and high accuracy at the expense of numerical simplicity. The analytical technique employed for a typical planar microstrip antenna includes transmission line model, cavity model, generalized transmission line model and multiport network model etc. Full wave methods are based on integral equations of solution of Maxwell's equation in time domain. Prominent numerical methods include integral equation analysis in spectral domain, integral equation analysis in space domain, Finite Element Method and Finite Difference Time Domain approach. The main objective of any numerical method is to develop an algorithm with minimum effort, maximum efficiency and flexibility to model any complicated structure.

Referring to the Fig 2.1 the analytical modeling of any electromagnetic field problem requires the following steps

- Description of the problem.
- Excitation of the structure.
- Computation of the electromagnetic field in the structure by solving Maxwell's equation subject to the appropriate boundary conditions.
- Extraction of the required parameters.

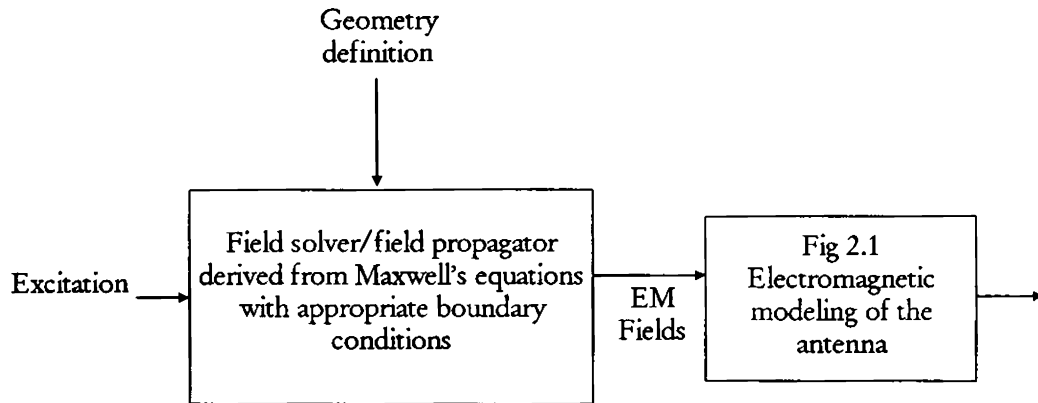


Fig 2.1 Electromagnetic modeling of the antenna

The most important stage of computational electromagnetics is the solution of Maxwell's equations [6]. These equations are linear but when subject to boundary and interface conditions the solution using analytical methods becomes complicated. The numerical methods for the solution of Maxwell's equations may be classified as shown in Table 2.1. The most commonly used methods in each category are listed in the table.

Table 2.1 Classification of Numerical methods for CEM.

SOLUTION OF MAXWELL'S EQUATIONS			
Frequency domain: Field solver. Requires Matrix inversion & system solution. Requires frequency samples across broad bandwidth, followed by a transform to obtain the result		Time domain: Field propagator. Requires initial values & boundary values. Values updated in time. Ideal for massive parallel architecture. Wide band performance results in a single calculation	
Integral equation	Differential method	Integral equation	Differential method
Method of moments: Electric field integral equations (EFIE) or Mixed potential Integral Equation (MPIE)	Finite element method	Time domain Integral Equation (TDIE)	Transmission line matrix (TLM) Finite Difference Time Domain Method (FDTD)

Apart from the time or frequency domain methods, hybrid methods are also used for the analysis of electromagnetic field problems. Hybrid methods, which combine the desirable features of two or more different techniques, are being developed by a number of authors to analyze complex electromagnetic problems that cannot be resolved conveniently and/or accurately, by using them individually [7-11]. A typical example included MoMTD which combines MoM and FDTD. These hybrid approaches considerably widens the scope of individual techniques, viz., FDTD, MoM and FEM.

This section presents a brief overview of the full wave techniques.

Method of Moments (MoM)

The *method of moments* (MoM) is a general procedure for solving linear operator equations [12]. The method owes its name to the process of taking moments by multiplying with appropriate weighing functions and integrating. The first use of Method of Moments in Computational Electromagnetics is attributed to

Harrington [13]. The origin and development of the moment method are fully documented by Harrington [14, 15]. The method of moments is essentially the method of weighted residuals hence applicable for solving both differential and integral equations. The use of MoM in EM has become popular since the work of Richmond [16] in 1965 and Harrington [4] in 1967. The method has been successfully applied to a wide variety of EM problems of practical interest such as radiation due to thin-wire elements and arrays, scattering problems, analysis of microstrip and lossy structures, propagation over an inhomogeneous earth, and antenna beam pattern etc. MoM is a method of solving a differential equation or an integral equation numerically by transforming the equation into simultaneous equations. Regarding antenna analysis integral equation for electric field on the surface of the conductor is usually used to obtain the surface current on the antenna. The substrate and ground plane are assumed to be infinite in lateral dimensions and formulation of the problem is based on rigorously enforcing the boundary condition. Analysis carried out in spatial domain uses Sommerfield type of integral equations where as in spectral domain approach uses exact Green's functions [17]. In Electric Field Integral Equation (EFIE) the boundary condition is applied to the total tangential electric field where as in Magnetic Field Integral Equation (MFIE) boundary condition is expressed in terms of magnetic field. Mixed Potential Integral Equations (MPIE) has both scalar and vector potentials in its formulation [18]. The integral equation is then solved either in spectral domain or spatial domain by taking appropriate transformations.

The procedure for applying MoM to solve an electromagnetic problem involves four steps:

- Derivation of the appropriate integral equation (IE)
- Conversion (discretization) of the IE into a matrix equation using basis (or expansions) functions and weighting (or testing) functions.

- Evaluation of the matrix elements
- Solving the matrix equation and obtaining the parameters of interest.

To solve Integral Equation it is discretised into set linear equations by means of moment method. By solving the matrix equation the surface current on the patch conductor can be obtained which is then used for extracting the radiation pattern, polarization, directivity etc. MoM depends upon expanding the unknown quantity in the equation in terms of known entire domain or sub domain basis functions with unknown coefficients. The selection of basis function is a very important step in the numerical solution since they have the ability to accurately represent and resemble the anticipated unknown function while minimizing computational effort [19-21]. The popularly used basis functions are piece wise sinusoidal, pulse basis and roof top basis functions. A set of equations is generated by enforcing the boundary conditions with a suitable set of testing functions. This results in a matrix whose order is proportional to the number of segments on which the current distribution is represented. The solution to the problem is found by inverting this matrix.

Finite Element Method (FEM)

The Finite element method is one of the classic tools of numerical analysis, suitable for the solution of a wide class of partial differential or integral equations. In the mid-1970's Mei, Morgan and Chang introduced the finite-element approach for the Helmholtz equation [12]. Later, in the early 1980's, they shifted their finite element research to direct solutions of Maxwell's curl equations. Finite element techniques require the entire volume of the configuration to be meshed as opposed to surface integral techniques, which require only the surfaces to be meshed. Each mesh element has completely different properties from those of neighbouring elements. In general, finite element techniques excel at modelling

complex inhomogeneous configurations. However, they do not model unbounded radiation problems as effectively as moment method techniques.

The finite element analysis of any problem involves basically four steps [22]:

- discretizing the solution region into a finite number of sub regions or elements,
- deriving governing equations for a typical element,
- assembling of all elements in the solution region, and
- Solving the system of equations.

An example of a discretised finite–element model is shown in Figure 2.2. The model contains information about the device geometry, material constants, excitations and boundary constraints. In each finite element, a simple (often linear) variation of the field quantity is assumed. The corners of the elements are called *nodes*. The goal of the finite-element analysis is to determine the field quantities at the nodes.

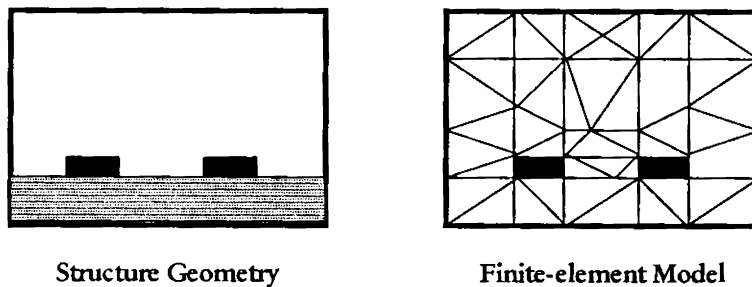


Fig. 2.2 Finite-element modeling example

Generally, finite element analysis techniques solve for the unknown field quantities by minimising energy functional. The energy functional is an expression describing all the energy associated with the configuration being analysed.

For 3-dimensional time-harmonic problems this functional may be represented as

$$F = \int_v \left(\frac{\mu |H|^2}{2} + \frac{\epsilon |E|^2}{2} - \frac{J \cdot E}{2j\omega} \right) dv \quad \dots\dots\dots(2.1)$$

The first two terms represent the energy stored in the magnetic and electric fields, and the third term is the energy dissipated by the conduction current. Expressing H in terms of E and setting the derivative of this functional with respect to E equal to zero, an equation of the form $f(J,E) = 0$ is obtained. A k^{th} order approximation of the function f is then applied at each node and boundary conditions enforced, resulting in the system of equations,

$$[J] = [Y][E] \quad \dots\dots\dots(2.2)$$

The elements of J are referred to as the source terms, representing the known excitations. The elements of the Y-matrix are functions of the problem geometry and boundary constraints. The elements of the E-matrix represent the unknown electric field at each node, obtained by solving the system of equations. In order to obtain a unique solution, it is necessary to constrain the values of the field at all boundary nodes. For example, the metal box of the model in Figure 1.3 constrains the tangential electric field at all boundary nodes to be zero. Therefore, a major weakness of FEM is that it is relatively difficult to model open configurations. However, in finite element methods, the electrical and geometric properties of each element can be defined independently. This permits the problem to be set up with a large number of small elements in regions of complex geometry and fewer, larger elements in relatively open regions. Thus it is possible to model complicated geometries with many arbitrarily shaped dielectric regions in a relatively efficient manner. Although the finite difference method (FDM) and the method of moments (MoM) are conceptually simpler and easier to program than the finite element method (FEM), FEM is a more powerful and versatile numerical technique for handling problems involving complex geometries and inhomogeneous media. The

systematic generality of the method makes it possible to construct general-purpose computer programs for solving a wide range of problems. Consequently, programs developed for a particular discipline have been applied successfully to solve problems in a different field with little or no modification.

Transmission Line Matrix Method (TLM)

Transmission-line modeling (TLM), otherwise known as the *transmission-line matrix method*, is a numerical technique for solving field problems using circuit equivalent. It is based on the equivalence between Maxwell's equations and the equations for voltages and currents on a mesh of continuous two-wire transmission lines. The main feature of this method is the simplicity of formulation and programming for a wide range of applications [23-24]. As compared with the lumped network model, the transmission-line model is more general and performs better at high frequencies where the transmission and reflection properties of geometrical discontinuities cannot be regarded as lumped [25]. Like other numerical techniques, the TLM method is a discretization process. Unlike other methods such as finite difference and finite element methods, which are mathematical discretization approaches, the TLM is a physical discretization approach. The nodes of the grids are interconnected by virtual transmission line. The excitation at the source node propagates to the adjacent nodes through these virtual transmission lines. Generally dielectric loading can be modeled by loading the nodes with reactive stubs and lossy media can be modeled by introducing the loss into the transmission line equations. Absorbing boundary is constructed in TLM meshes by terminating each boundary node transmission line by its characteristic impedance. Analysis is performed in time domain. The major advantage of the TLM method, as compared with other numerical techniques, is the ease with which even the most complicated structures can be analyzed. The great flexibility and versatility of the method reside in the fact that the TLM mesh incorporates the properties of EM fields and their interaction with the boundaries and material media. Hence, the EM problem need not be

formulated for every new structure. Another advantage of using the TLM method is that certain stability properties can be deduced by inspection of the circuit. There are no problems with convergence, stability or spurious solutions. The method is limited only by the amount of memory storage required, which depends on the complexity of the TLM mesh. Also, being an explicit numerical solution, the TLM method is suitable for nonlinear or inhomogeneous problems since any variation of material properties may be updated at each time step.

Finite Difference Time Domain method (FDTD)

The Finite Difference Time Domain (FDTD) method was first introduced by K.S.Yee in 1966 [26] and refined and reinvented by Taflov [27] in the 1970's. This method permits the modelling of electromagnetic wave interactions with a level of detail as high as that of the Method of Moments. Unlike MoM, however, the FDTD does not lead to a system of linear equations defined over the entire problem space. Updating each field component requires knowledge of only the immediately adjacent field components calculated one-half time step earlier. Therefore, overall computer storage and running time requirements for FDTD are linearly proportional to N , the number of field unknowns in the finite volume of space being modelled. The FDTD method has thus emerged as a viable alternative to the conventional Frequency Domain methods because of its dimensionally reduced computational burdens and ability to directly simulate the dynamics of wave propagation [28]. The rapid growth of FDTD in Computational Electromagnetics is presented in the survey paper by Shlager and Schneider [29]. Although FDTD and TLM are time domain methods there are some fundamental differences that make them complement each other than compete each other. TLM is a physical model based on Huygens' principle using interconnected transmission lines, but the FDTD is an approximate mathematical model directly based on Maxwell's equations. In the two-dimensional TLM, the magnetic and electric field components are located at the same position with respect to space and time, whereas in the corresponding two-

dimensional FDTD cell, the magnetic field components are shifted by half an interval in space and time with respect to the electric field components. Due to this displacement between electric and magnetic field components in Yee's FDTD, Chen et al. [30] modified the FDTD and the new formulation is exactly equivalent to the symmetric condensed node model used in the TLM method. This implies that the TLM algorithm can be formulated in FDTD form and vice versa. However, both algorithms retain their unique advantages. FDTD has a simpler algorithm where constitutive parameters are directly introduced, while the TLM has certain advantages in the modeling of boundaries and the partitioning of the solution region. Furthermore, the FDTD requires less than one-half of the CPU time spent by the equivalent TLM program under identical conditions. A detailed description of FDTD, the method used for the numerical analysis in the present investigation is presented in the following sections.

2.3 Numerical investigations : Finite Difference Time Domain

Finite difference Time Domain method proposed by Yee in 1966 is extensively used many areas of science and technology. FDTD, a technique that discretizes the problem domain in both time and space gives time and frequency domain information of the electromagnetic problem of interest. FDTD provides a direct solution of time dependant Maxwell's equation for electric and magnetic field intensities in a finite, piecewise homogenous media. Due to the lack of analytical preprocessing and modeling, FDTD is a potential tool for planar antenna problems. Moreover, this analysis approach can be used to include the effect of finite ground plane and substrate parameters which is very important in the present investigation, where printed monopole with truncated ground plane is the focus of this work. Specifically, certain characteristic strengths of FDTD attract the investigators to apply this algorithm in the antenna design and analysis.

Following are the striking features of this powerful modelling, simulation and analysis tool.

- From the mathematical point of view, it is a direct implementation of Maxwell's curl equations. Therefore, analytical processing of Maxwell's equations is almost negligible.
- It can model complex antenna geometries and feed and other structures in the model.
- It can model any type of materials of importance to electromagnetic technology, including conductors, dielectrics, dispersive and non linear medium.
- Impulsive excitations in Time Domain gives a broadband response in frequency domain in a single FDTD run through concurrently run Fourier transform.
- The complex near field information is an intrinsic part of FDTD model and the near to far field transformation offers the calculation of far field radiation pattern in single FDTD run.
- FDTD is accurate: It is good model of the physical world. The ready availability of time domain and frequency domain data provides a deep physical insight to the problem in different perspectives. Visualization of fields in time provides a clear insight to the actual physics behind the antenna radiation.

2.3.1 Fundamental concepts of FDTD

Analysis of antenna problem using FDTD starts with dividing the structure into various regions based on the material properties. The unbounded region, if any, is then bounded by terminating it with absorbing medium or a termination free from reflections. The entire structure is discretised in the form of number of

cuboids of volume $\Delta x \Delta y \Delta z$ called Yee cells, where Δx , Δy , Δz are the dimensions of cuboid in X, Y and Z directions. The Yee cell is the basic building block of the entire structure in which the Electric fields and Magnetic field are interleaved as shown in Fig.2.3. The time domain is also discretised with interval Δt . The structure is then excited by an electromagnetic pulse. The wave thus launched by the pulse in the structure is then studied for its propagation behavior. The stabilized time-domain waveform is numerically processed to determine the time-domain and frequency domain characteristics of the structures. Convergence, stability, accuracy and consistency are some of the issues to be addressed while implementing FDTD method.

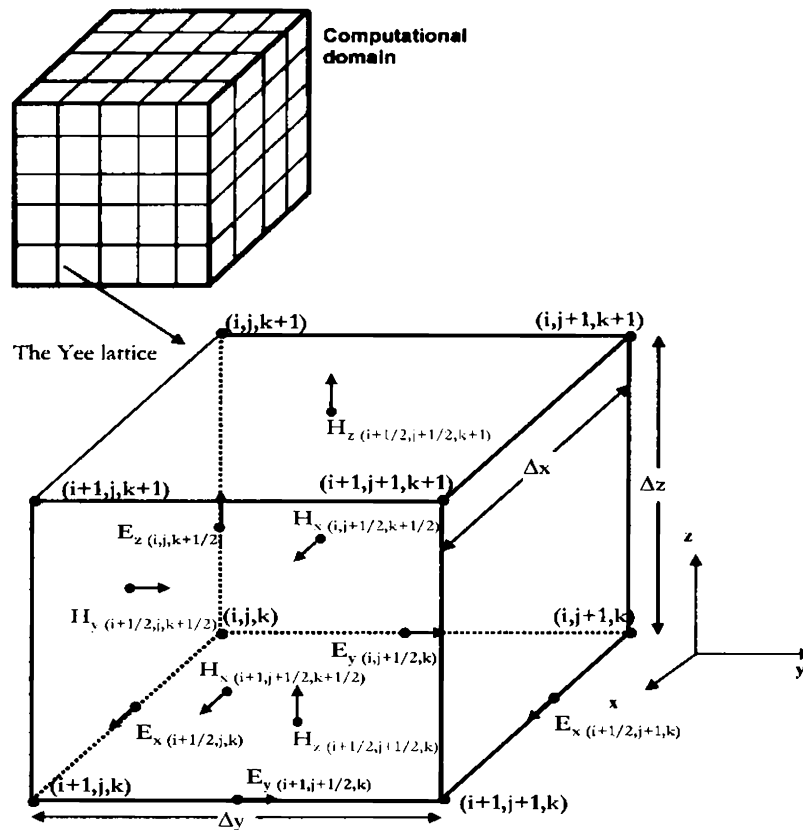


Fig 2.3 Yee cells illustrating E and H field vector placements

2.3.2 Implementation

FDTD method is a direct solution of Maxwell's time-dependent curl equations. The curl operators in the Maxwell's set of equation are discretized using central difference approximations of spatial and time derivatives. The orthogonal E field components (E_x, E_y, E_z) are staggered onto the edges of the Yee cell, where as H field components (H_x, H_y, H_z) are distributed at the face centers. Maxwell's Divergent equations are inherent in FDTD scheme if initial and boundary values are properly applied [31]. Yee defines the grid coordinates (i, j, k) as

$$(i, j, k) = (i\Delta x, j\Delta y, k\Delta z) \dots\dots\dots (2.3)$$

where $\Delta x, \Delta y$ and Δz are the actual grid separations and i, j and k are the space indices in x, y and z directions. Following Yee's notation the grid points in the solution region are defined as

$$(i, j, k) = (i\Delta x, j\Delta y, k\Delta z) \dots\dots\dots (2.4)$$

and any function of space and time can be defined as

$$F^n(i, j, k) = F(i\Delta x, j\Delta y, k\Delta z, n\Delta t) \dots\dots\dots (2.5)$$

where Δt is the time increment, n is the time index and $\Delta x, \Delta y, \Delta z$ is the space increment along the three coordinate axes.

The spatial and temporal derivatives of F are written using central finite difference approximations as follows

$$\frac{\partial F^n(i, j, k)}{\partial x} = \frac{F^n(i+1/2, j, k) - F^n(i-1/2, j, k)}{\Delta x} \dots\dots\dots (2.6a)$$

$$\frac{\partial F^n(i, j, k)}{\partial t} = \frac{F^{n+1/2}(i, j, k) - F^{n-1/2}(i, j, k)}{\Delta t} \dots\dots\dots (2.6b)$$

The starting point of the FDTD algorithm is the differential form of Maxwell's curl equations for an isotropic medium [Eqn 2.5 (a-b)].

$$\nabla \times \vec{E} = -\mu \frac{\partial \vec{H}}{\partial t} \quad \dots\dots\dots (2.7a)$$

$$\nabla \times \vec{H} = \sigma \vec{E} + \varepsilon \frac{\partial \vec{E}}{\partial t} \quad \dots\dots\dots (2.7b)$$

These curl equations can be expanded in Cartesian coordinates [Eqn. 2.6 (a-f)].

$$\frac{\partial H_x}{\partial t} = \frac{1}{\mu} \left(\frac{\partial E_y}{\partial z} - \frac{\partial E_z}{\partial y} \right) \quad \dots\dots\dots (2.8a)$$

$$\frac{\partial H_y}{\partial t} = \frac{1}{\mu} \left(\frac{\partial E_z}{\partial x} - \frac{\partial E_x}{\partial z} \right) \quad \dots\dots\dots (2.8b)$$

$$\frac{\partial H_z}{\partial t} = \frac{1}{\mu} \left(\frac{\partial E_x}{\partial y} - \frac{\partial E_y}{\partial x} \right) \quad \dots\dots\dots (2.8c)$$

$$\frac{\partial E_x}{\partial t} = \frac{1}{\varepsilon} \left(\frac{\partial H_z}{\partial y} - \frac{\partial H_y}{\partial z} - \sigma E_x \right) \quad \dots\dots\dots (2.8d)$$

$$\frac{\partial E_y}{\partial t} = \frac{1}{\varepsilon} \left(\frac{\partial H_x}{\partial z} - \frac{\partial H_z}{\partial x} - \sigma E_y \right) \quad \dots\dots\dots (2.8d)$$

$$\frac{\partial E_z}{\partial t} = \frac{1}{\varepsilon} \left(\frac{\partial H_y}{\partial x} - \frac{\partial H_x}{\partial y} - \sigma E_z \right) \quad \dots\dots\dots (2.8e)$$

By applying central difference approximations (Equn.2.4.a-2.4.b) to the above scalar equations, six coupled central difference equations (Equn.2.6.a-2.6.f) are obtained as

$$\begin{aligned}
 H_x^{n+1/2}(i, j+1/2, k+1/2) &= H_x^{n-1/2}(i, j+1/2, k+1/2) \\
 &+ \left[\frac{\Delta t}{\mu \Delta z} \right] \left(E_y^n(i, j+1/2, k+1) - E_y^n(i, j+1/2, k) \right) \\
 &- \left[\frac{\Delta t}{\mu \Delta y} \right] \left(E_z^n(i, j+1, k+1/2) - E_z^n(i, j, k+1/2) \right) \dots\dots (2.9a)
 \end{aligned}$$

$$\begin{aligned}
 H_y^{n+1/2}(i+1/2, j, k+1/2) &= H_y^{n-1/2}(i+1/2, j, k+1/2) \\
 &+ \left[\frac{\Delta t}{\mu \Delta x} \right] \left(E_z^n(i+1, j, k+1/2) - E_z^n(i, j, k+1/2) \right) \\
 &- \left[\frac{\Delta t}{\mu \Delta z} \right] \left(E_x^n(i+1/2, j, k+1) - E_x^n(i+1/2, j, k) \right) \dots\dots (2.9b)
 \end{aligned}$$

$$\begin{aligned}
 H_z^{n+1/2}(i+1/2, j+1/2, k) &= H_z^{n-1/2}(i+1/2, j+1/2, k) \\
 &+ \left[\frac{\Delta t}{\mu \Delta y} \right] \left(E_x^n(i+1/2, j+1, k) - E_x^n(i+1/2, j, k) \right) \\
 &- \left[\frac{\Delta t}{\mu \Delta x} \right] \left(E_y^n(i+1, j+1/2, k) - E_y^n(i, j+1/2, k) \right) \dots\dots (2.9c)
 \end{aligned}$$

$$\begin{aligned}
 E_x^{n+1}(i+1/2, j, k) &= E_x^n(i+1/2, j, k) \\
 &+ \left[\frac{\Delta t}{\epsilon \Delta y} \right] \left(H_z^{n+1/2}(i+1/2, j+1/2, k) - H_z^{n+1/2}(i+1/2, j-1/2, k) \right) \\
 &- \left[\frac{\Delta t}{\epsilon \Delta z} \right] \left(H_y^{n+1/2}(i+1/2, j, k+1/2) - H_y^{n+1/2}(i+1/2, j, k-1/2) \right) \dots\dots (2.9d)
 \end{aligned}$$

$$\begin{aligned}
 E_y^{n+1}(i, j+1/2, k) &= E_y^n(i, j+1/2, k) \\
 &+ \left[\frac{\Delta t}{\epsilon \Delta z} \right] \left(H_x^{n+1/2}(i, j+1/2, k+1/2) - H_x^{n+1/2}(i, j+1/2, k-1/2) \right) \\
 &- \left[\frac{\Delta t}{\epsilon \Delta x} \right] \left(H_z^{n+1/2}(i+1/2, j+1/2, k) - H_z^{n+1/2}(i-1/2, j+1/2, k) \right) \dots\dots (2.9e)
 \end{aligned}$$

$$E_z^{n+1}(i, j, k+1/2) = E_z^n(i, j, k+1/2) + \left[\frac{\Delta t}{\epsilon \Delta x} \right] \left(H_y^{n+1/2}(i+1/2, j, k+1/2) - H_y^{n+1/2}(i-1/2, j, k+1/2) \right) - \left[\frac{\Delta t}{\epsilon \Delta y} \right] \left(H_x^{n+1/2}(i, j+1/2, k+1/2) - H_x^{n+1/2}(i, j-1/2, k+1/2) \right) \dots (2.9f)$$

To implement these equations, in Yee cell of dimension $\Delta x \Delta y \Delta z$, the there electric field components and corresponding magnetic field components are interleaved at half discretization length and half time steps. Central difference approximation for time derivative is obtained by alternatively calculating the E and H fields at every half time step (Δt). The discretization in space and time which granted the name leap frog algorithm to this method is shown in Fig 2.4

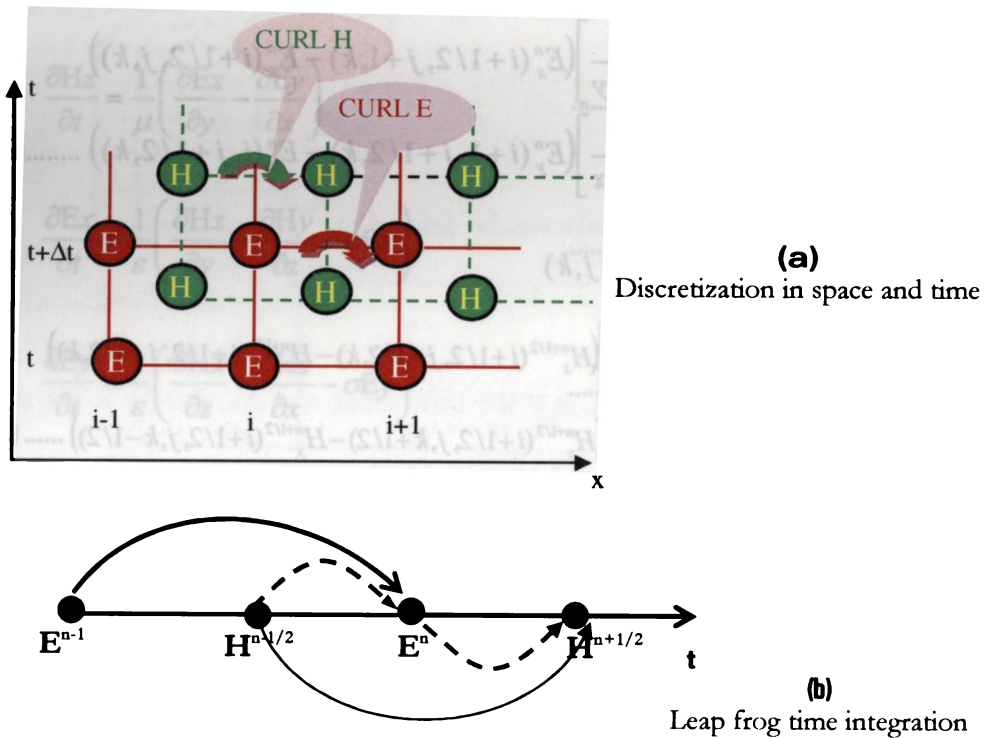


Fig 2.4 FDTD method proposed by Yee

Yee's algorithm is modified and simplified for easy programming by Sheen et al [32]. Hence for the computer implementation the explicit equations (Equ. 2.7.a-2.7.f) are modified as

$$H_{x,i,j,k}^{n+1/2} = H_{x,i,j,k}^{n-1/2} + \frac{\Delta t}{\mu\Delta z} (E_{y,i,j,k}^n - E_{y,i,j,k-1}^n) - \frac{\Delta t}{\mu\Delta y} (E_{z,i,j,k}^n - E_{z,i,j-1,k}^n) \quad \dots(2.10a)$$

$$H_{y,i,j,k}^{n+1/2} = H_{y,i,j,k}^{n-1/2} + \frac{\Delta t}{\mu\Delta x} (E_{z,i,j,k}^n - E_{z,i-1,j,k}^n) - \frac{\Delta t}{\mu\Delta z} (E_{x,i,j,k}^n - E_{x,i,j,k-1}^n) \quad \dots(2.10b)$$

$$H_{z,i,j,k}^{n+1/2} = H_{z,i,j,k}^{n-1/2} + \frac{\Delta t}{\mu\Delta y} (E_{x,i,j,k}^n - E_{x,i,j-1,k}^n) - \frac{\Delta t}{\mu\Delta x} (E_{y,i,j,k}^n - E_{y,i-1,j,k}^n) \quad \dots(2.10c)$$

$$E_{x,i,j,k}^{n+1} = E_{x,i,j,k}^n + \frac{\Delta t}{\epsilon\Delta y} (H_{z,i,j+1,k}^{n+1/2} - H_{z,i,j,k}^{n+1/2}) - \frac{\Delta t}{\epsilon\Delta z} (H_{y,i,j,k+1}^{n+1/2} - H_{y,i,j,k}^{n+1/2}) \quad \dots(2.10d)$$

$$E_{y,i,j,k}^{n+1} = E_{y,i,j,k}^n + \frac{\Delta t}{\epsilon\Delta z} (H_{x,i,j,k+1}^{n+1/2} - H_{x,i,j,k}^{n+1/2}) - \frac{\Delta t}{\epsilon\Delta x} (H_{z,i+1,j,k}^{n+1/2} - H_{z,i,j,k}^{n+1/2}) \quad \dots(2.10e)$$

$$E_{z,i,j,k}^{n+1} = E_{z,i,j,k}^n + \frac{\Delta t}{\epsilon\Delta x} (H_{y,i+1,j,k}^{n+1/2} - H_{y,i,j,k}^{n+1/2}) - \frac{\Delta t}{\epsilon\Delta y} (H_{x,i,j+1,k}^{n+1/2} - H_{x,i,j,k}^{n+1/2}) \quad \dots(2.10f)$$

using the above update equations present magnetic and electric fields are calculated from the immediate past corresponding fields and neighboring other fields. In each time step a set of electric and magnetic fields are used to generate a set of electric and magnetic field components at the next time step as shown in Fig.2.4(b).

2.3.3 Boundary conditions

Most of the Electromagnetic problems are unbounded or associated with open space regions. In the FDTD implementation of such problems requires exhaustive computational efforts and unlimited computational resources. Due to limited

computational resources, the simulation domain requires truncation, which may introduce spurious fields from the boundaries unless appropriate measures are taken. Size of the computational domain is selected based on the problem under analysis. The Boundary condition should ensure that the outgoing wave is completely absorbed at the boundary, making domain appear infinite in extent with minimum numerical back reflection. The first most widely used ABC was devised by Mur in 1981 [33]. This boundary condition is derived from a one-way wave equation. However, the attenuation of waves incident on the Mur ABC degrades as the incident angle (away from the normal) increases until at the grazing angle, the boundary becomes perfectly reflecting. Hence for most of the simulations using Mur's first order ABC at least 20 cells are required between the boundary and the radiating structure. As the number of cells between the radiator and boundary is increased the outward propagating wave from the radiator approaches to the normal incidence at the truncated boundary and are subsequently absorbed better than the waves at the near grazing angle. In 1994, Berenger [34] derived a new boundary condition referred to as a Perfectly Matched Layer (PML) which reduces reflections several orders of magnitude below other techniques. It uses a modified set of Maxwell's equations in which fields at the ABC-simulation space interface are split into two components and an artificial anisotropic material is introduced within the ABC. The result is a PML wave impedance perfectly matched to the simulation space and independent of incident angle. Incident waves are attenuated in the direction normal to the layers as they propagate through the artificial medium. Reflection coefficients as low as -80 dB have been demonstrated [35] for both 2-D and 3-D FDTD simulations.

Apart from ABC and PML, the implementation of the truncated ground plane printed monopole antennas involves simple boundary conditions such as Perfect Electric Conductor (PEC) and Dielectric interface boundary.

Perfect Electric Conductor (PEC) boundary

The PEC boundary is used to represent ideal conductors. This type of boundary condition deliberately reflects all incident wave energy back into the computational domain, thus limiting its size. The boundary conditions at a perfect electric conductor are such that the electric field components tangential to the surface must be zero, stated mathematically where \vec{n} is a surface normal vector,

$$\vec{n} \times \vec{E} = 0 \quad \dots\dots\dots(2.11)$$

in the Yee cell formulation the electric fields calculated at points on the surface of a PEC are always tangential to the surface. Thus by using the Yee cell in the FDTD scheme, the boundary condition at the surface of a PEC can be satisfied by simply setting $E_{\text{tan}} = 0$, they will remain *nearly* zero throughout the iterations. In materials finite conductivity, the update equation for the electric field component is

$$E^n = E^{n-1} \left[\frac{1 - \sigma\Delta t / 2\epsilon}{1 + \sigma\Delta t / 2\epsilon} \right] + \left[\frac{1}{1 + \sigma\Delta t / 2\epsilon} \right] \left[\frac{\Delta t}{\epsilon} \right] (\nabla \times H^{n-1/2}) \quad \dots\dots\dots(2.12)$$

when $\sigma \gg 1$ in the above equation, $E^n \cong E^{n-1}$. In the FDTD iteration procedure, once the boundary conditions on the tangential fields are satisfied, the boundary conditions on the normal fields will be automatically valid. PEC boundaries are used in the present investigation to model the finite ground plane and metallic strip of the printed strip monopole antenna.

Dielectric interface boundary

While modelling the monopole printed on a dielectric substrate at the interface between two media (Air and Dielectric) the discretization of Maxwell's equation become invalid. This is because in the difference equation only single value for material constants (ϵ and μ) are used, but in actual case there are two

separate values on either side of the interface (ϵ_1, μ_1 of air and ϵ_2, μ_2 of the dielectric). By applying the equivalent parameter approach introduced by Zhang and Mei [36] the condition at the interface is approximated as

$$\epsilon_{\text{eff}} = \frac{\epsilon_1 + \epsilon_2}{2} \dots\dots\dots (2.13)$$

a detailed description of the Boundary condition applied for the truncation of the computational domain is presented in the following section.

2.3.3.1 First order Mur's ABC

Mur's first order ABC is derived from differential equations. Differential based ABCs are generally obtained by factoring the wave equation and by allowing a solution that permits only outgoing waves. Mur's ABC was proposed after the theoretical work by Enquist and Majda [37]. It provides satisfactory absorption for a great variety of problems and is extremely simple to implement. Mur's first order ABC looks back one step in time and one cell into the space location. For the structure considered in the thesis, the pulses on the radiating monopoles will be normally incident to the outer boundary mesh walls and this leads to simple approximate boundary condition that the tangential electric field at the outer boundary obeys one dimensional wave equation in the direction normal to the mesh wall. For the x normal wall the one dimensional wave equation can be written as

$$\left(\frac{\partial}{\partial x} - \frac{1}{c} \frac{\partial}{\partial t} \right) E_{\text{tan}} = 0 \dots\dots\dots (2.14)$$

by imposing above equation on a wave normally incident on planar surface, absorbing condition for a normal incident wave with out reflection can be obtained as

$$\frac{\partial E(x,t)}{\partial x} = \frac{1}{c} \frac{\partial E(x,t)}{\partial t} \quad \text{Where } x=\Delta x/2, t = (n+1/2) \Delta t \dots\dots\dots(2.15)$$

for updating of the electric field at

$$x = \Delta x/2, t = (n + 1)\Delta t$$

in finite-difference form it can be written as follows:

$$\frac{E_1^{n+1/2} - E_0^{n+1/2}}{\Delta x} = \frac{1}{c} \frac{E_{1/2}^{n+1} - E_{1/2}^n}{\Delta t} \dots\dots\dots(2.16)$$

In this form, the finite-difference approximation is accurate to the second order in Δx and Δt . But the values at the half grid points and half time steps are not available, and can be averaged as

$$E_m^{n+1/2} = \frac{E_m^{n+1} + E_m^n}{2} \dots\dots\dots(2.17)$$

$$E_{m+1/2}^n = \frac{E_{m+1}^n + E_m^n}{2} \dots\dots\dots(2.18)$$

The equations 2.14, 2.15 and 2.16 yields a explicit finite difference equation

$$E_0^{n+1} = E_1^n + \left(\frac{c\Delta t - \Delta x}{c\Delta t + \Delta x} \right) (E_1^{n+1} - E_0^n) \dots\dots\dots(2.19)$$

Where E_0 represents the tangential electric field component on the mesh wall and E_1 represents the tangential electric field component on node inside of the mesh wall. Similar expressions are obtained for the other absorbing boundaries by using the corresponding normal directions for each wall. But while implementing the Mur's first order boundary conditions for truncated ground plane printed monopole it should be noted that boundary walls are far enough from the radiating monopole to ensure the normal incidence at the boundary walls. For the oblique incidence case the wave will reflected from the boundary walls.

2.3.3.2 Bergner's PML ABC

Berenger's perfectly matched layer (PML) type of has been the most widely accepted [38-39] and is set to revolutionize the FDTD method. In the perfectly matched layer (PML) truncation technique, an artificial layer of absorbing material is placed around the outer boundary of the computational domain. The goal is to ensure that a plane wave that is incident from FDTD free space to the PML region at an arbitrary angle is completely absorbed there without reflection. This is the same as saying that there is complete transmission of the incident plane wave at the interface between free space and the PML region. Thus the computational region and the PML region are said to be perfectly matched.

In the present investigation of printed monopole with truncated ground plane Mur's first order ABC requires a large computational domain to ensure normal incidence which increases the computational efforts and time. Hence FDTD method with PML concept is implemented by introducing Electric Flux Density (D) in discretized Maxwell's equations as proposed by Sullivan [40].

Initially the implementation of PML concept in FDTD is described and then discretized Maxwell's equations are derived. The iterative FDTD algorithm presented in this section does not use separate computer codes for PML section, but the generalized equation can be used for both normal media and PML by suitably enabling or disabling some medium dependent parameters in the equations.

Consider the following Maxwell's equations,

$$\frac{\partial D}{\partial t} = \frac{1}{\sqrt{\epsilon_0 \mu_0}} \nabla_x H \dots\dots\dots (2.20)$$

$$D(\omega) = \epsilon^*, (\omega) E(\omega) \dots\dots\dots (2.21)$$

Where $\epsilon^*, (\omega) = \epsilon_r + \frac{\sigma}{j\omega\epsilon_0}$ (2.22)

$$\frac{\partial H}{\partial t} = -\frac{1}{\sqrt{\epsilon_0\mu_0}} \nabla_x E$$

Consider a transverse magnetic wave (TM) propagating in a medium. The E and H field components are Ez, Hx and Hy. Now the above equations are reduced to

$$\frac{\partial D_z}{\partial t} = \frac{1}{\sqrt{\epsilon_0\mu_0}} \left(\frac{\partial H_y}{\partial x} - \frac{\partial H_x}{\partial y} \right) \dots\dots\dots (2.23a)$$

$$D(\omega) = \epsilon^*, (\omega)E(\omega) \dots\dots\dots(2.23b)$$

$$\frac{\partial H_x}{\partial t} = -\frac{1}{\sqrt{\epsilon_0\mu_0}} \frac{\partial E_z}{\partial y} \dots\dots\dots(2.23c)$$

$$\frac{\partial H_y}{\partial t} = \frac{1}{\sqrt{\epsilon_0\mu_0}} \frac{\partial E_z}{\partial x} \dots\dots\dots(2.23d)$$

If a wave is propagating in medium A and it impinges upon medium B, the amount of reflection is dictated by the intrinsic impedances of the two media

$$\Gamma = \frac{\eta_A - \eta_B}{\eta_A + \eta_B} \dots\dots\dots(2.24)$$

which are determined by the dielectric constant and permeability of the respective media

$$\eta = \sqrt{\frac{\mu}{\epsilon}} \dots\dots\dots(2.25)$$

Up to now, it is assumed that μ is a constant, so when a propagating pulse travels from ϵ_1 to ϵ_2 , it sees a change in impedance and reflects a portion of the pulse. However, if μ changed with ϵ so that η remains a constant, Γ would be zero and

no reflection will occur. This still doesn't solve the problem, because the pulse will continue propagating in the new medium. Hence the medium must be lossy so that the pulse will die out before it hits the boundary. This is accomplished by making both ϵ and μ of Eq. (2.25) complex because the imaginary part represents attenuation or loss.

by applying Fourier transform to the Eqn. 2.23.a-2.23.d

$$j\omega D_z = c_0 \left(\frac{\partial H_y}{\partial x} - \frac{\partial H_x}{\partial y} \right) \dots\dots\dots (2.26a)$$

$$D_z(\omega) = \epsilon^*_r(\omega) E_z(\omega) \dots\dots\dots (2.26b)$$

$$j\omega H_x = -c_0 \frac{\partial E_z}{\partial y} \dots\dots\dots (2.26c)$$

$$j\omega H_y = c_0 \frac{\partial E_z}{\partial x} \dots\dots\dots (2.26d)$$

It should be noted that ϵ and μ are eliminated from the spatial derivatives in the above equations for the normalized units. Instead of putting them back to implement the PML, we will add fictitious dielectric constants and permeabilities.

$$j\omega D_z \epsilon^*_{Fz}(x) \epsilon^*_{Fz}(y) = c_0 \left(\frac{\partial H_y}{\partial x} - \frac{\partial H_x}{\partial y} \right) \dots\dots\dots (2.27a)$$

$$D_z(\omega) = \epsilon^*_r(\omega) E_z(\omega) \dots\dots\dots (2.27b)$$

$$j\omega H_x \mu^*_{Fx}(x) \mu^*_{Fx}(y) = -c_0 \frac{\partial E_z}{\partial y} \dots\dots\dots (2.27c)$$

$$j\omega H_y \mu^*_{Fy}(x) \mu^*_{Fy}(y) = c_0 \frac{\partial E_z}{\partial x} \dots\dots\dots (2.27d)$$

It is worth noting that the fictitious values added in the equations have nothing to do with the real values of $\epsilon^*(\omega)$ which specify the medium.

Sacks et al. [41] showed that there are two conditions to form a PML:

1. The impedance going from the background medium to the PML must be constant

$$\eta_0 = \eta_m = \sqrt{\frac{\mu^*_{Fx}}{\epsilon^*_{Fx}}} = 1 \quad \dots\dots\dots(2.28)$$

In the direction perpendicular to the boundary the relative dielectric constant and relative permeability must be the inverse of those in the other directions

That is,

$$\epsilon^*_{Fx} = \frac{1}{\epsilon^*_{Fy}} \quad \dots\dots\dots(2.29)$$

$$\mu^*_{Fx} = \frac{1}{\mu^*_{Fy}} \quad \dots\dots\dots(2.30)$$

Each of these is a complex quantity of the form

$$\epsilon^*_{Fm} = \epsilon_{Fm} + \frac{\sigma D_m}{j\omega\epsilon_0} \text{ for } m=x \text{ or } y \quad \dots\dots\dots(2.31)$$

$$\mu^*_{Fm} = \mu_{Fm} + \frac{\sigma H_m}{j\omega\mu_0} \text{ for } m=x \text{ or } y \quad \dots\dots\dots(2.32)$$

The following selection of parameters satisfies Eq. 2.29 and 2.30

$$\epsilon_{Fm} = \mu_{Fm} = 1 \quad \dots\dots\dots(2.33)$$

$$\frac{\sigma D_m}{\epsilon_0} = \frac{\sigma H_m}{\mu_0} = \frac{\sigma D}{\epsilon_0} \quad \dots\dots\dots(2.34)$$

Substituting these values in (2.28)

$$\eta_0 = \eta_m = \sqrt{\frac{\mu_{Fx}^*}{\epsilon_{Fx}^*}} = \sqrt{\frac{1 + \sigma(x)/j\omega\epsilon_0}{1 + \sigma(x)/j\omega\epsilon_0}} = 1 \dots\dots\dots(2.35)$$

If σ increases gradually as it goes into the PML, (2.27.a -2.27.d) will cause Dz and Hy to be attenuated.

The PML is first implemented in the X direction. Therefore, the x dependent values of ϵ_F^* and μ_F^* will be retained.

$$j\omega D_z \epsilon_{Fz}^*(x) = c_0 \left(\frac{\partial H_y}{\partial x} - \frac{\partial H_x}{\partial y} \right) \dots\dots\dots(2.36)$$

$$j\omega H_x \mu_{Fx}^*(x) = -c_0 \frac{\partial E_z}{\partial y} \dots\dots\dots(2.37)$$

$$j\omega H_y \mu_{Fy}^*(x) = c_0 \frac{\partial E_z}{\partial x} \dots\dots\dots(2.38)$$

$$j\omega \left(1 + \frac{\sigma_D(x)}{j\omega\epsilon_0} \right) D_z = c_0 \left(\frac{\partial H_y}{\partial x} - \frac{\partial H_x}{\partial y} \right) \dots\dots\dots(2.39)$$

$$j\omega \left(1 + \frac{\sigma_D(x)}{j\omega\epsilon_0} \right)^{-1} H_x = -c_0 \frac{\partial E_z}{\partial y} \dots\dots\dots(2.40)$$

using the values of (2.33 and 2.34)

$$j\omega \left(1 + \frac{\sigma_D(x)}{j\omega\epsilon_0} \right) H_y = c_0 \frac{\partial E_z}{\partial x} \dots\dots\dots(2.41)$$

In the above equations the permeability of Hx is the inverse of that of Hy. Therefore the second requirement for the PML is fulfilled. Now the above equations have to be put into the FDTD formulation. Consider the left side of (2.36)

$$j\omega\left(1 + \frac{\sigma_D(x)}{j\omega\epsilon_0}\right)D_z = j\omega D_z + \frac{\sigma_D(x)}{\epsilon_0} D_z$$

Moving to the time domain, and then taking the finite difference approximations,

$$\begin{aligned} \frac{\partial D_z}{dt} + \frac{\sigma_D(i)}{\epsilon_0} D_z &\cong \frac{D_z^{n+1/2}(i,j) - D_z^{n-1/2}(i,j)}{\Delta t} + \frac{\sigma_D(i)}{\epsilon_0} \frac{D_z^{n+1/2}(i,j) + D_z^{n-1/2}(i,j)}{2} \\ &= D_z^{n+1/2}(i,j) \frac{1}{\Delta t} \left[1 + \frac{\sigma_D(i)\Delta t}{2\epsilon_0}\right] - D_z^{n-1/2}(i,j) \frac{1}{\Delta t} \left[1 - \frac{\sigma_D(i)\Delta t}{2\epsilon_0}\right] \end{aligned}$$

if this is substituted into Eq. (2.32) along with the spatial derivatives,

$$\begin{aligned} D_z^{n+1/2}(i,j) &= gi3(i)D_z^{n-1/2}(i,j) + \\ &gi2(i)0.5\left[H_y^n(i+1/2,j) - H_y^n(i-1/2,j) - H_x^n(i,j+1/2) - H_y^n(i,j-1/2)\right] \dots (2.42) \end{aligned}$$

the parameters gi2(i) and gi3(i) are given by

$$gi2(i) = \frac{1}{1 + \sigma_D(i)\Delta t / 2\epsilon_0} \dots (2.43)$$

$$gi3(i) = \frac{1 - \sigma_D(i)\Delta t / 2\epsilon_0}{1 + \sigma_D(i)\Delta t / 2\epsilon_0} \dots (2.44)$$

Similarly Hy can be formulated as,

$$H_y^{n+1}(i+1/2,j) = fi3(i+1/2)H_y^n(i+1/2,j) + fi2(i+1/2)0.5\left[E_z^{n+1/2}(i+1,j) - E_z^{n+1/2}(i,j)\right] \dots (2.45)$$

where

$$fi2(i+1/2) = \frac{1}{1 + \sigma_D(i+1/2)\Delta t / (2\epsilon_0)} \dots\dots\dots(2.46)$$

$$fi3(i+1/2) = \frac{1 - \sigma_D(i+1/2)\Delta t / (2\epsilon_0)}{1 + \sigma_D(i+1/2)\Delta t / (2\epsilon_0)} \dots\dots\dots(2.47)$$

These parameters are calculated at $i+1/2$ positions due to the $\frac{1}{2}$ cell position of the H component. (2.32) can be written as,

$$j\omega H_x = -c_0 \left[\frac{\partial E_z}{\partial y} + \frac{\sigma_D(x)}{\epsilon_0} \frac{1}{j\omega} \frac{\partial E_z}{\partial y} \right] \dots\dots\dots(2.48)$$

The spatial derivative will be written as,

$$\frac{\partial E_z}{\partial y} \cong \frac{E_z^{n+1/2}(i, j+1) - E_z^{n+1/2}(i, j)}{\Delta x} = -\frac{curl_e}{\Delta x} \dots\dots\dots(2.49)$$

implementing this into FDTD gives

$$\frac{H_x^{n+1}(i, j+1/2) - H_x^n(i, j+1/2)}{\Delta t} = -c_0 \left[\frac{-curl_e}{\Delta x} - \frac{\sigma_D(x)}{\epsilon_0} \Delta t \sum_{n=0}^T \frac{curl_e}{\Delta x} \right] \dots\dots\dots(2.50)$$

The extra Δt in front of the summation is the part of the approximation of the time domain integral.

$$\begin{aligned} H_x^{n+1}(i, j+1/2) &= H_x^n(i, j+1/2) + \frac{c_0 \Delta t}{\Delta x} curl_e + \frac{\Delta t c_0}{\Delta x} \frac{\sigma_D(x) \Delta t}{\epsilon_0} I_{Hx}^{n+1/2}(i, j+1/2) \\ &= H_x^n(i, j+1/2) + \frac{c_0 \Delta t}{\Delta x} curl_e + \frac{\sigma_D(x) \Delta t}{2\epsilon_0} I_{Hx}^{n+1/2}(i, j+1/2) \dots\dots\dots(2.51) \end{aligned}$$

(2.32) is implemented as the following series of equations:

$$\text{curl}_z e = [E_z^{n+1/2}(i, j) - E_z^{n+1/2}(i, j + 1)] \dots\dots\dots(2.52)$$

$$I_{Hx}^{n+1/2}(i, j + 1/2) = I_{Hx}^{n-1/2}(i, j + 1/2) + \text{curl}_z e \dots\dots\dots(2.53)$$

$$H_x^{n+1}(i, j + 1/2) = H_x^n(i, j + 1/2) + 0.5\text{curl}_z e + f1(i)I_{Hx}^{n+1/2}(i, j + 1/2) \dots\dots\dots(2.54)$$

With

$$f1(i) = \frac{\sigma(i)\Delta t}{2\epsilon_0} \dots\dots\dots(2.55)$$

In calculating the f and g parameters, it is not necessary to actually vary conductivities. Instead, we calculate an auxiliary parameter,

$$x_n = \frac{\sigma\Delta t}{2\epsilon_0} \dots\dots\dots(2.56)$$

that increases as it goes into the PML. The f and g parameters are then calculated:

$$x_n(i) = 0.333 \left(\frac{i}{\text{length_pml}} \right)^3 \quad i=1,2, \dots\dots, \text{length_pml} \dots\dots\dots(2.57)$$

$$f1(i) = x_n(i) \dots\dots\dots(2.58)$$

$$gi2(i) = \left(\frac{1}{1 + x_n(i)} \right) \dots\dots\dots(2.59)$$

$$gi3(i) = \left(\frac{1 - x_n(i)}{1 + x_n(i)} \right) \dots\dots\dots(2.60)$$

The factor 0.333 is found empirically to be the largest number that remained stable. The cubic factor is also found empirically to be the most effective variation.

The parameters vary in the following manner:

fi1(i) from 0 to 0.333

gi2(i) from 1 to 0.75

gi3(i) from 1 to 0.5

Throughout the main problem space, fi1 is zero, while gi2 and gi3 are 1. Therefore, there is a transition from the main part of the program to the PML. The above equations refer to the implementation of PML in x direction. Now the PML is to be implemented in y direction. Therefore instead of (2.36) one can write

$$j\omega \left(1 + \frac{\sigma_D(x)}{j\omega\epsilon_0}\right) \left(1 + \frac{\sigma_D(y)}{j\omega\epsilon_0}\right) D_z = c_0 \left(\frac{\partial H_y}{\partial x} - \frac{\partial H_x}{\partial y}\right) \dots\dots\dots (2.61a)$$

$$j\omega \left(1 + \frac{\sigma_D(x)}{j\omega\epsilon_0}\right)^{-1} \left(1 + \frac{\sigma_D(y)}{j\omega\epsilon_0}\right) H_x = c_0 \left(-\frac{\partial E_z}{\partial y}\right) \dots\dots\dots (2.61b)$$

$$j\omega \left(1 + \frac{\sigma_D(x)}{j\omega\epsilon_0}\right) \left(1 + \frac{\sigma_D(y)}{j\omega\epsilon_0}\right)^{-1} H_y = c_0 \frac{\partial E_z}{\partial x} \dots\dots\dots (2.61c)$$

Employing the same procedure in the previous section D, and H values becomes

$$D_z^{n+1/2}(i,j) = g\beta(i)g\beta(j)D_z^{n-1/2}(i) + g\beta(i)g\beta(j)0.5 \begin{bmatrix} H_y^n(i+1/2,j) - H_y^n(i-1/2,j) \\ -H_x^n(i,j+1/2) + H_x^n(i,j-1/2) \end{bmatrix}$$

In Y direction, Hy will require an implementation similar to the one used for Hx in the x direction.

$$curl_e = \left[E_z^{n+1/2}(i+1,j) - E_z^{n+1/2}(i,j) \right] \dots\dots\dots (2.62a)$$

$$I_{Hy}^{n+1/2}(i+1/2,j) = I_{Hy}^{n-1/2}(i+1/2,j) + curl_e \dots\dots\dots (2.62b)$$

$$H_y^{n+1}(i+1/2,j) = fi3(i+1/2)H_y^n(i+1/2,j) - fi2(i+1/2)0.5curl_e + \dots\dots\dots (2.63a)$$

$$fi1(j)I_{Hy}^{n+1/2}(i+1/2,j)$$

Finally, H_x in the x direction becomes

$$\text{curl}_e = \left[E_z^{n+1/2}(i, j) - E_z^{n+1/2}(i, j+1) \right]$$

$$I_{H_x}^{n+1/2}(i, j+1/2) = I_{H_x}^{n-1/2}(i, j+1/2) + \text{curl}_e$$

$$H_x^{n+1}(i, j+1/2) = f_3(j+1/2)H_x^n(i, j+1/2) + f_2(j+1/2)0.5\text{curl}_e + f_1(i)I_{H_x}^{n+1/2}(i, j+1/2)$$

The full set of parameters associated with the PML are,

- | | |
|---------------------------------------|-----------------|
| $f_1(i) \& f_1(j)$ | from 0 to 0.333 |
| $f_2(i), g_2(i), f_2(j)$ and $g_2(j)$ | from 1 to 0.75 |
| $f_3(i), g_3(i), f_3(j)$ and $g_3(j)$ | from 1 to 0.5 |

The PML can be turn off in the main part of the problem space by setting f_1 and f_1 to 0, and other parameters to 1.

The free space equations for D and H in three dimensions are,

$$\frac{\partial D_x}{\partial t} = \frac{1}{\sqrt{\epsilon_0 \mu_0}} \left(\frac{\partial H_z}{\partial y} - \frac{\partial H_y}{\partial z} \right) \dots\dots\dots(2.64a)$$

$$\frac{\partial D_y}{\partial t} = \frac{1}{\sqrt{\epsilon_0 \mu_0}} \left(\frac{\partial H_x}{\partial z} - \frac{\partial H_z}{\partial x} \right) \dots\dots\dots(2.64b)$$

$$\frac{\partial D_z}{\partial t} = \frac{1}{\sqrt{\epsilon_0 \mu_0}} \left(\frac{\partial H_y}{\partial x} - \frac{\partial H_x}{\partial y} \right) \dots\dots\dots(2.64c)$$

$$\frac{\partial H_x}{\partial t} = \frac{1}{\sqrt{\epsilon_0 \mu_0}} \left(\frac{\partial E_y}{\partial z} - \frac{\partial E_z}{\partial y} \right) \dots\dots\dots(2.64d)$$

$$\frac{\partial H_y}{\partial t} = \frac{1}{\sqrt{\epsilon_0 \mu_0}} \left(\frac{\partial E_z}{\partial x} - \frac{\partial E_x}{\partial z} \right) \dots\dots\dots(2.64e)$$

$$\frac{\partial H_z}{\partial t} = \frac{1}{\sqrt{\epsilon_0 \mu_0}} \left(\frac{\partial E_x}{\partial y} - \frac{\partial E_y}{\partial x} \right) \dots\dots\dots(2.64f)$$

The development of the PML for three dimensions closely follows the two dimensional version. The only difference is that we have to deal with three directions instead of two.

For instance (2.61.a) becomes

$$j\omega \left(1 + \frac{\sigma_x(x)}{j\omega\epsilon} \right) \left(1 + \frac{\sigma_y(y)}{j\omega\epsilon_0} \right) \left(1 + \frac{\sigma_z(z)}{j\omega\epsilon_0} \right)^{-1} D_z = c_0 \left(\frac{\partial H_y}{\partial x} - \frac{\partial H_x}{\partial y} \right) \dots\dots\dots(2.65)$$

$$\begin{aligned} j\omega \left(1 + \frac{\sigma_x(x)}{j\omega\epsilon} \right) \left(1 + \frac{\sigma_y(y)}{j\omega\epsilon_0} \right) D_z &= c_0 \left(1 + \frac{\sigma_z(z)}{j\omega\epsilon_0} \right) \left(\frac{\partial H_y}{\partial x} - \frac{\partial H_x}{\partial y} \right) 0 \\ &= c_0 \text{curl}_- h + c_0 \frac{\sigma_z(z)}{\epsilon_0} \frac{1}{j\omega} \text{curl}_- h \dots\dots\dots(2.66) \end{aligned}$$

$$\text{Let } I_{Dz} = \frac{1}{j\omega} \text{curl}_- h \dots\dots\dots(2.67)$$

Which is an integration when it goes to the time domain. Thus above Eq. becomes

$$j\omega \left(1 + \frac{\sigma_x(x)}{j\omega\epsilon} \right) \left(1 + \frac{\sigma_y(y)}{j\omega\epsilon_0} \right) D_z = c_0 \left(\text{curl}_- h + \frac{\sigma_z(z)}{\epsilon_0} I_{Dz} \right) \dots\dots\dots(2.68)$$

The implementation of this into FDTD parallels that of the two dimensional PML, except the right side contains the integration term I_{Dz} . Following previous procedure the equation can be written as

$$curl_h = \begin{bmatrix} H_y^n(i+1/2, j, k+1/2) - H_y^n(i-1/2, j, k+1/2) \\ H_x^n(i, j+1/2, k+1/2) + H_x^n(i, j-1/2, k+1/2) \end{bmatrix} \dots\dots\dots (2.69a)$$

$$I^n_{Dz}(i, j, k+1/2) = I^{n-1}_{Dz}(i, j, k+1/2) + curl_h \dots\dots\dots (2.69b)$$

$$D^{n+1/2}_z(i, j, k+1/2) = gi3(i)gj3(j)D^{n-1/2}_z(i, j, k+1/2) + gi2(i)gj2(j)0.5(curl_h + gk1(k)I^n_{Dz}(i, j, k+1/2)) \dots\dots\dots (2.69c)$$

The I_{Dz} is a three dimensional array that is dimensioned throughout the problem space, but used only at two edges. The three dimensional implementation will have a total of six such arrays, which increases the computational burden. For this reason, I_{Dz} will be broken up into small three-dimensional arrays, defined at the low values of k and one defined at the high values of k. Similarly equations for D_x, D_y, H_x, H_y, H_z can be derived. In the iterative FDTD algorithm, values of D are computed first and then E is computed as,

$$E_x = g_{ax} D_x$$

$$E_y = g_{ay} D_y$$

$$E_z = g_{az} D_z$$

$$\text{Where } g_{ax} = g_{ay} = g_{az} = 1 / (\epsilon_r + (\sigma * dt / \epsilon_0))$$

This is a medium dependent parameter. In the case of PECs (Perfect Electric Conductor), one can easily define it by making g_{ax}, g_{ay} and g_{az} as zero so that the respective field components of E becomes zero, thus the boundary conditions for PEC are automatically assigned in the computation. The components of H are computed from the computed E values.

For the analysis of printed monopole antenna presented in the thesis the above mentioned PML based FDTD technique is implemented using MATLABTM. This MATLAB based code can be used for extracting antenna characteristics

such as return loss, radiation pattern, gain and efficiency. Detailed descriptions of the classical methods used for extracting antenna characteristics are presented in the Section 2.4 of this chapter.

2.3.4 Numerical dispersion and stability criteria

The numerical algorithm for Maxwell’s curl equation defined by finite difference equation requires that time increment Δt have a specific bound relative to the lattice dimensions Δx Δy and Δz . This bound is necessary to avoid numerical instability, an undesirable possibility of computed results to spuriously increase without the limit as time marching progresses. To ensure the computational stability it is necessary to satisfy a relation between the space increment and time increment. To ensure the stability of the time-stepping algorithm, Δt is chosen to satisfy the Courant-Friedrichs-Lewy (CFL) Stability criterion:

$$\Delta t \leq \frac{1}{V_{\max}} \frac{1}{\sqrt{1/\Delta x^2 + 1/\Delta y^2 + 1/\Delta z^2}} \dots\dots\dots(2.70)$$

V_{\max} is the maximum velocity of light in the computational volume. Typically V_{\max} will be the velocity of light in free space unless the entire volume is filled with dielectric. These equations will allow the approximate solution of E and H in the volume of the computational domain or mesh. In the present investigation the maximum time step is limited as 99.5% of the value given by the above equation.

The discretization of Maxwell’s equations in space and time causes the variation of the phase constant of the propagating wave with frequency. For a fixed cell size different frequency components of a wave propagate at slightly different velocities. This phenomenon is referred to as numerical dispersion and is inherently present in the FDTD algorithm. Furthermore, velocity depends also on the angle of propagation with respect to the coordinate axis. This is called numerical anisotropy. For accurate and stable results, the grid dispersion error

must be reduced to an acceptable level, which can be readily accomplished by reducing the cell size. Accuracy of computation can be ensured by selecting the grid size as 10 cells per wavelength ($\lambda/10$) or less at the highest frequency. In the analysis presented in the thesis the accuracy and stability are ensured by selecting

$$\Delta x, \Delta y, \Delta z \leq \lambda_{\min} / 20.$$

2.3.5 Luebbers feed model for fast FDTD convergence

With the transient excitation in FDTD, impedance and scattering parameters over a wide frequency band can be calculated. One difficulty with FDTD is that for some applications, few thousands of time steps may be required for the transient fields to decay. This difficulty is common in the case of circuits having very high quality factor. One method to reduce the time steps required is to apply signal processing methods to predict the voltages and currents at later times from the results computed for early times. Instead of making FDTD calculations for the full number of time steps required for transients to dissipate, one might make actual FDTD calculations for some fraction of this total number of time steps, and use these results to predict those for the later times [43].

Applying the various prediction methods adds additional complexity to the FDTD calculation process. The prediction methods are complicated, and may require care and skill by the use to obtain accurate results. Most of the methods described require the use to determine the order of the prediction process, related to the number of terms of whatever expansion function is used to approximate the FDTD time signal. A poor choice for the order of the prediction model can result in larger precision errors.

Another simple approach is to include a source with internal resistance to excite the problem. By employing source with internal resistance which matches with the characteristic impedance of the transmission line provided accurate results while greatly reduces the number of time steps required for convergence.

2.3.5.1 Resistive source model

FDTD transient calculations are often excited by a hard voltage source, whose internal source resistance is zero ohms. These sources are very easy to implement in an FDTD code. The electric field at the mesh edge where the source is located is determined by some function of time rather than by the FDTD update equations. A common choice is a Gaussian pulse, but other functions may also be used. The Gaussian pulse is significantly greater than zero amplitude for only a very short fraction of the total computation time, especially for resonant geometries such as many antennas and micro strip circuits.

Once the pulse amplitude drops the source voltage becomes essentially zero, the source effectively becoming a short circuit. Thus, any reflections from the antenna or circuit which return to the source are totally reflected. The only way the energy introduced into the calculation space can be dissipated is through radiation or by absorption by lossy media or lumped loads. For resonant structures, there are frequencies for which this radiation or absorption process requires a relatively long time to dissipate the excitation energy. Using a source with an internal resistance to excite the FDTD calculation provides an additional loss mechanism for the calculations.

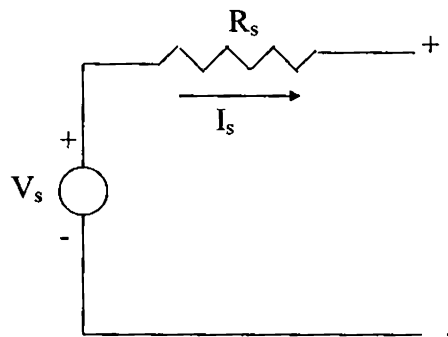


Fig 2.5 FDTD source with source resistance

Consider that it is desired to excite an FDTD calculation with a voltage source that corresponds to an electric field E in the z direction at a certain mesh location $i_s \Delta x, j_s \Delta y, k_s \Delta z$, described using the usual Yee notation. The corresponding equivalent circuit for a voltage source which includes an internal source resistance R_s is illustrated in Fig. 2.5. If the source resistance R_s is set to zero then the usual FDTD electric field at the source location is simply given by

$$E_s^n(i_s, j_s, k_s) = \frac{V_s(n\Delta t)}{\Delta z} \dots\dots\dots(2.71)$$

V_s is any function of time, often a Gaussian pulse.

However, with the source resistance included, the calculation of the source field $E_s^n(i_s, j_s, k_s)$ at each time step is complicated slightly. To determine the terminal voltage V of Fig. 2.4 and, thus, the FDTD electric source field $E_s^n(i_s, j_s, k_s)$, the current through the source must be determined. This can be done by Ampere's circuital law, taking the line integral of the magnetic field around the electric field source location. The current through the source is then given by

$$I_s^{n-1/2} = (H_x^{n-1/2}(i_s, j_{s-1}, k_s) - H_x^{n-1/2}(i_s, j_s, k_s)) \Delta x + (H_y^{n-1/2}(i_s, j_s, k_s) - H_y^{n-1/2}(i_{s-1}, j_s, k_s)) \Delta y \dots\dots\dots(2.72)$$

so that by applying Ohm's law to the circuit of Fig. 2.4 the electric source field is given by

$$E_s^n(i_s, j_s, k_s) = \frac{V_s(n\Delta t)}{\Delta z} + \frac{I_s^{n-1/2} R_s}{\Delta z} \dots\dots\dots(2.73)$$

if $R_s=0$, in this equation, then the usual hard-voltage source results. The value of the internal resistance does not appear to be critical. A reasonable choice for R_s is

to use the value of the characteristic impedance of the transmission line. In the thesis R_s is selected as 50Ω .

2.3.5.2 Staircase transition for microstrip line feed

The microstrip excitation presented in the thesis is implemented by using Luebber's [43] approach of stair cased FDTD mesh transition from electric field sources location to the full width of the microstrip transmission line. Compared to the "hard" voltage source excitation this approach provides accurate results with reduced computational time. For implementing the stair cased transition in microstrip line the substrate is discretized in order to incorporate more than one Yee cell. A gap feed model can be obtained by applying the excitation field between the microstrip line and the ground plane using a stair cased mesh transition as shown in Fig2.6

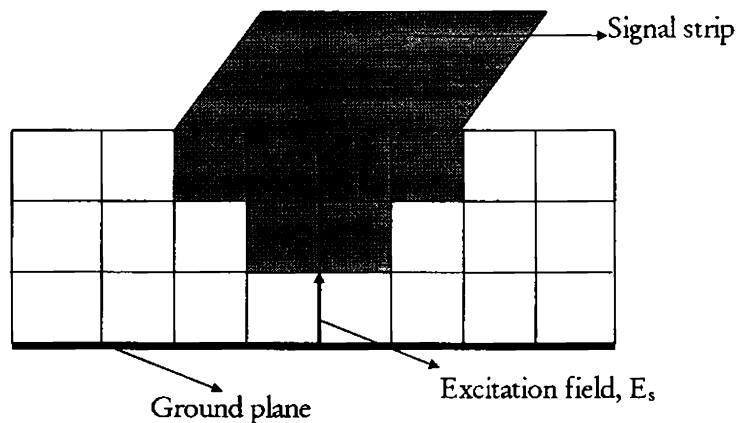


Fig 2.6 Stair cased feed model for microstrip line in FDTD

2.3.6 Excitation source modeling.

Proper excitation of the computational domain excites a field distribution closely resembling that of the physical structure. On the other hand, improper excitation leads to spurious solutions. For the antenna analysis in time-domain a narrow pulse is usually used as the excitation pulse to extract the frequency-domain parameters in the entire frequency range of interest by Fourier transform

of the transient results. The frequency band of interest decides the width of the pulse. A narrow pulse ensures wide band performance. To avoid the unnecessary noise appearing in the FDTD generated response, the excitation pulse and its spectrum must have a smooth roll off and low side lobes.

A sine wave or a Gaussian pulse can be used as the input signal for the 3D FDTD method. However, a Gaussian pulse plane wave is the most widely specified incident field as it provides a smooth roll off in frequency content and is simple to implement. In addition, the frequency spectrum of a Gaussian pulse is also Gaussian and will therefore provide frequency domain information from dc to the desired cut off frequency by adjusting the pulse width. The Gaussian input is of the form

$$g(t) = e^{-\left(\frac{(t-t_0)^2}{T^2}\right)} \dots\dots\dots(2.74)$$

where t_0 is the pulse delay and T relates to the Gaussian half width, which sets the required cut off frequency. Writing in the discrete form,

$$g(n\Delta t) = e^{-\left(\frac{(n\Delta t-t_0)^2}{T^2}\right)} \dots\dots\dots(2.75)$$

where $T = N \Delta t$ and $t_0 = 3T$. Thus the pulse is sampled N times in a pulse half width T. The Gaussian pulse and its spectrum are shown in Figure 2.7. It is evident from the figure that the pulse provides relatively high signal levels up to the desired frequency. The parameter N can be changed to achieve sharper frequency roll off. In the FDTD method, all functions are assumed to be causal. Therefore, to satisfy the initial condition of zero excitation at the zeroth time step, the time of origin of the Gaussian pulse must be shifted by t_0 ($t_0 \gg 1$). To ensure proper initial value conditions a time delayed Gaussian pulse $t_0 = 3^*T$ is employed in the thesis.

In order to simulate a voltage source excitation in a Microstrip fed structure, a vertical electric field E_s can be imposed in between the ground plane and the microstrip line as shown in Fig 2.5. This electric field is defined using the Eqn.2.58 with the voltage source as Gaussian pulse.

$$V_s = e^{-\left(\frac{(t-t_0)^2}{T^2}\right)} \dots\dots\dots(2.76)$$

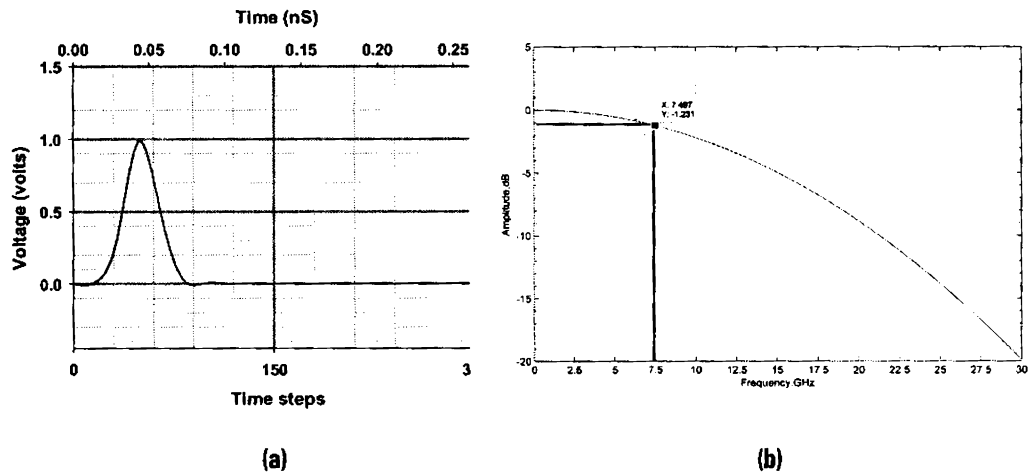


Fig. 2.7 (a) Gaussian pulse (b) Gaussian spectrum

Gaussian pulse is usually used for the extracting the antenna characteristics such as return loss, impedance bandwidth, input impedance etc. Sinusoidal excitation is usually used to extract the radiation characteristics at a particular frequency of interest. A sinusoidal function of the following form is usually used for extracting the near field data at a particular frequency.

$$E(t) = E_0 \sin(2\pi ft)$$

Where E_0 determines the peak amplitude and ' $t=n*\Delta t$ ' is the current instant of time.

2.3.7 Flowchart of Yee algorithm

MATLAB based numerical code is developed for the parametric analysis of the antenna. The Flow chart used for extracting the antenna reflection characteristics are depicted in Fig.2.8

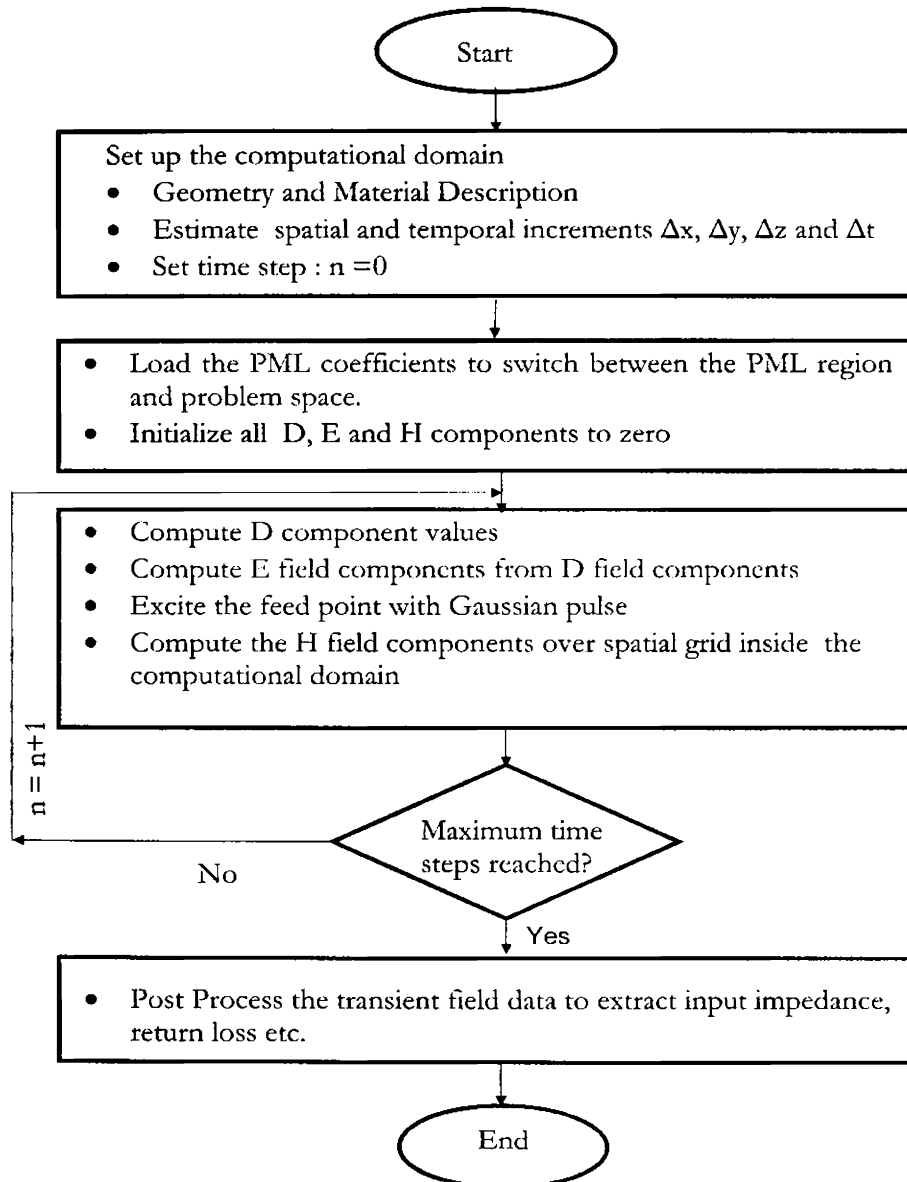


Fig.2.8. The FDTD flow chart

2.4 Antenna characteristics using FDTD

FDTD algorithm performs the transient analysis of the antenna under investigation. Fourier transform of the transient data gives the frequency domain information over the frequency range of interest. Current and voltage samples are taken from the fixed points in the FDTD grid and Fast Fourier Transform (FFT) is used to compute the frequency domain information. Since for our analysis FFT can provide results with good accuracy FFT is used instead of DFT. By suitably post processing this information the reflection characteristics can be extracted as outlined in the section below.

2.4.1 Reflection characteristics

2.4.1.1 Return loss, Resonant frequency and 2:1 VSWR Band width

The voltage at the input port location is computed from the E_z field components at the feed point over the entire simulation time interval. The current at the feed point is calculated from the H field values around the feed point using Ampere's circuital law. The input impedance of the antenna is computed from the Eqn 2.61

$$Z_{in}(\omega) = \frac{FFT(V^n, P)}{FFT(I^{n-1}, P)} \dots\dots\dots(2.77)$$

Where P is the suitable Zero padding used for taking FFT, $V^n = E_z * \Delta z$ and I^{n-1} is given by equation 2.57.

Since microstrip line is modeled using Leubber's staircase approach as explained in section 2.3.5.1., the internal impedance of source resistance R_s is taken as the characteristic impedance (Z_0) of microstrip line.

Reflection coefficient is given as $\Gamma(\omega) = \frac{Z_{in} - Z_0}{Z_{in} + Z_0} \dots\dots\dots(2.78)$

Return loss in dB, $S_{11} = 20 \log_{10} |\Gamma(\omega)| \dots\dots\dots(2.79)$

The return loss computed in the above process is processed for extracting the fundamental resonant frequency and 2:1 VSWR bandwidth corresponding to the -10dB return loss.

2.4.2 Radiation characteristics

Theoretical analysis procedure for predicting the radiation characteristics of the antenna usually employs formulating the theoretical model of the antenna and applying different numerical approximations. But the main problem with these approximations is that discrepancies may occur due to the inaccurate modeling and approximations. Moreover, most of the modeling techniques use modeling the current on the conducting surface to predict the radiation characteristics. Even though the computational time is less, wide band performance can not be achieved using these techniques, while using FDTD transient calculations can be done more efficiently for most of the antenna geometries than by applying frequency domain methods. FDTD is capable of computing transient far zone radiations of the antennas excited by non sinusoidal sources using transient near to far field transformation [28]. Hence from one FDTD computation wide band gain and radiation characteristics can be extracted. But using these transient near to far field transformation computational effort is more if number of frequencies involved is high. In applications requiring transient results in wideband frequency domain the fully transient approach involving Fast Fourier Transform is more desirable than applying a Discrete Fourier Transform in every time step. This method utilizes computing the transient far field Electric and Magnetic vector potentials on closed surface in the computational domain by running summation at each time step [44]. Procedure employed in this thesis for computing the radiation characteristics of the antenna is presented in the following section.

2.4.2.1 Principal plane radiation patterns.

To extract the radiation pattern at the resonant frequency a sinusoidal source is used as the excitation source. Initially using the Gaussian pulse the resonant frequency of the antenna is extracted and thus obtained resonant frequency f_r is used for FDTD run for pattern computation. The source voltage for pattern computation is given by

$$V(n\Delta t) = \sin(2\pi f_r n\Delta t)$$

A near field transformation surface layer is selected just above the printed monopole layer as the transformation layer for field computations. The surface S is chosen to be in the near field of radiating monopole with proper dimensions to ensure that tangential E field components are negligible outside this boundary. Usually a rectangular surface as shown in Fig.2.9 is chosen for the easy implementation of near to far field transformation algorithm.

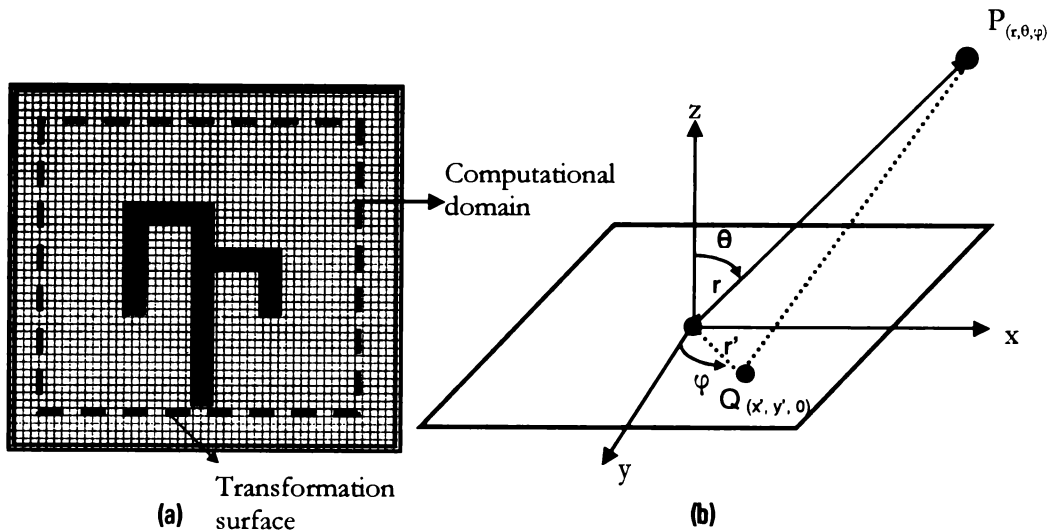


Fig 2.9. Radiation pattern computation using FDTD.

- (a) Near field transformation surface
- (b) Spatial point Q in near field and far field point P.

The tangential near field Electric and Magnetic Field vectors on this surface are sampled and converted to equivalent surface currents.

$$\bar{J}_s = \bar{a}_n \times \bar{H}_A \dots\dots\dots(2.80)$$

$$\bar{M}_s = \bar{E}_A \times \bar{a}_n \dots\dots\dots(2.81)$$

Where \bar{a}_n is the unit outward normal from the transformation surface ($\bar{a}_n = \bar{z}$). The far field at any point outside this transformation surface is computed from the electric and magnetic vector potential derived from the surface current equivalence principle. The far field E field vectors tangential to the direction of propagation is given by

$$E_\theta = -\mu \frac{\partial A_\theta}{\partial t} - \frac{1}{c} \frac{\partial F_\phi}{\partial t} \dots\dots\dots(2.82)$$

$$E_\phi = -\mu \frac{\partial A_\phi}{\partial t} + \frac{1}{c} \frac{\partial F_\theta}{\partial t} \dots\dots\dots(2.83)$$

where A and F represents magnetic and electric vector potentials and θ and ϕ denotes the coordinates in the spherical coordinate system. Suppressing the $e^{j\omega t}$ variation [44] the electric field in the free space can be written as

$$E(r, \theta, \phi) = j\omega \cdot \eta_0 \cdot (F_\theta \cdot \bar{a}_\phi - F_\phi \cdot \bar{a}_\theta) \dots\dots\dots(2.84)$$

E_θ and E_ϕ are derived by transforming into spherical coordinate system as

$$E_\theta = j\omega \cdot \eta_0 \cdot (F_x \cdot \text{Sin}(\phi) - F_y \cdot \text{Cos}(\phi)) \dots\dots\dots(2.85)$$

$$E_\phi = j\omega \cdot \eta_0 \cdot \text{Cos}(\theta) (F_x \cdot \text{Cos}(\phi) + F_y \cdot \text{Sin}(\phi)) \dots\dots\dots(2.86)$$

Following assumptions are made for the near to far field transformation

- The antenna radiates into the $z > 0$ and $z < 0$ region from the aperture in the $z = 0$ plane
- r is in the far field i.e ($r \gg (x'^2 + y'^2)^{1/2}$) & $k_0 r \gg 1$
- Transformation surface dimensions are proper so that tangential electric fields are negligible outside the transformation aperture boundary.

Eqn 2.84 now becomes

$$E = j \cdot \exp(-jkr) / (\lambda \cdot r) \bullet \begin{pmatrix} \cos(\theta) \cdot (f_x \cos(\phi) + f_y \sin(\phi)) \vec{a}_\phi \\ - (f_x \sin(\phi) - f_y \cos(\phi)) \vec{a}_\theta \end{pmatrix} \dots\dots\dots (2.87)$$

Where

$$f_x = \iint_S E_x(x', y', 0) \cdot \exp(jk(x' \sin(\theta) \cos(\phi) + y' \sin(\theta) \sin(\phi))) \cdot dx' dy'$$

The E field components $E_x(x', y', 0)$ can be computed by the technique proposed by Zimmerman et.al [45] as

$$E_{x^*}(x', y', z'=0) = (1/N) \sum_{n=1}^N E_x(n) \cdot \exp(j2\pi \cdot n / N) \dots\dots\dots (2.88)$$

Where $E(n)$ correspond to the corresponding tangential electric field components E_x^n and E_y^n sampled at the point on the transformation surface point $Q(x', y', 0)$ at the n^{th} time step. N corresponding to time steps for one period of sinusoidal excitation frequency. From the E_θ and E_ϕ values obtained using the above computation the E-plane and H-plane pattern can be derived. A complete flow chart illustrating the radiation pattern computation algorithm is illustrated in the Fig 2.10

2.4.2.2 Antenna gain

For calculating the wide band gain, the input power fed to the antenna is needed. The equivalent steady state input power can be obtained at each frequency from the complex Fourier transforms of source voltage and source current (Equation 2.72).

$$P_{in}(\omega) = \text{Re}[V_s(\omega) * I_s^*(\omega)] \dots\dots\dots(2.89)$$

Far zone electric field in the desired direction can be obtained from the equation 2.87, and then antenna gain in the θ, ϕ direction relative to an isotropic antenna is given by

$$Gain(\omega, \theta, \phi) = \frac{[E(\omega, \theta, \phi)]^2 / \eta_0}{P_{in}(\omega) / 4\pi} \text{ where } \eta_0 \text{ is the impedance of the free space.}$$

2.4.2.3 Efficiency

Antenna efficiency is determined from the input power and dissipated power. Dissipated power can also be computed quite simply [46].

$$Efficiency = \frac{P_{in} - P_{dis}}{P_{in}} .$$

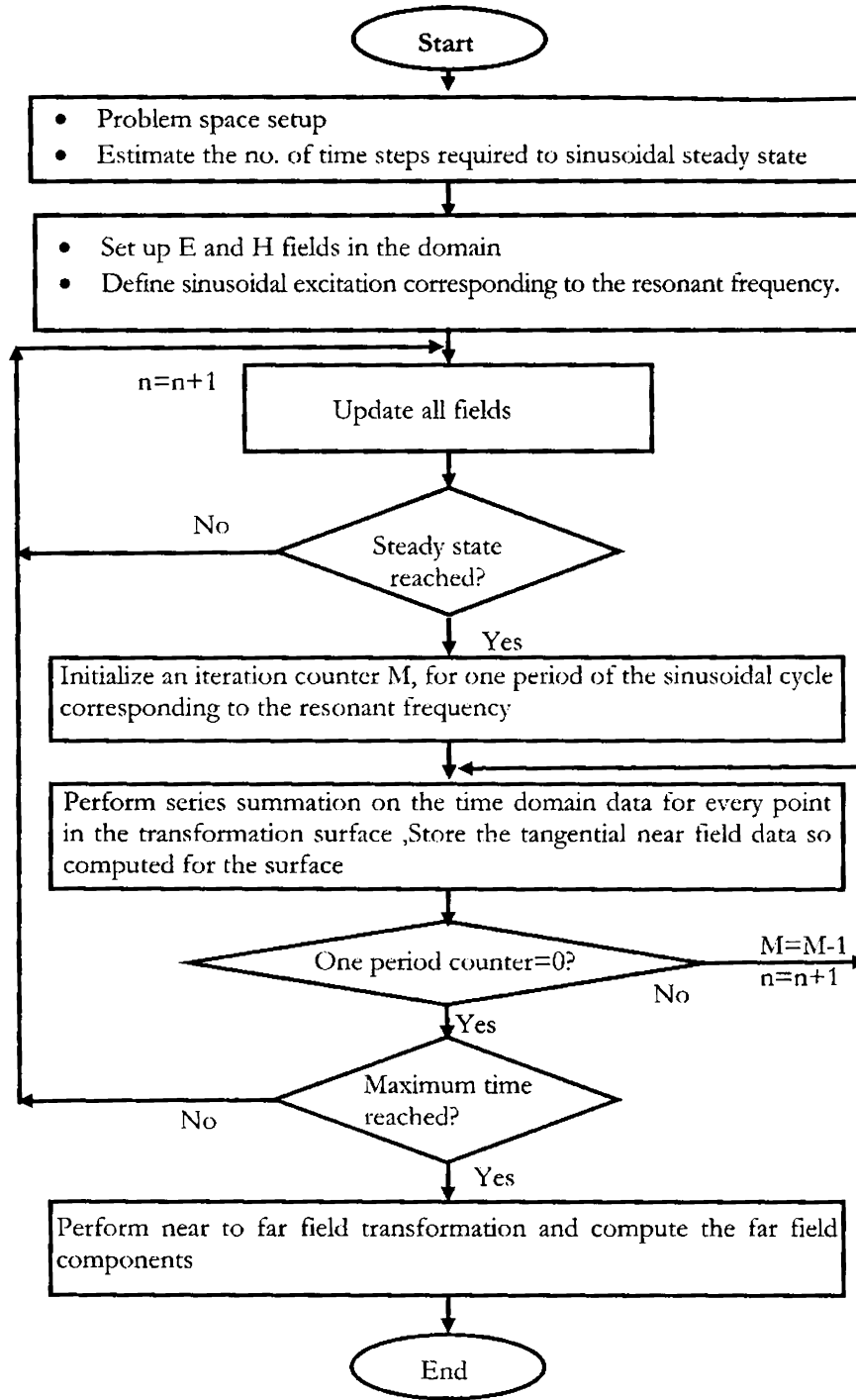


Fig 2.10. Flow chart for radiation pattern computation

2.5 Experimental analysis

This section outlines the fabrication method and basic facilities used for the experimental investigation of the printed monopole antenna.

2.5.1. Antenna fabrication: photolithography technique

Printed antennas are usually fabricated on microwave substrate materials using standard photolithographic techniques or chemical etching methods. Selection of proper substrate material is the essential part in antenna design. The dielectric constant, loss tangent, homogeneity, isotropicity and dimensional strength of the substrate all are of importance. High loss tangent substrate adversely affects the efficiency of the antenna especially at high frequencies. The selection of dielectric constant of the substrate depends on the application of the antenna and the radiation characteristics specifications. High Dielectric constant substrates causes surface wave excitation and low bandwidth performance. After the proper selection of the substrate material a computer aided design of the geometry is initially made and a negative mask of the geometry to be generated is printed on a butter paper. A double side copper cladded substrate of suitable dimension is properly cleaned using acetone and dried in order to avoid the discontinuity caused by the impurities. Any disparity in the etched structure will shift the resonant frequency from the predicted values, especially when the operating frequency is very high. A thin layer of negative photo resist material is coated using spinning technique on copper surfaces and it is dried. The mask is placed onto the photo resist and exposed to UV light. After the proper UV exposure the layer of photo-resist material in the exposed portions hardens which is then immersed in developer solution for few minutes. The hardened portions will not be washed out by the developer. The board is then dipped in the dye solution in order to clearly view the hardened photo resist portions on the copper coating. After developing phase the unwanted copper portions are etched off using Ferric Chloride (FeCl_3) solution to get the required antenna geometry on the substrate. The etched board is rinsed in running

water to remove any etchant. $FeCl_3$ dissolves the copper parts except underneath the hardened photo resist layer after few minutes. The laminate is then cleaned carefully to remove the hardened photo resist using acetone solution. The various steps involved in the fabrication process is illustrated in Fig.2.11

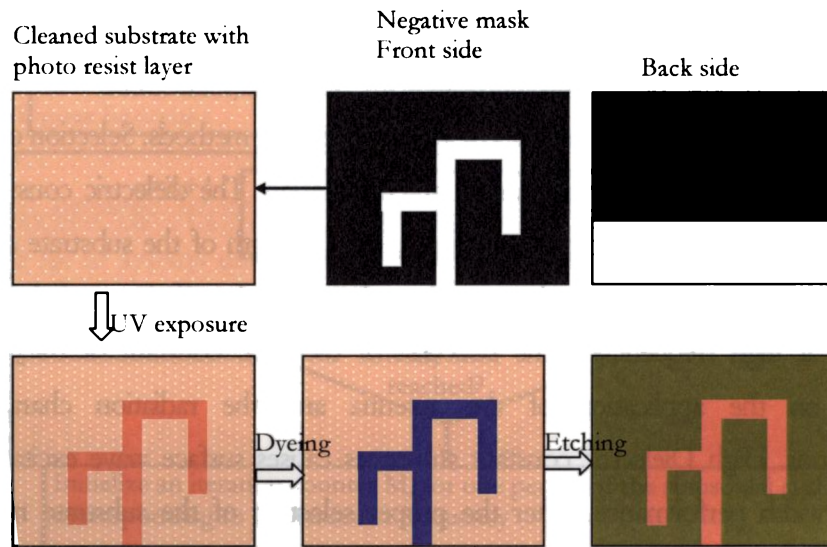


Fig 2.11. Antenna fabrication process using photolithography

2.5.2 Experimental setup.

An epigrammatic overview of the equipments and facilities used for extracting the antenna reflection and radiation characteristics is presented in this section with details of the measurement procedure.

2.5.2.1 HP 8510C Vector Network analyzer (VNA)

HP8510C is sophisticated equipment capable of making rapid and accurate measurements in frequency and time domain [47]. The NWA can measure the magnitude and phase of the S parameters. 32 bit microcontroller MC68000 based system can measure two port network parameters such as S_{11} , S_{12} , S_{22} , S_{21} and it's built in signal processor analyses the transmit and receive data and displays the results in many plot formats. The NWA consists of source, S parameter test set, signal processor and display unit. The synthesized sweep generator HP 83651B uses an open

loop YIG tuned element to generate the RF stimulus. It can synthesize frequencies from 10 MHz to 50 GHz. The frequencies can be set in step mode or ramp mode depending on the required measurement accuracy. The antenna under test is connected to the two port S parameter test set unit, HP8514B and incident and reflected wave at the port are then down converted to an intermediate frequency of 20MHz and fed to the detector. These signals are suitably processed to display the magnitude and phase information in the required format. These constituent modules are interconnected through HPIB system bus. An in-house developed MATLAB based data acquisition system coordinates the measurements and saves the data in the text format. Schematic diagram of HP8510C NWA and setup for reflection characteristic measurement is shown in Fig.2.12. HP 8510C NWA is mainly used for the antenna radiation pattern measurements.

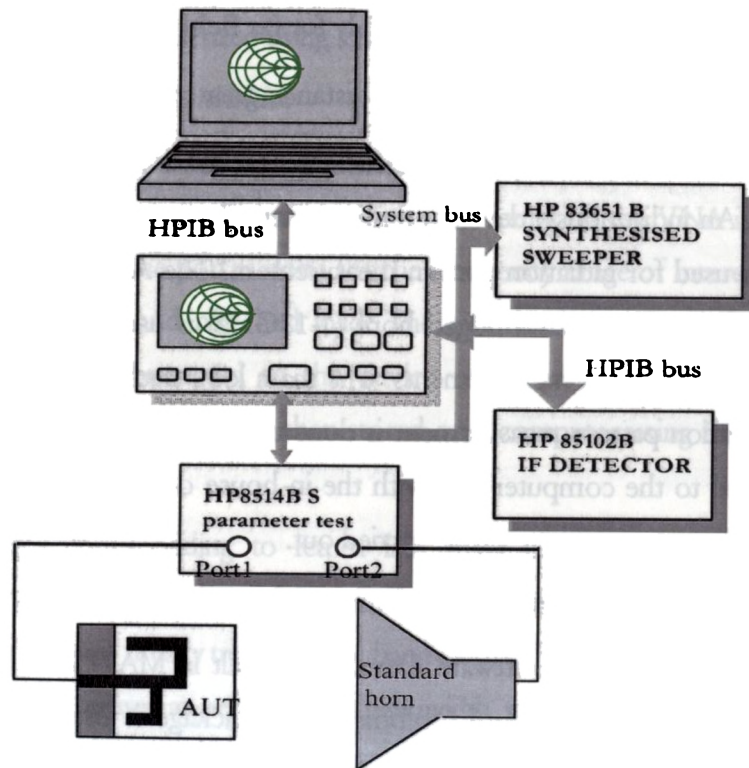


Fig.2.12 Experimental setup for antenna characterization

2.5.2.2 E8362B programmable Network Analyzer (PNA)

The Agilent E8362B Vector Network Analyzer is a member of the PNA Series Network Analyzer platform and provides the combination of speed and precision for high frequency measurements. The operation range is from 10 MHz to 20 GHz. For antenna measurements it provides exceptional results with more points and faster measurement speed. It has 16,001 points per channel with < 26 μ sec/point measurement speed and 32 independent measurement channels. Windows operating system and user interface mouse makes measurement procedure much easier. Embedded help system with full manual, extensive measurement tutorials, and complete programming guide helps to carry out accurate measurement of antenna characteristics promptly. This instrument is used for reflection studies in this Thesis.

2.5.2.3 Automated turn table assembly for far field measurement

The turn table assembly kept at distance greater than $2 * D^2 / \lambda$ consists of a stepper motor driven rotating platform for mounting the Antenna under Test (AUT). An indigenously developed microcontroller based antenna positioner STIC 310C is used for radiation pattern measurement. The AUT is used as the receiver and a standard wideband ridged horn (1-18GHz) is used as transmitting antenna for radiation pattern measurements. The main lobe tracking for gain measurement and radiation pattern measurement is done using this setup. Antenna positioner is interfaced to the computer and with the in-house developed software '*Crema Soft*' automatic measurements can be carried out.

2.5.2.4 *Crema Soft*: Automated antenna measurement

The user friendly software *CremaSoft* is built in MATLAB™ environment. The powerful instrument control toolbox of the package is used for communicating with the stepper motor control and Network Analyzer using the GPIB interface.

This automated software can be used for calibration, antenna measurements and material characterization of the substrate used for the antenna design.

Measurement of Antenna characteristics

The experimental procedures followed to determine the antenna characteristics are discussed in the following sections. Power is fed to the antenna from the S parameter test set of antenna through different cables and connectors. The connectors and cables will have its losses associated at higher microwave bands. Hence the instrument should be calibrated with known standards of open, short and matched loads to get accurate scattering parameters. There are many calibration procedures available in the network analyzer. Single port, full two port and TRL calibration methods are usually used. The two port passive or active device scattering parameters can be accurately measured using TRL calibration method. Return loss, VSWR and input impedance can be characterized using single port calibration method.

Return loss and 2:1 VSWR bandwidth

The return loss characteristic of the antenna is obtained by connecting the antenna to any one of the network analyzer port and operating the VNA in s_{11}/s_{22} mode. The calibration of the port is done for the frequency range of interest using the standard open, short and matched load. The calibrated instrument including the port cable is now connected to the device under test. The frequency vs reflection parameter (s_{11}/s_{22}) values is then stored on a computer using the 'Crema Soft' automation software.

The frequency corresponding to return loss minimum is taken as resonant frequency of the antenna. The range of frequencies for which the return loss value is within the -10dB points is usually treated as the bandwidth of the antenna. The antenna bandwidth is usually expressed as percentage of bandwidth, which is defined as

$$\%Bandwidth = \frac{bandwidth}{centrefrequency} * 100$$

Far field radiation pattern

The measurement of far field radiation pattern is conducted in an anechoic chamber or using the time gating facility of Vector Network Analyzer HP8510C to ensure a reflection free environment. The AUT is placed in the quiet zone of the chamber on a turn table and connected to one port of the network analyzer. A wideband horn is used as a transmitter and connected to the other port of the network analyzer. The turn table is controlled by a STIC positioner controller. The automated radiation pattern measurement process is coordinated by the '*Crema Soft*' software in the remote computer.

In order to measure the radiation pattern, the network analyzer is kept in S_{21}/S_{12} mode with the frequency range within the -10dB return loss bandwidth. The number of frequency points are set according to the convenience. The start angle, stop angle and step angle of the motor is also configured in the '*Crema Soft*'. The antenna positioner is boresighted manually. Now the THRU calibration is performed for the frequency band specified and saved in the CAL set. Suitable gate parameters are provided in the time domain to avoid spurious radiations if any. The *Crema Soft* will automatically perform the radiation pattern measurement and store it as a text file

Antenna Gain

The gain of the antenna under test is measured using the gain Transfer method [48-49]. The experimental setup is similar to the radiation pattern measurement setup. A standard antenna is placed in the antenna positioner and boresighted. THRU calibration is made for the frequency range of interest. Standard antenna is then replaced by the AUT and the change in S_{21} is noted. Note that the AUT should be aligned so that the gain in the main beam direction is measured. This is the relative gain of the antenna with respect to the reference

antenna. The absolute gain of the antenna is obtained by adding this relative gain to the original gain of the standard antenna, provided by the manufacturer.

Antenna Efficiency

Efficiency of the antenna is measured using the Wheeler cap method [50-51]. The method involves making only two input impedance measurement of antenna under test: one with conducting cap enclosing the antenna and one without. For the Wheeler cap, a conducting cylindrical box is used whose radius is radius of the antenna and to completely enclose the test antenna. Input impedance of the test antenna is measured with and without the cap using E8362B PNA. Since the test antenna behaves like a series resonant RLC circuit near resonance the efficiency is calculated by the following expression:

$$\text{Efficiency, } \eta = \frac{R_{no_cap} - R_{cap}}{R_{no_cap}}$$

2.6 Simulation studies

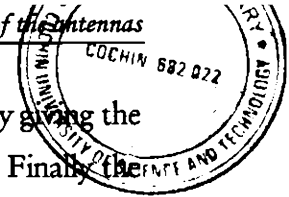
2.6.1 IE3D Electromagnetic software

IE3D is a full-wave, method-of-moments (MoM) based EM tool [52]. IE3D is a highly accurate, efficient and highly flexible full-wave EM engine. The MS-Windows based object-oriented GUI allows interactive construction of 3D and multilayer metallic structures as a set of polygons. Numerous editing capabilities are implemented to ease the construction and manipulation of these polygons. IE3D solves Maxwell's equations in integral form and its solutions include the wave effects, discontinuity effects, coupling effects, and radiation effects. The simulation results include S-, Y-, Z-parameters, VSWR, RLC-equivalent circuits, current distribution, near field, radiation patterns, directivity, efficiency, and RCS. IE3D is an extremely powerful tool in the design of monolithic microwave integrated circuits (MMIC), RF integrated circuits (RFIC), RF PCB, microstrip antennas, wire antennas, RFID antennas and other RF antennas. CURVIEW is the

Post processor for display and animation of current distribution and field distribution. CURVIEW also provides complete information on the directivity, return loss, efficiency, axial ratio, 3 dB beam width, and RCS. Most of the field solvers model ground and substrate as infinite while solving circuit and antenna problems. In antenna design for wireless communication and handheld application the infinite ground plane is not practical. IE3D is able to model structures with finite ground plane. MGRID is the layout editor for construction of geometry and defining the material parameter such as substrate thickness, dielectric constant, and metallic properties of the antenna structure. The simulation setup window can be used to specify the frequency range of interest and accuracy of the results. The simulation results are available in MODUA window available with IE3D.

2.6.2 HFSS: 3D Electromagnetic simulator

HFSS (High frequency Structure Simulator) is a 3D electromagnetic field simulator based on Finite Element Method for modelling arbitrary volumetric structures [53]. It integrates simulation, modelling, visualization and automation in an easy to learn environment. With adaptive meshing and brilliant graphics the HFSS gives an unparalleled performance and complete insight to the actual radiation phenomenon in the antenna. With HFSS one can extract the parameters such as S, Y, and Z, visualize 3D electromagnetic fields (near- and far-field), and optimize design performance. An important and useful feature of this simulation engine is the availability of different kinds of port schemes. It provides lumped port, wave port, incident wave scheme etc. The accurate simulation of coplanar waveguides and microstrip lines can be done using wave port. The parametric set up available with HFSS is highly suitable for Antenna engineer to optimize the desired dimensions. The first step in simulating a system in HFSS is to define the geometry of the system by giving the material properties and boundaries for 3D or 2D elements available in HFSS window. The suitable port excitation scheme is then given. A radiation boundary filled with air is then defined surrounding the



structure to be simulated. Now, the simulation engine can be invoked by giving the proper frequency of operations and the number of frequency points. Finally the simulation results such as scattering parameters, current distributions and far field radiation pattern can be displayed. The vector as well as scalar representation of E, H, J values of the device under simulation gives a good insight in to the antenna under analysis.

2.7 References

T
621 395 67
R

- [1] K.H. Huebner and E.A. Thornton, *The Finite Element Method for Engineers*. New York: John Wiley and Sons, 1982, Chap. 3, pp. 62–107.
- [2] Keller J.B., "Geometrical Theory of Diffraction" *J. Optical Society of America* vol.52, 1962, pp. 116-130.
- [3] Kouyoumjian R.G and P.H Pathak "A uniform geometrical theory of diffraction for an edge in a perfectly conducting surface", *Proc. IEEE* vol.62, 1974, pp 1448-1461.
- [4] Constantine A Balanis., "Advanced Engineering Electromagnetics," John Wiley and Sons, USA, 1989.
- [5] Umashankar K.R., "Numerical analysis of electromagnetic wave scattering and interaction based on frequency domain integral equation and method of moments techniques" *Wave motion*, vol.10, 1988, pp.493-525.
- [6] Roberto Sorrentino, "Modelling and Design of Millimetre wave passive circuits: from 2 to 3D," *Proc. 24th European Microwave conference*, September 1994.
- [7] G. A. Thiele, "Overview of selected hybrid methods in radiating system analysis," *Proc. IEEE*, vol. 80, no. 1, pp. 66–78, Jan. 1992.
- [8] E. Abenius, U. Anderson, and F. Edelvik, "Hybrid time domain solvers for the Maxwell equations," *Int. J. Numerical Methods Eng.*, vol. 9, pp. 2185–2199, 2002.
- [9] J. Gong, J. L. Volakis, A. Woo, and H. Wang, "A hybrid finite element- boundary integral method for the analysis of cavity-backed antennas of arbitrary shape," *IEEE Trans. Antennas Propagat.*, vol. 42, pp. 1233–1242, Sept. 1994.

- [10] D. Jankovic, M. LaBelle, D. C. Chang, J. M. Dunn, and R. Booton, "A hybrid method for the solution of scattering from inhomogeneous dielectric cylinders of arbitrary shape," *IEEE Trans. Antennas Propagat.*, vol. 42, pp. 1215–1222, Sept. 1994.
- [11] M. A. Mangoud, R. A. Abd-Alhameed, and P. S. Excell, "Simulation of human interaction with mobile telephones using hybrid techniques over coupled domains," *IEEE Trans. Microwave Theory Techniques*, pt. 2, vol. 48, pp. 2014–2021, Nov. 2000.
- [12] Karoda Umashankar and Allan Taflov, "Computational Electromagnetics," Artech House, Norwood, MA, 1993.
- [13] R.F. Harrington, *Field Computation by Moment Methods*. Malabar, FL: Krieger, 1968.
- [14] B.J. Strait, *Applications of the Method of Moments to Electromagnetics*. St. Cloud, FL: SCEEE Press, 1980.
- [15] R.F. Harrington, "Origin and development of the method moments for field computation," in E.K. Miller et al., *Computational Electromagnetics*. New York: IEEE Press, 1992, pp. 43–47.
- [16] J.H. Richmond, "Digital computer solutions of the rigorous equations for scattering problems," *Proc. IEEE*, vol. 53, Aug. 1965, pp. 796–804.
- [17] Mosig, J.R., And Gardiol, F.E, "Analytical and numerical techniques in Green's function treatment of microstrip antennas and scatterers", *IEE Proc. Microwaves Opt. Antennas H*, 1983, 132, pp. 175-1 82
- [18] Mosig, J.R., "Arbitrarily shaped microstrip structures and their analysis with a mixed potential integral equation", *IEEE Trans.*, 1988, MTT-36, pp. 314-323.
- [19] R.Mitra and C.A Klein, "Stability and Convergence of Moment Method solutions", in *Numerical and Asymptotic Techniques in Electromagnetics*, R.Mitra (Ed.),Springer Verlag, New York,1975,Chpater 5, pp 129-163
- [20] T.K Sarkar, "A Note on the choice of weighing function sin the Method of Moments", *IEEE Trans. Antennas and Propogat.* ,vol AP-33,no.4,pp 436-441, April 1985.
- [21] T.K Sarkar, A.R Djordjevic and E.Arvas, "On the choice of expansion and weighing function in the solution of operator equations", *IEEE Trans. Antennas and Propogat.* vol AP-33,no.9,pp 988-996,September 1985.

- [22] M.N.O. Sadiku, "A simple introduction to finite element analysis of electromagnetic problems," *IEEE Trans. Educ.*, vol. 32, no. 2, May 1989, pp. 85–93.
- [23] W.J.R. Hoefer, "The transmission-line matrix method—theory and applications," *IEEE Trans. Microwave Theory Tech.*, vol. MTT-33, no. 10, Oct. 1985, pp. 882–893.
- [24] C. Christopoulos, *The Transmission-Line Modeling Method (TLM)*. New York: IEEE Press, 1995.
- [25] N. Marcovitz and J. Schwinger, "On the reproduction of the electric and magnetic fields produced by currents and discontinuity in wave guides", I. *J. Appl. Phys.*, vol. 22, no. 6, June 1951. pp. 806–819.
- [26] K.S.Yee, "Numerical solution of initial boundary value problems involving Maxwell's equations in isotropic media," *IEEE Trans. Antennas Propagat.*, vol.14, no.4, pp.302-307, May 1966.
- [27] Allen Taflove, "Numerical issues regarding finite-difference time-domain modelling of Microwave structures," *Time-Domain Methods for Microwave structures – Analysis and Design*, Ed. Tatsuo Itoh and Bijan Houshmand, *IEEE Press*.
- [28] Allen Taflove and Morris E. Brodwin, "Numerical solution of steady –state electromagnetic scattering problems using the time-dependent Maxwell's equations," *IEEE Trans. Microwave Theory Tech.*, vol.23, pp.623-630, August 1975.
- [29] Kurt L. Shlager and John B. Schneider, "A selective survey of the Finite-Difference Time-Domain literature," *IEEE Antennas Propagat. Mag.*, vol.37, no.4, pp.39-57, August 1995.
- [30] Z. Chen, M. Ney, and W.J.R. Hoefer, "A new finite-difference time-domain formulation and its equivalence with the TLM symmetrical condensed node," *IEEE Trans. Micro. Theo. Tech.*, vol. 39, no. 12, Dec. 1992, pp. 2160–2169.
- [31] Andrew F. Peterson, Scott L. Ray and Raj Mittra, "Computational methods for Electromagnetics", University Press, India, 2001, Ch.12.
- [32] David M. Sheen, Sami M. Ali, Mohamed D. Abouzahra and Jin Au Kong, "Application of the Three-Dimensional Finite-Difference Time-Domain method to the analysis of planar Microstrip circuits," *IEEE Trans. Microwave Theory Tech.*, vol.38, no.7, pp.849-857, July 1990.
- [33] G. Mur, "Absorbing Boundary Conditions for the Finite Difference Approximation of the Time-Domain Electromagnetic Field Equations," *IEEE Trans. Electromagn. Compat.*, Vol .EMC-23, Nov. 1981, pp. 377-382.

- [34] J. P. Berenger, "A Perfectly Matched Layer for the Absorption of Electromagnetic Waves," *J. Computational Phys.*, Vol. 114, 1994, pp. 185-200.
- [35] D. S. Katz, E. T. Thiele, and A. Taflov, "Validation and Extension to Three Dimensions of the Berenger PML Absorbing Boundary Condition for FD-TD Meshes," *IEEE Microwave Guided Wave Lett.*, Vol. 4, No. 8, Aug. 1994, pp. 268- 270.
- [36] X.Zhang,J.Fang,y.Liu and K.K Mei , "Calculation of dispersive characteristics of Microstripes by time domain finite difference method", *IEEE Trans.Mirowave theory and tech.* vol 36,pp.263-267,1988.
- [37] Enquist and Majada, "Absorbing Boundary Conditions for the Numerical simulation of waves", *Mathematics of computation*, Vol. 31, 1977, pp. 629-651.
- [38] D.S. Katz, E.T. Thiele, and A. Taflove, "Validation and extension to three dimensions of the Berenger PML absorbing boundary conditions for FD-TD meshes," *IEEE Micro. Guided Wave Lett.*, vol. 4, no. 6, Aug. 1994, pp. 268– 270.
- [39] J.P. Berenger, "Perfectly matched layer for the FDTD solution of wave structure interaction problems," *IEEE Trans. Ant. Prop.*, vol. 44, no. 1, Jan. 1996, pp. 110–117.
- [40] Sullivan Dennis M, "Electromagnetic simulation using the FDTD method", IEEE press series on RF and Microwave Technology, USA.
- [41] Z. S Sacks, D. M. Kingsland, R. Lee, and J.F. Lee, "A perfectly matched anisotropic absorber for use as an absorbing boundary condition", *IEEE Transactions on Antennas and Propagation*, Vol. 43. December 1995, pp. 1460-1463.
- [42] V. Jandhyala, E. Michielssen, and R. Mittra, "FDTD signal extrapolation using the forward-backward autoregressive model", *IEEE Microwave and guide wae letters*, Vol. 4, June 1994, pp. 163-165.
- [43] R.J Leubbers and H.S Langdon., "A simple feed Model that reduces Time steps Needed for FDTD Antenna and Microstrip Calculations" *IEEE Trans. Antennas and Propogat.*Vol.44,No.7,July 1996, pp.1000-1005.
- [44] R.J Leubbers,Karl s Kunz,Micheal Schneider and Forrest Hunsberger.," A finite difference time Domain near zone to far zone transformation", *IEEE Trans. Antennas and Propogat.*vol.39,pp429-433,April 1991.

- [45] Martin L Zimmerman and Richard Q Lee, "Use of FDTD method in the design of microstrip antenna arrays", *Int.Journal of Microwave and Millimeter wave Comp. aided Engg.* vol.4, no. 1, pp 58-66, 1994.
- [46] R.J Leubbers, Karl s Kunz, " Finite difference time domain method for electromagnetics", CRC press, New York 1993.
- [47] HP8510C Network Analyzer operating and programming manual, Hewlett Packard, 1988.
- [48] C. A. Balanis, "Antenna Theory: Analysis and Design", Second Edition, John Wiley & Sons Inc. 1982.
- [49] John D. Kraus, "Antennas", Mc. Graw Hill International, second edition, 1988.
- [50] H.A Wheeler, "The Radiansphere around a small antenna", in *Proc. IRE*, August 1959, pp 1325-1331.
- [51] E.Newman, P.Hohley and C.H Walter, " Two methods for the measurement of antenna efficiency", *IEEE trans. Antennas and Propogat.* Vol.23, No.4, pp 457-461, July 1975.
- [52] IE3D User's manual, Release 7, Zeland Software Inc. December 1997.
- [53] HFSS User's manual, version 10, Ansoft Corporation, July 2005

THEORETICAL AND EXPERIMENTAL ANALYSIS OF PRINTED STRIP MONOPOLE ANTENNA

Experimental results derived from investigations on the truncated ground plane dimensions of printed strip monopole antenna are presented in this chapter. FDTD based numerical computation is performed to predict the effect of ground plane truncation on the impedance and radiation characteristics of the printed strip monopole antenna. The predicted results are experimentally verified by fabricating and testing different printed monopole antennas. This chapter highlights the step by step procedure to derive a broadband printed monopole antenna from a simple printed strip monopole antenna.

The chapter begins with the description of resonance and radiation characteristics of printed strip monopole antenna on an infinite ground plane. It is followed by a detailed study of the ground plane truncation effects on antenna characteristics. The truncation of ground plane is effectively utilized to design a wide band printed strip monopole antenna. The detailed parametric analysis of wide band printed monopole is enabled to derive simple design equation for wide band performance. Experimental and theoretical analysis of compact monopole antenna derived from parametric analysis of a wide and printed monopole is presented for application in modern wireless communication systems. The chapter concludes with some of the typical strip monopole antenna designs along with its radiation characteristics suitable for wireless communication gadgets.

3.1 Introduction

The Monopole antenna is attractive for modern communication systems due to its simple structure, broad bandwidth and nearly omnidirectional radiation characteristics. The monopoles are usually placed vertical to the ground plane which increases the system complexity, size and volume. These types of antennas may create constraints to the performance of the system and uneasiness to the user. Printed monopoles on the other hand, are conformal for modular design and can be fabricated along with the printed circuit board of the system, which make the design simpler and fabrication easier. Usually in the printed monopole designs ground plane is printed on the same substrate parallel to the radiator either on the same side of radiator or at the opposite side. These has made antenna low in profile and low in volume along with added advantage of easy to fabricate and integrate in the system circuit board of communication device. The limited space of circuit board will impose another constraint on the size of the ground plane. It is found that the size of the ground plane, adversely affect the antenna performance considerably. Thus the ground plane, an inevitable part of the mobile gadget and its effect on antenna performance are the important issues that have to be addressed in the present scenario. The exhaustive explorations of the ground plane effects have resulted an interesting inference that the bandwidth of a conventional printed strip quarter wave monopole can be broadened more than 60% by prudently truncating the ground plane width. These inferences can be put forward as a solution to the everlasting problem that the radiation characteristic of monopole degrades when ground plane sizes are limited.

In other words, the length of the ground plane can be reduced to many folds by properly selecting its width. Thus compact monopole antennas can be designed on truncated ground planes with the additional advantage of broad

band behaviour without loosing its omni-directional radiation properties. This intervening property is elaborately discussed in this chapter. The FDTD algorithm is used to predict the antenna input impedance characteristics and field distributions. These results can provide more insight to the problem. Exhaustive parametric analysis were carried out to optimize the ground plane truncation. From the parametric studies an optimum ground plane dimension to fix the resonance at desired frequency is derived. Using the optimum ground plane a compact strip monopole antenna is designed and experimentally characterized. A wide band printed strip monopole is thus derived can find application in laptop computers, PDA's WLAN and WiMAX bands. The design equations are confirmed by extending the designs to meet requirements of modern wireless gadgets. These designs confirm that printed monopole antenna is highly suitable in wireless gadgets where the size of the antenna is the major concern.

3.2 Microstrip fed printed strip monopole antenna

A microstrip fed printed monopole and the ground truncation effects on the antenna characteristics is the main theme of the present chapter. A strip of length L_m and width W_m is printed on a low loss substrate of dielectric constant ϵ_r and height h . The length of the antenna is selected as $\lambda/4$ of the design frequency. For the present analysis the width of the radiating monopole is selected as the width of 50Ω microstrip line. A rectangular ground plane of dimensions $W_g \times L_g$ is printed on the other side of the substrate parallel and symmetric to the strip. This antenna is simulated using FDTD code implemented in MATLAB™. The built in FFT function of the MATLAB is used to extract the frequency domain characteristics. The entire computational domain is divided into Yee cells of dimensions $\Delta x = \Delta y = \Delta z = 0.5 \text{mm}$ which ensures the minimum discretization error. Maximum frequency of operation is

selected as 7GHz so that spatial discretization is less than $\lambda/20$ of the maximum frequency of operation. The substrate is discretized as 3 cells in the Z direction and 10 air cells were assigned on each side of the substrate periphery to ensure the practical condition of surrounding air. The layer of cell just above the printed strip monopole and underneath the ground plane is assigned with effective dielectric constant value to ensure the air dielectric interface. 10 cells are assigned surrounding the antenna to truncate the problem space with PML ABC which ensures the complete absorption of any incident wave at the truncation boundary. Microstrip feed is modeled using Leubber's technique as outlined in Section 2.3.5.2. The input Gaussian pulse facilitates to extract the wideband characteristics of the printed strip monopole antenna. From the near field data far field radiation pattern and gain of the antenna are computed as outlined in Section 2.4.2. Sinusoidal excitation is used to extract the field components at the resonant frequency. The following sections describe the experimental and theoretical observations in detail. The geometry of the proposed microstrip fed printed strip monopole and the layout of the computational domain is depicted in Fig.3.1. For the initial experimental investigations the strip monopole is printed on FR4 substrate of $\epsilon_r = 4.4$ and height $h=1.6\text{mm}$.

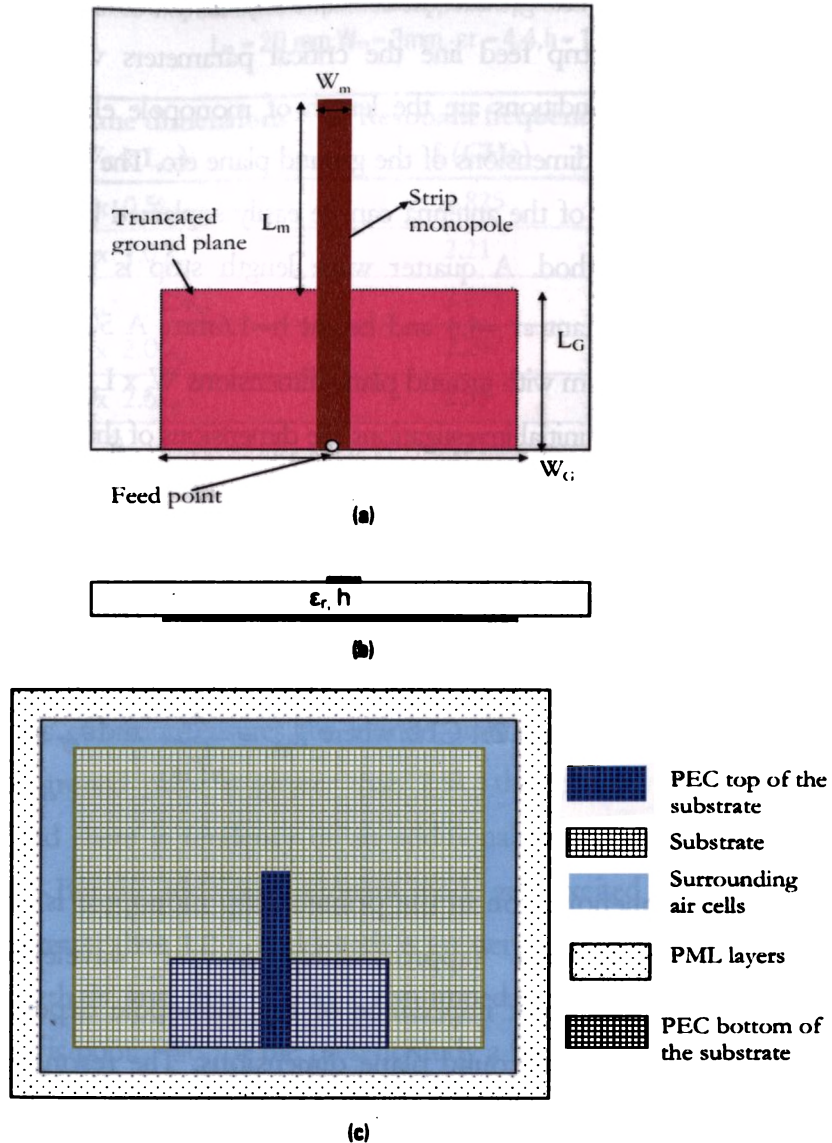


Fig 3.1 (a) Top view of the geometry of the proposed antenna
 (b) Side of the geometry
 (c) The layout of the computational domain

3.3 Resonance and radiation in microstrip fed printed strip monopole

In conventional wire monopole antennas fed by a transmission line, the effective terminal impedance depends not only on the length and diameter of the wire but also

up on the dimensions of the ground plane. Similarly in printed strip monopole antenna excited by microstrip feed line the critical parameters which affect the radiation and resonance conditions are the length of monopole element, width to length ratio of the element, dimensions of the ground plane etc. The actual resonance and radiation phenomenon of the antenna can be easily explained by modelling the antenna using FDTD method. A quarter wave length strip is printed on FR4 substrate of dielectric constant $\epsilon_r = 4.4$ and height $h = 1.6\text{mm}$. A 50Ω characteristic impedance line of width 3mm with ground plane dimensions $W_g \times L_g$ is used to excite the strip monopole. For the initial investigations the dimensions of the ground plane is varied from several wavelengths ($5\lambda_d \times 5\lambda_d \text{ mm}^2$) to fraction of wavelengths ($0.5\lambda_d \times 0.5\lambda_d \text{ mm}^2$), where $\lambda_d = \frac{\lambda_0}{\sqrt{\epsilon_r}}$. Large ground plane dimensions ensures an infinite ground plane transitions for the quarter wavelength monopole. The length of the monopole, $L_m = 0.25\lambda_{eff} = 20\text{mm}$ at 2.4 GHz where $\lambda_{eff} = \frac{\lambda_0}{\sqrt{\epsilon_{eff}}}$ and $\epsilon_{eff} = \frac{\epsilon_r + 1}{2}$.

3.3.1 Resonance phenomenon

The resonance phenomenon in the printed strip monopole is akin to the conventional near -resonant (approximately quarter wavelength) wire monopole antennas. The input impedance of the monopole depends on the length of the monopole and ground plane dimensions. The resonance can be explained on the basis of sinusoidal current variation along the strip monopole above finite or infinite ground plane. When the strip monopole is excited by microstrip line with finite ground plane the ground plane underneath the microstrip line operates in the propagating mode without any field deterioration. The variation of resonant frequency with ground plane parameters obtained from FDTD computation is presented in Table 3.1.

Table 3.1 Resonance characteristics of printed strip monopole on various ground plane dimensions.
 $L_m = 20 \text{ mm}, W_m = 3 \text{ mm}, \epsilon_r = 4.4, h = 1.6 \text{ mm}$

Ground plane dimensions ($W_G \times L_G$)	Resonant frequency f_r (GHz)	Additional resonance (GHz)
$0.5\lambda_d \times 0.5\lambda_d$	2.825	Nil
$1.0\lambda_d \times 1.0 \lambda_d$	2.21	Nil
$1.25\lambda_d \times 1.25\lambda_d$	2.075	3.05
$2.0\lambda_d \times 2.0 \lambda_d$	2.247	2.99
$2.5\lambda_d \times 2.5\lambda_d$	2.35	2.875
$5\lambda_d \times 5\lambda_d$	2.35	2.875
$1.25\lambda_d \times 1.0 \lambda_d$	2.079	3.0
$1.25\lambda_d \times 0.5\lambda_d$	2.029	3.4576

From the Table 3.1 it is found that the resonant frequency is independent of ground plane dimensions if the ground plane parameters are greater than $2.5\lambda_d \times 2.5\lambda_d$. Hence this condition ensures the infinite ground condition. When the width and length of ground plane is greater than $2.5\lambda_d$ the ground plane is considered as infinite and there is tendency of an additional resonance near the fundamental resonance. But the additional resonant mode gets excited when the ground plane width is greater than $1.0 \lambda_d$ and length is greater than $0.5 \lambda_d$. But when the ground plane length is less than $0.5 \lambda_d$ the impedance matching for the additional resonance is poor. So for the present study a finite ground plane width of $0.5 \lambda_d$ and infinite ground plane width of $2 \lambda_d$ are selected so as to optimize the ground plane width for maximum bandwidth performance.

The simulated surface current distribution of a typical monopole antenna above a finite ground plane is shown in Fig. 3.2. The length of the strip monopole is $\lambda_d / 4$ and width W_m is 3mm. From the figure it is very clear that there is quarter wavelength variation of field along the strip.

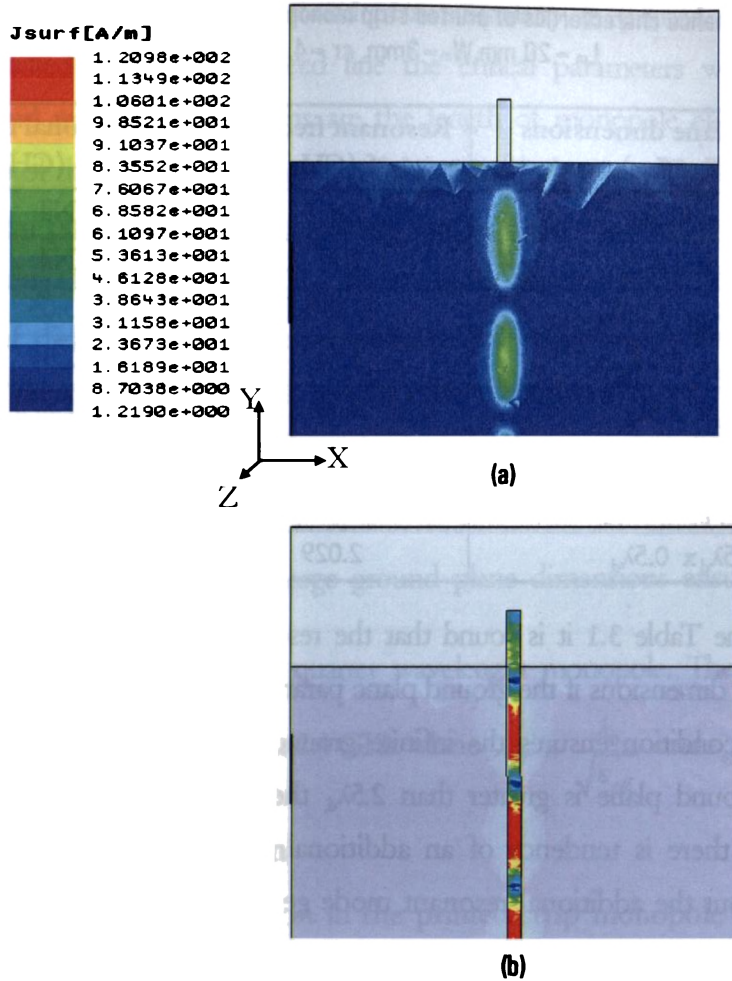


Fig 3.2 Simulated surface current distribution of finite ground plane printed monopole antenna.

$$W_g = 0.5\lambda_d \text{ mm} \quad L_g = 0.5\lambda_d \text{ mm}, L_m = 20\text{mm}, W_m = 3\text{mm}, \epsilon_r = 4.4, h = 1.6\text{mm}$$

(a) Current distribution on the ground plane.

(b) Surface current distribution on the strip.

From the surface current distribution it can be inferred that the surface current at the tip of the monopole is minimum. Maximum surface current is observed near the ground truncation. The simulated current distributions confirm that antenna is resonant with quarter wavelength current variation along the strip. But there is no current variation on the finite ground plane at the resonant frequency. But it can be observed that at the edges along the width of the ground

plane there is feeble current which varies with the dimensions of the ground plane. Hence it can be concluded that the ground plane transition from infinite to finite can tailor the resonance and radiation characteristics of the strip monopole. Variation of input impedance characteristics on antenna resonance characteristics can easily explained with quarter wavelength monopole with infinite and finite ground plane dimensions. FDTD computed input impedance characteristics of the printed strip monopole are depicted in Fig.3.3.

At resonance the reactive part of the input impedance vanishes and the system becomes purely resistive. But on either sides of the resonant frequency the reactive part becomes either inductive or capacitive

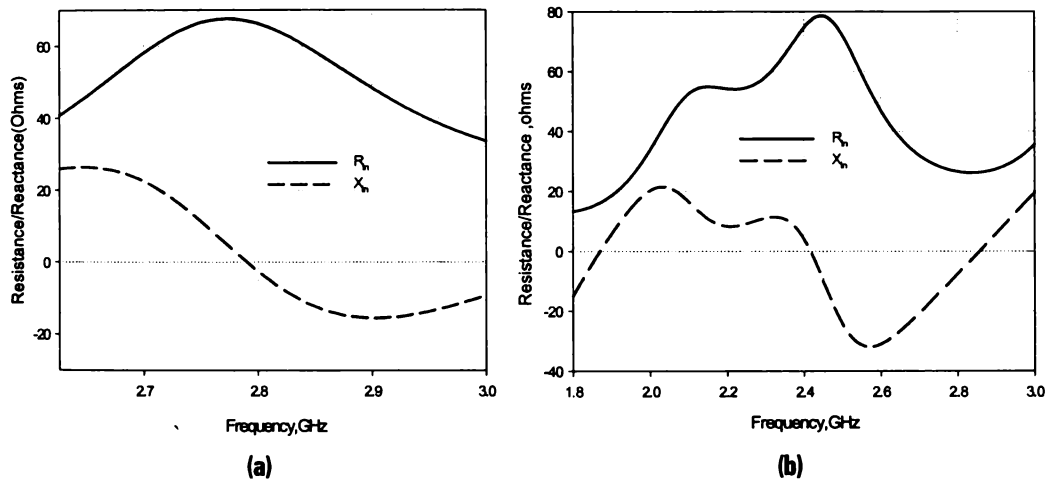


Fig 3.3 Input impedance characteristics of the printed strip monopole antenna

(a) Finite ground plane $W_0 = 45$ mm, $L_0 = 45$ mm, $L_m = 20$ mm, $W_m = 3$ mm, $\epsilon_r = 4.4$, $h = 1.6$ mm

(b) Infinite ground plane $W_0 = 150$ mm, $L_0 = 45$ mm, $L_m = 20$ mm, $W_m = 3$ mm, $\epsilon_r = 4.4$, $h = 1.6$ mm

From the input impedance characteristics it can be inferred that at resonance the input impedance is purely resistive and both the sides of the resonant frequency the impedance becomes either inductive or capacitive. Computed return loss characteristics of the antenna presented in Fig 3.4 gives a clear insight of the above mentioned inferences. For a finite ground monopole the resonance occurs around

2.8GHz where the input impedance is approximately 50Ω and at the lower end of resonant frequency the impedance is inductive while at the upper edge the reactance becomes capacitive. But when the ground plane dimensions is infinite the impedance characteristics reveals that there is a tendency of an additional resonance at 3.1GHz near the fundamental mode. In this case the antenna is resonating at 2.3GHz, which is lower than the finite ground plane. The important conjecture arrived from the above investigation is that by properly optimizing the ground plane a new resonant mode can be generated near the fundamental resonant frequency of the monopole. These studies also reveals that the resonant frequency is altered due to the transition of the ground plane dimensions but the variation is negligible.

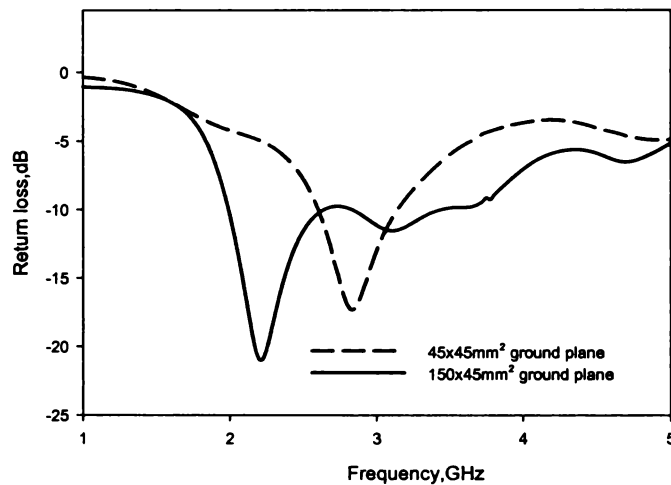


Fig 3.4 Return loss characteristics of the microstrip fed printed strip monopole antenna.
 $L_m = 20\text{mm}$, $W_m = 3\text{mm}$, $\epsilon_r = 4.4$, $h = 1.6\text{mm}$

3.3.2 Radiation characteristics

Computed radiation characteristics using FDTD for the strip monopole with infinite and finite ground plane dimensions are shown in Fig.3.5. Computed radiation characteristics reveal that the radiation from printed strip monopole is analogous to the typical monopole mode with a null along X direction when the monopole is placed along XY plane as shown in Fig 3.5. For both the cases antenna is linearly

polarized along Y direction. For truncated infinite ground plane the H plane radiation patterns shows four nulls along $0^\circ, 90^\circ, 180^\circ, 270^\circ$. It is very interesting to note that for finite ground plane the pattern is almost omnidirectional with low cross polarization. This is because for finite ground plane dimensions the vertical monopole is strongly radiating at the resonant frequency where as the ground plane currents has negligible effect on the radiation characteristics. But when the infinite ground plane is truncated the ground plane edge currents distorts the image and the radiation characteristics varies considerably. Moreover, horizontal edge currents along the ground plane width affects the cross polarization level.

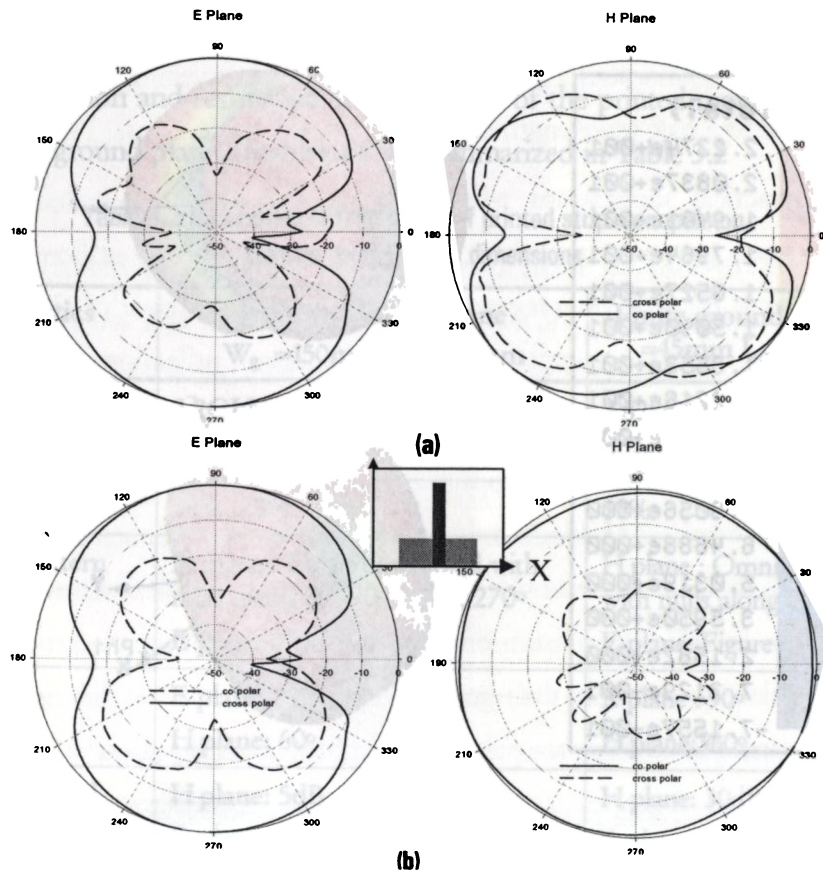


Fig 3.5 Computed radiation patterns at the resonant frequency
 (a) Infinite ground plane $W_0 = 150\text{mm}, L_0 = 45\text{mm}, L_m = 20, W_m = 3\text{mm}, \epsilon_r = 4.4, h = 1.6\text{mm}$
 (b) finite ground plane $W_0 = 45\text{mm}, L_0 = 45\text{mm}, L_m = 20\text{mm}, W_m = 3\text{mm}, \epsilon_r = 4.4, h = 1.6\text{mm}$

3.3.2.1 3D Radiation patterns

3D radiation pattern is computed using simulation software Ansoft HFSS. Simulated radiation patterns are similar to the FDTD computed radiation characteristics. For a finite ground plane the 3D radiation pattern is doughnut shaped similar to the dipole pattern. But for infinite ground plane the pattern shows feeble nulls in the bore sight direction hence the pattern is some what distorted in the H plane losing its omni directionality. Fig 3.6 clearly depicts the variation of the pattern with ground plane transitions.

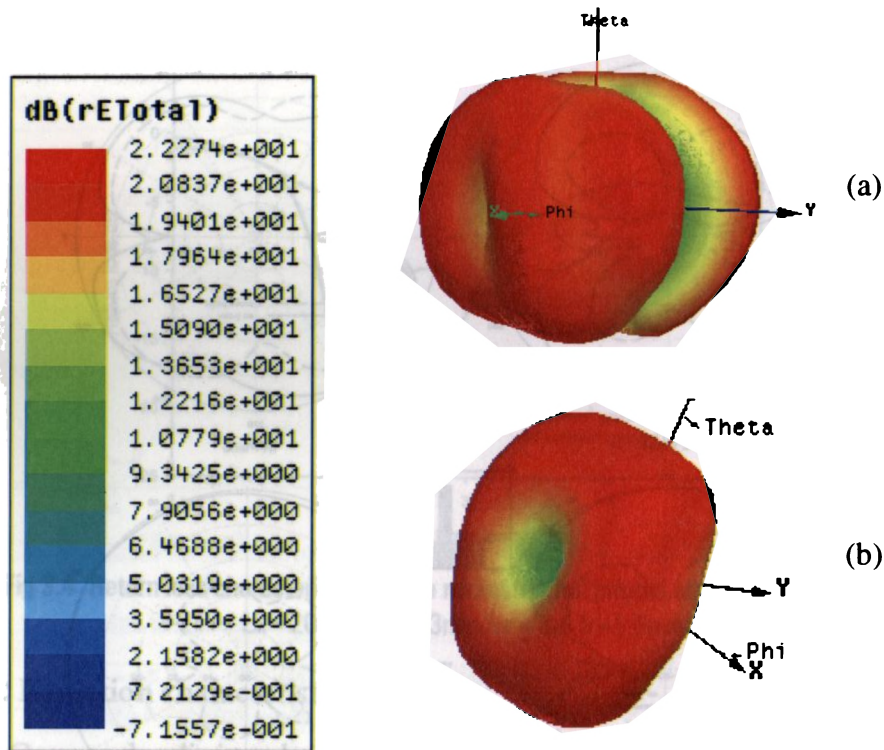


Fig 3.6 Simulated 3D radiation pattern of the printed strip monopole

- (a) Infinite ground plane $W_g = 150\text{mm}$, $L_g = 45\text{mm}$, $L_m = 20\text{mm}$, $W_m = 3\text{mm}$, $\epsilon_r = 4.4$, $h = 1.6\text{mm}$
 (b) finite ground plane $W_g = 45\text{mm}$, $L_g = 45\text{mm}$, $L_m = 20\text{mm}$, $W_m = 3\text{mm}$, $\epsilon_r = 4.4$, $h = 1.6\text{mm}$

3.3.2.2 Gain and efficiency

Gain of the antenna is measured using gain transfer method. Measured gain of the antenna for finite ground plane is 2.65dBi where as for infinite ground plane the gain is 3.4dBi. For infinite ground plane the gain enhancement is observed due to the increased directivity. This can be clearly observed from the 3D radiation patterns. The efficiency of the antenna is 86.4% for finite ground plane printed strip monopole where as efficiency is 79% for infinite ground plane case. A slight degradation of efficiency is observed for the large ground plane is due to the increased ohmic losses in the ground plane. The computed efficiency is 84% for finite ground printed strip monopole antenna where as the efficiency is 76.5% for infinite ground condition.

The radiation and resonance characteristics of the printed monopole antenna on different ground plane dimensions are summarized in Table 3.2

Table 3.2 Resonance charectartics of printed strip monopole on various ground plane dimensions

Characteristics	Infinite ground plane $W_g = 150\text{mm}$ $L_g = 45\text{ mm}$	Finite ground plane $W_g = 45\text{mm}$ $L_g = 45\text{ mm}$
Resonant frequency	2.2GHz , 3.1GHz (Two distinct resonant modes)	2.825GHz (single resonance)
Band width	30%, 20%	19%
Radiation pattern	H plane : Omni directional with nulls along 0° , 90° , 180° , 270° E plane: Figure of eight	H plane : Omni directional with nulls along 0° 180° E plane: Figure of eight
HPBW	E plane : 90° H plane: 60°	E plane : 90° H plane: 360°
Cross polar level along bore-sight direction	H plane: 5dB E plane: 30dB	H plane: 30dB E plane: 30dB
Gain	3.4dBi	2.65dBi
Efficiency	79%	86%

The important conclusions of this initial analysis can be summarized as

- The ground plane dimensions of the feed line of a microstrip excited printed monopole plays a crucial role in the resonance and radiation characteristics of the printed monopole antenna.
- The ground plane truncation can be effectively utilized to control the impedance bandwidth of the antenna.
- The ground plane can be properly tailored to generate an additional resonance near the fundamental mode which can be effectively used to broaden the bandwidth of the printed strip monopole.
- Radiation characteristics of a monopole with truncated ground plane are similar to a half wavelength dipole.
- In practical applications where the antenna and feed system shares a common ground plane, these effects can be effectively utilized to design antennas that can be integrated with in the limited space of the electronic gadgets without compromising the antenna reflection and radiation characteristics.

These inferences initiated for optimization of the ground plane for maximum bandwidth performance. After exhaustive numerical and experimental analysis a broad band width of 60% is achieved by properly optimizing the ground plane dimensions. The optimum ground plane dimensions required to fix the resonance at a particular frequency is also derived from the numerical analysis. The detailed discussions of the truncated ground plane effects are presented in the following sections.

3.3.3 Truncated Ground plane effects on antenna characteristics

The initial investigation on the ground plane truncation reveals that by judiciously truncating the ground plane a second resonant mode can be excited near the fundamental resonant frequency. This resonant mode can be merged with the

fundamental monopole mode to yield wide band performance. To ensure the identical radiation characteristics in the entire band the ground plane dimensions should be selected in such a way that the edge currents on the ground plane do not alter the radiation characteristics. The investigations on the ground plane optimization for maximum bandwidth performance is elaborately presented in the next section.

3.3.3.1 Effect of ground plane width W_g

The investigations on the printed strip monopole presented in the last section reveals that there is a possibility of an additional resonance when the ground plane is altered. Hence for the present investigation the ground plane length is selected approximately as half wave length. The ground plane width is varied from infinite to finite dimensions. Effect of ground plane dimensions on antenna characteristics are illustrated in the following sections

Reflection characteristics

The ground plane width (W_g) is varied from 20 mm to 150 mm. The computed return loss characteristics are shown in Fig.3.7. From the reflection characteristics it is evident that when the width of the ground plane is varied there is a tendency for another resonance near the first fundamental mode. When the ground plane width is of the order of $0.5\lambda_d$, the antenna is resonating at 2.925GHz with bandwidth of 22%. When the ground plane width exceeds $1.0\lambda_d$ the frequency is lowered and an additional resonance at 3.2GHz is observed. But the impedance matching is poor in this case. Further optimization of W_g the fundamental resonance and additional resonance merge together and bandwidth is increased to 60%. But the width of the ground plane is a decisive parameter for the impedance matching of the antenna. When the ground plane length is approximately half wavelength then $W_g/2$ should be approximately half wavelength to provide better impedance matching at the fundamental resonant mode. Thus by properly optimizing the structural parameters the additional mode excited in the structure

can be merged with the fundamental mode to get a wide band performance. But the interesting inference obtained during these studies is that even though the second mode is not at all the second harmonic of the monopole mode the radiation characteristics of this mode are similar to the fundamental monopole mode. Hence properly truncating the ground plane width band widening can be achieved. Variation of resonant frequency and bandwidth of the antenna for different ground plane widths are presented in Fig3.8 (a) and (b) respectively. From the figure it is evident that when the ground plane width is approximately half wavelength there is no considerable change in the first fundamental mode. But when the width increases beyond full wavelength then due to the presence of additional mode the centre frequency of the operating band is shifted. At the optimum ground plane width centre frequency of the antenna system is due to the merging of the ground plane resonant mode and monopole mode. A maximum band width of 60% can be achieved by proper truncation of the ground plane. Computed FDTD results are verified by simulation and experiment and good agreement is observed. Computed maximum bandwidth is 58% while the experimental bandwidth is 60%.

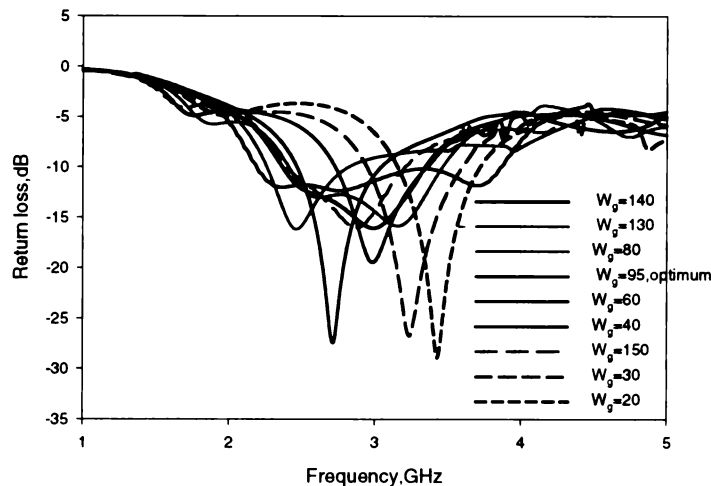


Fig 3.7 Computed return loss characteristics of the printed strip monopole antenna for W_g variation. $L_g = 45\text{mm}$, $L_m = 20\text{mm}$, $W_m = 3\text{mm}$, $\epsilon_r = 4.4$, $h = 1.6\text{mm}$

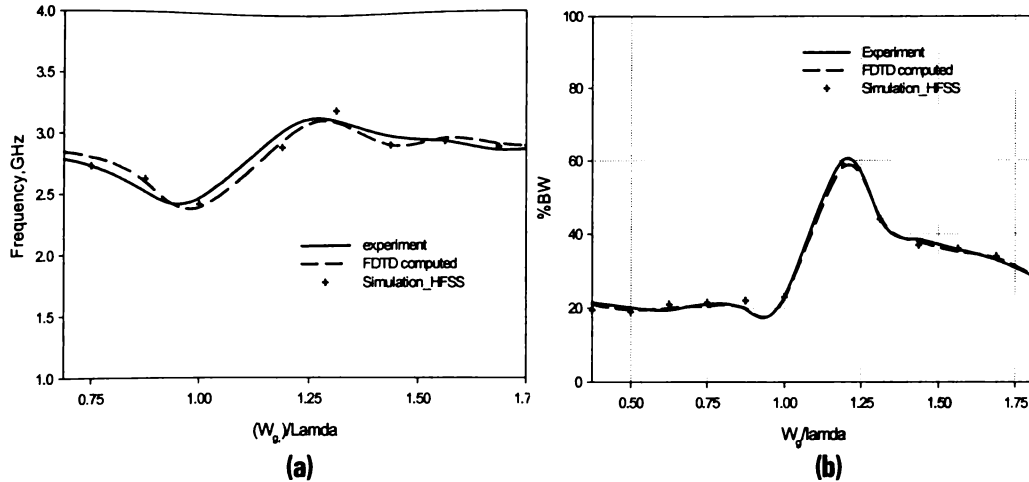


Fig 3.8 (a) Variation of resonant frequency with width of the ground plane W_g
(b) Variation of % bandwidth with W_g , $L_g = 45\text{mm}$, $L_m = 20\text{mm}$, $W_m = 3\text{mm}$, $\epsilon_r = 4.4$, $h = 1.6\text{mm}$

Radiation characteristics

The radiation characteristics of the wide band printed strip monopole can be explained from the simulated current distribution excited on the antenna structure.

In the present design a wide band width is obtained with the merging of two resonant modes. The first dip in the resonance is due to the monopole mode. From the surface current distribution in Fig.3.9 it is clearly evident that monopole is strongly radiating at this frequency and the ground plane has negligible effect on the radiation. At the fundamental resonance the electric field is polarized along Y direction. From the surface current distribution, it can be observed that the feeble current existing on either sides of the feed are equal and out of phase. This strongly indicates that there is negligible radiation from the ground plane and monopole alone is radiating at this frequency. Hence the radiation pattern at this frequency is typical omni directional in the H plane and figure of eight in the E plane. Since the contribution from the

ground plane is virtually small, the radiation from the monopole is along the y direction (along the length of the monopole)

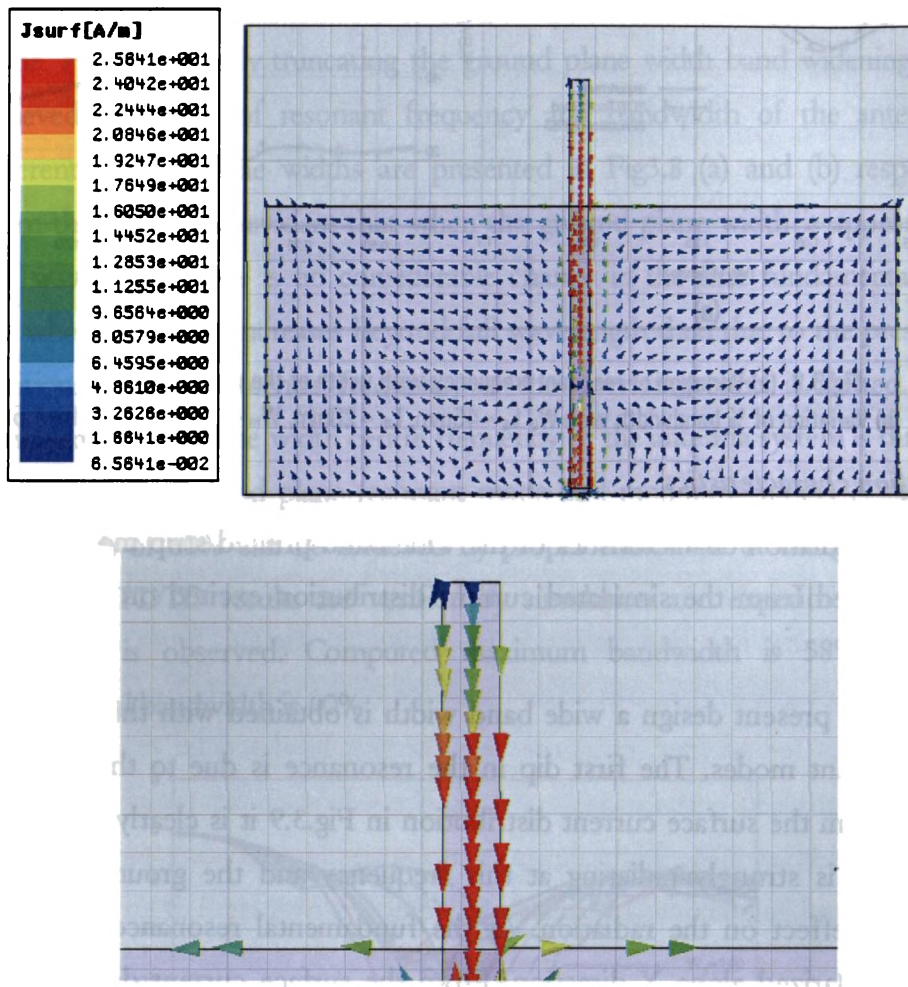
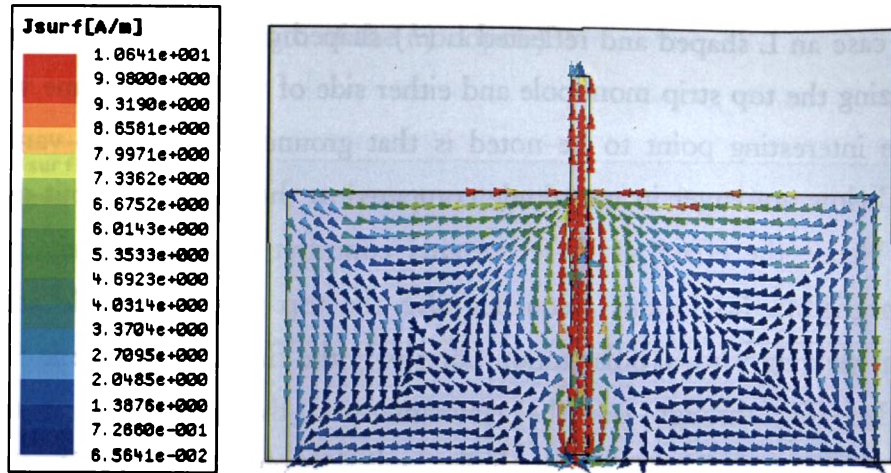


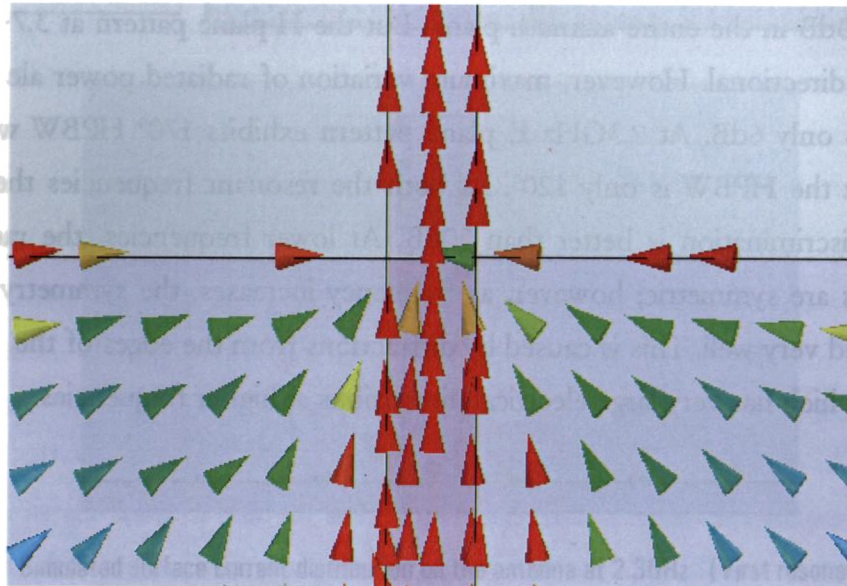
Fig 3.9 Simulated surface current distribution on the antenna at 2.3GHz (First resonance) $W_0 = 95\text{mm}$, $L_0 = 45\text{mm}$, $L_m = 20\text{mm}$, $W_m = 3\text{mm}$, $\epsilon_r = 4.4$, $h = 1.6\text{mm}$

A close look at the current distribution at the second resonance in the return loss response is shown in Fig.3.10.b. According to the current distribution even though the monopole and ground plane are separate entities,

they excites a common mode by utilizing the current paths as shown in Figure. In this case an L shaped and reflected L (\perp) shaped current paths are formed by utilizing the top strip monopole and either side of the ground plane width. But the interesting point to be noted is that ground strip current variation shown below are larger in magnitude compared to the earlier case but out of phase. Hence the effect of these currents contributing towards radiation is again negligible. So in this frequency also the top strip monopole acts as radiator, yielding vertical polarization same as in the first case. Hence it can be concluded that through out the resonant band the antenna is vertically polarized along Y direction with similar radiation characteristics. Computed radiation patterns in the bands are shown in Fig 3.11. It is found that at 2.3GHz the H plane pattern is almost omnidirectional. The maximum variation is only 3dB in the entire azimuth plane. But the H plane pattern at 3.7GHz is slightly directional. However, maximum variation of radiated power along this plane is only 6dB. At 2.3GHz E plane pattern exhibits 170° HPBW while at 3.7GHz the HPBW is only 120°. At both the resonant frequencies the cross polar discrimination is better than 20dB. At lower frequencies, the radiation patterns are symmetric; however, as frequency increases, the symmetry is not observed very well. This is caused by diffractions from the edges of the ground plane, which has very large electrical dimensions at higher frequencies.



(a)



(b)

Fig.3.10 (a) Simulated current distribution at the 3.7 GHz second dip of the wide band.
 $W_0 = 95\text{mm}$, $L_0 = 45\text{mm}$, $L_m = 20\text{mm}$, $W_m = 3\text{mm}$, $\epsilon_r = 4.4$, $h = 1.6\text{mm}$.
(b) Current distribution indicating L shaped and reflected L shaped paths.

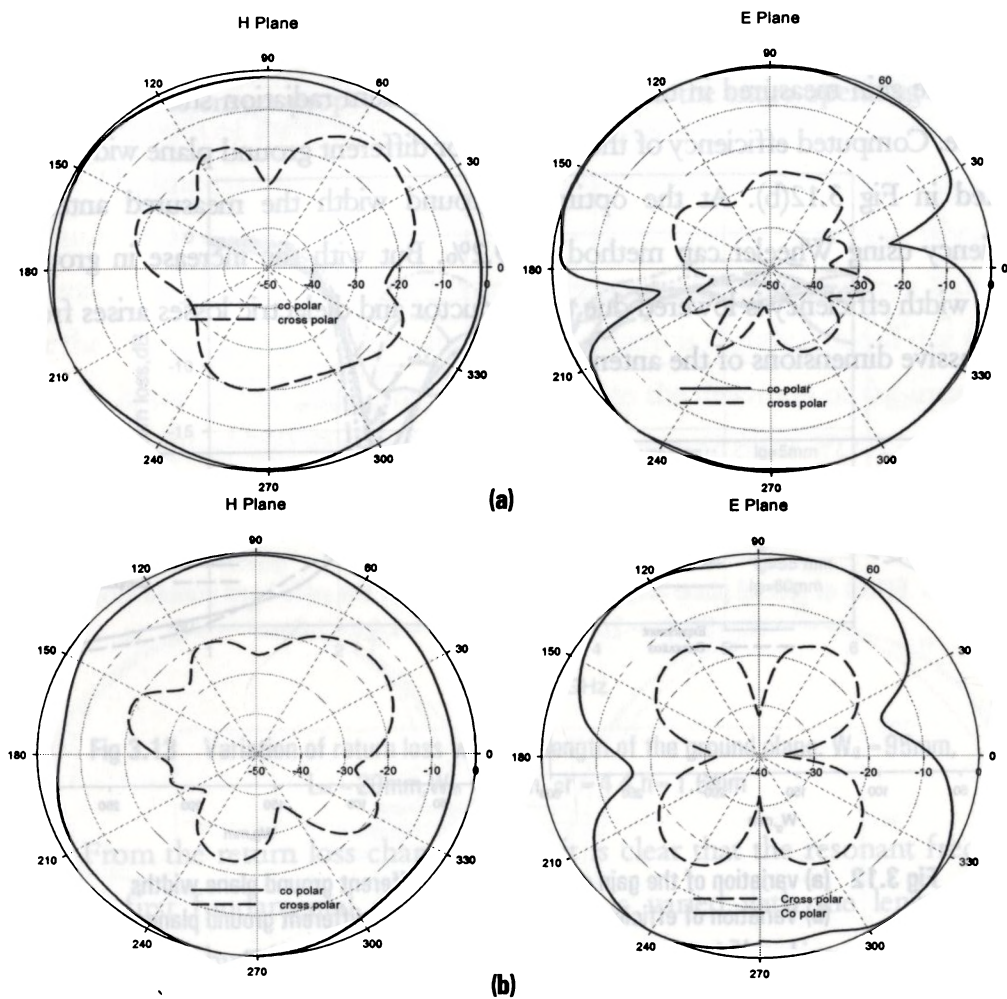


Fig 3.11 computed principal plane radiation patterns of the wide band printed strip monopole antenna,
 $W_0 = 95\text{mm}$, $L_0 = 45\text{mm}$, $L_m = 20\text{mm}$, $W_m = 3\text{mm}$, $\epsilon_f = 4.4$, $h = 1.6\text{mm}$
(a) at 2.3GHz
(b) at 3.7 GHz

Gain and efficiency

Gain of the antenna for different ground plane width is measured using gain transfer method and compared with theoretical computation (Fig.3.12 (a)). It is observed that when the ground plane width is very large the gain increases considerably because of the increased electrical size of the antenna. Moreover,

when the ground plane width is greater than the optimum value the pattern losses its omni directionality in one plane and becomes more directive with side lobes. Hence the gain measured in the direction of maximum radiation shows a gradual increase. Computed efficiency of the antenna for different ground plane widths are plotted in Fig 3.12(b). At the optimum ground width the measured antenna efficiency using Wheeler cap method is 89.2%. But with the increase in ground plane width efficiency is lowered due to conductor and dielectric losses arises from the massive dimensions of the antennas.

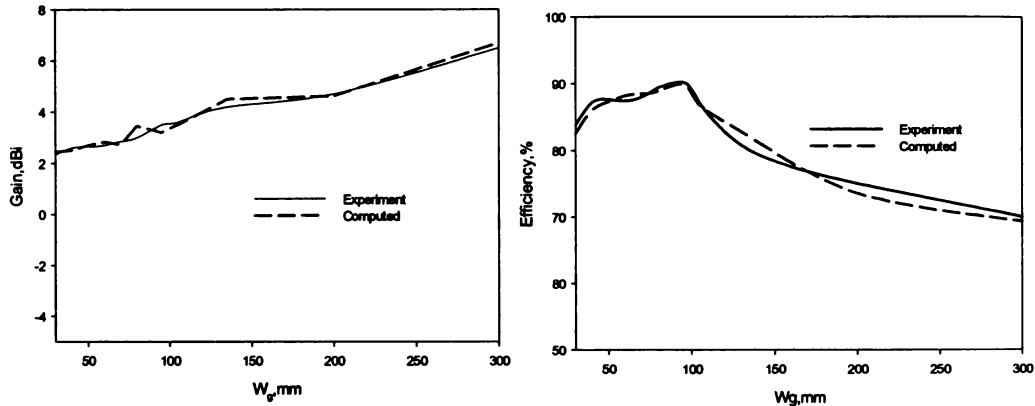


Fig 3.12 (a) variation of the gain of antenna with different ground plane widths
 (b) Variation of efficiency of the antenna with different ground plane widths.
 $L_g = 45\text{mm}$, $L_m = 20\text{mm}$, $W_m = 3\text{mm}$, $\epsilon_r = 4.4$, $h = 1.6\text{mm}$

3.3.3.2 Effect of ground plane length L_g

Return loss, resonant frequency and bandwidth

This section describes the radiation characteristics of the antenna by varying the ground plane length. Fig 3.13 shows the effect of variation of ground plane length on the reflection characteristics of the antenna. L_g is varied from 5 mm to 60 mm keeping the monopole length as constant. FDTD Computed return loss characteristics indicate that length of the ground plane is virtually independent of the resonant frequency. But the ground plane length is critical for merging the two resonant modes. This parametric study again ensures that the first dip in the wide

band response is solely due to the monopole mode and second resonance due to the width of the ground plane. But the ground length should be of the order of half wavelength to ensure proper impedance matching in the entire operating band.

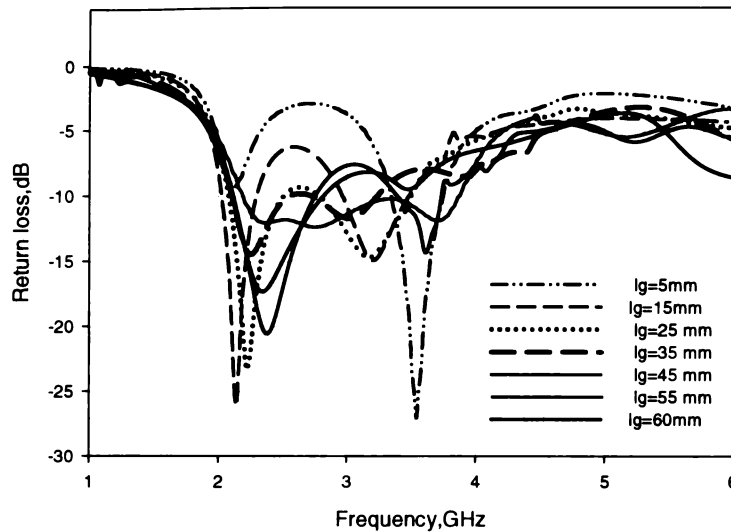


Fig 3.13 Variation of return loss with the length of the ground plane. $W_0 = 95\text{mm}$,
 $L_m = 20\text{mm}$, $W_m = 3\text{mm}$, $\epsilon_r = 4.4$, $h = 1.6\text{mm}$

From the return loss characteristics it is clear that the resonant frequency of the first fundamental monopole mode is varied with the length of the ground plane but the effect being negligible. But at the optimum length of the ground plane the two resonant modes merge together and a wide band width of 60% is obtained. This is shown as red curve in fig 3.13 with $l_g = 45\text{mm}$. Fig 3.14 shows the variation of resonant frequencies and bandwidths of the two modes for different ground plane lengths. The % bandwidth due to the monopole mode alone is of the order of 20%. At optimum length when the monopole mode merges with newly excited mode wide band response is achieved. The variation of % bandwidth with the length of the ground plane is depicted in Fig 3.15.

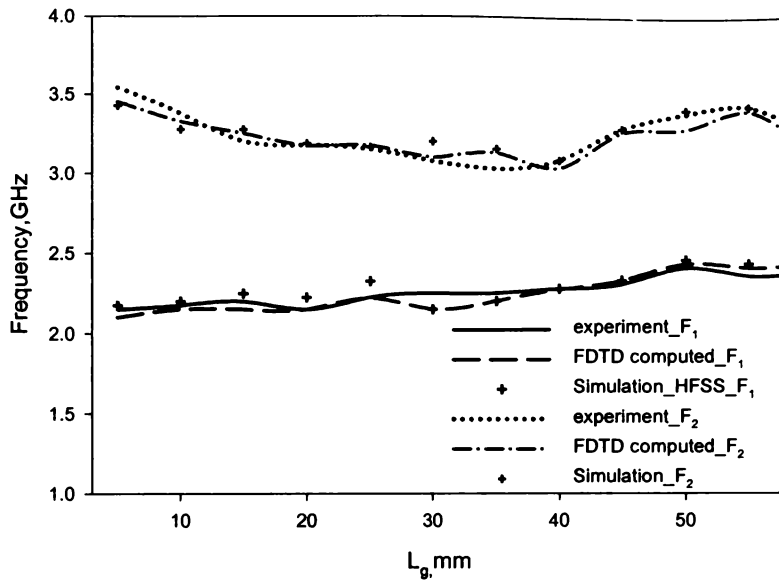


Fig 3.14 Effect of ground plane length on the two modes of the wide band printed strip design.
 $W_g = 95, L_m = 20, W_m = 3\text{mm}, \epsilon_r = 4.4, h = 1.6\text{mm}$

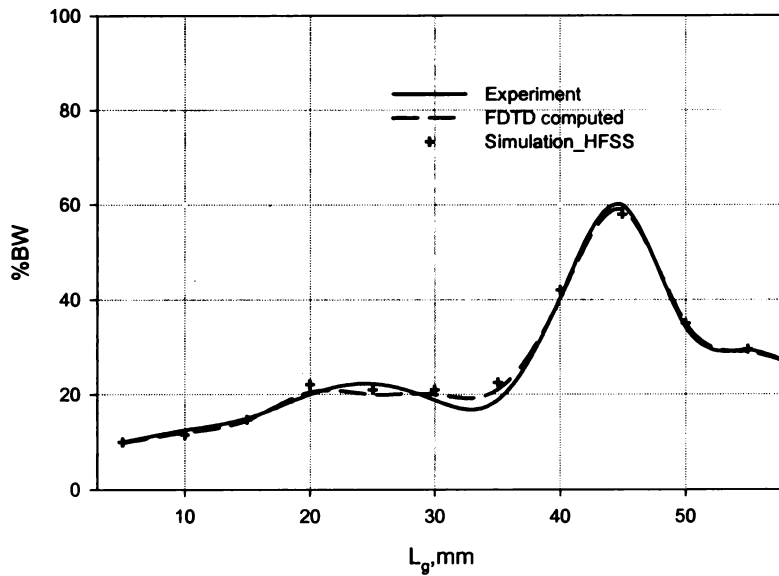


Fig 3.15 Variation of % bandwidth with the length of the ground plane.
 $W_g = 95\text{mm}, L_m = 20\text{mm}, W_m = 3\text{mm}, \epsilon_r = 4.4, h = 1.6\text{mm}$

Radiation pattern

Radiation characteristics studies reveal the ground plane length variation affects the nulls of the E plane pattern where as the beam width is varied slightly in the H plane pattern. When the ground plane length is very low the E plane patterns become more dipole like than classical monopoles. Moreover, when the ground plane length is very high it acts as reflector and back radiation is reduced. For the H plane pattern the broadness of the pattern is slightly reduced due to the increase in the ground plane length. This is due to the distortion of the image due to the edge diffractions occurring from large sized ground plane. FDTD computed radiation patterns for different ground plane length is shown in Fig.3.16

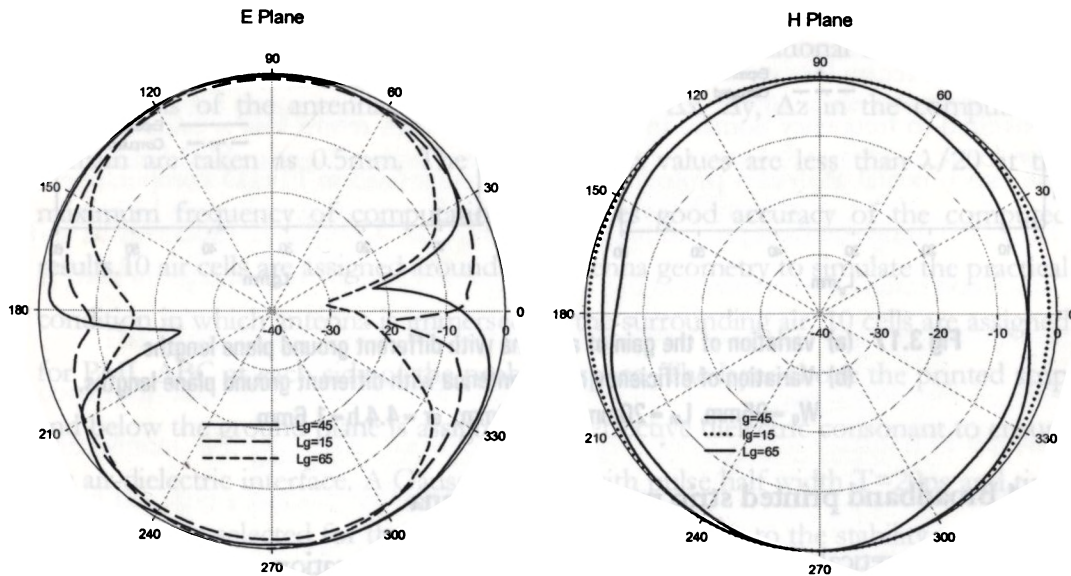


Fig.3.16 Computed radiation patterns for different ground plane lengths.

$W_0 = 95\text{mm}$, $L_m = 20\text{mm}$, $W_m = 3\text{mm}$, $\epsilon_r = 4.4$, $h = 1.6\text{mm}$

Gain and efficiency

Gain variation of the printed strip monopole antenna for different ground plane length is depicted in Fig 3.17(a). From the figure it can be observed that

there is negligible effect of the ground plane on the gain of the antenna. But as ground plane length is very much higher than the monopole length then gain increases slightly due the decrease in beam width of the pattern. In other words pattern becomes directional with the increase in the ground plane length. Antenna efficiency is slightly reduced due to the large variation in computed E field due to the variation in ground plane length. Variation of efficiency with ground plane length is shown in Fig. 3.17(b)

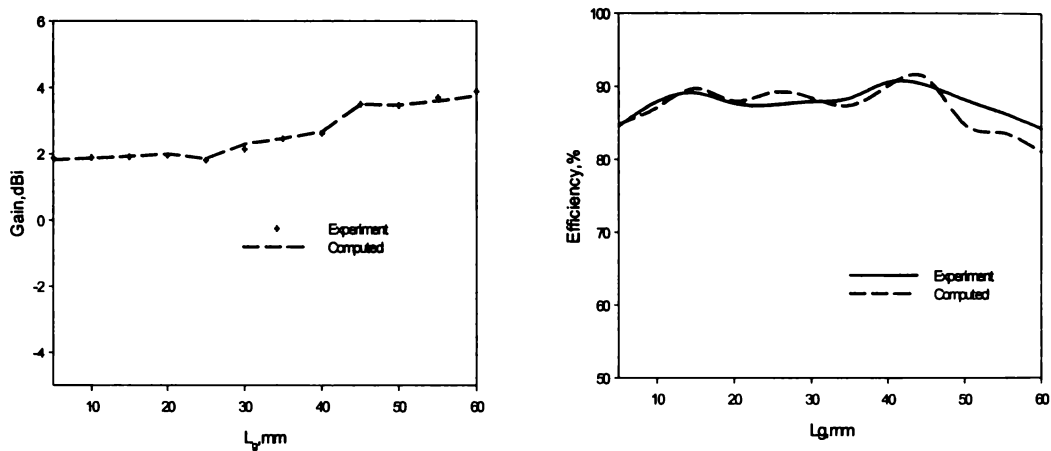


Fig 3.17 (a) variation of the gain of antenna with different ground plane lengths
 (b) Variation of efficiency of the antenna with different ground plane lengths.
 $W_0 = 95\text{mm}$, $L_m = 20\text{mm}$, $W_m = 3\text{mm}$, $\epsilon_r = 4.4$, $h = 1.6\text{mm}$

3.3.4 Broadband printed strip monopole antenna

The theoretical investigations on ground plane truncation arrives at a novel conclusion that truncated ground plane is an important concept for the design of printed strip monopole antennas with wide impedance bandwidth. The ground plane currents can be suitably modified and effectively utilized for dual band or broad band applications. A detailed description of the strip monopole antenna with maximum bandwidth obtained after rigorous ground plane optimization is presented in the following section. FDTD computed field distributions are utilized to illustrate

the band widening behavior of printed strip monopole. These studies give an insight to actual resonance and radiation phenomenon explained in the previous section. The exhaustive numerical analysis arrived at a conjecture that a quarter wavelength monopole resonating at 2.4 GHz excited by a microstrip line of ground plane dimensions $95 \times 45 \text{ mm}^2$ yields a maximum bandwidth of 60%. These results are confirmed with experiment. A strip monopole of length $L_m = 20 \text{ mm}$ and width $W_m = 3 \text{ mm}$ is printed on a substrate of dielectric constant $\epsilon_r = 4.4$ and thickness 1.6 mm . The strip monopole is excited with a microstrip line of characteristic impedance 50Ω . Width of the strip is 3 mm , same as that of a 50Ω microstrip line. From the previous analysis the optimum ground plane dimensions of the microstrip line are selected as $W_g = 95 \text{ mm}$ and $L_g = 45 \text{ mm}$. For the theoretical analysis the antenna is modeled using FDTD algorithm. Total computational domain used for the analysis of the antenna is $230 \times 180 \times 23$ cells. Δx , Δy , Δz in the computation domain are taken as 0.5 mm . The discretization values are less than $\lambda/20$ at the maximum frequency of computation and gives good accuracy of the computed results. 10 air cells are assigned around the antenna geometry to simulate the practical condition in which antenna is immersed in the surrounding air. 10 cells are assigned for PML ABC at each side of the problem space. The layer above the printed strip and below the ground plane is assigned with effective dielectric constant to ensure the air-dielectric interface. A Gaussian pulse with pulse half width $T = 20 \text{ ps}$ and time delay $t_0 = 3T$ is selected for the present analysis. According to the stability criteria the calculated time step is $\Delta t = 0.95 \text{ ps}$. Leubbers feed model is employed to implement the microstrip line. Gaussian pulse value is employed as the voltage sources for calculating the time domain response. The computed time domain response at the feed point is depicted in Fig 3.18. The electric field component is settled by around 5000 time steps.

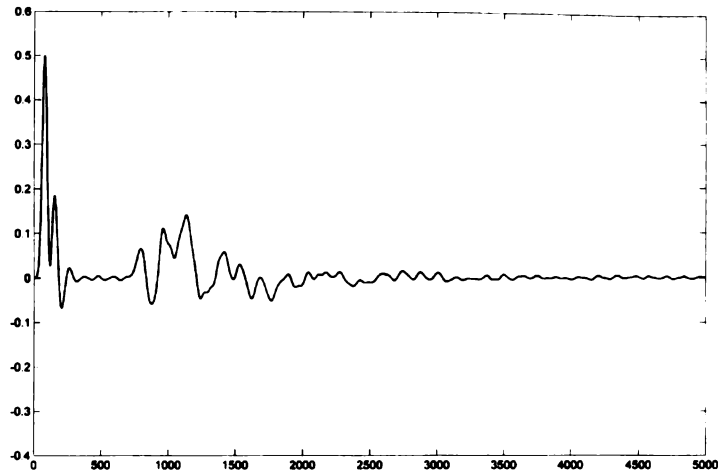


Fig. 3.18 Computed time domain characteristics at the feed point

When the launched Gaussian pulse is completely settled down in the computation domain the return loss value of the device is calculated. The time domain data are first converted to frequency domain by taking FFT and then return loss is calculated. For the experimental analysis a prototype of the antenna used in FDTD computation is fabricated using standard photolithographic techniques. Computed, experimental and simulation results are compared in Fig. 3.19.

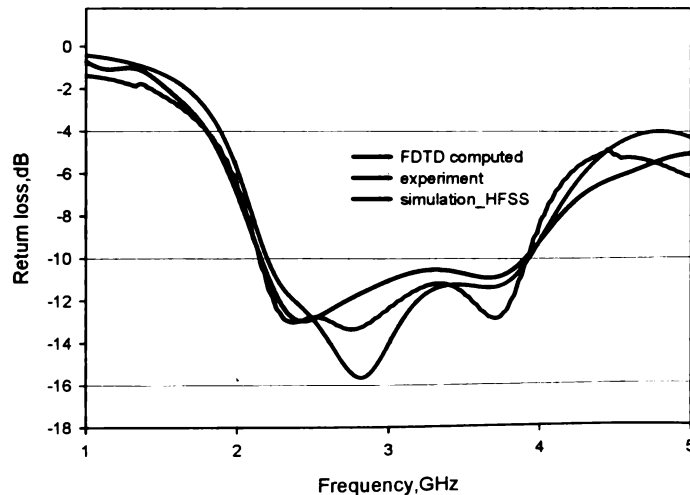


Fig 3.19 Reflection characteristics of the wide band printed strip monopole antenna.
 $W_n = 95\text{mm}$, $l_n = 45\text{mm}$, $l_m = 20\text{mm}$, $W_m = 3\text{mm}$, $\epsilon_r = 4.4$, $h = 1.6\text{mm}$

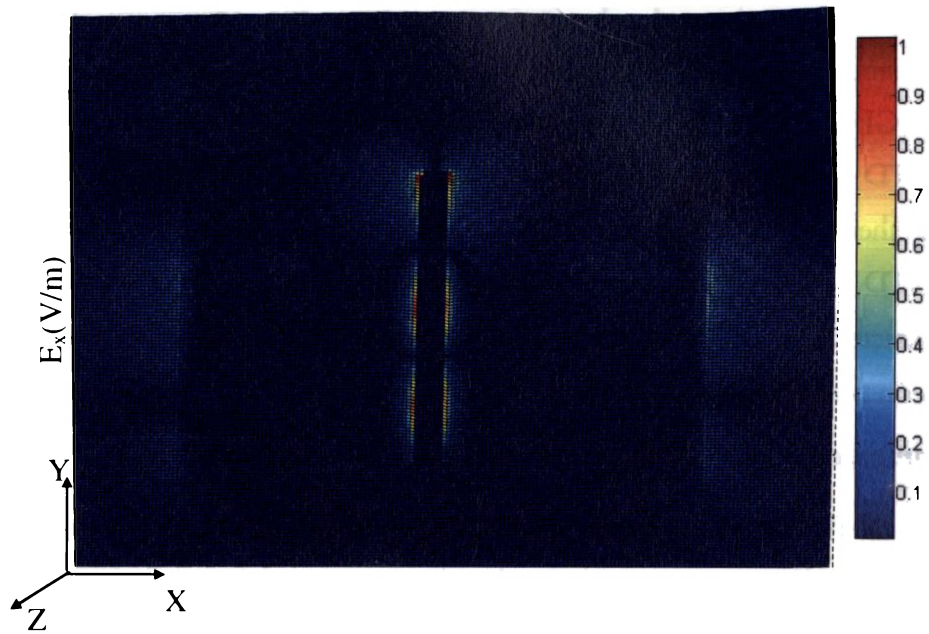
The experimental observations confirm the theoretical predications. Measured return loss characteristics exhibit a wide band width 1.78 GHz from 2.15GHz to 3.93GHz corresponding to a fractional bandwidth of 60%. Computed FDTD results shows that antenna resonates with two different modes merged together to yield a wide band width 1.7GHz from 2.175GHz to 3.925 GHz. The FDTD results differ from the experimental results only by 1.68%. Return loss characteristics of the antenna simulated using HFSS again confirms that the theoretical prediction of the wide band performance.

Computed E field values at different layers of the problem space

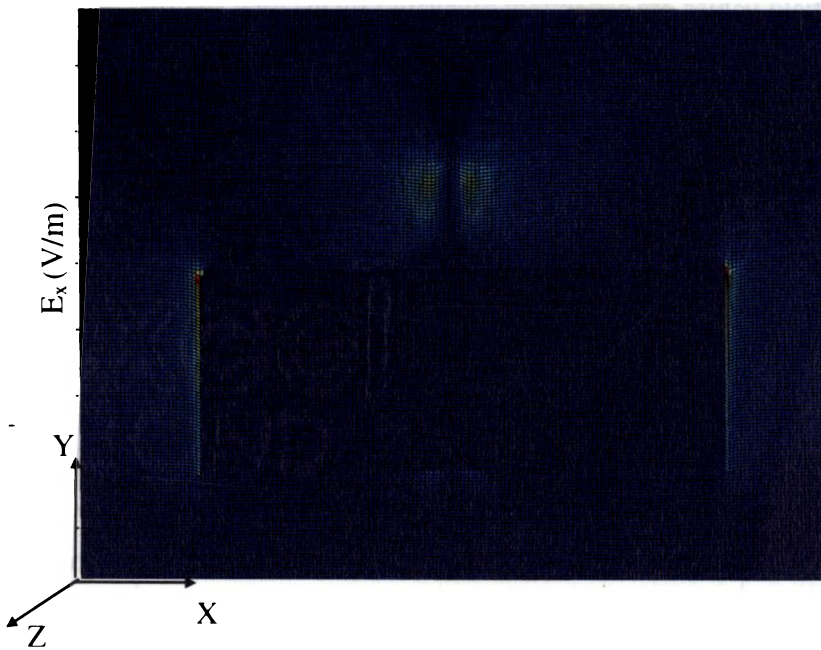
The reflection characteristics of the printed strip monopole antenna discussed in the previous section concludes that the antenna exhibits wide band due to the merging of two resonant modes with similar radiation characteristics. Computed E field values are presented at the two resonant modes of the wide operating band. Computed field values are separately calculated by exciting the problem space with sinusoidal excitation at the two desired frequencies of interest.

E field component at first resonance.

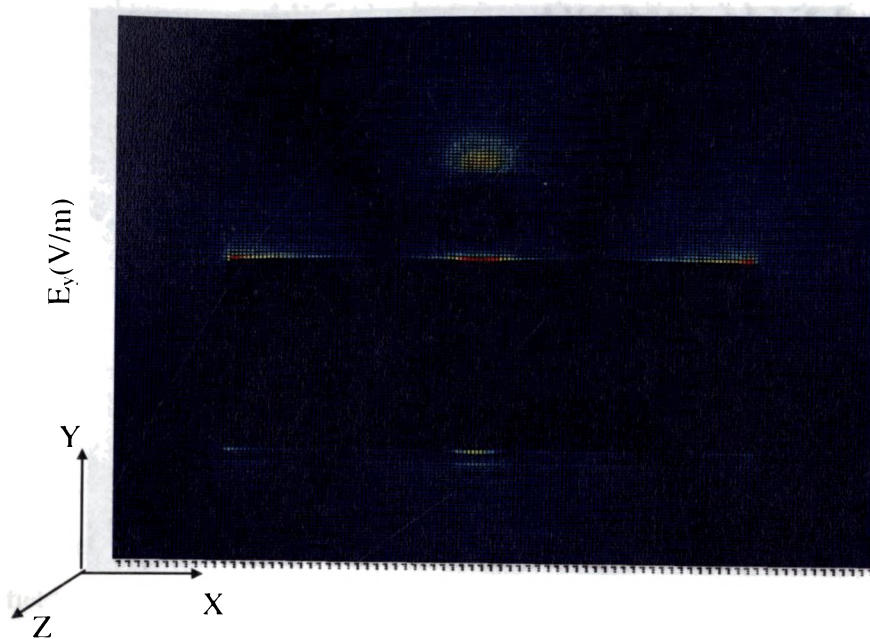
The Computed E field distribution at the first dip of the wide band response corresponding to the monopole mode is shown in Fig.3.20. From the E_x field component, it is observed that there is a quarter wave length variation of the field along the strip length. E_x field is maximum at the open circuit end of the strip and minimum at the ground end. In this case the microstrip line is in the propagating mode. The E_x field variation on the ground at the fundamental mode indicates that there is no significant variation of the field at the ground truncation edges. Even though there is a feeble variation of the field along the width of the truncated edges, the effect in resonance or radiation is negligible. Hence, it can be concluded that at the fundamental mode strip monopole is radiating strongly.



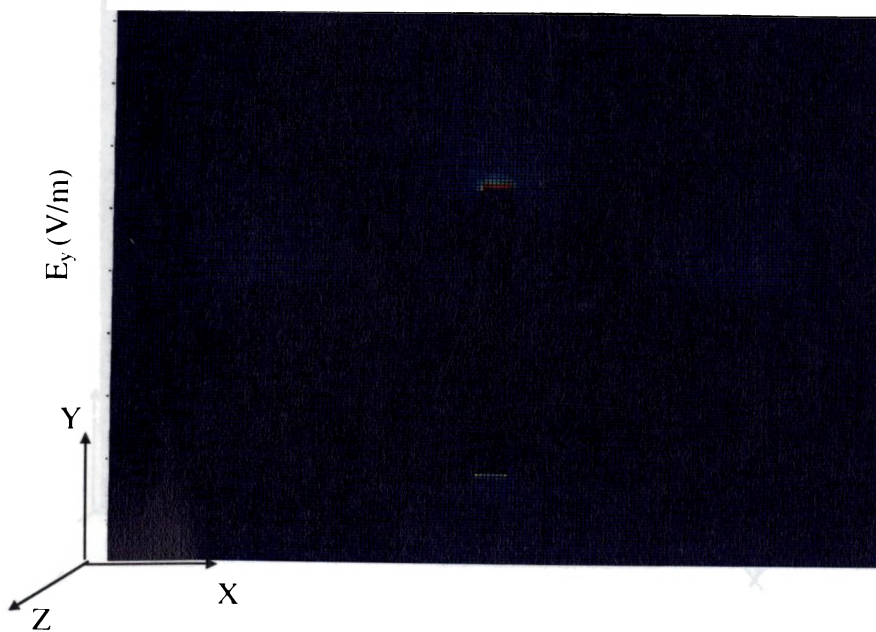
3.20 (a) Computed E_x component at the top strip at 2.4GHz
 $W_0 = 95\text{mm}$, $L_0 = 45\text{mm}$, $L_m = 20\text{mm}$, $W_m = 3\text{mm}$, $\epsilon_r = 4.4$, $h = 1.6\text{mm}$



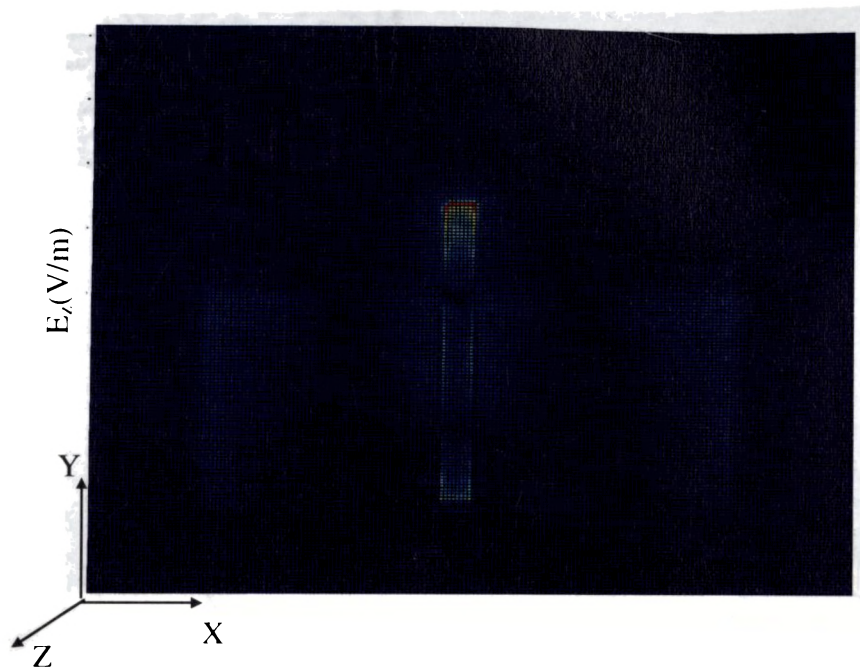
3.20 (b) Computed E_x component at the bottom ground at 2.4GHz
 $W_0 = 95\text{mm}$, $L_0 = 45\text{mm}$, $L_m = 20\text{mm}$, $W_m = 3\text{mm}$, $\epsilon_r = 4.4$, $h = 1.6\text{mm}$



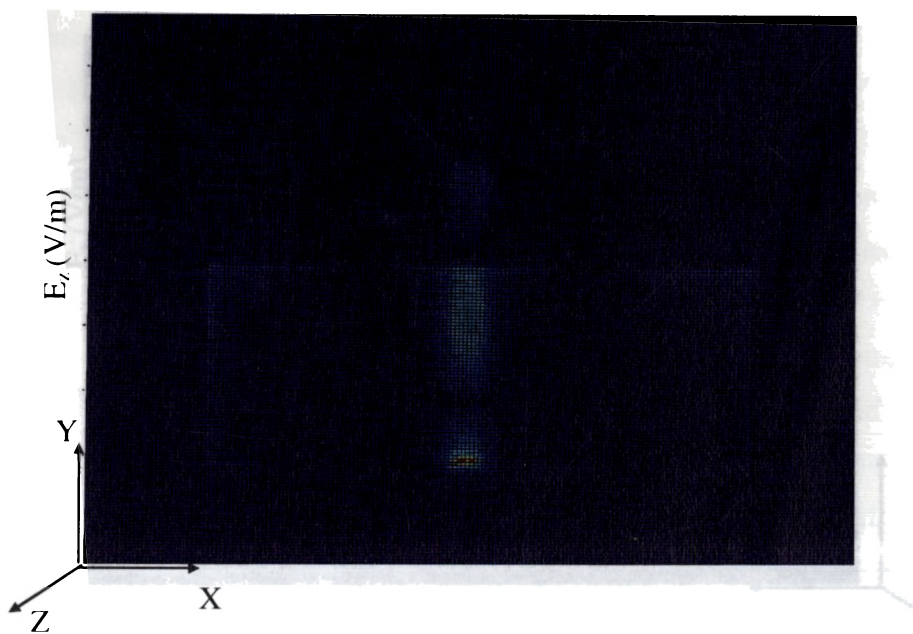
3.20 (c) Computed E_y component at the bottom ground
 $W_g = 95\text{mm}$, $L_g = 45\text{mm}$, $L_m = 20\text{mm}$, $W_m = 3\text{mm}$, $\epsilon_r = 4.4$, $h = 1.6\text{mm}$



3.20 (d) Computed E_y component at the strip
 $W_g = 95\text{mm}$, $L_g = 45\text{mm}$, $L_m = 20\text{mm}$, $W_m = 3\text{mm}$, $\epsilon_r = 4.4$, $h = 1.6\text{mm}$

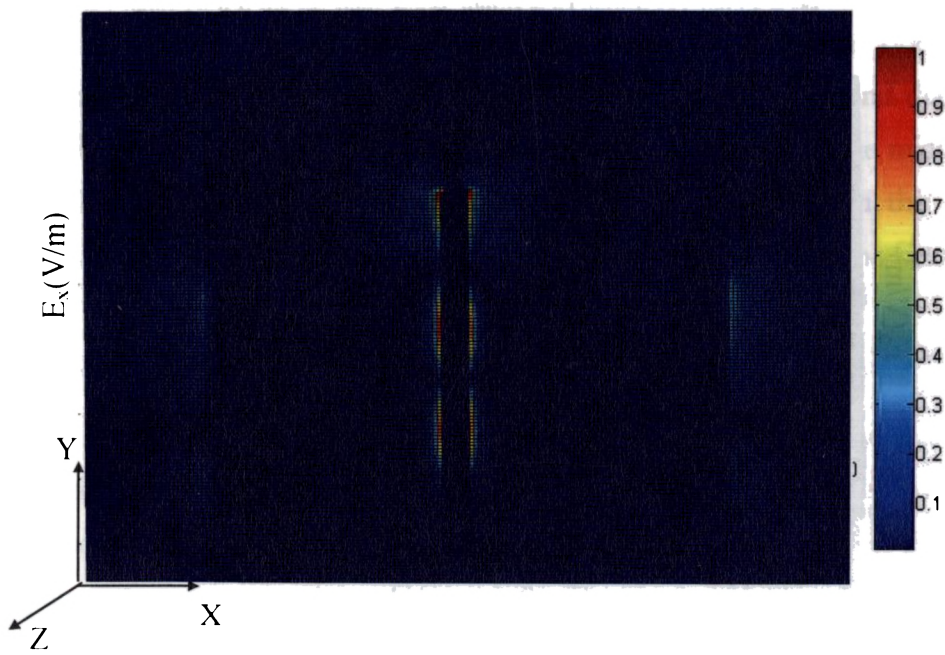


3.20 (e) Computed E_z component at the top strip

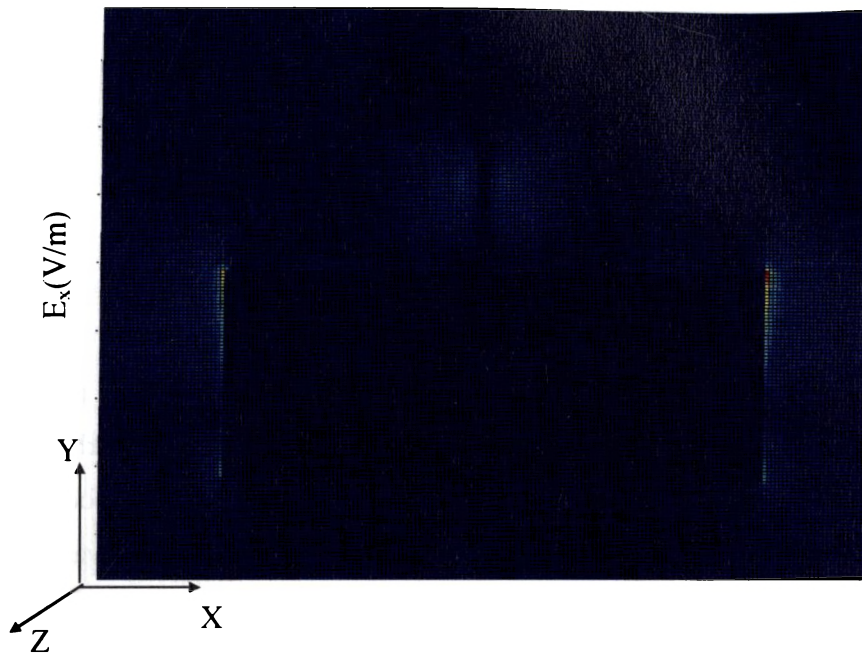


3.20 (f) Computed E_z component at the bottom ground

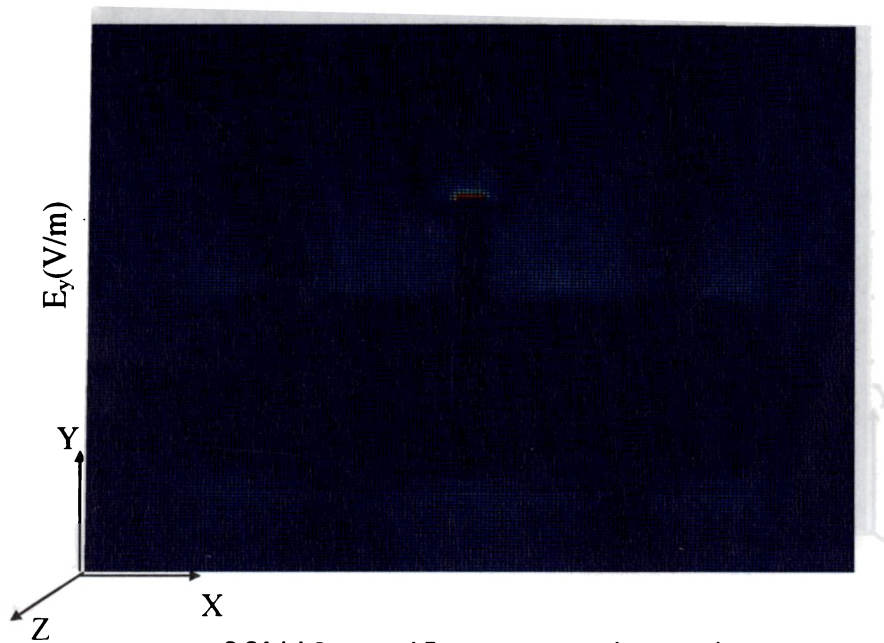
From the computed E field values, it can be concluded that the fundamental resonant mode corresponding to the first dip in the wide return loss response, the monopole is strongly radiating. The effect of ground plane truncation in this mode is negligible even though there is feeble variation of field along the width of the truncated ground plane. For large values of the ground plane width the truncation edge effect becomes strong which will affect the radiation pattern considerably. But for smaller ground plane dimension this effect is negligible and radiation pattern is omnidirectional in the XY plane and figure of eight in the EZ plane with polarization along Y direction. Computed E field corresponding to the second resonant mode is shown in Fig 3.21. From the field variations it can be inferred that at the second mode there is an L shaped and reflected L shaped variation of the field due to the strong coupling between the ground plane and radiating strip. This full wave variation corresponds to the second resonance.



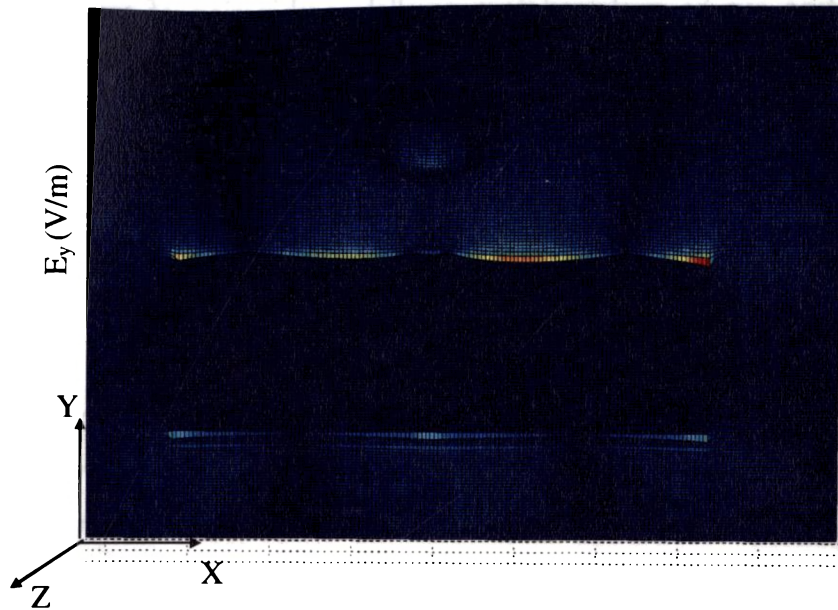
3.21 (a) Computed E_x component at the top strip
 $W_g = 95\text{mm}$, $L_g = 45\text{mm}$, $L_m = 20\text{mm}$, $W_m = 3\text{mm}$, $\epsilon_r = 4.4$, $h = 1.6\text{mm}$



3.21 (b) Computed E_x component at the bottom ground
 $W_0 = 95\text{mm}, L_0 = 45\text{mm}, L_m = 20\text{mm}, W_m = 3\text{mm}, \epsilon_r = 4.4, h = 1.6\text{mm}$



3.21 (c) Computed E_y component at the top strip
 $W_0 = 95\text{mm}, L_0 = 45\text{mm}, L_m = 20\text{mm}, W_m = 3\text{mm}, \epsilon_r = 4.4, h = 1.6\text{mm}$



3.21 (d) Computed E_y component at the bottom ground
 $W_g = 95\text{mm}$, $L_g = 45\text{mm}$, $L_m = 20\text{mm}$, $W_m = 3\text{mm}$, $\epsilon_r = 4.4$, $h = 1.6\text{mm}$

From the computed field values inference obtained for wide band operation is explained in the following section. From the earlier analysis it is found that the electric fields at the width of the truncation edges on either sides of the midpoint are equal in magnitude and out of phase. So the contribution from this field cancels each other at the far field. So the entire radiation is only from the fields on the strips.

Principle of wide band operation

From the computed E field it can be observed that in the case of Microstrip line fed printed strip monopole two distinct resonance are observed and these two modes merged together to yield a wide band response. But the computed field components confirm that the second resonance is not the second harmonic frequency of the fundamental resonant mode. But it is due to the effect of an interesting phenomenon occurring in the truncated ground plane of the monopole excited by microstrip line. A monopole over a truncated

ground plane can be explained as a parallel combination of two asymmetric dipoles (an L shaped and reflected L shaped) excited at the common point by a microstrip line as shown in Fig. 3.22.

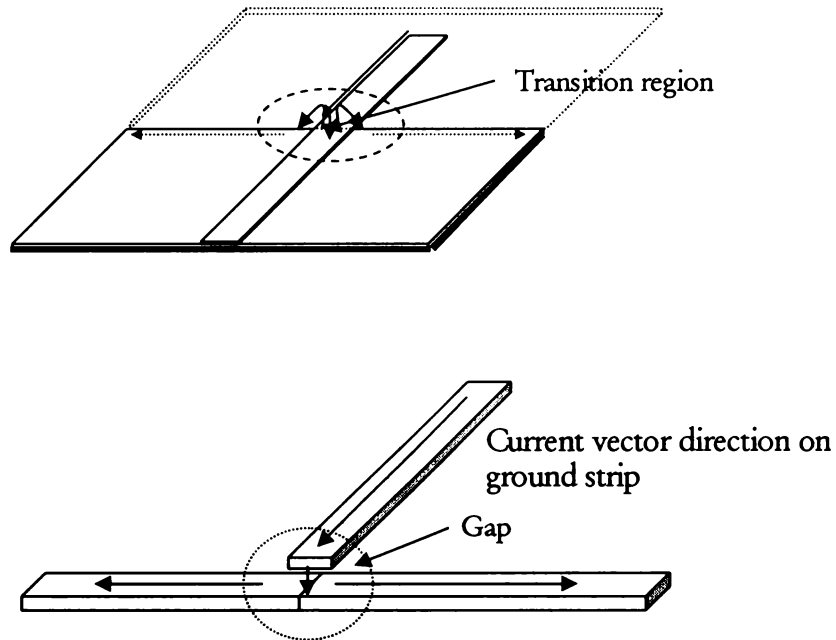


Fig 3.22 (a) vertical monopole on truncated ground plane with an L shaped and reflected L shaped asymmetric dipoles
 (b) Asymmetric dipole with gap source

A conventional dipole usually consists of two metallic strips each of which is quarter wavelength and excited exactly at the middle. Even half wavelength line excited at middle will produce a current distribution on it for achieving the dipole pattern. In conventional printed dipole antenna systems excited by microstrip line, several technologies are employed to transfer the microstrip line transmission line mode to the dipole mode of the antenna. Techniques such as ground tapering near the dipole, balanced parallel wire designs and microstrip to slot line transitions are usually employed to obtain an unbalanced to balance (baluns) transition. These

baluns are not broadband in performance and thus dipoles employing these techniques are high Q devices.

In the present design of wide band printed strip monopole over a truncated ground plane, the Quasi TEM mode propagating through the microstrip line encounters a discontinuity at the microstrip transition region. For the second resonance case the field forms two asymmetric dipole configurations through the substrate. In other word the current distribution established on the monopole strip and one side of the ground plane truncation along the width forms two asymmetric dipoles. The excitation mechanism at the second resonance for these asymmetric dipoles is shown in Fig.3.22 (b). The important point to be noted that two arms of the dipoles are lying on the two layers of the substrate. Hence substrate thickness will affect the impedance matching of the antenna at the frequency where it behaves as asymmetric dipole. These two dipoles with a full wave length field variation (Refer Fig.3.10 for better clarity) corresponding to second resonant frequency are matched by the same microstrip line used for exciting the first monopole mode. But according to the current distribution the horizontal current paths are 180° out of phase and hence this field is cancelled at the far field. In effect the vertical strip is strongly radiating at the second resonance. But the current illumination in this case is slightly different from the monopole mode hence a slightly different radiation characteristics (in terms of directivity) but with exactly similar monopole like radiation pattern is obtained for the second resonant mode. This implies that in the printed strip monopoles excited by truncated ground plane, by properly selecting the ground plane width two different modes with exactly similar radiation characteristics can be merged together to form wide band. Even though the current distribution on the edges along the width of the truncated ground plane is essential for this mode to sustain, it is not at all contributing in the radiation. The radiation can be approximated to

the radiation from a vertical metallic strip printed on the substrate. Thus similar to the monopole mode an omni directional H plane pattern and figure of eight E plane pattern is resulted from this new resonant mode. It should be noted that the current distribution is more pronounced at the ground plane truncation edges and the current is not spread on the entire ground portion. In effect we can utilize the ground plane for a new resonance, with out affecting the propagating mode of the microstrip line and usual function of the ground plane in typical communication system where the ground plane is shared by the antenna and RF circuit. It can be concluded that truncated ground plane is suitable concept for wide band antenna applications.

Experimental and Computed radiation patterns of the wide band printed strip monopole antenna

The inference obtained from the above discussion concluded that the radiation pattern of a wide band printed strip monopole over a truncated ground plane is nearly omni directional in one plane and figure of eight in the other plane. Fig 3.23 shows the experimental and computed radiation patterns at the start, centre and end frequency points of the wide band monopole. Experimental radiation pattern are nearly similar to the theoretically computed radiation patterns. The antenna has almost identical radiation patterns through out the 2:1 VSWR bandwidth. Moreover, antenna exhibits cross polar level better than 20dB in both the planes. At higher frequencies small distortion in the pattern is observed because the edge currents near the ground truncation becomes more dominant at higher frequencies.

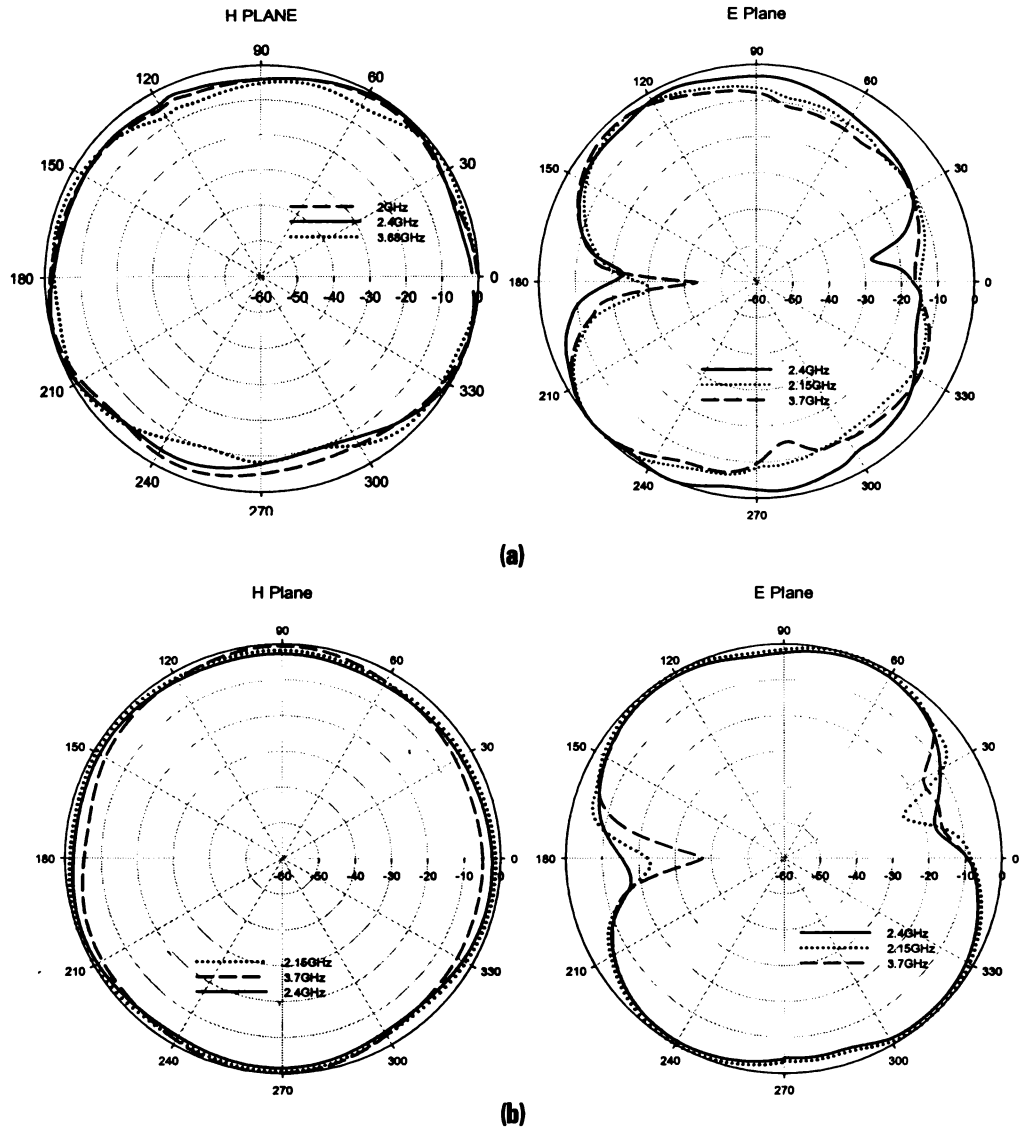


Fig 3.23 Principal plane radiation patterns of the wide band printed strip monopole antenna.

$W_0 = 95\text{mm}$, $L_0 = 45\text{mm}$, $L_m = 20\text{mm}$, $W_m = 3\text{mm}$, $\epsilon_r = 4.4$, $h = 1.6\text{mm}$.

(a) experimental

(b) FDTD computed

Gain and efficiency of the wide band printed strip monopole antenna.

Gain of the antenna measured using gain transfer method is shown in Fig 3.24. Antenna exhibits an average gain of 3.5dBi in the operating band. Gain variations are less than 1.5dBi in the entire operating band. At higher frequencies gain is increased considerably due to the slight directional characteristics. Computed average gain of the antenna is 3.62dBi which is in good agreement with the measured value of 3.5dBi. Measured antenna efficiency at 3.1 GHz is 89.9% where as computed efficiency is 90.2%.

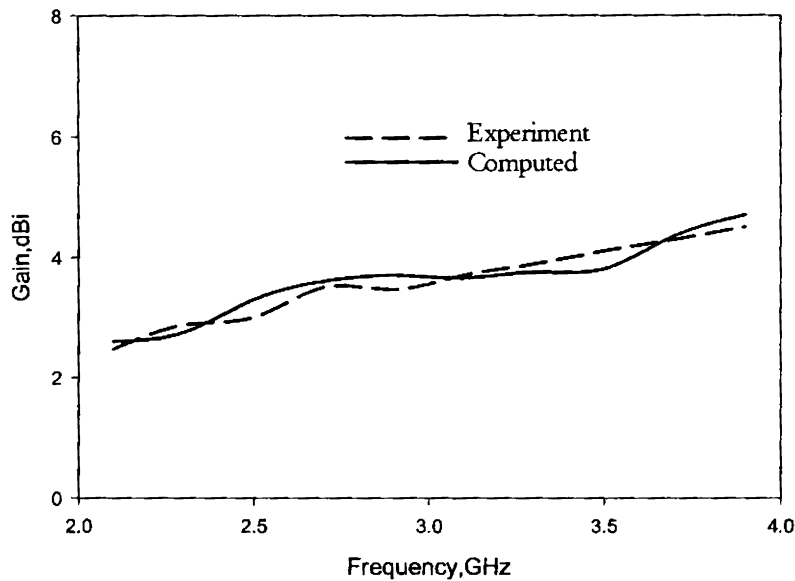


Fig 3.24. Experimental and computed gain of the wide band printed strip monopole antenna.
 $W_g = 95\text{mm}$, $L_g = 45\text{mm}$, $L_m = 20\text{mm}$, $W_m = 3\text{mm}$, $\epsilon_r = 4.4$, $h = 1.6\text{mm}$.

Experimental and theoretical radiation characteristics of wide band printed strip monopole antenna is summarized in Table 3.3

Table 3.3 Characteristics of Wide band printed monopole antenna,
 $W_0 = 95$ mm, $L_0 = 45$ mm, $L_m = 20$ mm, $W_m = 3$ mm, $\epsilon_r = 4.4$, $h = 1.6$ mm.

Characteristics	Experiment	Theory
Resonant frequency	2.425GHz , 3.65GHz	2.36GHz, 3.7GHz
Band width	1.78GHz (2.15GHz-3.93GHz)	1.7GHz (2.175GHz-3.925GHz)
Radiation pattern	H plane : Omni directional E plane: Figure of eight	H plane : Omni directional E plane: Figure of eight
HPBW	E plane : 100° H plane: 215°	E plane : 90° H plane: 220°
Cross polar level	H plane: 18dB E plane: 20dB	H plane: 22dB E plane: 22dB
Gain	3.5dBi	3.62 dBi
Efficiency	89.9%	90.2%

3.3.5 Parametric analysis

From the ground plane optimization studies of quarter wavelength monopole antenna excited by microstrip feed line we derived an optimum ground plane for wide band operation. In this section the effect of the strip dimensions and substrate parameters on the wide band antenna performance is illustrated. This parametric analysis led to the formulation of simple design equations to design the wide band printed strip monopole antenna for any wireless communication band of interest.

3.3.5.1 Effect of monopole length L_m

Fig 3.25 shows the effect of length of the monopole on the wide band printed monopole antenna. When monopole length is varied the first resonance corresponding to the monopole mode is significantly affected. For the second

resonant mode the length of the vertical monopole along with the ground plane width is decisive for forming the two asymmetric dipoles. Hence variation in length of the monopole slightly affects the second resonance mode. But when the monopole length is increased the two modes separates as the width of the ground plane is not sufficient to merge them. This observation again confirms our earlier argument that the first resonance is solely due to the strip monopole and the second mode is the combined effect of strip monopole and the ground plane. It is found that when the length is large the first resonance occurs at lower frequency as expected. This resonance frequency can be increased by decreasing the length of the radiating strip. Almost similar behavior is observed for second resonant mode also. As stated earlier this variation is rather small compared to the first resonance. Hence by proper selection of the length of the radiating strip and ground plane the two resonant modes can be merged together to obtain large bandwidth.

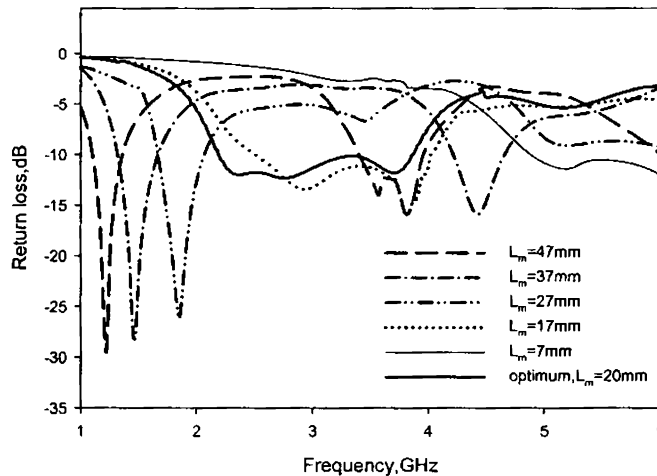


Fig 3.25 Effect of length of the monopole L_m on the reflection characteristics.

$W_g = 95\text{mm}$, $L_g = 45\text{mm}$, $W_m = 3\text{mm}$, $\epsilon_r = 4.4$, $h = 1.6\text{mm}$.

An important inference arrived from the parametric study of the monopole length is that a quarter wavelength monopole excited by microstrip line with

truncated ground plane will yield wide band response only when the ground plane length is twice the monopole length or in other words ground plane length should be half wavelength.

3.3.5.2 Effect of monopole width W_m

In the previous analysis width of the strip is sets as width of the microstrip line. The width of the monopole is varied from 3 mm to 25mm to study the effect on the 2:1 VSWR bandwidth. Fig 3.26 shows the variation of reflection characteristics with width of the monopole. When width of the monopole is increased higher order resonant modes occurs in the radiating structure. But the impedance matching for the higher order resonant modes is poor due to the coupling between the ground plane. An important thing to be noted here is that there should be minimum separation between the monopole and truncation edge to avoid the capacitive coupling which affects the impedance matching. In this case the separation between the monopole and ground plane is optimized for good impedance matching as 1.5mm. This separation is very critical to merge the different resonant modes to yield ultra wide band response. When the width of the monopole is 15mm with a separation gap $g=1.5\text{mm}$ the antenna exhibits a 2:1 VSWR bandwidth of 4.4:1. The coupling between the truncated ground plane and the monopole acts as an impedance matching element to control the impedance matching of the different resonant modes. FDTD computed results satisfies 10dB return loss requirement from 1.87GHz to 8.2GHz corresponding to extremely wide band operation. A wide band operation is resulted due to the merging of different modes with almost similar radiation characteristics. The variation of bandwidth performance with the width of the monopole is presented in Table 3.4.

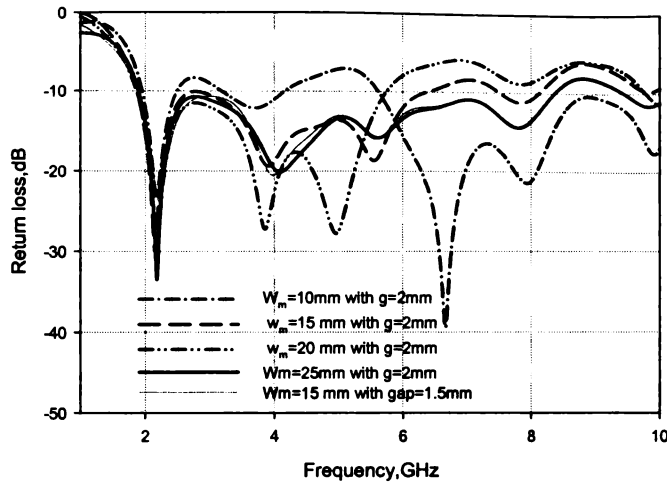


Fig.3.26. Variation of return loss with width of the monopole.
 $W_0 = 95\text{mm}$, $L_0 = 45\text{mm}$, $L_m = 20\text{mm}$, $\epsilon_r = 4.4$, $h = 1.6\text{mm}$

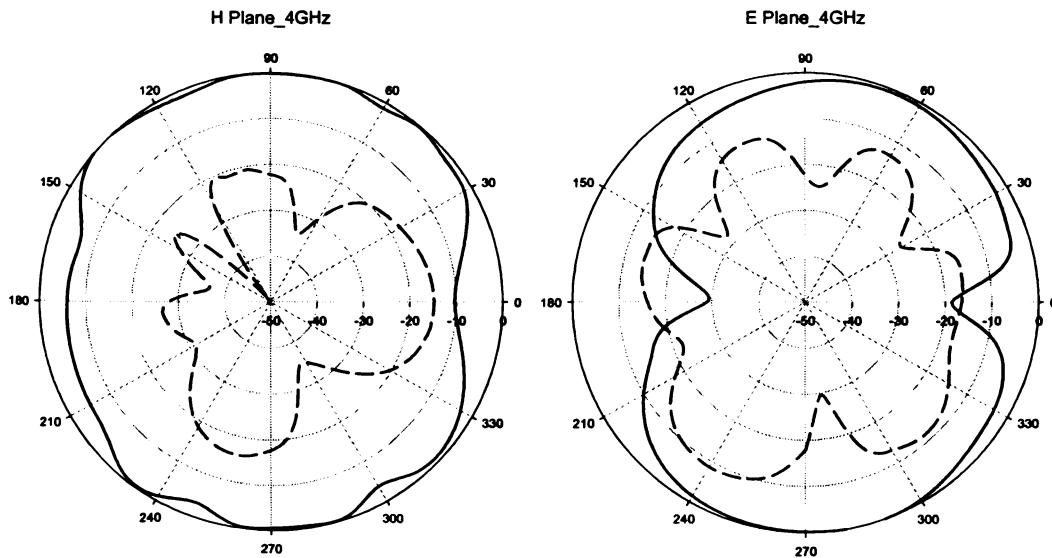
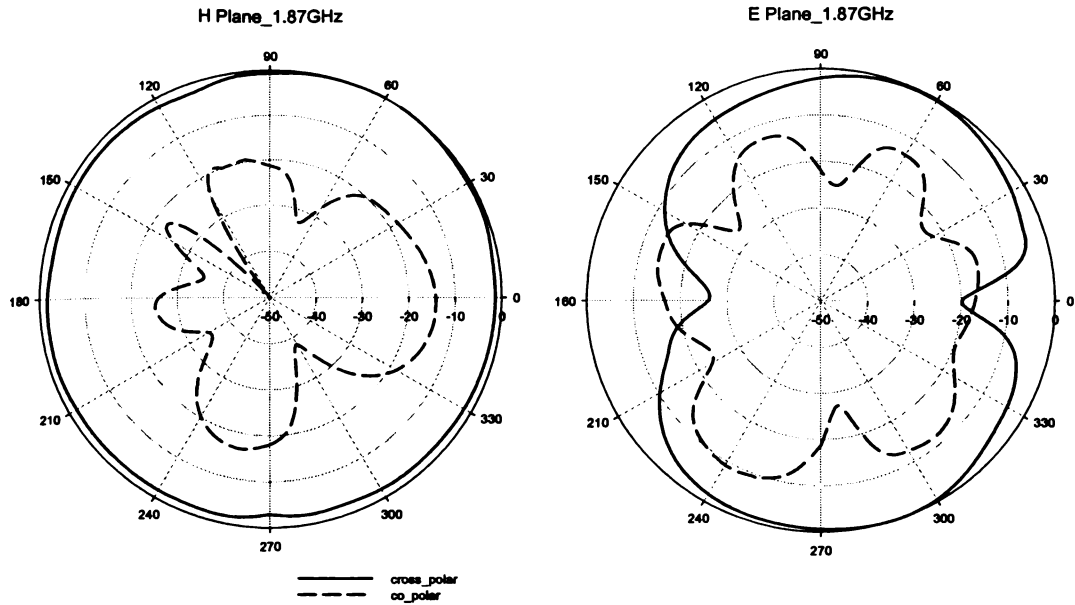
Table 3.4 Variation of band width with width of the monopole, W_m

Width of the Monopole, W_m (mm)	Gap 'g' (mm)	Band width
10	2	1.954 GHz-2.503 GHz
15	2	1.873 GHz-6.39 GHz
20	2	1.864 GHz-5.752 GHz
25	2	1.90 GHz-8.362 GHz
15	1.5	1.88 GHz-8.359 GHz

When the width of monopole is increased the higher order modes merges with the fundamental modes. But the gap is decisive parameter for the merging of resonant modes to yield wide band response.

Hence a microstrip fed printed strip monopole with truncated ground plane with wide strip can be used for Ultra wide Band applications. Computed radiation patterns confirm that radiation patterns are almost identical with in the 2:1 VSWR bandwidth. The *E*-plane pattern is dipole-like and the *H*-plane pattern is nearly omni directional over the entire band, as shown in Fig 3.27.

Theoretical and experimental analysis of printed strip monopole antenna



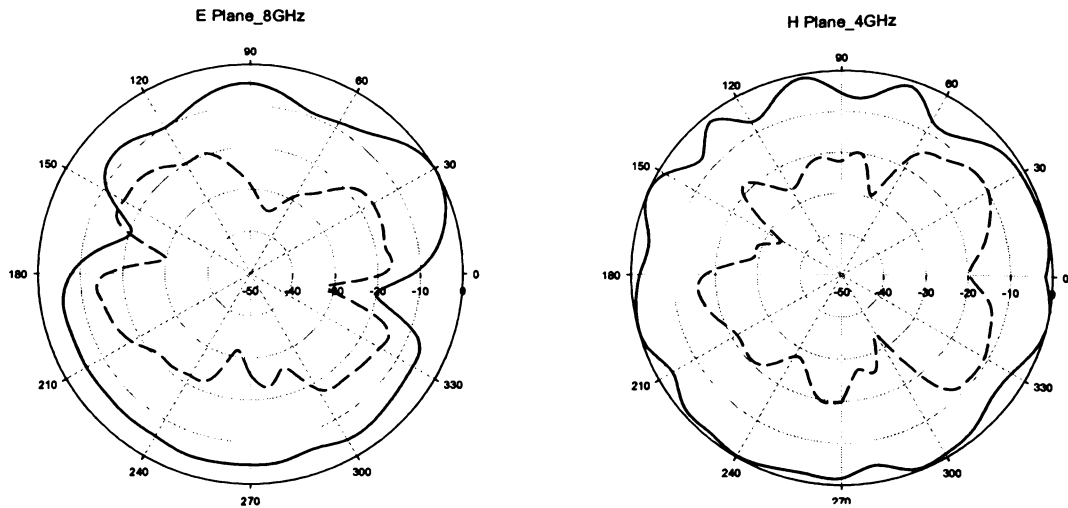


Fig.3.27. Computed radiation patterns of the wide band antenna at different frequencies with in the band spectrum. $W_0 = 95\text{mm}$, $L_0 = 45\text{mm}$, $L_m = 20\text{mm}$, $\epsilon_r = 4.4$, $h = 1.6\text{mm}$

E plane patterns are slightly squinted and look like doughnut shaped. H plane patterns are nearly omni directional at lower frequencies. With increase in frequency to second and third resonant modes patterns become distorted because of the enhanced perturbing effect of the ground plane truncation on antenna characteristics. But the H plane pattern retains satisfactory omni directionality with less than 10dB variations in most directions over the entire bandwidth.

Gain of the antenna with Ultra Wide Band response is also computed and it is found that antenna exhibits an average gain of 4.6dBi with in the entire operating band. Computed average efficiency is 78% at 5.8GHz. Computed gain and efficiency of the Ultra Wide Band printed monopole antenna is depicted in Fig3.28. Stable radiation patterns, average gain and good radiation efficiency of this antenna project it as a potential candidate for Ultra Wide Band applications.

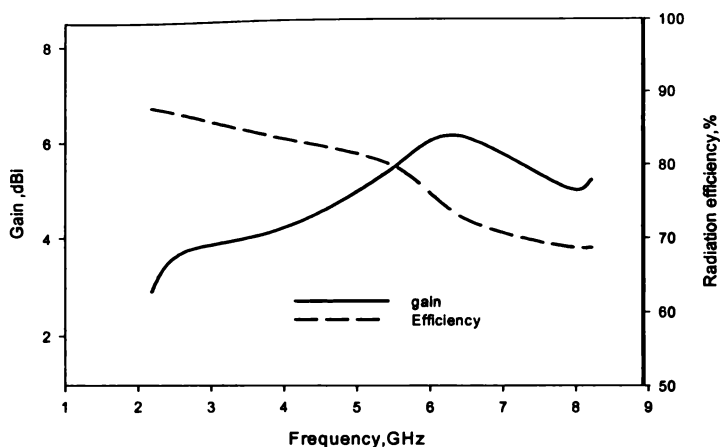
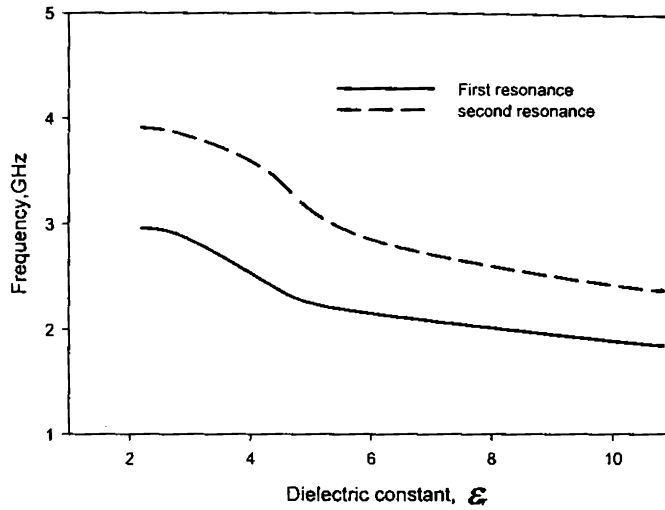


Fig.3.28. Computed gain and radiation efficiency in the entire Ultra wide Band.
 $W_0 = 95\text{mm}$, $L_0 = 45\text{mm}$, $L_m = 20\text{mm}$, $\epsilon_r = 4.4$, $h = 1.6\text{mm}$

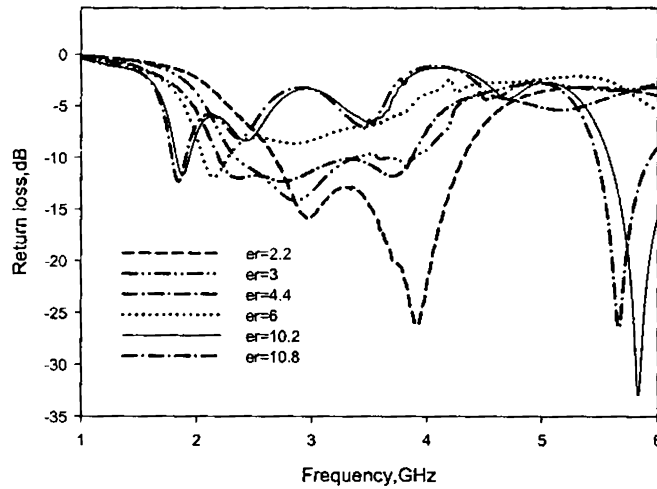
3.3.5.3 Effect of dielectric constant of substrate

The dielectric constant of the substrate material has great influence on the resonant frequencies of the two modes leading to the wide band operation. Effect of the dielectric constant on the two resonant modes leading to the wide band operation is depicted in Fig 3.29 (a). When the dielectric constant of the substrate is changed then two resonant frequencies are changed. When dielectric constant changes from 2.2 to 10.8 the monopole mode frequency changes by 1.1GHz where as corresponding to dipole mode the frequency variation is 1.5GHz. Since the two modes are substrate dependent the average dielectric constant value of the substrate has to be considered while calculating the resonant frequency. When the dielectric constant is changed the characteristics impedance of the microstrip line is changed which in turn modifies the return loss. The effect of the dielectric constant on the return loss characteristics of the antenna is shown in Fig.3.29 (b). For high dielectric constant substrates the bandwidth is considerably degraded due to the high Q of the antenna. For high dielectric constant substrates antenna efficiency is considerably degraded due to the excitation of the surface waves.

Moreover, the radiation patterns are distorted due to the edge diffraction caused by the surface wave excitation.



(a)



(b)

Fig 3.29. Effect of dielectric constant on the two resonant modes of the antenna.

$W_g = 95\text{mm}$, $L_g = 45\text{mm}$, $L_m = 20\text{mm}$, $W_m = 3\text{mm}$, $h = 1.6\text{mm}$

(a) Resonant frequency variation

(b) Return loss variation

3.3.5.4 Effect of substrate height.

Fig 3.30 depicts the variation of the two resonant modes with height of the substrate. For the first resonant mode there is no significant variation with respect to the height of the substrate. When the substrate height varied from 1mm to 5mm the first resonance frequency is slightly shifted from 2.55GHz to 1.975GHz (525MHz). But when the dielectric thickness is increased the effect on the second resonant mode is drastic. For the second resonant mode the frequency shifts from 3.8GHz to 2.45GHz (1.35GHz). When the height of the substrate is increased the electrical length corresponding to monopole mode is increased which decreases the resonant frequency corresponding to this mode. This again confirms the fact that the second mode is decided by the effective length of the strip including the path through the substrate and ground plane. When the substrate height is within the range of 1.5mm to 3mm, bandwidth variation is negligible. But for thin substrates due to strong coupling between the ground plane and vertical monopole the matching for the dipole mode is poor. Hence bandwidth is reduced. But when the substrate height is greater than 3mm spurious higher order modes affects the impedance characteristics and radiation patterns. Moreover, thick substrates give rise to the increased spurious radiation from the microstrip line. Hence for practical application substrate thickness should be less than $0.024\lambda_0$ for achieving wide band operation. Variation of % bandwidth with thickness of the substrate is presented in Fig 3.31(a). The return loss variation with substrate thickness is depicted in Fig 3.31(b). Increase in substrate thickness degrades the radiation efficiency of the antenna due to the increased surface waves. This surface wave excitation may lead to the degradation in the radiation pattern also. Hence substrate dielectric constant and thickness should be selected in such a way that the deterioration in radiation or resonance characteristics of the antenna is minimum.

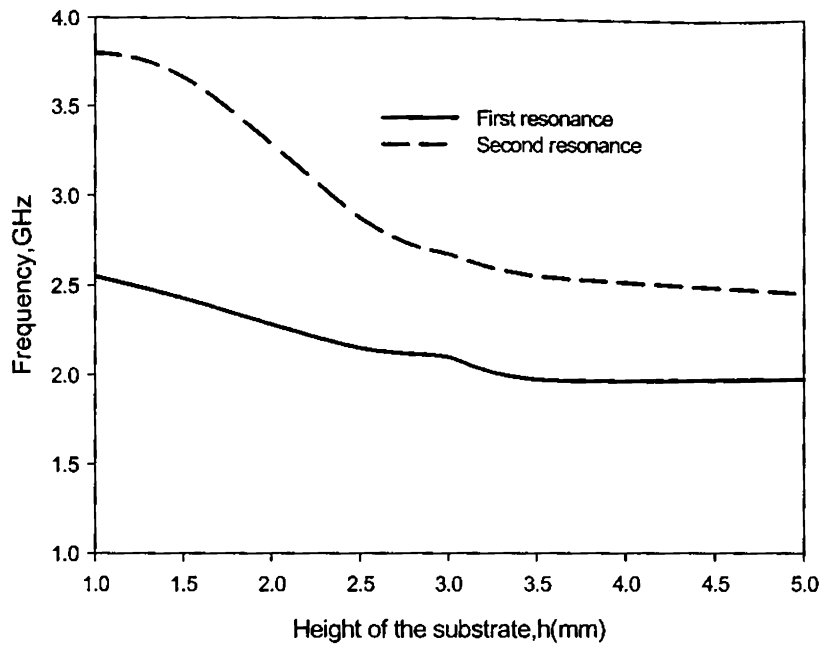
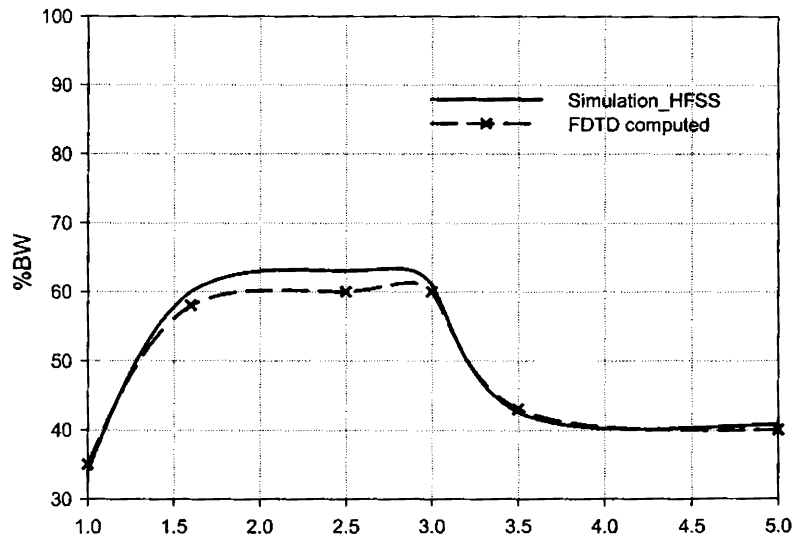
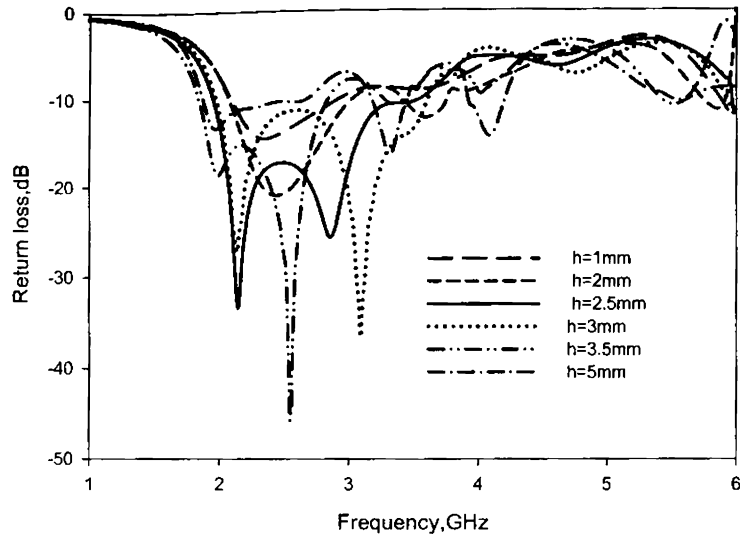


Fig 3.30 Effect of substrate thickness on the two resonant modes
 $W_g = 95\text{mm}$, $L_g = 45\text{mm}$, $L_m = 20\text{mm}$, $W_m = 3\text{mm}$, $\epsilon_r = 4.4$



(a)



(b)
Fig 3.31 (a) Effect of substrate thickness on impedance bandwidth
(b) Effect of substrate thickness on the reflection characteristics

3.3.6 Compact printed strip monopole antenna with optimum ground plane dimensions.

From the ground plane optimization studies we derived an optimum ground plane to fix the resonant frequency at the desired value. The input impedance variation corresponding to half wavelength and quarter wavelength resonant modes with optimum ground plane is shown in Fig.3.32 (a). When the ground plane length is extremely low the impedance matching for the fundamental mode is very poor. For the optimum ground plane length, the input resistance at the fundamental mode is very low which can not be matched with the 50Ω microstrip line. At the optimum ground plane case the antenna resonates at 4.38 GHz corresponding to the half wavelength mode of the strip monopole. Hence to fix the resonance at 2.4GHz the length of the strip should be half wavelength corresponding to the frequency. This arrives at an important conclusion that when the ground plane length is optimum the second harmonic of the fundamental mode is excited. To match the fundamental resonant mode complicated baluns are required which increases the

system complexity. Hence considering the compactness into account a half wavelength monopole with an optimum ground plane width of half wavelength is selected as the monopole with optimum ground plane. For the optimum length monopole the variation of input impedance with different ground plane width is shown in Fig.3.32(b). From the impedance studies it is observed that the width of half wavelength is required to match the impedance to 50Ω for a particular frequency. When the ground plane length is less than half wavelength the resonant matching frequency is shifted to higher end of the 2:1 VSWR band.

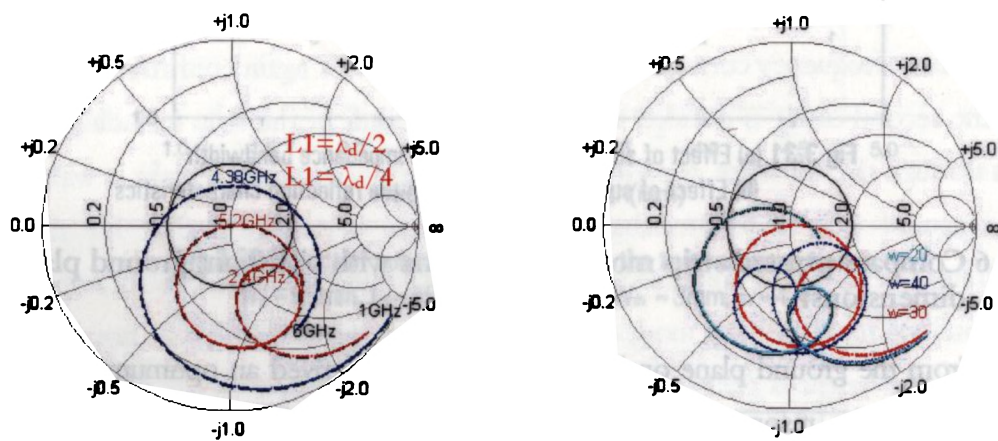


Fig 3.32 (a) Input impedance variation of optimum ground plane printed monopole antenna with different monopole length. $L_g = 3\text{mm}$ $W_g = 30\text{mm}$ $W_m = 3\text{mm}$
(b) Input impedance variation with different ground plane widths, W_g

Consider a strip monopole excited by a 50Ω microstrip line with truncated ground plane of dimensions $L_g \times W_g$. The length and width of the truncated ground plane is optimized for maximum bandwidth without affecting the impedance matching. For the design convenience the strip width of the monopole is set as 3 mm for $\epsilon_r = 4.4$, $h = 1.6\text{mm}$, width of 50Ω microstrip line. Fig 3.33(a) shows the structural parameters of the optimum ground plane printed strip monopole antenna. Experimental, FDTD computed and HFSS simulated reflection characteristics are compared in Fig.3.33 (b).

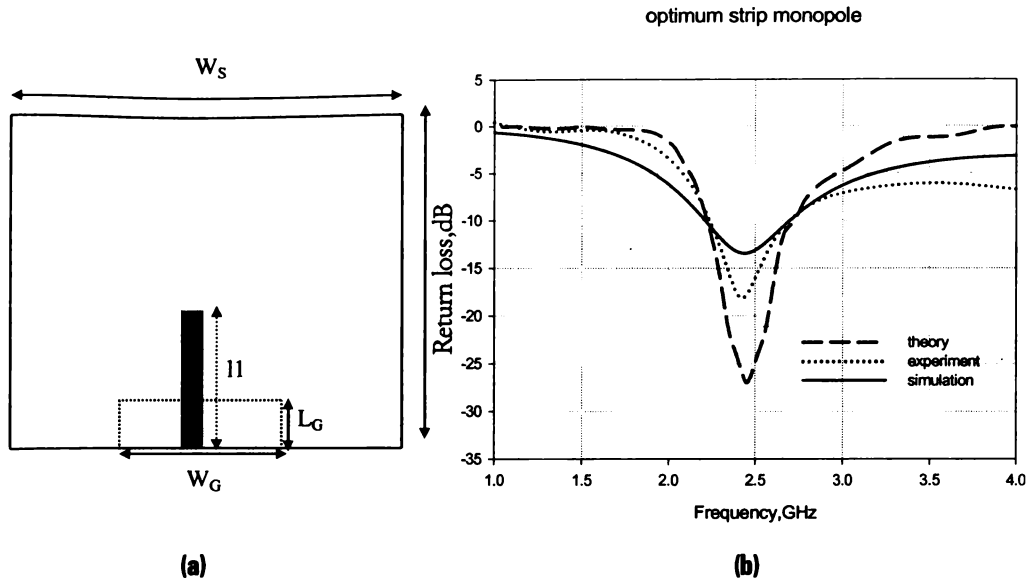


Fig 3.33 (a) Geometry of the optimum ground compact microstrip fed printed monopole antenna. $L_G = 3\text{mm}$ $W_G = 30\text{mm}$ $L_S = 35\text{mm}$ $W_S = 30\text{mm}$. $l_1 = 32\text{mm}$. Area = $32 \times 35\text{mm}^2$
(b) Return loss characteristics

With the optimum ground plane dimensions the maximum % bandwidth achieved is 23%. In this case the antenna dimensions is only $32 \times 35\text{mm}^2$ with an area reduction of 15% compared to standard planar microstrip rectangular patch antenna. From the experimental and theoretical investigations it can be inferred that antenna resonates at 2.454GHz with 2:1 VSWR band width of 575 MHz(2.19GHz-2.768GHz) corresponding to a wide band width of 23%. A detailed investigation on the optimum ground plane printed strip monopole is presented in the following section.

Computed E field distribution

FDTD computed E field distribution reveal that there is half wavelength variation of the field along the length of the monopole. From the computed E field distribution it can also be inferred that the variation of field along the ground truncation edges is negligible. With an optimum ground plane the monopole

behaves more like a dipole than conventional monopole. Computed E field distribution corresponding to the first resonant mode is depicted in Fig.3.34. From the field distribution it is evident that the strip monopole is vertically polarized along the length of the monopole.

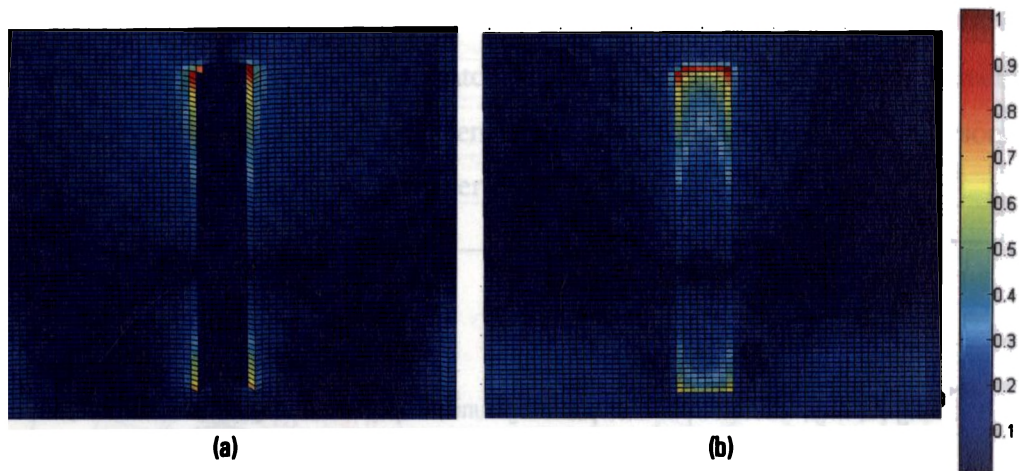


Fig 3.34 Computed E field distribution of the optimum strip monopole at 2.454GHz
 $L_G = 3\text{mm}$ $W_G = 30\text{mm}$, $L_S = 35\text{mm}$ $W_S = 30\text{mm}$ $l_1 = 32\text{mm}$
(a) E_x at the top of the substrate
(b) E_z at top of the substrate

Radiation characteristics

The Principal plane radiation pattern of the optimum strip monopole antenna computed using FDTD technique is shown in Fig.3.35. The radiation patterns are omni directional in the H plane and figure of eight in the E plane similar to that of conventional dipole antenna. The simulated 3D pattern shown in fig 3.35 (b) again confirms that for an optimum ground plane printed strip monopole the radiation pattern is doughnut shaped like the dipole pattern.

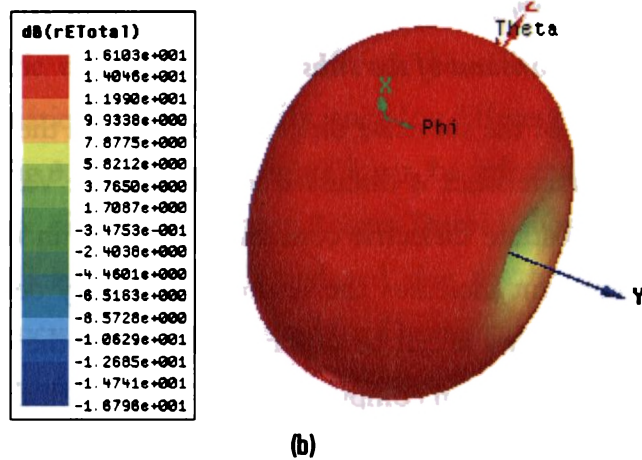
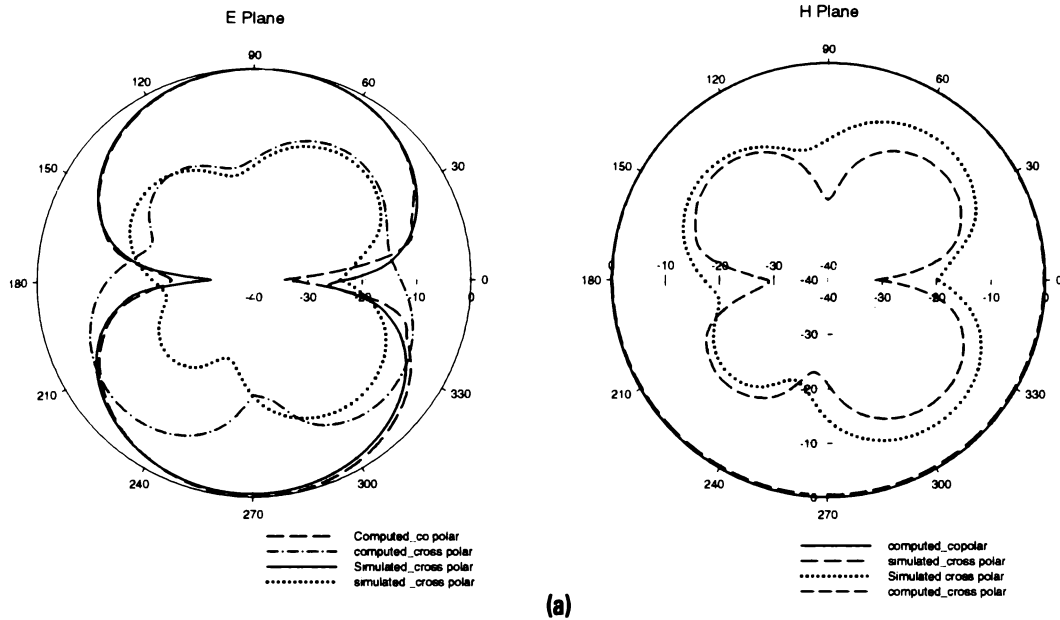


Fig 3.35 (a) Simulated and computed radiation pattern of the optimum design
 (b) Simulated 3D radiation pattern of the proposed antenna.
 $L_G = 3\text{mm}$ $W_G = 30\text{mm}$, $L_s = 35\text{mm}$ $W_s = 30\text{mm}$, $l_1 = 32\text{mm}$

Antenna gain and efficiency

Gain of the optimum strip printed monopole antenna is measured using gain transfer method. Antenna exhibits an average gain of 2.5dBi with in the entire

operating band. Simulated gain is in close agreement with the measured values. The measured antenna gain and efficiency is presented in Fig3.36. The average efficiency of the antenna is 86%.

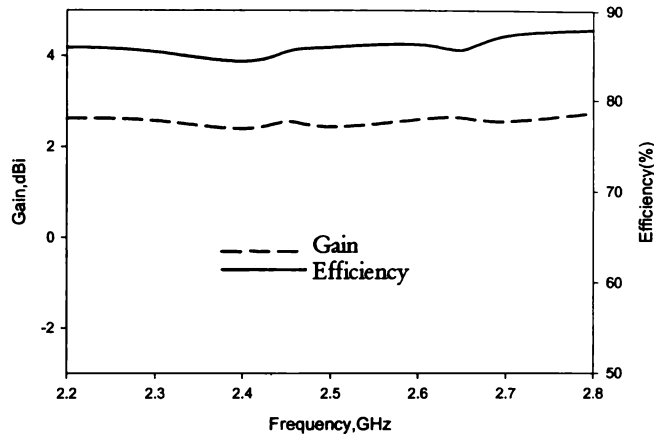


Fig 3.36 Measured gain and efficiency of the compact monopole antenna.
 $L_6 = 3\text{mm}$, $W_6 = 30$, $L_s = 35\text{mm}$, $W_s = 30\text{mm}$, $l_1 = 32\text{mm}$

Effect of dielectric constant of the substrate

The influence of the substrate dielectric constant on the antenna reflection and radiation characteristics is discussed in this section. Variation of resonant frequency with substrate dielectric constant is depicted in the Fig 3.37(a). As the dielectric constant increases the resonant frequency decreases. From the computed E field values it can be observed that when the dielectric constant increases there is variation in computed E field underneath the strip. Hence the effective dielectric constant value should be accounted while calculating the resonant frequency. Increase in dielectric constant affects the impedance characteristics as the Q of the antenna varies when the dielectric constant is changed. For high dielectric constant substrates the computed results shows that bandwidth is reduced due to the high Q of the antenna. Variation of reflection characteristics for different dielectric constant values is depicted in Fig3.37 (b).

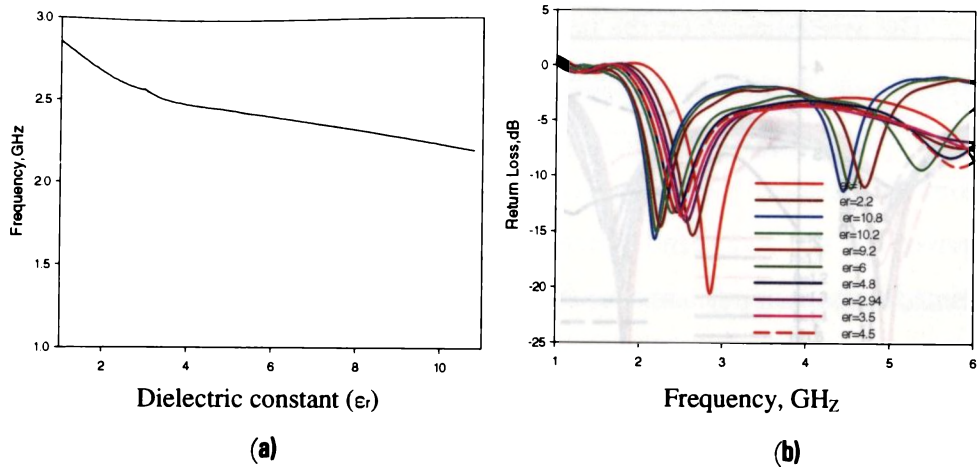


Fig 3.37 (a) Effect of dielectric constant on the resonant Frequency of optimum strip monopole
(b) variation of reflection characteristics $L_G = 3\text{mm}$ $W_G = 30\text{mm}$ $L_S = 35\text{mm}$
 $W_S = 30\text{mm}$ $l_1 = 32\text{mm}$ height of the substrate $h = 1.6\text{mm}$

For the optimum strip monopole printed on a dielectric substrate, the substrate dielectric constant variation affects the efficiency and gain of the antenna. The variation of gain and efficiency for different dielectric laminates is presented in Fig 3.38. From the figure it can be inferred that the efficiency is highest for low dielectric constant Rogers-Duroid substrate. But for FR4 substrate the efficiency is slightly reduced due to the high loss tangent. Maximum efficiency of 89% is achieved for Duroid substrate while the gain is 3dBi.

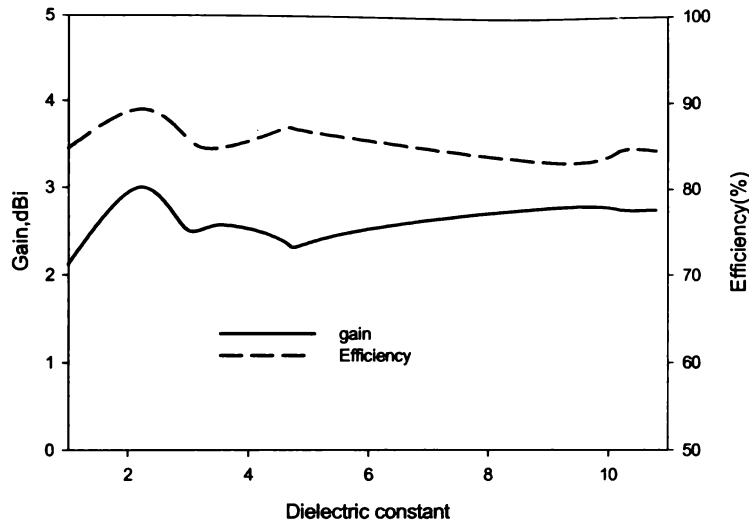
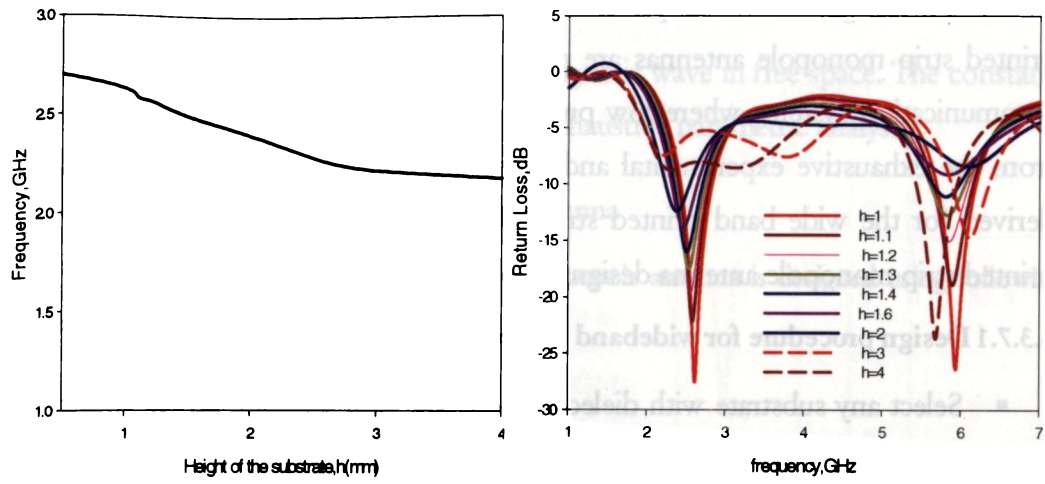


Fig 3.38 Variation in gain and efficiency with substrate dielectric constant. $L_G = 3\text{mm}$
 $W_G = 30\text{mm}$ $L_S = 35\text{mm}$ $W_S = 30\text{mm}$ $l_1 = 32\text{mm}$. height of the substrate $h = 1.6\text{mm}$

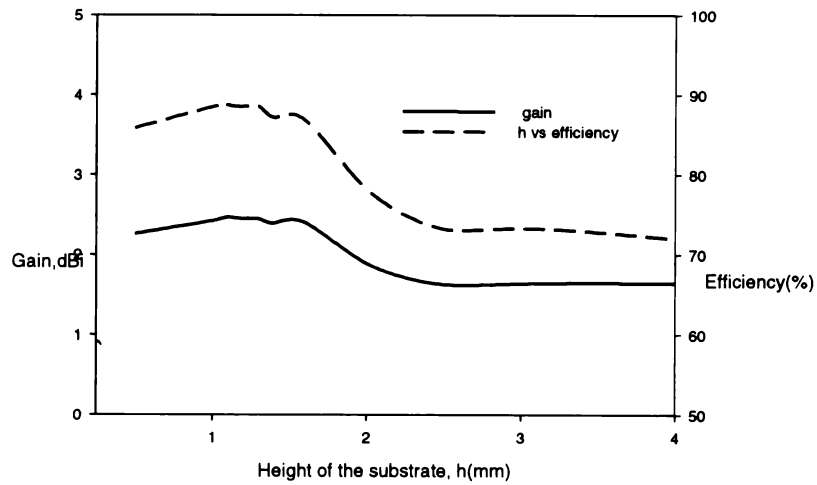
Effect of substrate thickness

Influence of substrate thickness on the antenna characteristics is depicted in Fig.3.39. From the figure it can be observed that when the substrate height varies from 0.5mm to 4mm corresponding resonant frequency variation is only 540MHz. But the gain of the antenna is considerably reduced for the thick substrates due to the degradation in radiation efficiency caused by the surface wave excitation. Effect of substrate thickness on gain and efficiency is presented in Fig.3.39(c). But as the substrate height increases the Q of the antenna is low. Hence bandwidth increases considerably as shown in Fig.3.39 (b). Return loss characteristics reveal that thickness of the substrate affects impedance matching considerably. For thick substrates the impedance matching is poor.



(a)

(b)



(c)

Fig 3.39 Effect of substrate height on

(a) resonant frequency

(b) reflection characteristics

(c) Gain and efficiency

$L_G = 3\text{mm}$ $W_G = 30\text{mm}$, $L_S = 35\text{mm}$ $W_S = 30\text{mm}$. $l_1 = 32\text{mm}$

3.3.7 Design procedure

The investigations on the printed strip monopole leads to the conclusion that printed strip monopole antennas are potential candidate for broadband wireless communication systems where low profile antennas are in great demand. Hence from the exhaustive experimental and numerical analysis simple equations were derived for the wide band printed strip monopole antenna as wells as compact printed strip monopole antenna design.

3.3.7.1 Design procedure for wideband performance

- Select any substrate with dielectric constant ϵ_r and height h . The width of the monopole is set as width of 50Ω microstrip feed line.
- Since the field components are not confined to the substrate alone effective dielectric constant has to be used in calculation.

$$\epsilon_{eff} = \frac{\epsilon_r + 1}{2} (1 + 0.3 * h) \dots\dots\dots(3.1)$$

Where h is the height of the substrate and ϵ_r is the dielectric constant of the substrate.

- Length of the monopole, L_m

$$L_m = \frac{0.25c}{f_r * \sqrt{\epsilon_{eff}}} \dots\dots\dots(3.2)$$

- Ground plane dimensions are then calculated using the following equations

$$L_G = \frac{0.59c}{f_r * \sqrt{\epsilon_{eff}}} \dots\dots\dots(3.3)$$

$$W_G = \frac{1.25c}{f_r * \sqrt{\epsilon_{eff}}} \dots\dots\dots(3.4)$$

Where 'c' is the velocity of electromagnetic wave in free space. The constants in the above equations are derived from exhaustive parametric analysis.

3.3.7.2. Design procedure for Compact antenna

An optimum ground plane printed monopole antenna is designed using following design equations.

- Length of the monopole, L_1

$$L_1 = \frac{0.48c}{f_r * \sqrt{\epsilon_{eff}}} \dots\dots\dots(3.5)$$

- Ground plane dimensions are then calculated using the following equations

$$L_G = \frac{0.0375c}{f_r * \sqrt{\epsilon_{eff}}} \dots\dots\dots(3.6)$$

$$W_G = \frac{0.5c}{f_r * \sqrt{\epsilon_{eff}}} \dots\dots\dots(3.7)$$

3.3.8 Printed monopole designs in modern communication bands

In order to confirm the validity of the above design equations wide band printed monopoles are designed for various communications bands of interest. Return loss characteristics of the wide band printed strip monopole antenna operating in various frequency bands are depicted in Fig.3.40. The reflections

characteristics confirm that predicted frequency and bandwidth are in good agreement with measured values.

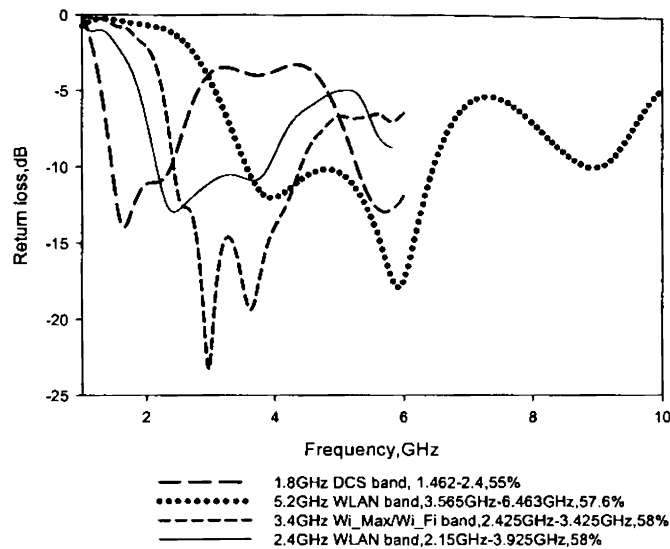


Fig 3.40 Wide band printed strip monopole designs in various wireless communication bands

The antenna parameters and characteristics of the various prototypes are summarized in table 3.5. Printed strip monopole antenna designed at DCS band exhibits a wide bandwidth of the order of 938MHz corresponding to 55% bandwidth. The bandwidth is wide enough to cover the DCS (1710&1880 MHz) and PCS (1850-1990 MHz) bands. The average gain of the antenna 3dBi with in the operating bandwidth and efficiency is 90%. Wide band printed monopole antenna designed at 2.4 GHz WLAN band exhibits broad bandwidth of the order of 1.7GHz corresponding to 58% bandwidth. The average gain of the antenna is 3.5dBi with efficiency of 89%. The prototype designed at 5.2GHz exhibits a bandwidth of the order of 2.8GHz covering HYPER LAN bands. In all the designs antenna exhibits wide band performance with bandwidth better than 55% confirming the suitability of the design in wireless communication applications.

Table 3.5 Wide band printed monopole antenna characteristics in different wireless standards.

Wireless Standard	Antenna parameters (mm)	Band	%Band width	Gain (dBi)	Efficiency (%)
DCS	$L_m=26.6, W_m=3$ $L_G=47, W_G=123$	1.46GHz- 2.4GHz	55	3.0	85.4
2.4GHz WLAN	$L_m=20, W_m=3$ $L_G=45, W_G=95$	2.15GHz- 3.925 GHz	58	3.4	89.9
5.2GHz WLAN	$L_m=3.5, W_m=3$ $L_G=19.7, W_G=43$	3.565GHz- 6.463GHz	57.6	4.2	86.2
Wi_Max/Wi_Fi	$L_m=13, W_m=3$ $L_G=29, W_G=63.6$	2.425GHz- 3.425GHz	58	3.8	87.8

The validity of compact optimum printed strip monopole design is also confirmed in modern wireless communications bands. Fig 3.41 shows the antenna designs suitable for compact antenna applications. Note that even though optimum ground plane printed monopole antenna is half wavelength resonant structure the overall dimensions of the antenna including the ground plane is only $0.5\lambda_d \times 0.5\lambda_d$. Hence compared to broadband design with truncated large ground plane, the optimum ground plane printed monopole is compact in dimensions. The optimum ground plane printed strip monopole antenna occupies slightly lower area compared to a standard rectangular patch resonating at the same frequency. The characteristics of the printed strip monopole antenna with optimum ground plane is presented in Table 3.6.

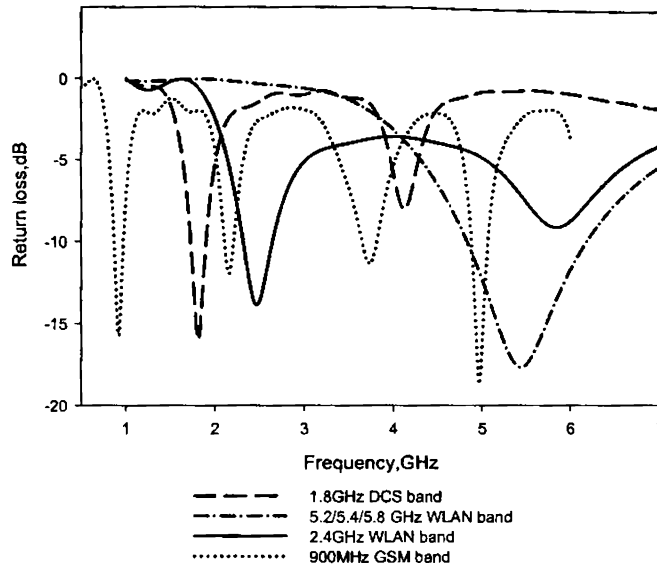


Fig 3.41 Compact printed monopole antenna design in various wireless communication bands

Table 3.6 Wide band printed monopole antenna characteristics in different wireless standards.

Wireless Standard	Antenna parameters (mm)	Band	Resonant Frequency (GHz)	%Band width	Gain (dBi)	Efficiency (%)
DCS	$L_m=40, W_m=3$ $L_G=4, W_G=40$	1.72GHz- 1.909GHz	1.819	10%	2.1	84.6
2.4GHz WLAN	$L_m=30, W_m=3$ $L_G=3, W_G=30$	2.19GHz- 2.768GHz	2.454	23%	2.5	86
5.2GHz WLAN	$L_m=14, W_m=3$ $L_G=1, W_G=14$	4.834GHz - 6.175GHz	5.4370	24%	2.75	89.2
GSM	$L_m=80, W_m=3$ $L_G=8, W_G=80$	868MHz- 973 MHz	918MHz	11.4	1.98	80.5

3.4 Comparison of printed strip monopole with standard planar antennas

Evolution of the printed antenna design started with the introduction of conformal low profile microstrip antennas. Table 3.7 compares some of the merits and demerits of the printed strip monopole with the conventional low profile planar rectangular microstrip antenna.

Table 3.7 Comparison of printed monopole with rectangular microstrip antenna.

Property	Rectangular microstrip antenna	Wide band printed strip monopole antenna	Compact printed strip monopole antenna
Size	Half wavelength resonant structure	Quarter wavelength resonant structure	Half wavelength resonant structure
Fabrication economy	Ease of fabrication and integration to MMICs	Ease of fabrication and integration to MMICs	Ease of fabrication and integration to MMICs
Bandwidth	Narrow bandwidth of the order of 3%	Extremely Broad band width of the order of 60%	Broad band width of the order of 23%
Gain	Average gain of 7dBi on RT Duroid substrate	4 dBi on RT Duroid substrate	Average of 3dBi on RT Duroid substrate
Substrate losses	Substrate losses are very high since the radiation depends on the fringing fields	Substrate losses are minimum compared to RMSA	Substrate losses are minimum compared to RMSA
Radiation patterns	Uni polar radiation pattern	Nearly omni directional radiation pattern in one plane and figure of eight radiation pattern in the other plane	Typical doughnut shaped radiation pattern similar to dipole radiation pattern.

3.5 Summarized conjecture at a glance

Inference obtained from the theoretical and experimental investigation of printed strip monopole with different ground plane dimensions are summarized in this section

- Truncated ground plane is an important concept for the modular design of wide band printed monopole antennas excited by microstrip feed line.
- The impedance bandwidth of the printed strip monopole antenna can be controlled by properly truncating the ground plane.
- By properly truncating the ground plane width an additional resonance near the fundamental mode can be excited which merges with the fundamental mode to yield wide band response.
- Truncation of ground plane forms additional currents on the edges of the ground plane. These edge currents are not spread all over the ground surface
- Currents on the edges of ground plane form an asymmetric dipole configuration along with the vertical monopole.
- Same microstrip line is able to match the vertical monopole mode and asymmetric dipole mode.
- Edge currents have negligible effects on the radiation as they cancels at the far field.
- Effectively utilizing a small area of the ground plane a second resonance is excited, which has similar radiation characteristics as that of first resonance, with out any additional balun.
- The ground plane edge currents can be effectively utilized for the generation of various current paths leading to the design of multiband antennas.

- Complicated balun structures which are limiting the bandwidth of the antenna are not at all required in the present design. By properly utilizing a portion of ground plane a wide band performance can be achieved without raising any spurious electromagnetic problems.
- When the ground plane dimensions are very large there may be distortion in the radiation pattern
- For finite ground plane printed monopole the radiation pattern is similar to the dipole.
- With optimum ground plane dimensions the impedance matching for the quarter wavelength fundamental mode is poor. But half wavelength mode with truncated optimum ground plane ensures the size reduction than quarter wavelength mode with truncated ground plane.
- For a half wavelength monopole ground plane width should be at least of the order of half wavelength when the ground plane length is optimum.

3.6 Conclusions

A planar monopole antenna with extremely wide band is designed by properly truncating the ground plane of the feeding microstrip line. An extremely wide band of 60% can be achieved by properly truncating the ground plane. The proposed antenna offers wide band width, moderate gain and nearly omnidirectional radiation characteristics suitable for application in modern wireless gadgets. A compact printed strip monopole antenna with band width of the order of 23% is derived from optimum ground plane dimensions. The proposed optimum design is a potential candidate in wireless communications systems where compact efficient antennas are in great demand.

DOUBLE FOLDED STRIP MONOPOLE ANTENNA FOR DUAL BAND APPLICATIONS

This chapter highlights the experimental and theoretical outcome of a double folded strip monopole antenna for dual band application and size reduction. A printed strip monopole antenna is suitably folded to make a low profile, small size folded strip monopole antenna. A folded strip antenna has generally narrow band characteristics than the straight vertical strip monopole antenna. Investigations are carried to broaden the bandwidth of the folded strip monopole antenna by judiciously placing another folded strip. By incorporating an additional strip at the opposite location, the bandwidth of the folded strip monopole can be increased with a bonus of an additional resonance to yield dual band response. Thus a novel compact planar branched monopole antenna is derived for dual band wireless communication applications. Experimental and numerical analysis of planar branched monopole antenna is presented with detailed discussion of the effect of the coupling between the arms. From the exhaustive numerical analysis simple design equation are presented at the concluding section of the chapter.

4.1 Reactive loading for antenna miniaturization: an overview.

The latest trends in handset unit in the cellular phone are to reduce the size and weight. The antennas used for such handsets must follow downsizing of the wireless gadget yet keep the antenna performance unchanged or even improved. Furthermore, built in antennas are becoming more intense requirements of the mobile gadgets. The reduction of antenna size imposes fundamental limitations on the antenna performance. Along with size reduction the antenna should cater the needs of gain and bandwidth. In conventional wire monopole antennas, one simple way to reduce the size of a monopole antenna is to load a positive reactance component, such as a coil, at the feed point or a short-circuited transmission line with length less than a quarter wavelengths etc. The resistance of short antenna becomes very low at the resonant frequency when the size of the antenna is reduced. Another problem then arises, where the actual gain of such a small antenna will be reduced owing to its low radiation resistance and low profile. Folding technique is extensively used in the design of short antennas because they exhibit higher input impedance than conventional monopoles of the same height. This is achieved as a result of impedance transformation which arises from distributed coupling between driven and folded sections. Input impedance of the folded monopole antenna is given by $Z_{in} = \frac{4Z_t Z_d}{Z_t + 2Z_d}$ Where Z_d is the input impedance of the parallel monopole antenna and Z_t is the terminal impedance of the transmission line with length H . $Z_t = jZ_0 \tan(\beta H)$ where β is the phase constant. When H equals the quarter wavelength then input impedance of the folded monopole antenna becomes four times the input impedance of the conventional quarter wave monopole. Thus folding can be effectively utilized to increase the impedance of the small antennas. This folding technique is

effectively utilized in the present investigation to design a compact folded monopole antenna as illustrated in the present chapter. But when the monopole antenna is folded the parallel arm has strong coupling with ground plane. This strong coupling adversely affects the input impedance characteristic of the antenna. Hence there is small degradation in the bandwidth performance. In the present chapter investigations are made to improve the bandwidth performance of the folded monopole antenna by deliberately placing another loaded arm which loads reactance at the antenna input impedance. Thus a dual folded monopole antenna is derived for broadband performance. The additional folded arm not only increases the bandwidth performance but also generates a new resonance due to an additional resonant path. Thus a compact dual branched or dual folded monopole antenna is derived for dual band applications. The experimental and theoretical investigations of the folded monopole and dual branched monopole are presented in the following sections.

4.2 FDTD analysis of Folded strip monopole antenna (FSMA) for size reduction.

In the previous chapter we reached at an important conjecture that for an optimum ground plane printed monopole antenna it is difficult to match the resonant frequency at the desired value with quarter wavelength strip. Thus a strip monopole with half wavelength is selected to fix the resonant frequency at the desired value. By properly folding the strip monopole considerable reduction in overall size can be achieved with out deteriorating antenna performance. The strip monopole antenna shown in Fig.4 (a) can be transformed to folded strip as shown in Fig.4.1 (b).

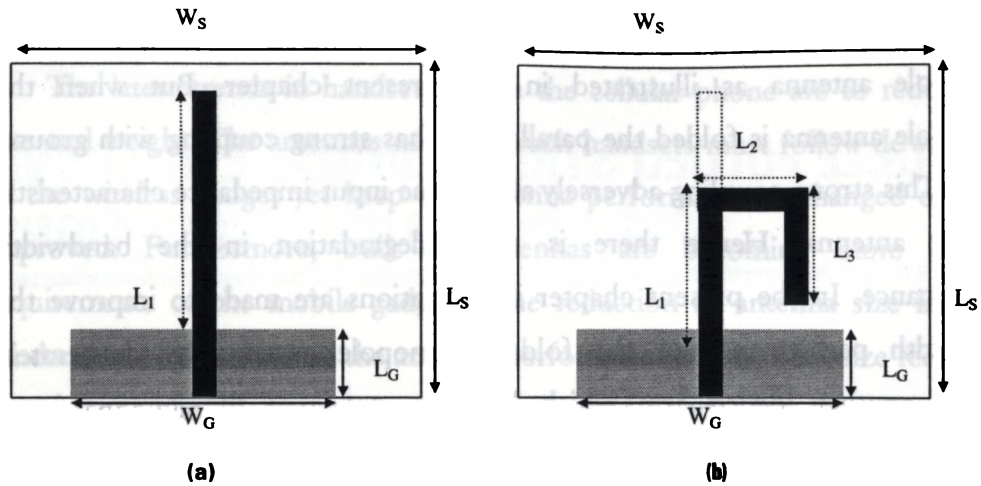


Fig 4.1 (a) Antenna 1: Printed strip monopole antenna over truncated optimum ground plane
(b) Antenna 2: folded monopole antenna over truncated optimum ground plane

For the numerical analysis a folded strip monopole with design parameters $L_G = 3\text{mm}$, $W_G = 40\text{mm}$, $L_1 = 24\text{mm}$, $L_2 = 13\text{mm}$, $L_3 = 16\text{mm}$ is printed on a substrate of dielectric constant 4.4 and thickness $h = 1.6\text{mm}$ is considered. The antenna is modeled in FDTD with discretization parameters $\Delta x = \Delta y = 0.5\text{mm}$ and $\Delta z = 0.4\text{mm}$. The computational domain corresponding to this problem contains $110 \times 100 \times 25$ number of Yee cells. The antenna is excited with 50Ω microstrip feed line which is modeled using Leubber's feed model as explained in chapter 2. The FDTD analysis will compute the frequency response of the antenna by exciting with a Gaussian pulse. The antenna parameters like input impedance reflection coefficient and field distribution corresponding to the resonant frequency etc are computed as explained in chapter 2. For a strip monopole with the following parameters $L_G = 3\text{mm}$, $W_G = 40\text{mm}$, $L_m = 21\text{mm}$ $w = 3\text{mm}$ the computed input impedance characteristics is shown in Fig.4.2. A quarter wavelength strip monopole characteristics is also compared in the same figure.

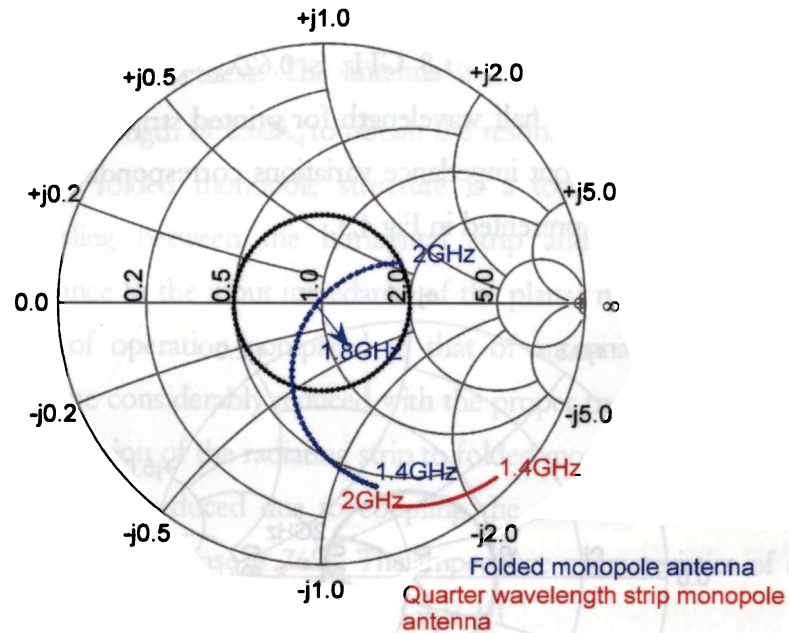


Fig 4.2 Computed input impedance characteristics of the printed monopole and folded strip monopole shown in Fig.4.1

Antenna1: $\lambda/4$ Printed strip monopole $L_G = 3\text{mm}$, $W_G = 40\text{mm}$, $L_1 = 21\text{mm}$, $w = 3\text{mm}$

Antenna2: $\lambda/2$ Folded strip monopole $L_G = 3\text{mm}$, $W_G = 40\text{mm}$, $L_1 = 24\text{mm}$, $L_2 = 13\text{mm}$, $L_3 = 16\text{mm}$ $w = 3\text{mm}$

In the previous chapter we found that it is very difficult to match the quarter wavelength strip monopole with optimum ground plane. The printed strip monopole antenna (Antenna1) is not resonating in the 1.4GHz to 2 GHz band even though the length is quarter wavelength. The real part of the resistance is 12.59Ω which is very low at 1.8GHz. Similarly imaginary part of the impedance is very high. The same antenna is loaded with a parallel arm of length L_3 with a connecting strip of length L_2 (Antenna 2) then impedance is nearly $49.2 - j0.81$. Now we can say that antenna is resonating at 1.8GHz with excellent matching. This is very clear from Fig 4.2. Thus it was confirmed from the input impedance analysis that folding can be effectively utilized to increase the resistance part to obtain good impedance matching. Note that when an additional arm is top loaded

to quarter wave monopole then total effective length of the folded strip required to fix the resonant frequency at 1.8 GHz is $0.62\lambda_d$. In this case width of the ground plane is selected as half wavelength for printed strip monopole as well as folded monopole. The input impedance variations corresponding to the different ground plane widths are presented in Fig.4.3.

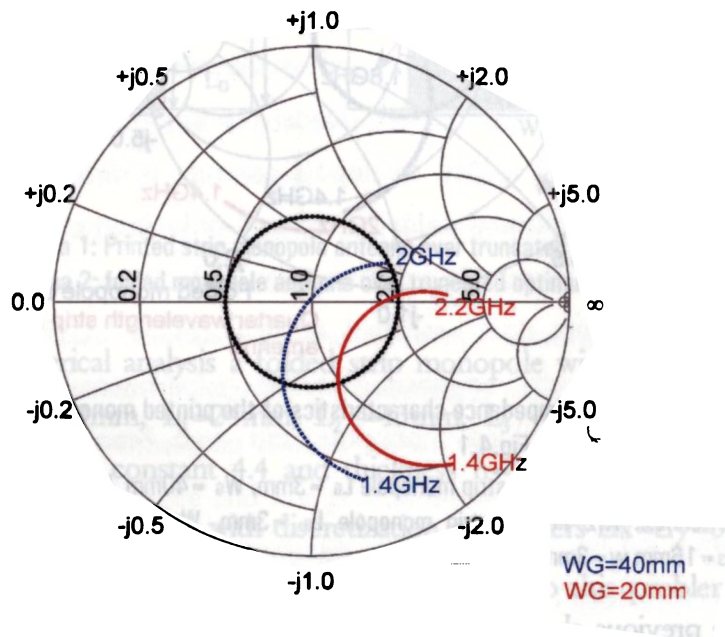


Fig 4.3 Computed input impedance characteristics of the folded monopole antenna for different ground plane widths.

$L_6 = 3\text{mm}$, $L_1 = 24\text{mm}$, $L_2 = 13\text{mm}$, $L_3 = 16$, $\epsilon_r = 4.4$, $h = 1.6\text{mm}$.

When the ground plane width is reduced to quarter wavelength the capacitive coupling between the ground plane and horizontal connecting strip L_2 adds capacitive reactance to the input impedance of the monopole antenna. From the numerical analysis it is investigated that Antenna 1, $\lambda_d/2$ strip monopole excited by 50Ω microstrip line requires truncated optimum ground plane width of $\lambda_d/2$ to fix the resonant frequency at the desired value (Chapter 3). Even though wide band width is achieved with this configuration the antenna occupies same area compared to standard rectangular patch resonating at the same frequency. The

antenna 1 is modified by meandering the strip monopole to a folded monopole in order to achieve compactness. The antenna 2 with ground plane width $\lambda_d / 4$ require a resonant length of $0.62\lambda_d$ to obtain the resonant frequency at the desired value. Since the folded monopole structure is a top loaded planar strip the capacitive coupling between the horizontal strip and ground plane adds a capacitive reactance to the input impedance of the planar monopole which lowers the bandwidth of operation compared to that of antenna 1. But the antenna dimensions can be considerably reduced with the proper truncation of the ground plane and modification of the radiating strip to folded monopole. Even though the bandwidth is slightly reduced due to coupling the area reduction compared to rectangular patch in this case is 76%. The impedance characteristics of different antenna configurations are summarized in Table 4.1

Table 4.1 Input impedance characteristics of printed monopole.

Antenna	Antenna parameters (mm)	Resonant frequency f_r (GHz)	Input impedance (Ω)
Quarter wavelength printed monopole with half wavelength ground plane	$L_m=20, w=3, L_G=3, W_G=40$	No matching	12.59-j83.47
half wavelength printed monopole with optimum (half wavelength)ground plane	$L_m=40, w=3, L_G=3, W_G=40$	1.8 GHz	49.83-j29.9
Folded monopole with half wavelength ground plane	$L_1=24, L_2=13, L_3=16, w=3, L_G=3, W_G=40$	1.8 GHz	49.2-j0.81
Folded monopole with optimum (quarter wavelength) ground plane	$L_1=24, L_2=13, L_3=16, w=3, L_G=3, W_G=20$	1.82 GHz	48.60-j35.88

4.2.1 Resonant modes in folded monopole antenna

Resonant phenomenon in folded monopole is identified from the FDTD computed E field distribution. The E field is computed at different layers of the antenna. The computed E field components are shown in Fig 4.4. Computed E field indicate that when the monopole is folded there is approximately a half wavelength variation along the length of the folded arm. The computed field distribution indicates that the folded arm must be loaded at a height of approximately quarter wavelength (which corresponds to E minimum) to avoid the radiation from the bend edges. When the loading height is greater or less than the quarter wavelength there may be radiation from the bend edges of the folded monopole. This will affect the radiation characteristics considerably. Hence loading height is selected according to the frequency requirements. From the E_x field components it is clearly evident that there is half wavelength variation of the field along the strip length of the folded monopole. Hence it can be concluded that antenna is polarized vertically along the Y direction. For the E_y components there is no variation of the field along L_1 and L_3 . But slight field intensity can be observed along the horizontal strip, L_2 which indicates that there may be horizontal component of E field due to the horizontal strip of the folded monopole. This indicates that cross polar level will be increased due to the effect of horizontal strip. The computed E_z component at the top layer of the strip is shown in Fig.4.4 (c). The E_z components again confirms that the half wavelength field variation along the length of the strip. Feeble field intensity can also be observed along the horizontal strip of the folded arm. Due to the horizontal field variation there will be coupling between this arm and ground plane which can affect the impedance matching characteristics of the folded monopole antenna. Simulated E field distribution is shown in Fig4.4 (d). This again confirms that there is a half wave variation of Electric field in the entire length of the antenna.

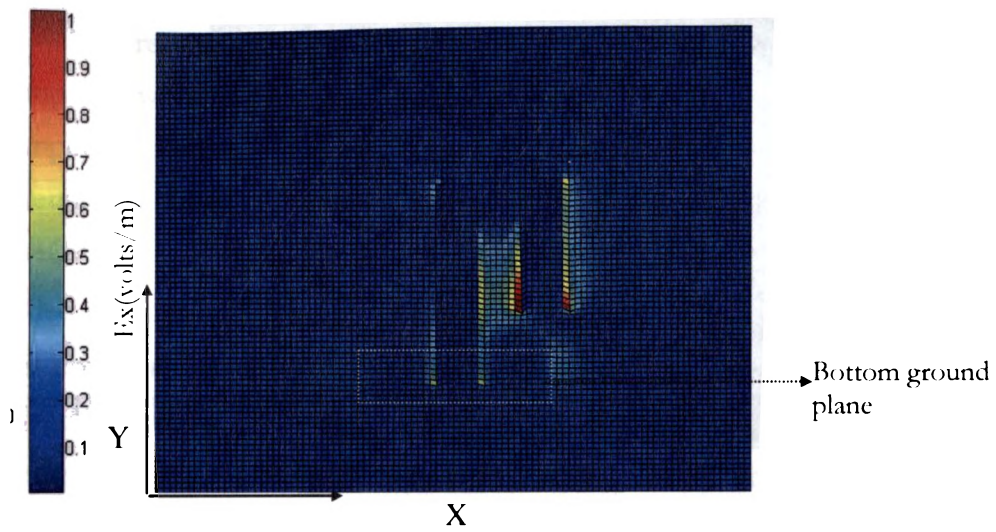


Fig.4.4 (a) FDTD computed E_x field distribution at the top of the folded strip monopole antenna at 1.8GHz, $L_G=3\text{mm}$, $W_G=20\text{mm}$ $L_1=24\text{mm}$, $L_2=13\text{mm}$, $L_3=16\text{mm}$, $w=3\text{mm}$

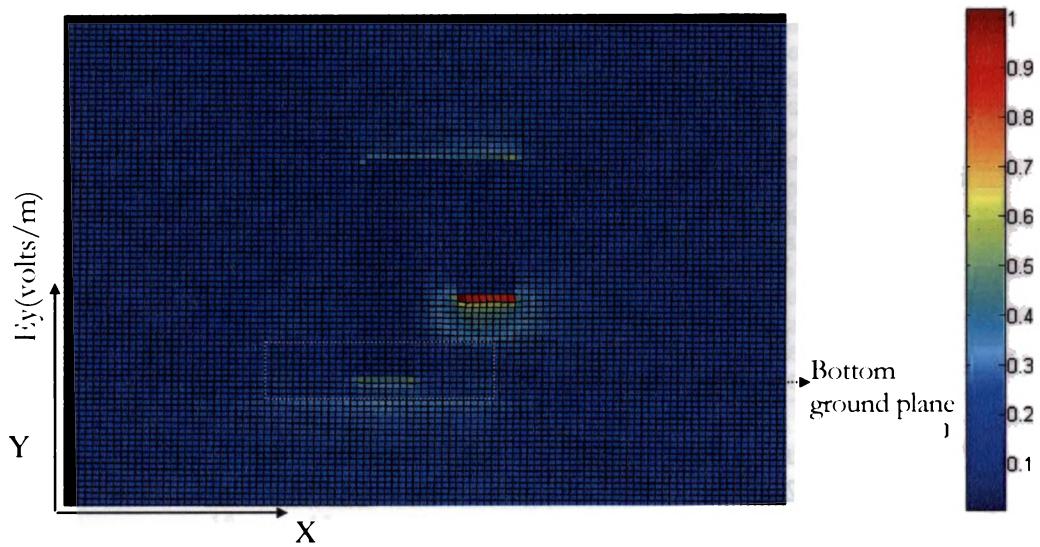


Fig.4.4 (b) FDTD computed E_y field distribution at the top of the folded strip monopole antenna at 1.8GHz, $L_G=3\text{mm}$, $W_G=20\text{mm}$ $L_1=24\text{mm}$, $L_2=13\text{mm}$, $L_3=16\text{mm}$, $w=3\text{mm}$

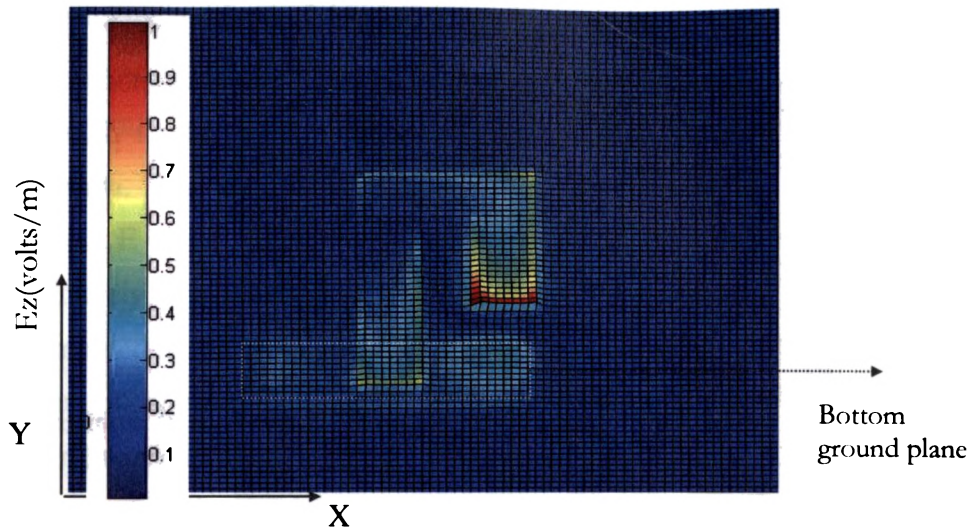


Fig.4.4 (c) FDTD computed E_z field distribution at the top of the folded strip monopole antenna at 1.8GHz, $L_G = 3\text{mm}$, $W_G = 20\text{mm}$, $L_1 = 24\text{mm}$, $L_2 = 13\text{mm}$, $L_3 = 16\text{mm}$, $w = 3\text{mm}$

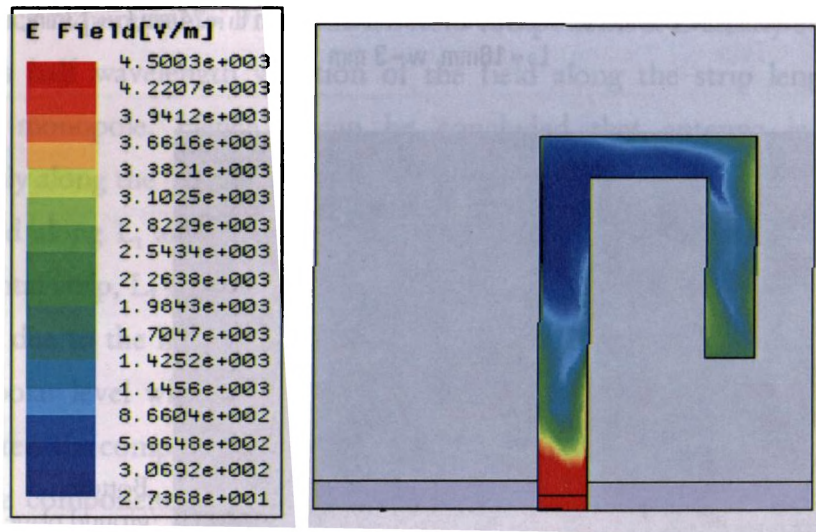


Fig 4.4. (d) Simulated field distribution of monopole antenna at 1.8GHz. $L_G = 3\text{mm}$, $W_G = 20\text{mm}$, $L_1 = 24\text{mm}$, $L_2 = 13\text{mm}$, $L_3 = 16\text{mm}$, $\epsilon_r = 4.4$, $h = 1.6\text{mm}$.

4.2.2 Effect of folding on antenna characteristics

The effect of folding on input impedance characteristics is presented in the previous section. The influence of folding on the reflection and radiation characteristics of the antenna is presented in the following sections.

4.2.2.1 Return loss characteristics

The return loss characteristic of the folded monopole antenna is compared with half wavelength strip monopole antenna in Fig.4.5. FDTD computed reflection characteristics predicts that the folded monopole antenna resonates at 1.8GHz with 2:1 VSWR bandwidth of 290MHz from 1.64GHz to 1.93GHz corresponding to fractional bandwidth of 16%. The folded monopole antenna is fabricated on a substrate of $\epsilon_r=4.4$ and $h=1.6\text{mm}$ and characterized using Agilent E8362B Programmable Network Analyzer. The measured return loss characteristics are in good agreement with the theoretically predicted result. The measured 2:1 VSWR impedance bandwidth of the antenna is 280MHz (1.675GHz-1.954GHz) with resonant frequency centered at 1.8GHz with fractional bandwidth of 15.5%. From the reflection characteristics it can be observed that an unfolded monopole antenna exhibits a bandwidth of 387.5MHz (11.6375GHz-2.025GHz) with resonant frequency centered at 1.825GHz corresponding to 22% fractional bandwidth.

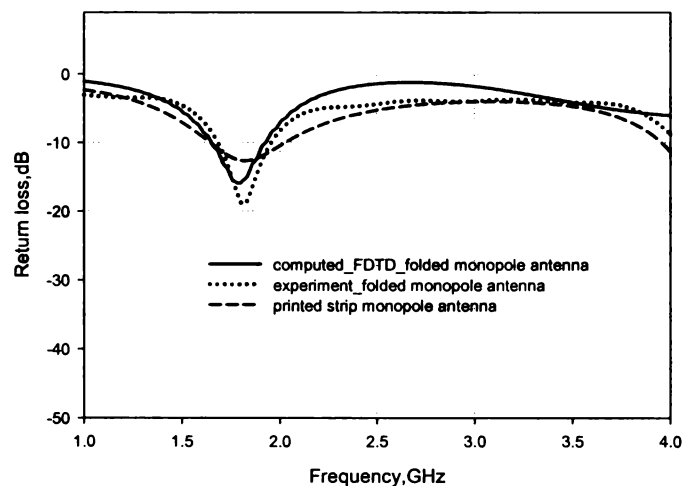


Fig 4.5 Reflection characteristics of the folded monopole antenna. $L_G = 3\text{mm}$, $W_G = 20\text{mm}$

$L_1 = 24\text{mm}$, $L_2 = 13\text{mm}$, $L_3 = 16$, $\epsilon_r = 4.4$, $h = 1.6\text{mm}$.

Strip monopole antenna $L_G = 3\text{mm}$, $W_G = 40\text{mm}$ $L_1 = 40\text{mm}$

Note that for the half wavelength strip monopole antenna the ground plane width required to fix the resonance at 1.8GHz is half wavelength and for quarter wavelength there is no impedance matching due to very low value of resistance at the input impedance. From the input impedance studies in the previous section we observed that when a quarter wavelength monopole is top loaded with folded arm the capacitive coupling between the ground plane and horizontal strip adds capacitive reactance to the input impedance of the antenna. Hence bandwidth of the antenna is slightly reduced than a vertical unfolded strip monopole. But with the folded arm technique the antenna size can be considerably reduced than unfolded monopole. Moreover, a vertical strip monopole of half wavelength requires an optimum ground plane of ~~half~~ wavelength in order to fix the resonant frequency at the desired value where as a quarter wavelength monopole top loaded with folded arm requires only a quarter wavelength ground plane width to fix the resonant frequency. Hence it can be concluded that folding the monopole is a suitable concept for size reduction even though bandwidth is slightly reduced.

4.2.2.2 Far field radiation pattern

From the computed E field distribution it can be observed that the variation of the field is dominant along the length of the monopole. The computed radiation patterns predict that the radiation from folded monopole is similar to dipole pattern with omnidirectional H plane and Figure of Eight E plane radiation patterns. Simulated 3D radiation characteristics again confirm that radiation characteristics are akin to a dipole. Radiation characteristics at the centre frequency of the impedance bandwidth are shown in Fig.4.6. The slight squinting in radiation patterns is due to the asymmetry of the folded monopole structure. The radiation characteristics reveal that the antenna is linearly polarized along Y direction. HFSS Simulated 3D radiation characteristics are shown in Fig 4.7. Simulated radiation characteristics again confirm that radiation pattern is nearly omnidirectional in one plane and figure of eight in the other plane. Even though the

radiation pattern of the folded monopole is similar to the strip monopole the beam is slightly tilted due to the asymmetry in the radiating structure. Thus from the theoretical and experimental investigations it is concluded that folded monopole exhibits a slight squinting in the radiation characteristics.

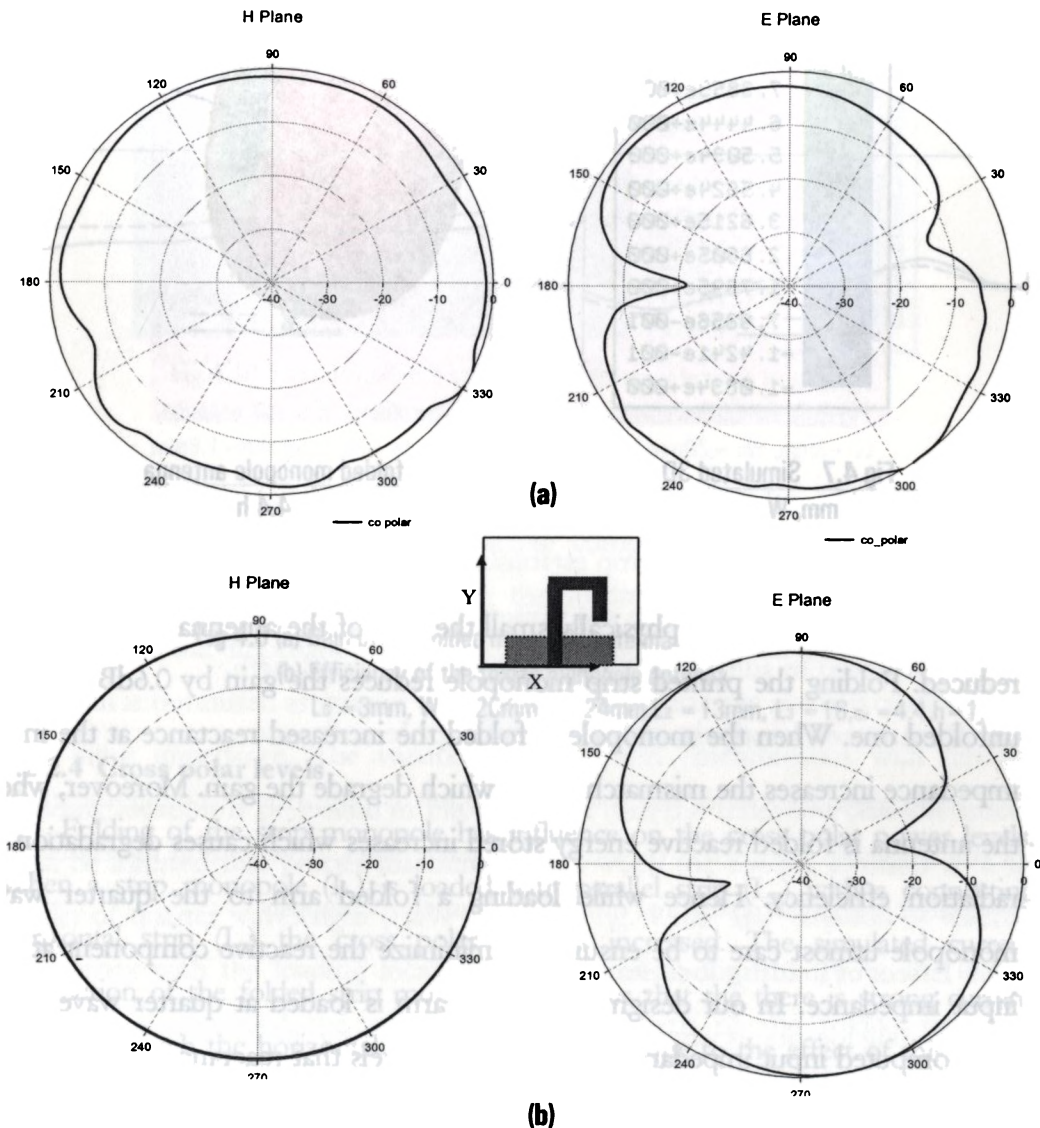


Fig 4.6 (a) Measured radiation patterns of the folded monopole at 1.8GHz
 (b) FDTD computed radiation patterns of the folded monopole at 1.8GHz.
 $L_6 = 3\text{mm}$, $W_6 = 20\text{mm}$, $L_1 = 24\text{mm}$, $L_2 = 13\text{mm}$, $L_3 = 16$, $\epsilon_r = 4.4$, $h = 1.6\text{mm}$.

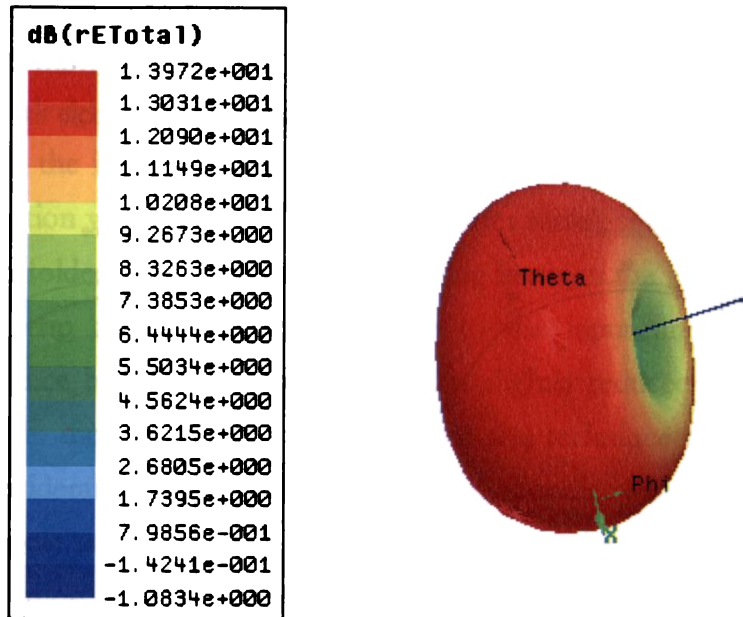


Fig 4.7 Simulated 3D radiation pattern of the folded monopole antenna
 $L_G = 3\text{mm}$, $W_G = 20\text{mm}$, $L_1 = 24\text{mm}$, $L_2 = 13\text{mm}$, $L_3 = 16$, $\epsilon_r = 4.4$, $h = 1.6\text{mm}$.

4.2.2.3 Gain and efficiency

When antenna size is physically small the gain of the antenna is considerably reduced. Folding the printed strip monopole reduces the gain by 0.6dBi than an unfolded one. When the monopole is folded the increased reactance at the input impedance increases the mismatch losses which degrade the gain. Moreover, when the antenna is folded reactive energy stored increases which causes degradation in radiation efficiency. Hence while loading a folded arm to the quarter wave monopole utmost care to be ensured to minimize the reactive component at the input impedance. In our design the parallel arm is loaded at quarter wavelength and computed input impedance characteristics reveals that reactance at the input is minimum hence efficiency is not that much degraded compared to vertical monopole of same length. Gain characteristics of the folded monopole are shown in Fig.4.8(a). The computed average gain of the antenna in the operating band is

2.26dBi where as the measured gain is 2.0dBi. The slight discrepancy is due to mismatch losses arising from the feed connector connected to a physically small folded monopole antenna which is not incorporated in FDTD analysis. Antenna efficiency measured using wheeler cap method shows that folded monopole antenna efficiency is 79% where as the computed efficiency is only 78%. The radiation efficiency of the antenna is shown in Fig.4.8 (b).

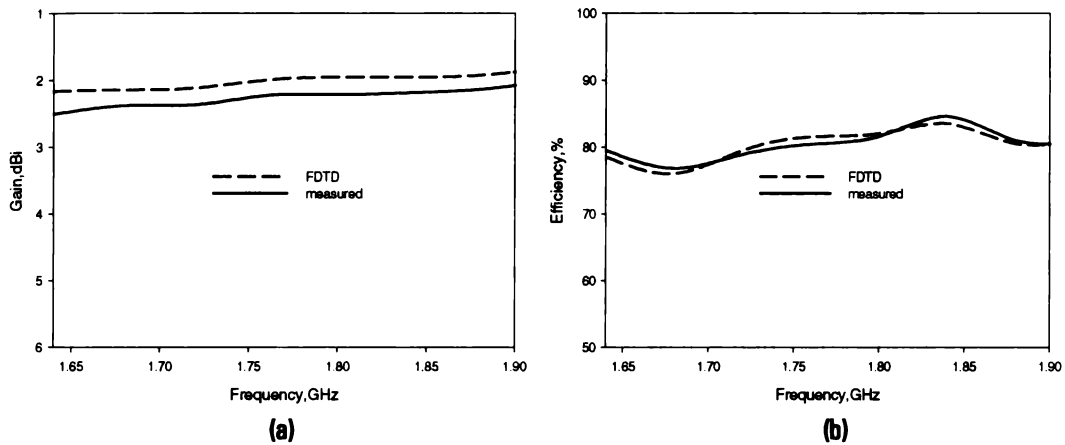


Fig 4.8 (a) Gain of the folded monopole antenna

(b) Efficiency of the folded monopole antenna

$L_6 = 3\text{mm}$, $W_6 = 20\text{mm}$, $L_1 = 24\text{mm}$, $L_2 = 13\text{mm}$, $L_3 = 16$, $\epsilon_r = 4.4$, $h = 1.6\text{mm}$.

4.2.2.4 Cross polar levels

Folding of the strip monopole has influence on the cross polar power levels. When a strip monopole (L_1) is loaded with parallel strip (L_3) with a connecting horizontal strip (L_2) the cross polar level is increased. The simulated current distribution of the folded strip monopole indicates that there is strong current flowing through the horizontal connecting strip L_2 . Due to the effect of this strong horizontal current polarization purity is low in the direction of maximum radiation. The simulated current distribution showing the effect of horizontal current variation is presented in Fig.4.9.

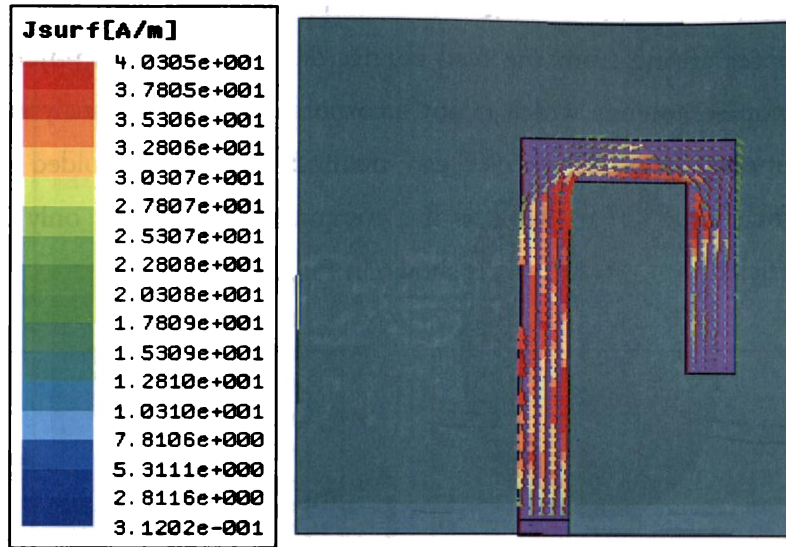


Fig 4.9. Simulated current distribution of the folded monopole antenna.
 $L_G = 3\text{mm}$, $W_G = 20\text{mm}$, $L_1 = 24\text{mm}$, $L_2 = 13\text{mm}$, $L_3 = 16$, $\epsilon_r = 4.4$, $h = 1.6\text{mm}$

When the horizontal strip length is lower then the coupling between the strip monopole and loaded parallel strip establishes a strong horizontal current and then cross polar level is very low. In the present design a cross polar level better than 20dB is achieved by suitably selecting the horizontal strip length.

4.3 Parametric analysis of folded monopole antenna.

Parametric analysis of the folded monopole is performed to study the effect of the structural parameters on antenna characteristics. This section illustrates the computed numerical results for different parameter variations.

4.3.1 Effect of loading location L_1

Loading location is very critical in determining the impedance matching of the antenna. The input impedance variation for different loading height L_1 is plotted in Fig 4.10.

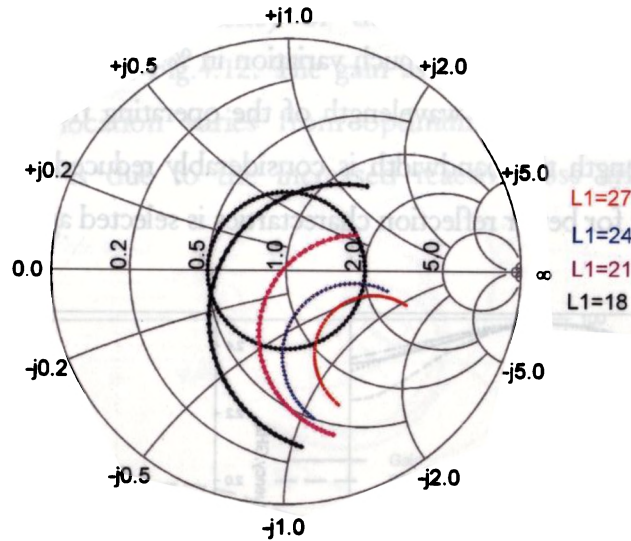


Fig 4.10. Input impedance variation for different loading Heights L_1 .
 $L_G = 3\text{mm}$, $W_G = 20\text{mm}$, $L_2 = 13\text{mm}$, $L_3 = 16$, $\epsilon_r = 4.4$, $h = 1.6\text{mm}$

Investigations on input impedance reveals that when the loading location is greater than quarter wavelength reactive component at the input impedance becomes more capacitive and when the loading location is less than quarter wavelength the impedance moves to the inductive region. Hence the loading location is optimized as quarter wavelength to minimize the reactive component at the input impedance. The variation of reflection characteristics with different loading location is presented in Fig.4.11 (a). From the reflection characteristics it can be inferred that proper matching occurs when the loading location is of the order of quarter wavelength (curve $L_1=21$ in fig. 4.10). The variation of resonant frequency with the loading location is presented in Fig.4.11 (b). As the loading location is increased the effective resonant length of the folded monopole increases and obviously the resonant frequency is decreased. Due to the increased reactance component at the input impedance of the folded monopole the bandwidth degradation is observed when loading location varies from quarter wavelength as shown in Fig.4.11(c). Computed maximum bandwidth that can be

achieved from the folded monopole is 16.4%. When the length L_1 is varied from 21 mm to 24 mm there is not much variation in % BW as the two values are very much close to the quarter wavelength of the operating frequency. But for larger variation of length the bandwidth is considerably reduced. Hence the optimum loading height for better reflection characteristics is selected as $\lambda_d/4$.

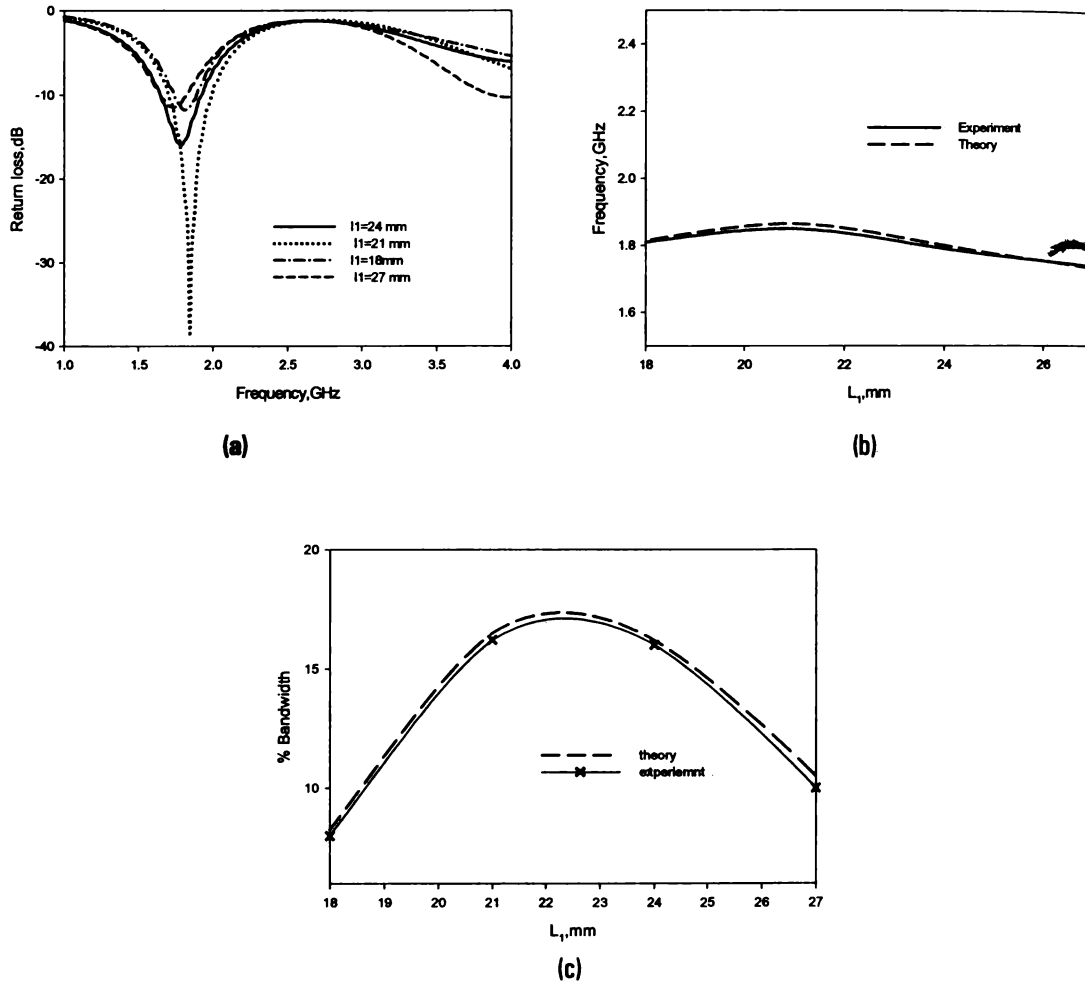


Fig 4.11. (a) Reflection characteristics for different loading locations L_1 .
 (b) Variation in resonant frequency with different loading locations
 (c) Variation in %BW with different loading heights
 $L_6 = 3\text{mm}$, $W_6 = 20\text{mm}$, $L_2 = 13\text{mm}$, $L_3 = 16$, $\epsilon_r = 4.4$, $h = 1.6\text{mm}$

Computed gain and efficiency of the antenna for different loading locations are presented in Fig.4.12. The gain as well as efficiency is degraded when the loading location varies from optimum value. The variation in radiation efficiency is due to the increased reactive loss arising from the reactive components.

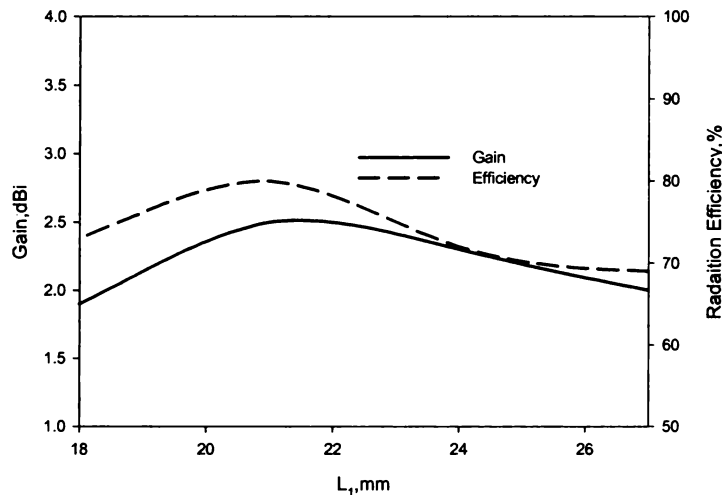


Fig 4.12. Computed gain and efficiency for different loading locations
 $L_6 = 3\text{mm}$, $W_6 = 20\text{mm}$, $L_2 = 13\text{mm}$, $L_3 = 16$, $\epsilon_r = 4.4$, $h = 1.6\text{mm}$

4.3.2 Effect of spacing between parallel strip and monopole arm, L_2

As already described in the section 4.2.2.4 the spacing has effect on the radiation characteristics of the folded monopole especially in the cross polarization purity. In this section effect of the spacing L_2 on the reflection characteristics is narrated. When the horizontal strip length is varied the effective length of the strip monopole changes and the resonant frequency varies accordingly. But when the horizontal length is very small the coupling between the arms increases which results in increased capacitive reactance at the input impedance of the folded monopole antenna as shown in Fig.4.13.

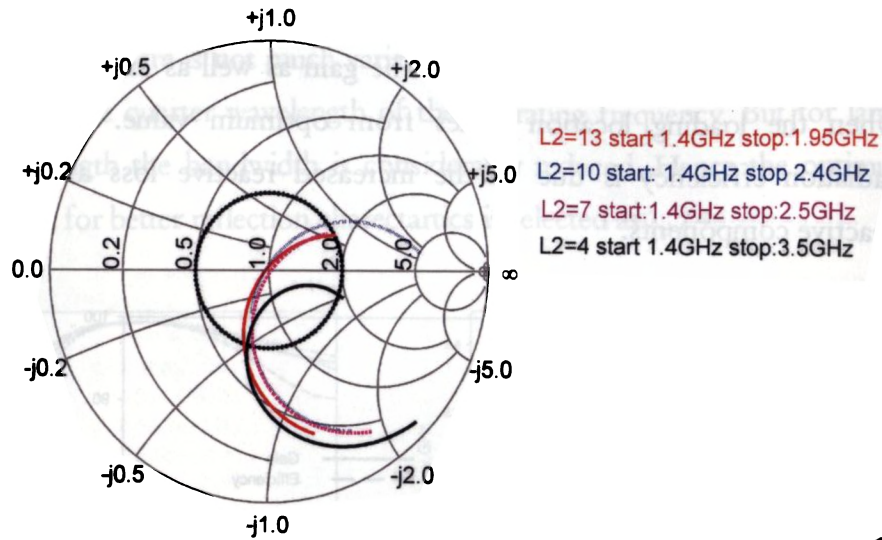


Fig. 4.13. Input impedance characteristics for different horizontal strip lengths.
 $L_6 = 3\text{mm}$, $W_6 = 20\text{mm}$, $L_1 = 21\text{ mm}$, $L_3 = 16$, $\epsilon_r = 4.4$, $h = 1.6\text{mm}$

Computed input impedance characteristics reveals that when the horizontal strip length is very low the vertical arm and loaded arm comes close to each other. This in turn decreases the Q of the antenna. Computed reflection characteristics for different horizontal arm lengths are presented in Fig.4.14 (a). From the Fig.4.14 (b) it can be observed that when L_2 changes the effective resonant length $L_1+L_2+L_3$ varies and hence resonant frequency changes by 1GHz when the horizontal strip length is varied from 4mm to 13mm. When the horizontal strip length is 4mm the %BW increases drastically due to the decreased Q of the device. Variation of %BW is presented in Fig. 4.14 (c). Even though wide bandwidth is obtained when the length L_2 is 4mm, the resonant frequency is increased. When the length L_2 is less than 4mm the two strips merge together to act as a single vertical strip with half wavelength. Hence concept of folding is lost in that case and antenna shows poor impedance matching. To fix the resonant frequency at the desired value without compromising the size L_2 is optimized as 13mm in this case.

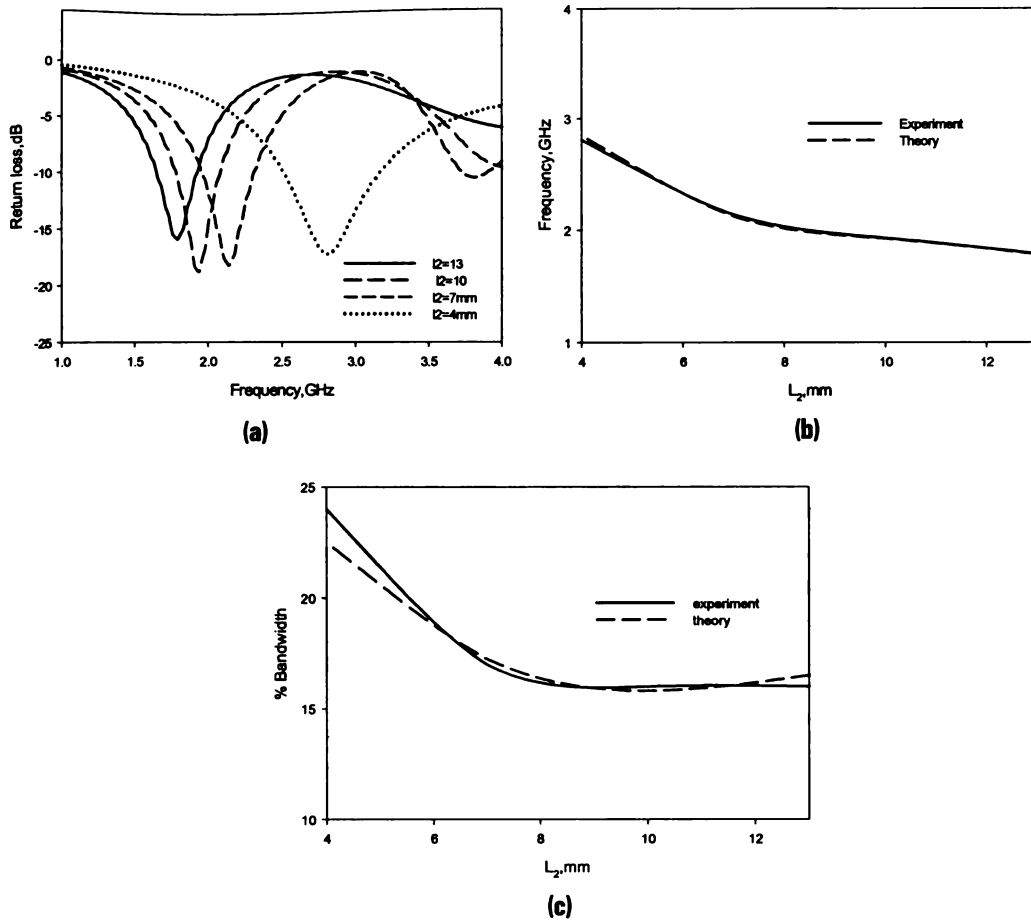


Fig. 4.14. (a) Reflection characteristics of the folded monopole antenna
 (b) Variation of resonant frequency with L_2
 (c) Variation of % BW with L_2 . $L_s = 3$ mm, $W_s = 20$ mm, $L_1 = 21$ mm,
 $L_3 = 16$, $\epsilon_r = 4.4$, $h = 1.6$ mm

Gain of the folded monopole antenna for different horizontal ground plane is measured using gain comparison methods. Gain variation is less for horizontal strip length variation from 7 mm to 13mm. But when the horizontal strip length is 4mm even though the antenna is properly matched the reactive component at the input impedance is high which causes reactive losses. The gain and efficiency is considerably reduced due to these reactive losses. Gain and efficiency characteristics are shown in Fig.4.15.

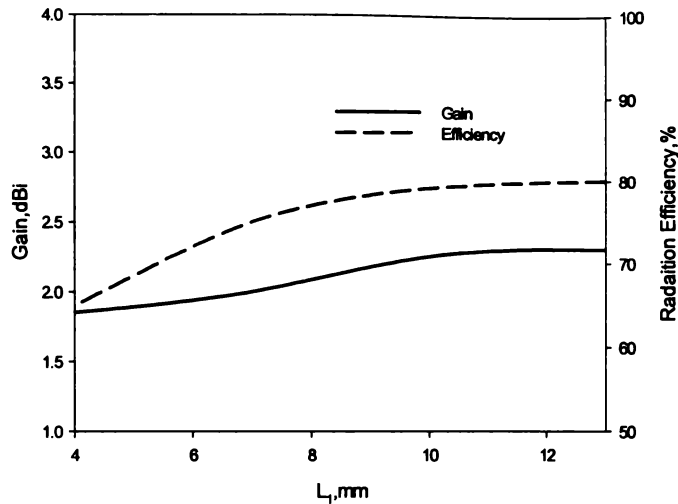


Fig. 4.15. Influence of horizontal arm length L_2 on gain and efficiency
 $L_6 = 3\text{mm}$, $W_6 = 20\text{mm}$, $L_1 = 21\text{mm}$, $L_3 = 16$, $\epsilon_r = 4.4$, $h = 1.6\text{mm}$

4.3.3 Effect of loaded parallel strip, L_3

When the loaded parallel strip length is varied from 4mm to 20mm the resonant frequency variation is only 450MHz (Fig4.16 (b)). When the loaded strip length increases the effective resonant path length increases which decreases the resonant frequency of the folded monopole antenna. But the computed reflection characteristics reveal that there is no considerable degradation in bandwidth of the antenna. The influence of loaded arm length on the reflection characteristics is depicted in Fig.4.16 (a). The % bandwidth remains almost constant with L_3 variation. But when the length of the parallel arm is considerably increased the bandwidth of operation degrades hence for the present design parallel arm length is selected less than quarter wavelength in the dielectric. When the loaded parallel arm length is equal to quarter wavelength the antenna exhibits high Q and the bandwidth is considerably reduced. Variation of % bandwidth with the length of parallel arm L_3 is shown in Fig.4.156(c).

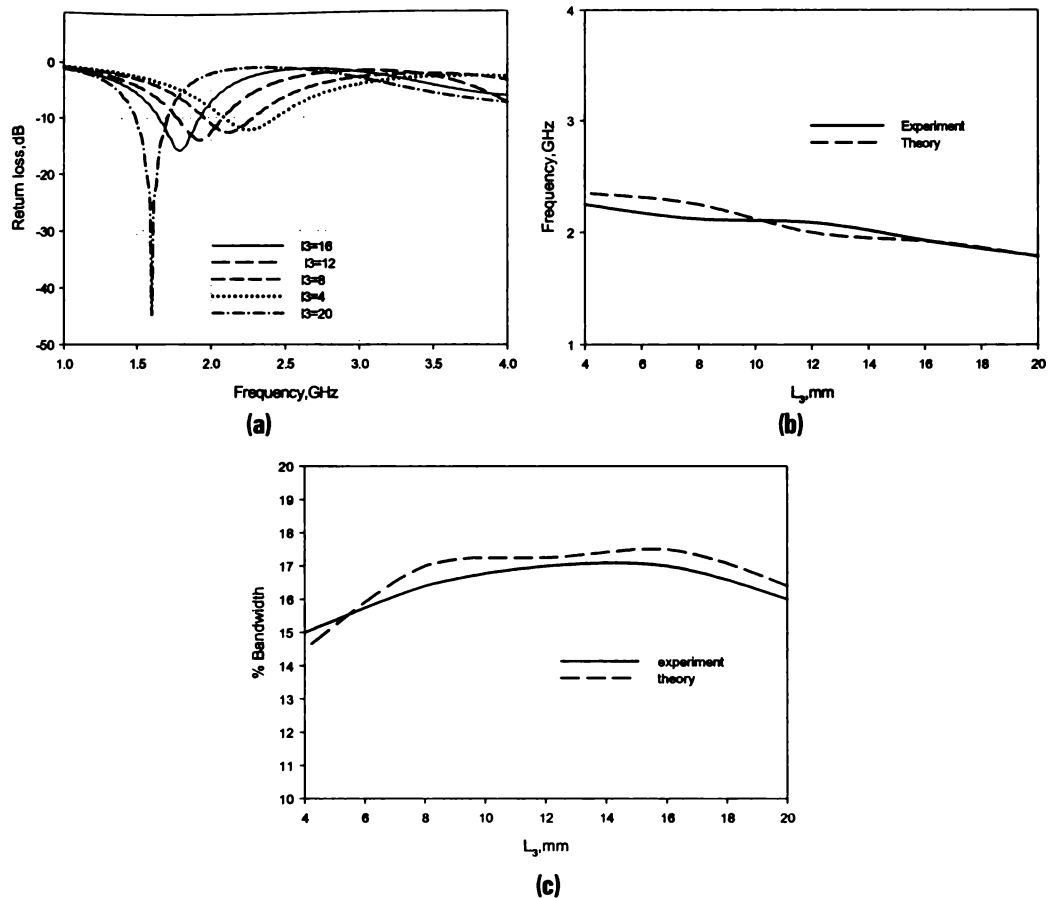


Fig. 4.16. (a) Reflection characteristics of the folded monopole antenna
 (b) Variation of resonant frequency with L_3
 (c) Variation of % BW with L_3 . $L_6 = 3$ mm, $W_6 = 20$ mm, $L_1 = 21$ mm, $L_2 = 10$,
 $\epsilon_r = 4.4$, $h = 1.6$ mm

4.3.4 Effect of Dielectric constant of the substrate, ϵ_r

The dielectric constant of the substrate material has influence on the resonant frequency of the folded monopole antenna. When the folded monopole antenna is fabricated on a dielectric substrate the change in dielectric constant will affect the characteristics impedance of the feed line which in turn modifies the return loss characteristics. Variation of reflection characteristics with different dielectric substrates is depicted in Fig.4.17 (a). When dielectric constant varies from 2.2 to

10.2 corresponding frequency change is 430MHz as shown in Fig.4.17 (b). For high dielectric constant substrates the bandwidth is reduced due to the high Q of the device. For dielectric constant with in the range of 2 to 6 the bandwidth performance is with in the acceptable limit. Influence of dielectric constant on the bandwidth of the folded monopole antenna is shown in Fig.4.17(c).

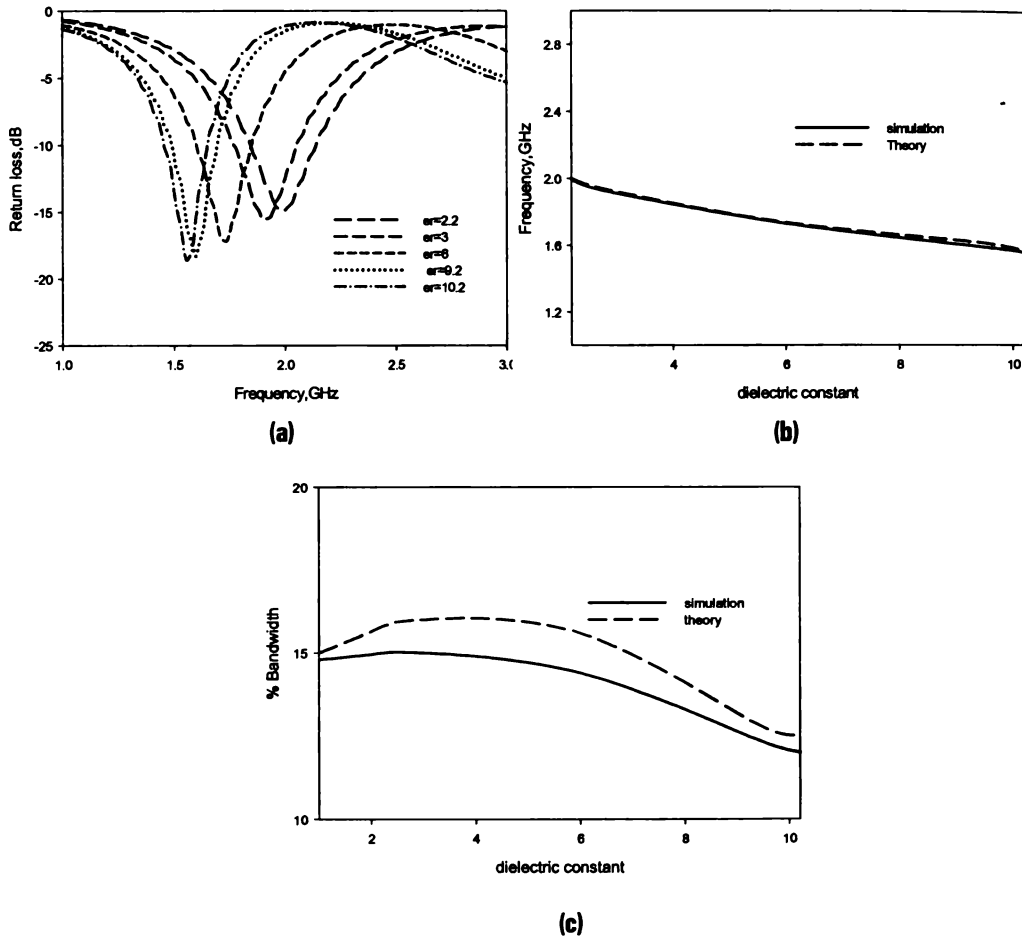


Fig. 4.17. (a) Effect of dielectric constant on the reflection characteristics of the folded monopole antenna
 (b) Variation of resonant frequency with dielectric constant
 (c) Variation of % BW with ϵ_r . $L_6 = 3\text{mm}$, $W_6 = 20\text{mm}$, $L_1 = 21\text{mm}$, $L_2 = 10$, $L_3 = 16\text{mm}$, $h = 1.6\text{mm}$

Variation in dielectric constant affects the radiation efficiency of the folded monopole antenna. The radiation efficiency decreases for high dielectric constant substrates. Computed results indicates a maximum efficiency of 87% when the antenna is printed on substrate of dielectric constant $\epsilon_r=2.2$. For $\epsilon_r=10.2$ the efficiency is only 84%. The measured average efficiency on an FR4 substrate is 78%. Efficiency is low in this case because of high loss tangent of FR4 substrate.

4.3.5 Effect of substrate height, h

Height of the substrate has considerable influence on the input impedance of the folded monopole antenna. This in turn affects the reflection characteristics considerably. The influence of the height of the substrate on the input impedance characteristics is shown in Fig. 4.18.

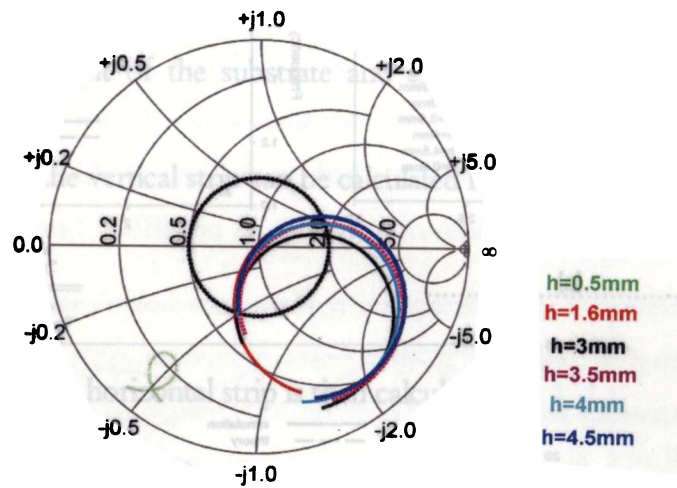


Fig.4.18. Input impedance variation of folded monopole antenna with height of the substrate.
 $L_G = 3\text{mm}$, $W_G = 20\text{mm}$, $L_1 = 21\text{mm}$, $L_2 = 10$, $L_3 = 16\text{mm}$, $\epsilon_r = 4.4$

For thin substrate the coupling between the bottom ground plane and the radiating folded monopole adds high capacitive reactance to the input impedance of the folded monopole antenna. Hence it is difficult to match the characteristic impedance of the feed line and the folded monopole antenna exhibits high reflection loss. The computed reflection characteristics for different substrate

thickness are presented in Fig.4.19 (a). From the figure it is clear that when the substrate is very thin impedance matching is very poor. When substrate thickness is varied from 1mm to 4.5mm the corresponding frequency change is 340MHz. From the computed E field values it is observed that when substrate thickness is varied field intensity varies on the different layers of the substrate. Hence substrate height should be accounted while calculating the resonant frequency of the folded monopole antenna. Variation in resonant frequency for different substrate thickness is shown in Fig.4.19 (b). For thick substrates Q is very low and bandwidth increases considerably as shown in Fig.4.19(c).

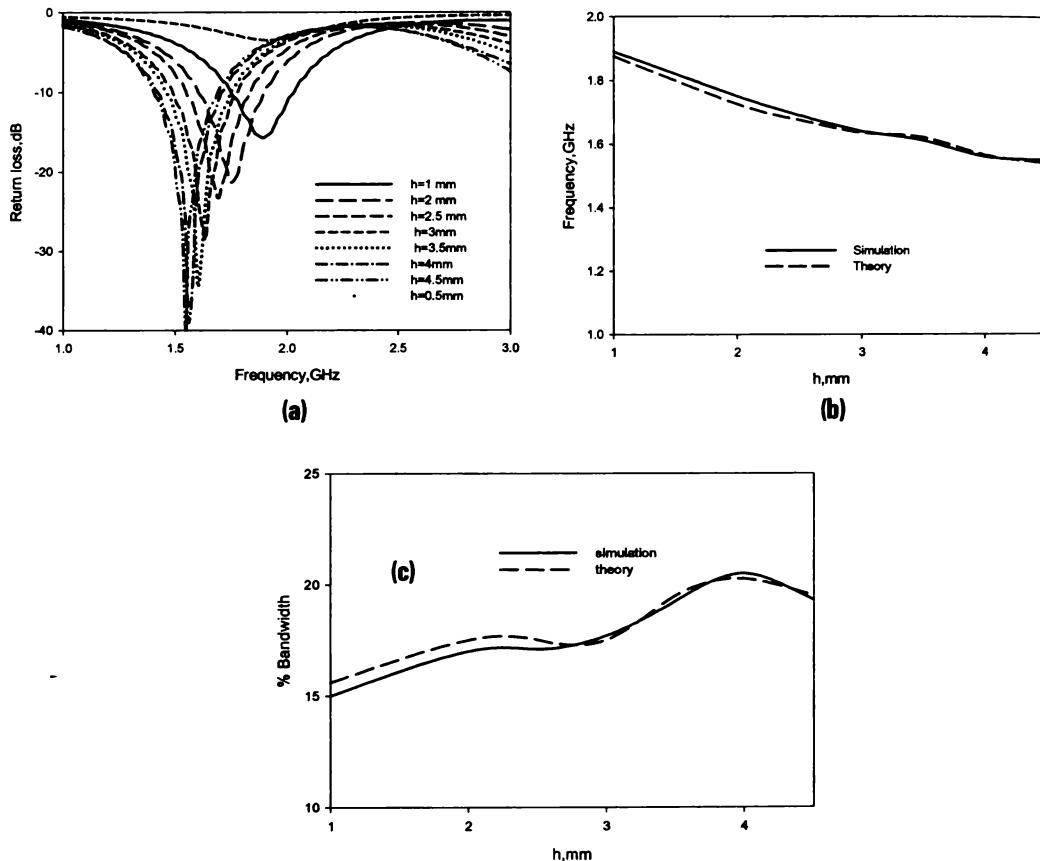


Fig. 4.19. (a) Effect of substrate thickness on reflection characteristics of the folded monopole antenna
 (b) Variation of resonant frequency with height of the substrate
 (c) Variation of % BW with h. $L_G = 3\text{mm}$, $W_G = 20\text{mm}$, $L_1 = 21\text{ mm}$, $L_2 = 10$, $L_3 = 16\text{ mm}$, $h = 1.6\text{mm}$, $\epsilon_r = 4.4$

4.4 Design procedure for a compact folded monopole antenna.

From the exhaustive numerical analysis and experimental observations a simple design criteria is formulated for the design of the folded monopole antenna. The following design equations can be used to design the antenna with good reflection and radiation characteristics.

- Select any substrate with dielectric constant ϵ_r and height h . The width of the folded monopole is set as width of 50Ω microstrip feed line.
- Since the field components are not confined to the substrate alone effective dielectric constant has to be used in calculation.

$$\epsilon_{eff} = \frac{\epsilon_r + 1}{2} (1 + 0.3 * h) \dots\dots\dots(4.1)$$

Where h is the height of the substrate and ϵ_r is the dielectric constant of the substrate.

- Length of the vertical strip can be calculated from the following equation

$$L_1 = \frac{0.25c}{f_r * \sqrt{\epsilon_{eff}}} \dots\dots\dots(4.2)$$

- Length of the horizontal strip is then calculated as

$$L_2 = \frac{0.1625c}{f_r * \sqrt{\epsilon_{eff}}} \dots\dots\dots(4.3)$$

- Length of the loaded strip is given by the equation below as

$$L_3 = \frac{0.2c}{f_r * \sqrt{\epsilon_{eff}}} \dots\dots\dots (4.4)$$

- Ground plane dimensions are then calculated using the following equations

$$L_G = \frac{0.0375c}{f_r * \sqrt{\epsilon_{eff}}} \dots\dots\dots(4.5)$$

$$W_G = \frac{0.25c}{f_r * \sqrt{\epsilon_{eff}}} \dots\dots\dots(4.6)$$

Where 'c' is the velocity of electromagnetic wave in free space. The constants 0.25 and 0.0375 are derived empirically after studying the effect of ground plane dimensions.

4.5 Antenna designs in various wireless communication standards

The validity of design equations are confirmed by fabricating the folded monopole antenna at desired wireless communication bands of interest. Return loss characteristics of antenna designed in various wireless communication standards are depicted in Fig.4.20.

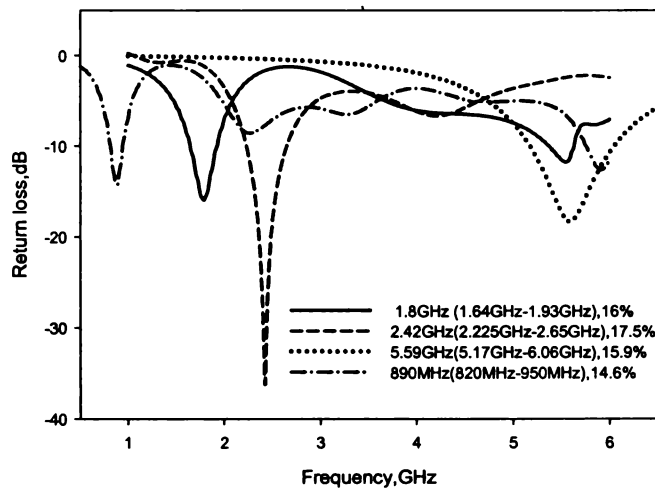


fig.4.20 Folded monopole antenna in various wireless communication standards.

Table 4.2 summarizes the antenna characteristics in different wireless standards.

Wireless Standard	Antenna parameters (mm)	Resonant frequency f_r (GHz)	Band	%Band width	Gain (dBi)	Efficiency (%)
DCS	$L_1=20, L_2=13, L_3=16$ $L_G=3, W_G=20$	1.8GHz	1.64GHz- 1.93GHz	16	2	78
2.4GHz WLAN	$L_1=15.6, L_2=10,$ $L_3=12.5, L_G=2.4\text{mm}$ $W_G=15.6,$	2.42GHz	2.225GHz -2.65GHz	17.5	3	80
5.2GHz WLAN	$L_1=7.2, L_2=4.7, L_3=5.78$ $L_G=1.1, W_G=7.2$	5.59GHz	5.17GHz- 6.06GHz	15.9	3.5	83
GSM	$L_1=42, L_2=27,$ $L_3=33, L_G=6.25, W_G=42$	890MHz	820MHz- 950MHz	14.6	1.78	74

In all the cases the antenna is operating with a bandwidth better than 14% and gain better than 1.75dBi and nearly omni directional radiation coverage.

The area of the folded monopole is compared with a standard rectangular patch and vertical strip monopole resonating at designed frequency. An area reduction of 79% can be achieved compared to rectangular microstrip resonating at the same frequency. Even though an area reduction of 77% compared to vertical monopole can be achieved with the folded monopole antenna a 3% reduction in bandwidth is observed when the antenna is folded. This bandwidth reduction can be eliminated by judiciously placing another strip whose length is properly selected so that the capacitive reactance arising from the folding can be nullified with the inductive stub. The Design of such a wide band folded monopole antenna with an additional arm is presented in the next section. The suitable location of the second arm increases the bandwidth of the first mode at

the same time an additional second mode is excited due to the various current paths excited in the antenna structure. Theoretical and experimental investigations of thus derived dual folded monopole antenna are elaborately recited in the following section.

4.6 FDTD analysis of Double Folded strip monopole antenna (DFSMA) for dual band operation.

The dual folded strip monopole antenna is derived from a single folded strip monopole antenna by modifying it with an additional arm placed at the appropriate location. This modified structure shown in Fig.4.21 consists of two different meandered current paths resulting in dual band operation.

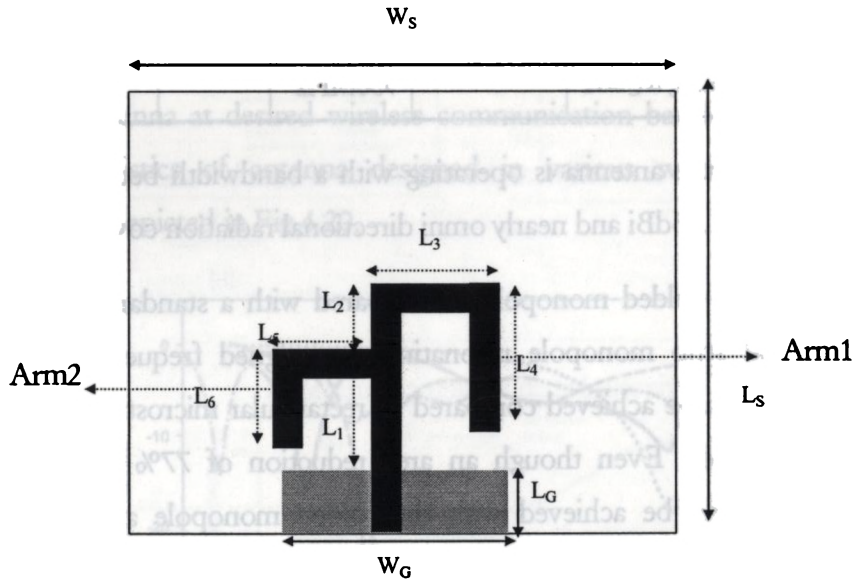


Fig.4.21. Geometry of the proposed dual branched folded monopole antenna. $L_G = 3\text{mm}$, $W_G = 15\text{mm}$, $L_S = 30\text{mm}$, $W_S = 30\text{mm}$, $L_1 = 15\text{mm}$, $L_2 = 5\text{mm}$, $L_3 = 13\text{mm}$, $L_4 = 16\text{mm}$, $L_5 = 10\text{mm}$, $L_6 = 12\text{mm}$, $h = 1.6\text{mm}$, $\epsilon_r = 4.4$.

For a printed strip monopole antenna described in the previous section with single arm the bandwidth performance is limited due to the capacitive coupling

between the parallel strip L and ground plane. This capacitive coupling adds a reactive component to the input impedance of the antenna. By judiciously placing another arm of length greater than quarter wavelength the capacitive reactance at the input impedance can be compensated. If the new arm is placed at proper location then the entire length of the second arm constitutes an additional current and second resonant mode is excited in the radiating structure. Thus by adding the second arm the bandwidth of the folded monopole is increased with an additional advantage of a new resonant mode. From the experimental investigations on folded monopole antenna operating at 1.8GHz we arrived at a conjecture that the length of the second arm required to ascertain the proper impedance matching is $0.275\lambda_d$ corresponding to the frequency of operation. The new arm is placed at a height of about $0.25\lambda_1$ corresponding to 2.4GHz a second resonance is generated in the radiating structure with frequency centered at 2.4GHz. These predicted results are verified by modelling a dual arm folded monopole antenna using FDTD algorithm. For this double folded monopole antenna with the parameters $L_G=3\text{mm}$, $W_G=15\text{mm}$, $L_S=30\text{mm}$, $W_S=30\text{mm}$, $L_1=15\text{mm}$, $L_2=5\text{mm}$, $L_3=13\text{mm}$, $L_4=16\text{mm}$, $L_5=10\text{mm}$, $L_6=12\text{mm}$ are implemented on a substrate of thickness 1.6mm and dielectric constant 4.4. Computed reflection characteristics are verified by fabricating a prototype and testing using E8362B PNA. The details of experimental, theoretical and simulated results are presented in the following section.

4.6.1 Resonance and radiation phenomenon in DFSMA.

The resonance in the double folded monopole antenna is associated with various current paths excited in the DFSMA structure. The longer arm1 of the monopole contributes for lower resonance and shorter arm 2 contributes for second resonance. From the computed Ex field distribution corresponding to the lower frequency, it can be observed that there is a half wavelength variation of the field along the longer arm of the folded monopole as shown in

Fig.4.22(a). The longer arm is strongly radiating at this frequency with polarization along Y direction. But there is feeble field variation along the shorter arm too. Hence it can be concluded that there is effect of the coupling of arm 2 on arm1. The computed E_y values shown in Fig.4.22 (b) indicates that there is slight field variation along the horizontal arms L_3 and L_5 . But for the lower resonant modes these field variations are equal and opposite and their effect cancels in the far field. So for the lower resonant mode better cross polarization discrimination can be expected. The E_z field plotted in Fig.4.22(c) again confirms the half wavelength variation of the field along the longer arm1 of the dual folded monopole antenna.

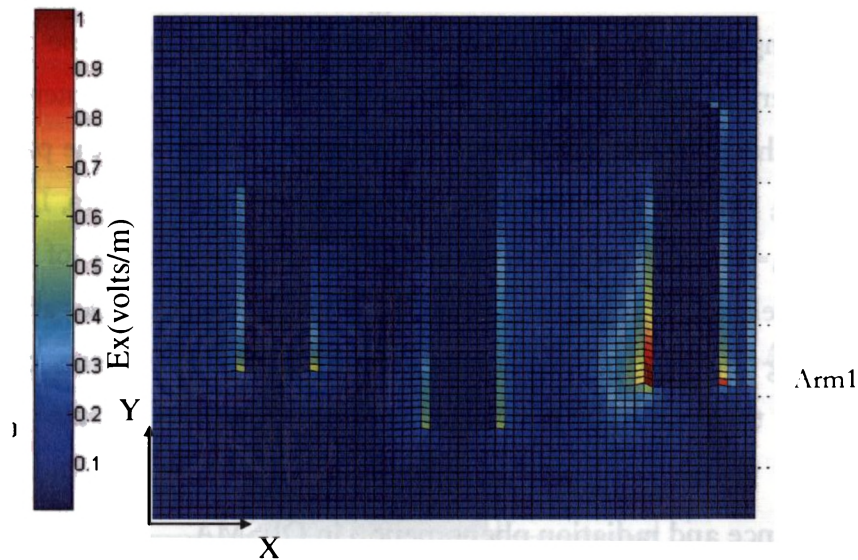


Fig. 4.22(a) computed E_x at the strip layer for first resonant mode(at 1.725GHz)
 $L_6 = 3\text{mm}$ $W_6 = 15\text{mm}$, $L_1 = 15\text{ mm}$, $L_2 = 5\text{ mm}$, $L_3 = 13\text{ mm}$, $L_4 = 16\text{ mm}$, $L_5 = 10\text{ mm}$, $L_6 = 12\text{ mm}$

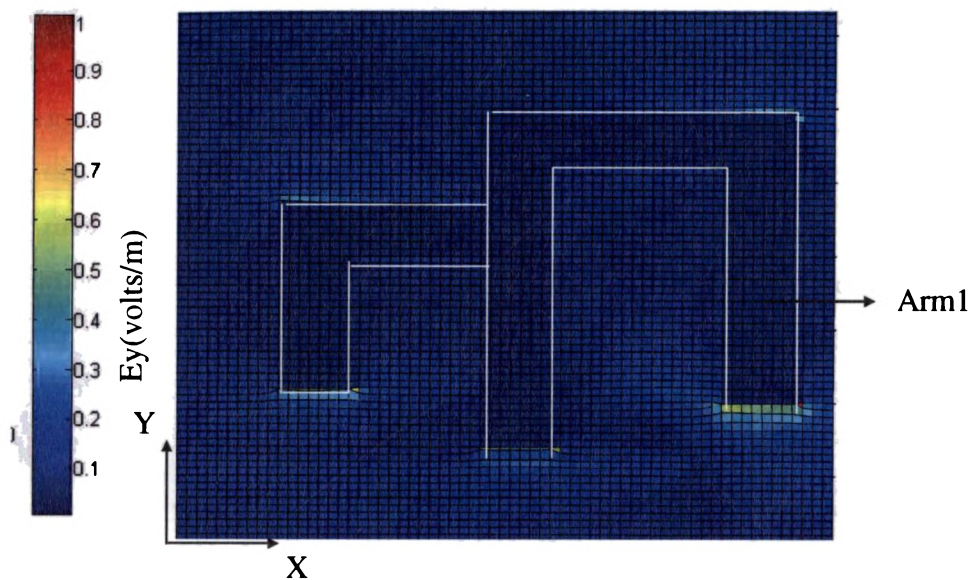


Fig. 4.22(b) computed E_y at the strip layer at first resonant mode(at 1.725GHz)
 $L_6 = 3\text{mm}$ $W_6 = 15\text{mm}$, $L_1 = 15\text{ mm}$, $L_2 = 5\text{ mm}$, $L_3 = 13\text{ mm}$, $L_4 = 16\text{ mm}$, $L_5 = 10\text{ mm}$, $L_6 = 12\text{ mm}$

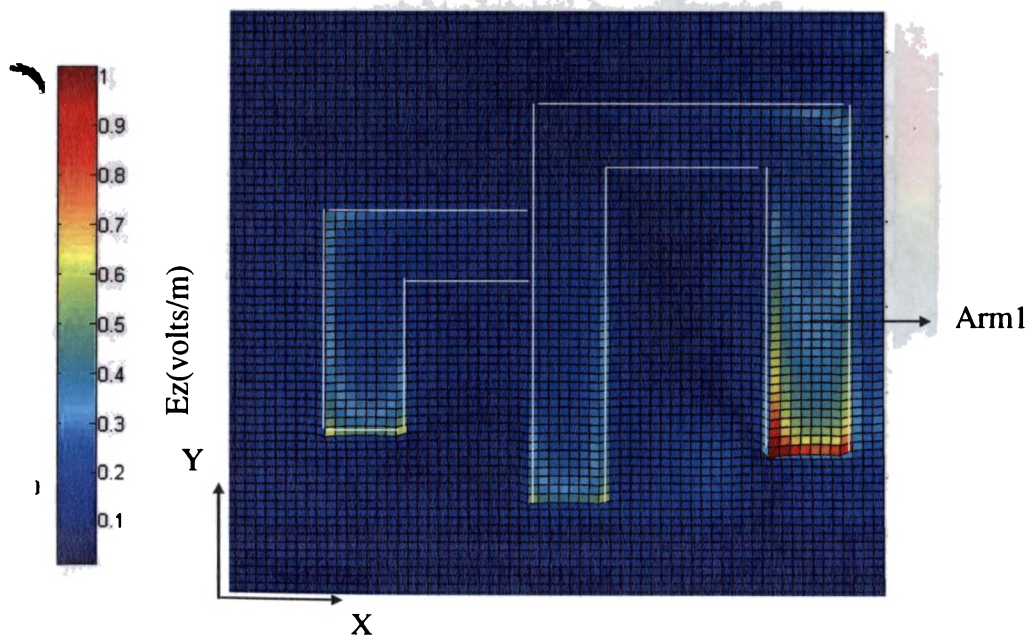


Fig. 4.22(c) computed E_z at the strip layer at first resonant mode(at 1.725GHz)
 $L_6 = 3\text{mm}$ $W_6 = 15\text{mm}$, $L_1 = 15\text{ mm}$, $L_2 = 5\text{ mm}$, $L_3 = 13\text{ mm}$, $L_4 = 16\text{ mm}$, $L_5 = 10\text{ mm}$, $L_6 = 12\text{ mm}$

For the second resonant mode E field distribution is computed by assigning a sinusoidal excitation corresponding to the second resonant frequency. From the computed E_x field distribution a half wavelength variation of the field can be observed along shorter arm as shown in Fig.4.23 (a). In the second resonant mode there is no effect of the longer arm. But E_y distribution shown in Fig.4.23 (b) reveals that there is feeble variation of electric field along the horizontal strip. In this case the field is in phase and their effect adds in the far field. Hence a high cross polar power level can be expected for the second resonant mode. The E_z field distribution depicted in Fig.4.23(c) again confirms the half wavelength variation along the shorter arm length. From the computed E field components it can be inferred that antenna is polarized along Y direction.

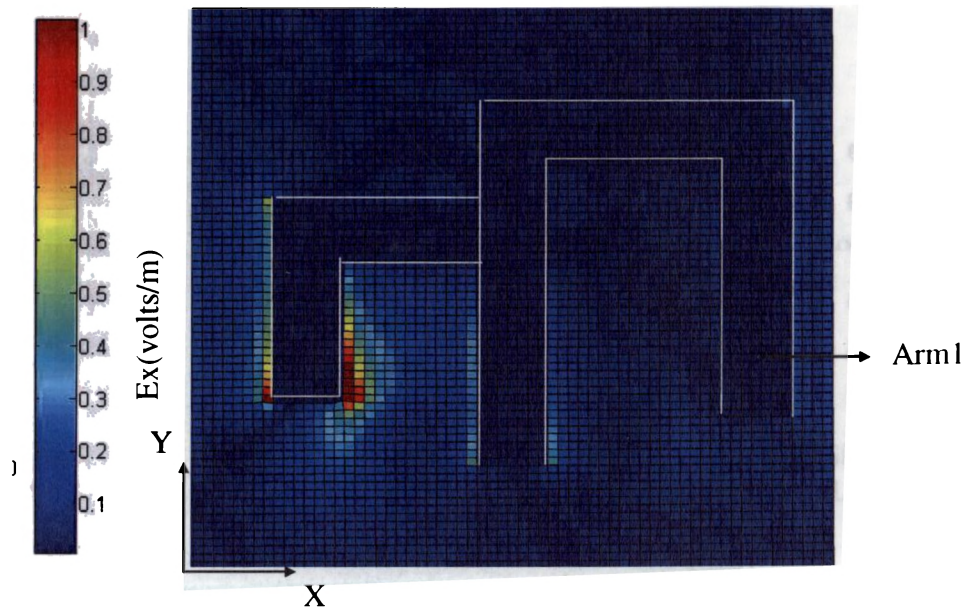


Fig. 4.23(a) computed E_x at the strip layer at second resonant frequency (at 2.4GHz)
 $L_G = 3\text{mm}$ $W_G = 15\text{mm}$, $L_1 = 15\text{ mm}$, $L_2 = 5\text{ mm}$, $L_3 = 13\text{ mm}$, $L_4 = 16\text{ mm}$, $L_5 = 10\text{ mm}$, $L_6 = 12\text{ mm}$

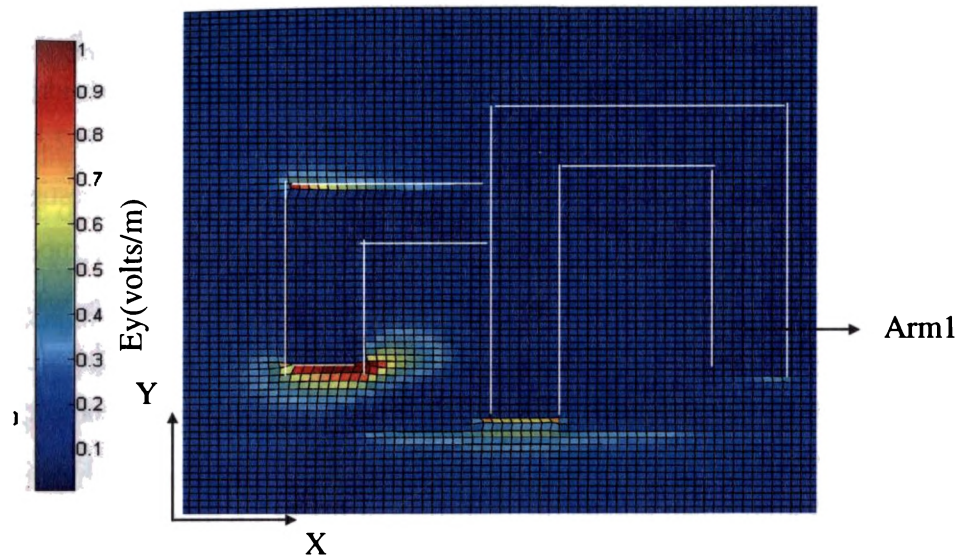


Fig. 4.23(b) computed E_y at the strip layer at second resonant frequency (at 2.4GHz)
 $L_6 = 3\text{mm}$ $W_6 = 15\text{mm}$, $L_1 = 15\text{ mm}$, $L_2 = 5\text{ mm}$, $L_3 = 13\text{ mm}$, $L_4 = 16\text{ mm}$, $L_5 = 10\text{ mm}$, $L_6 = 12\text{ mm}$

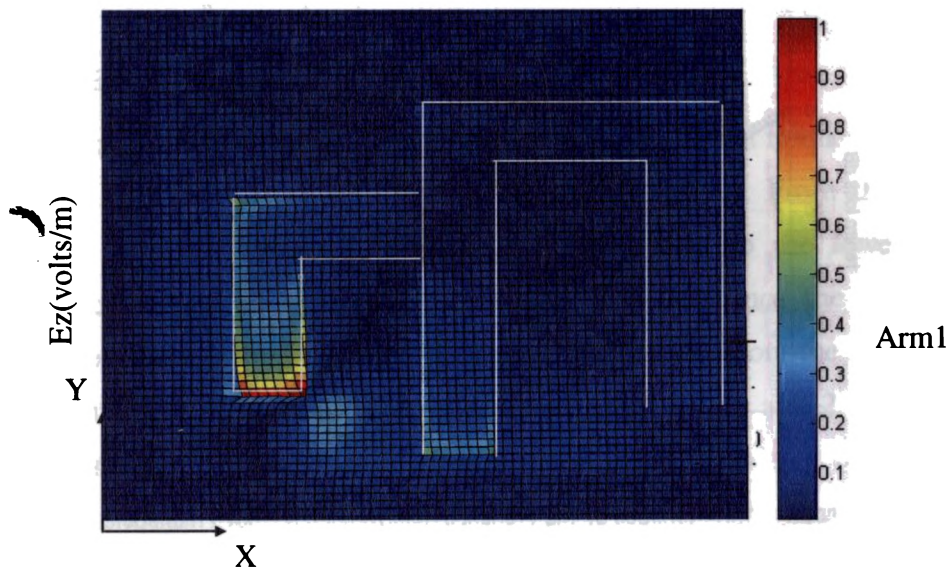


Fig. 4.23(c) computed E_z at the strip layer at second resonant frequency(at 2.4GHz)
 $L_6 = 3\text{mm}$ $W_6 = 15\text{mm}$, $L_1 = 15\text{ mm}$, $L_2 = 5\text{ mm}$, $L_3 = 13\text{ mm}$, $L_4 = 16\text{ mm}$, $L_5 = 10\text{ mm}$, $L_6 = 12\text{ mm}$

monopole antenna offers two distinct resonant modes at 1.725GHz and 2.45GHz respectively. The lower impedance band due to arm 1 provides a 2:1 VSWR bandwidth of 505MHz from 1.375GHz-1.88GHz which corresponds to 29% bandwidth. The upper resonance due to arm 2 reaches 220MHz from 2.33GHz-2.55GHz corresponding to 9% bandwidth. From the experimental and theoretical investigations it is found that optimum width of ground plane required to ensure proper impedance matching is quarter wavelength of the higher resonant frequency. Thus with two different resonant lengths constitutes dual band operation as predicted from theoretical inferences. Theoretically predicted results are in good agreement with experimental and simulated results. The dual frequency monopole antenna occupies an area of 30x25mm² when printed on a substrate of height 1.6 mm and 4.4 dielectric constant. Thus dual folded monopole antenna offers an area reduction 67% corresponding to conventional planar microstrip antenna.

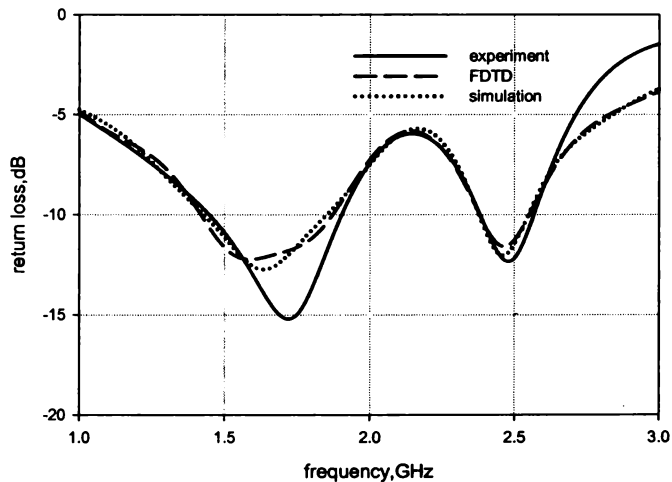


Fig.4.24. Reflection characteristics of the proposed dual frequency folded monopole antenna. $L_6 = 3\text{mm}$, $W_6 = 15\text{mm}$, $L_S = 30\text{mm}$, $W_S = 30\text{mm}$, $L_1 = 15$, $L_2 = 5$, $L_3 = 13$, $L_4 = 16$, $L_5 = 10$, $L_8 = 12$, $h = 1.6\text{mm}$, $\epsilon_r = 4.4$, $\epsilon_r = 4.4$.

The two different arms of the folded monopole have influence on each of the resonance characteristics. The following section describes the effect of the coupling of the arms on the reflection and radiation characteristics.

4.6.2 Double Folding for dual frequency: A case study

A double folded monopole antenna with two branched folded arms offers a dual resonance characteristics due to different meandered current paths excited in the radiating structure. The longer arm1 of the folded monopole excites a lower resonance of the dual frequency response and shorter arm excites the higher frequency. But for the lower frequency shorter arm of the monopole increases the inductive reactance as the length of the arm2 is approximately quarter wavelength of the shorter arm. Thus the capacitive impedance due the coupling between the ground plane and horizontal strip of the arm1 is minimized and antenna exhibits bandwidth enhancement in the lower order mode. But for the second resonant mode arm1 length is half wavelength order of the second resonant frequency hence arm 1 adds more capacitive reactance to the input impedance of the second resonant frequency. Thus for second mode degradation in bandwidth is observed .The effect of this mutual coupling on antenna characteristics is illustrated in the subsequent section.

4.6.2.1 Effect of mutual coupling of arms

The effect of mutual coupling of the two arms of dual frequency monopole antenna affects the reflection and radiation charectartics. From the simulated current distribution shown in Fig.4.25 corresponding to the lower resonant frequency it can be observed that for the first resonance the arm2 of the monopole even though exhibits a feeble current variation the effect of the horizontal current causing the coupling is cancelled by the arm 2. Moreover the horizontal strip of the arm1 of the folded monopole causes a horizontal field variation which increases the cross polar power of the antenna. But for lower resonant mode this horizontal current cancels at the far field due to the arm2 as the horizontal strip current in the arm 2 is opposite in phase with arm 1 current. Thus better cross polar discrimination is obtained for lower resonant mode.

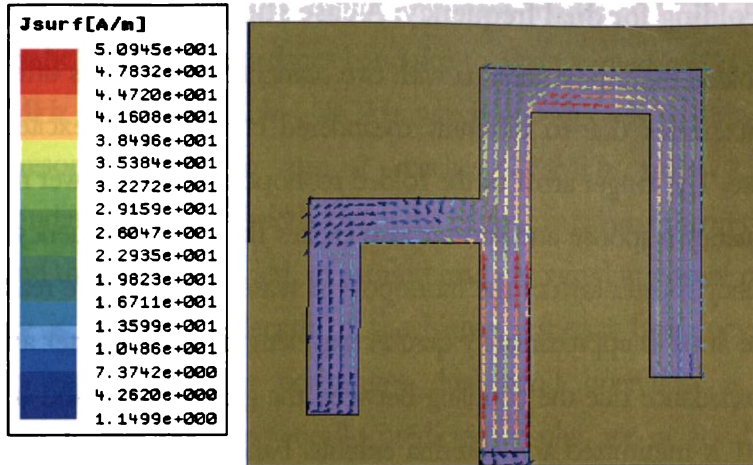


Fig.4.25 Simulated current distribution of the dual frequency folded monopole antenna at 1.8GHz..
 $L_6 = 3\text{mm}$ $W_6 = 15\text{mm}$, $L_S = 30\text{mm}$ $W_S = 30\text{mm}$, $L_1 = 15$, $L_2 = 5$, $L_3 = 13$, $L_4 = 16$, $L_5 = 10$,
 $L_6 = 12$, $h = 1.6\text{mm}$, $\epsilon_r = 4.4$

But for the higher resonant mode the arm 1 of the monopole excites a horizontal current in phase with the current on the horizontal strip of arm 2. Hence the resultant will add in the far field and polarization purity is very poor for the second resonant mode. The current distribution corresponding to the second resonant mode is shown in Fig.4.26.

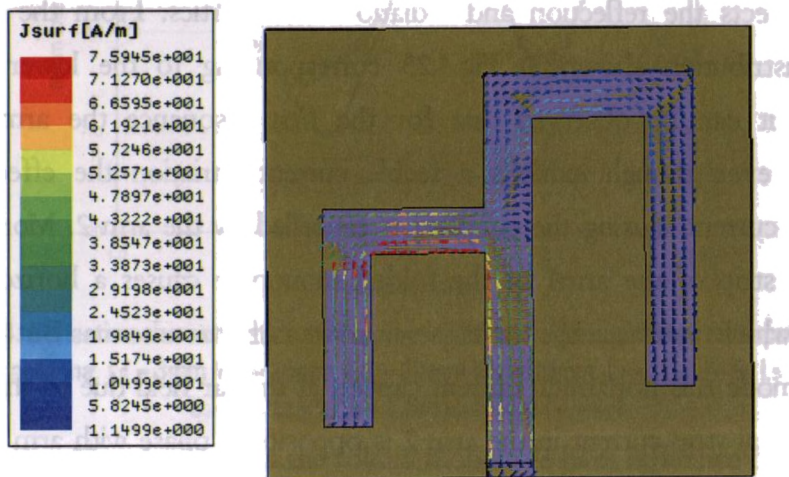


Fig.4.26. Simulated current distribution of the dual frequency folded monopole antenna at 2.4 GHz.
 $L_6 = 3\text{mm}$ $W_6 = 15\text{mm}$, $L_S = 30\text{mm}$ $W_S = 30\text{mm}$, $L_1 = 15$, $L_2 = 5$, $L_3 = 13$, $L_4 = 16$, $L_5 = 10$, $L_6 = 12$,
 $h = 1.6\text{mm}$, $\epsilon_r = 4.4$ $\epsilon_r = 4.4$.

4.6.2.2 Effect of arm 2 on first resonance.

The influence of arm 2 on the input impedance characteristics of the arm 1 is shown in Fig.4.27. With out arm 2, the antenna is resonating at 1.79GHz with a bandwidth of 16%. By the introduction of arm2 the resonant frequency is found to be slightly changed to 1.725GHz. When arm 2 is added the capacitive reactance caused by the folding of arm1 is cancelled due to the arm 2 . Thus bandwidth enhancement is observed in arm 1 band due to addition of arm2. For folded monopole operating at 1.8GHz a maximum % bandwidth obtained by suitably placing this additional strip is 29%. Note that for single folded monopole the bandwidth performance was only 16% and a vertical strip monopole the bandwidth was 21%. Computed return loss characteristics shown in Fig.4.28 summarizes the above inferences. It is interesting to note the additional advantage of a second resonance by adding arm 2.

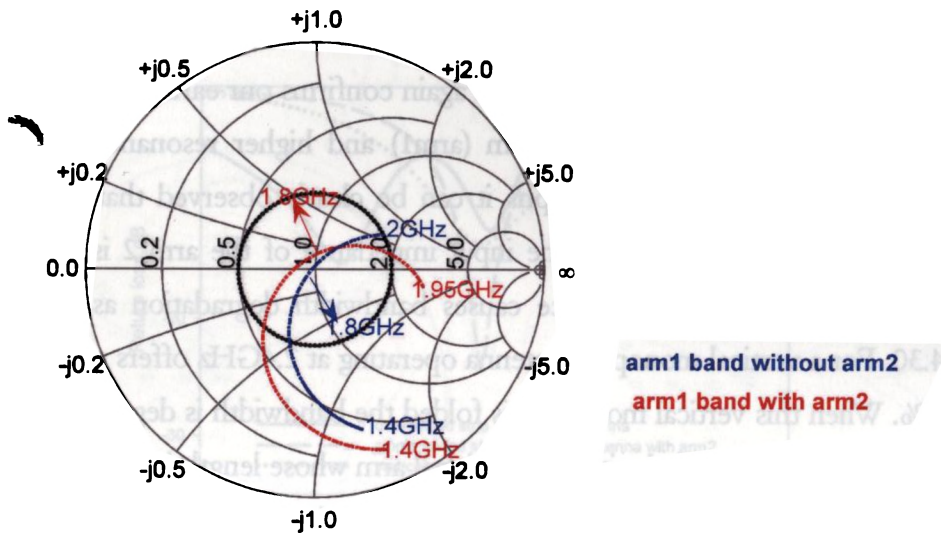


Fig.4.27 computed input impedance characteristics of the dual folded monopole antenna at lower band $L_6 = 3\text{mm}$ $W_6 = 15\text{mm}$, $L_S = 30\text{mm}$ $W_S = 30\text{mm}$, $L_1 = 15$, $L_2 = 5$, $L_3 = 13$, $L_4 = 16$, $L_5 = 10$, $L_6 = 12$, $h = 1.6\text{mm}$, $\epsilon_r = 4.4$

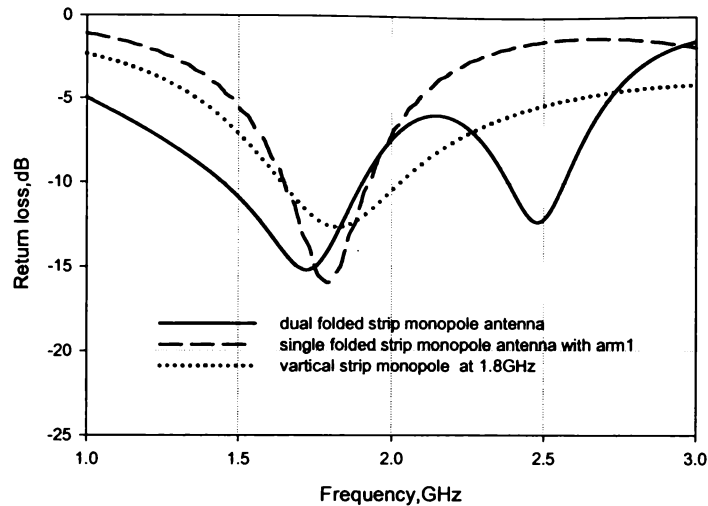


Fig.4.28. Reflection characteristics of different antennas operating at 1.8GHz

4.6.2.3 Effect of arm 1 on second resonance

Fig.4.29 clearly indicates the influence of arm 1 on the input impedance characteristics of the arm 2 band. Single folded antenna is resonating at 2.437GHz with a bandwidth of 14%. By the addition of arm 1 an additional resonance at 1.79GHz is introduced. This observation again confirms our earlier argument that lower resonance is due to longer arm (arm1) and higher resonance is due to shorter arm (arm2). From the graphs it can be clearly observed that by adding arm1 the capacitive reactance at the input impedance of the arm 2 is increased. This increased capacitive reactance causes bandwidth degradation as shown in Fig.4.30. For a vertical monopole antenna operating at 2.4GHz offers a wide band of 23%. When this vertical monopole is folded the bandwidth is degraded to 16%. But when the arm is loaded with an additional arm whose length is greater than half wavelength of arm 1 the bandwidth is further reduced to 10%.

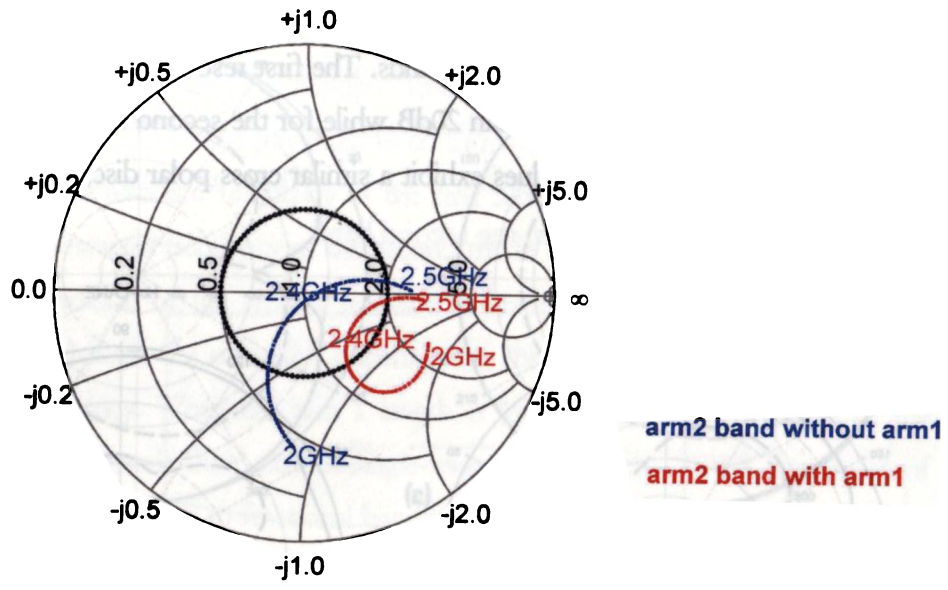


Fig.4.29 FDTD Computed input impedance charectartics at the second band. $L_6 = 3\text{mm}$
 $W_6 = 15\text{mm}$, $L_S = 30\text{mm}$ $W_S = 30\text{mm}$, $L_1 = 15$, $L_2 = 5$, $L_3 = 13$, $L_4 = 16$, $L_5 = 10$, $L_6 = 12$,
 $h = 1.6\text{mm}$, $\epsilon_r = 4.4$ $\epsilon_r = 4.4$.

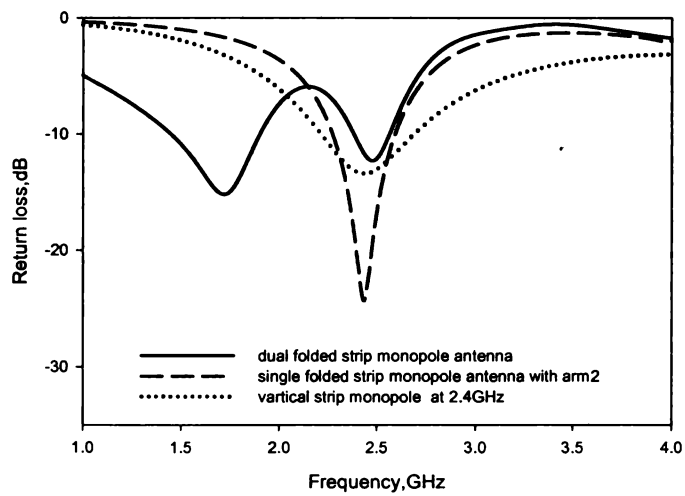
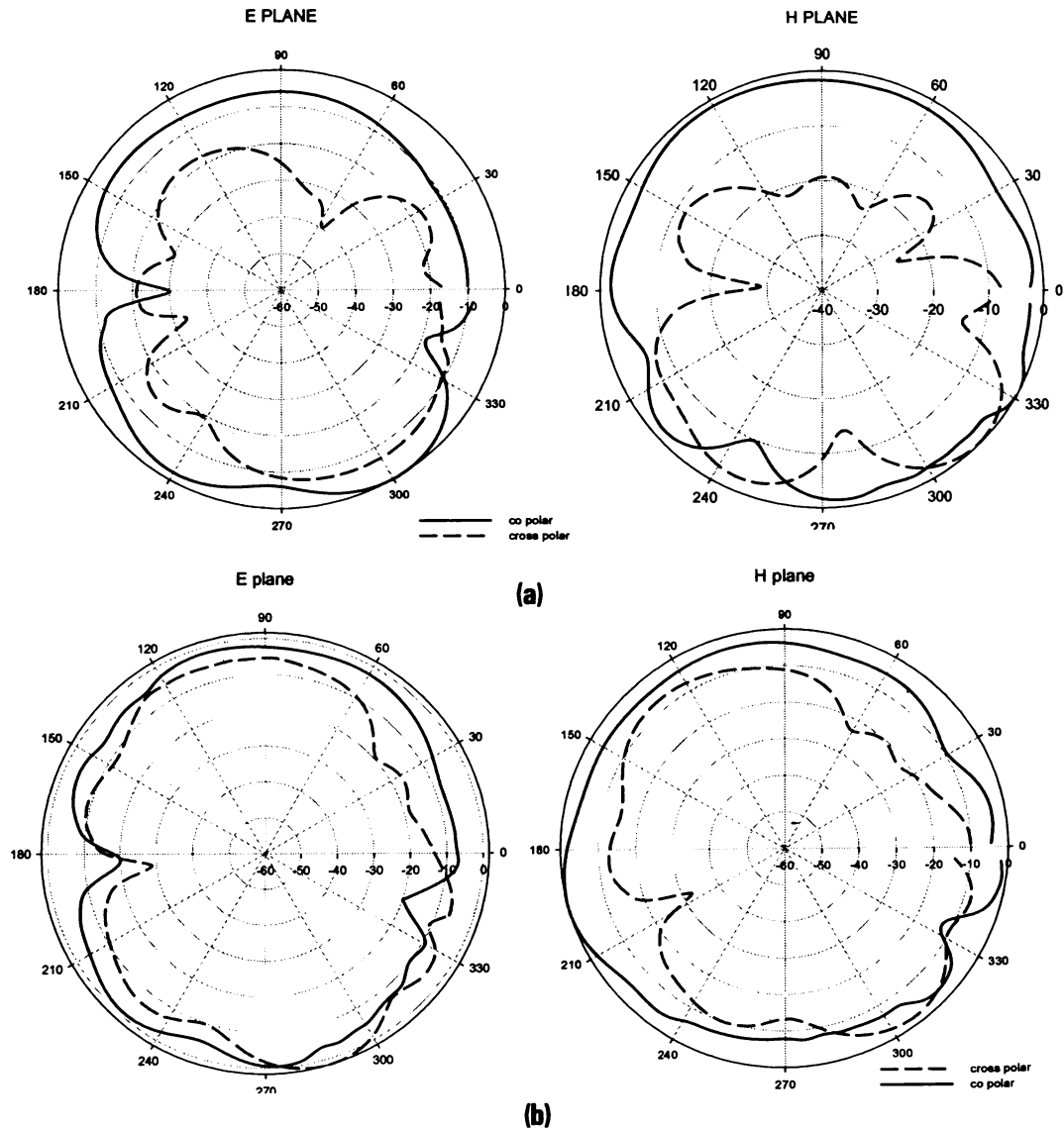


Fig.4.30. Reflection characteristics of different antennas operating at 2.4GHz.

Computed and experimental radiation patterns at the two resonant frequencies of the dual folded monopole antenna are shown in Fig.4.31. The antenna is vertically polarized along Y direction in the two bands. The first resonant frequency exhibits a cross polar discrimination better than 20dB while for the second resonance the cross polar level is high. Measured values exhibit a similar cross polar discrimination in the two bands.



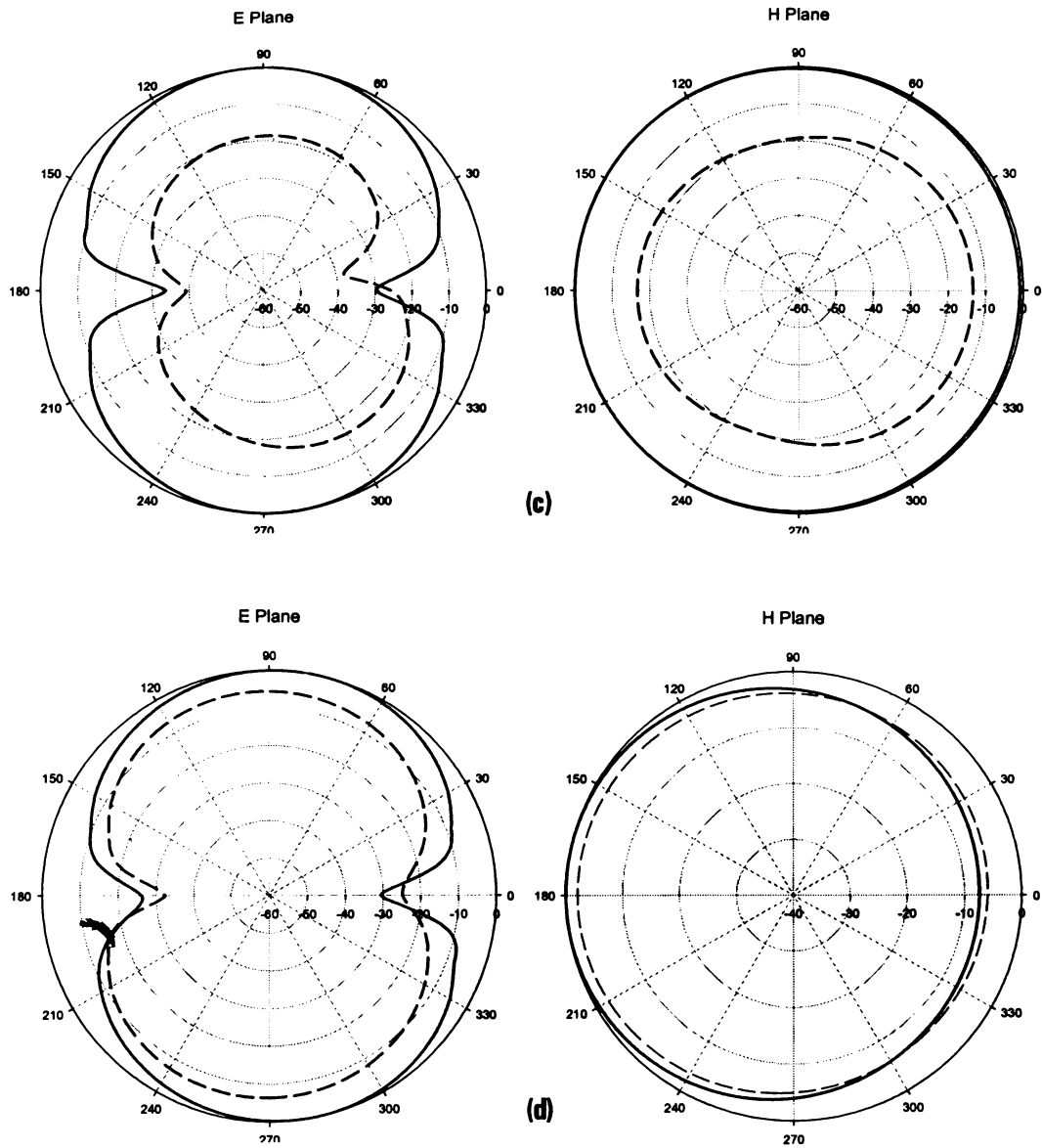


Fig.4.31 Radiation patterns of the double folded dual band antenna

$L_6 = 3\text{mm}$ $W_6 = 15\text{mm}$ $L_S = 30\text{mm}$ $W_S = 30\text{mm}$ $L_1 = 15$ $L_2 = 5$ $L_3 = 13$ $L_4 = 16$
 $L_5 = 10$ $L_8 = 12$ $h = 1.6\text{mm}$ $\epsilon_r = 4.4$

(a) experimental at 1.8GHz (b) Computed at 1.8GHz

(c) Experimental at 2.4GHz (d) Computed at 2.4GHz

Gain of the antenna is measured using gain comparison method and average gain obtained in the 1.8GHz band is 2.53dBi. For the second resonant mode the average gain is 2.1dBi. Measured gains of the antenna in the two bands are shown in Fig.4.32. Measured efficiency of the antenna in the first resonant frequency is 80.1% and second resonant frequency is 73.6%. Where as computed efficiency is 85% in the first band and 76% in the second band.

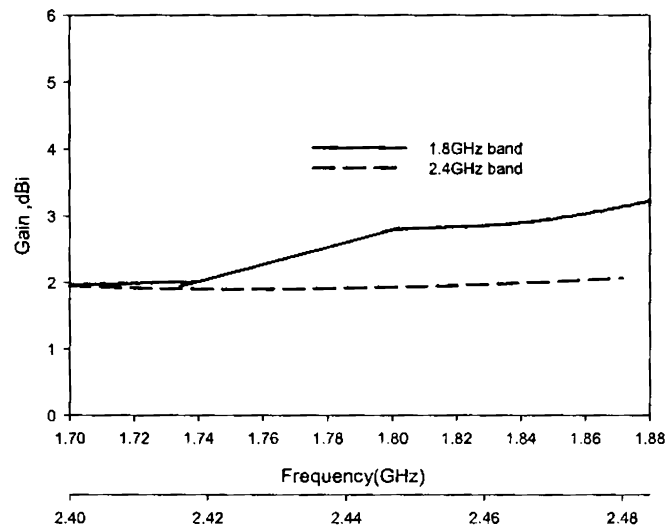


Fig.4.32 Gain of the double folded dual band antenna in the two resonant bands. $L_G = 3\text{mm}$
 $W_G = 15\text{mm}$, $L_S = 30\text{mm}$ $W_S = 30\text{mm}$, $L_1 = 15$, $L_2 = 5$, $L_3 = 13$, $L_4 = 16$, $L_5 = 10$, $L_6 = 12$,
 $h = 1.6\text{mm}$, $\epsilon_r = 4.4$

4.6.3 Parametric analysis of double folded monopole antenna.

Parametric analysis of the antenna is performed to confirm predicted resonant modes and effect of each parameter on the antenna characteristics. The resonant frequency and impedance bandwidth are the main characteristics being investigated. Parametric analysis leads to the formulation of simple equations to design the dual band folded monopole antenna for any two bands of operation.

4.6.3.1 Effect of folded arm1

Effect of the entire resonant length of arm 1 $L_1 = L_1 + L_2 + L_3 + L_4$ is varied to study the effect on the two resonant frequencies. Investigation on variation of individual strip length is also presented to confirm our earlier arguments. When arm 1 length is varied resonant frequency of the first mode changes considerably but the variation of resonant frequency of the second mode is negligible. But the impedance matching condition of the second resonant frequency changes considerably as the arm1 length changes the capacitive impedance at the input impedance of the second resonant frequency. When the arm 1 length is lower than half wavelength of the second resonant mode there exists a single wide band with 2:1 VSWR bandwidth of 670 MHz corresponding to fractional bandwidth of 34 % as shown in Fig.4.33. This study again confirms that arm1 is responsible for first mode and its length affects the impedance matching condition of the second mode. As expected, the resonant frequency decreases with increase of arm1 length L_1 .

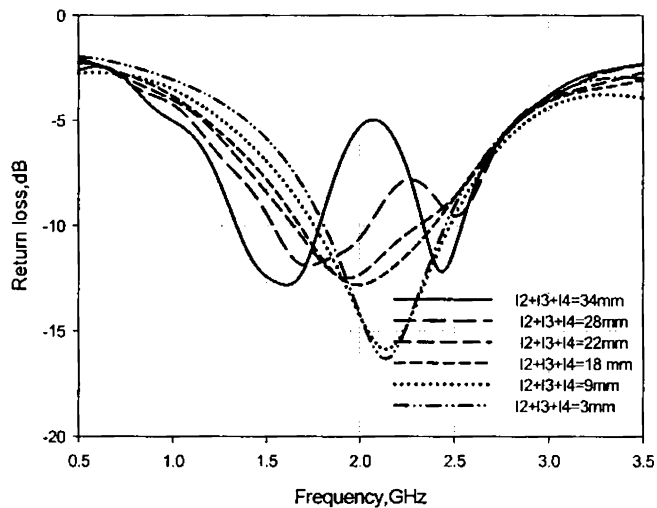


Fig.4.33 Influence of arm 1 length on the return loss characteristics of the dual folded monopole antenna. $L_6 = 3$ mm $W_6 = 15$ mm, $L_5 = 30$ mm $W_5 = 30$ mm, $L_1 = 15$, $L_5 = 10$, $L_6 = 12$, $h = 1.6$ mm, $\epsilon_r = 4.4$

The individual strip lengths of the arm 1 are varied separately to study the effect of them on the dual frequency characteristics. When length L_2 is varied the entire resonant length corresponding to first frequency changes which in turn varies the first resonant frequency. From the reflection characteristics shown in Fig.4.34 (a) it is again confirmed that the total loading height $L_1 + L_2$ should be of the order of quarter wavelength in dielectric corresponding to first resonant frequency to ensure the proper impedance matching of the first mode. The variation of horizontal strip of the arm1, L_3 causes the first resonant frequency to change considerably and decrease in length L results in merging of the individual modes to form a wide band (Fig. 4.34(b)). As length L_3 affects the cross polar level of the second mode length of the horizontal strip is optimized as 13mm favorable for both the modes. When the loaded parallel strip L_4 is varied the resonant frequency of the first mode changes and merges with the second mode as shown in Fig.4.34(c). So proper care is required for the selection of L_3 . If bandwidth is the major concern we have to select the optimum L_3 . If cross polarization is the major concern we have to reduce L_3 by sacrificing the bandwidth.

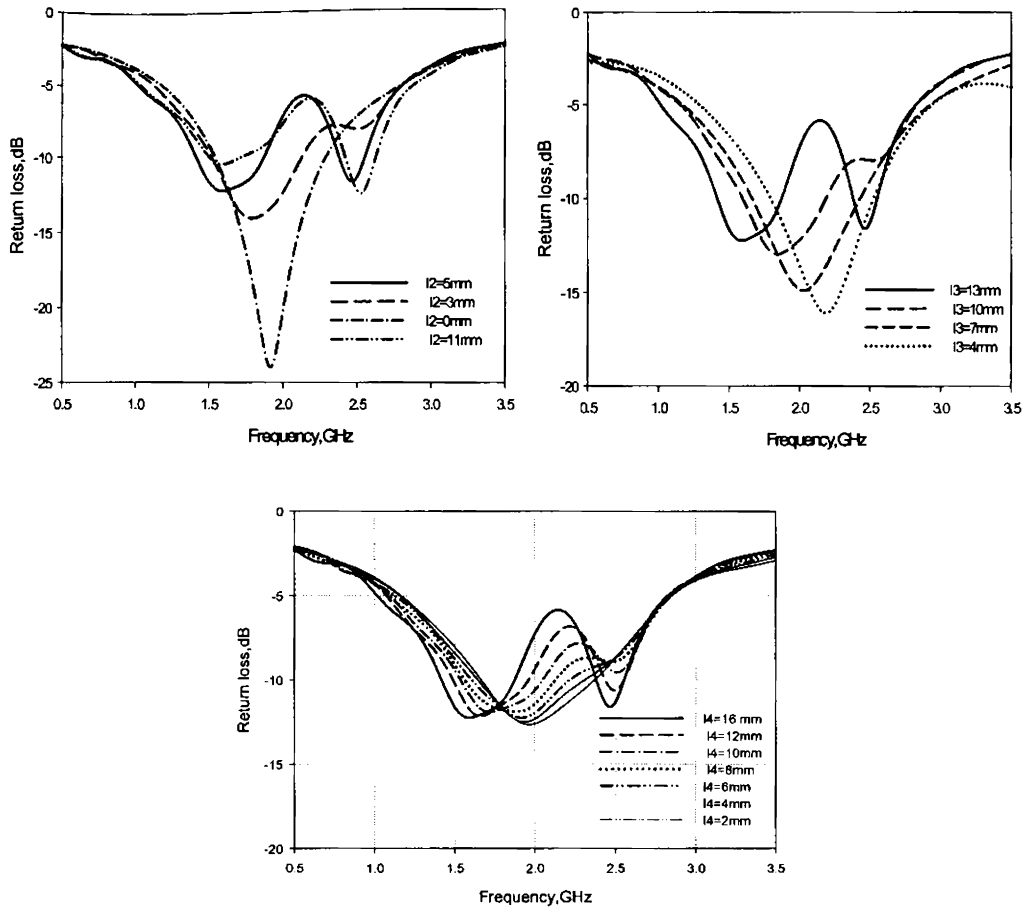


Fig.4.34 Influence of individual strip lengths of arm 1 length on the return loss characteristics of the dual folded monopole antenna. $L_6 = 3\text{mm}$ $W_6 = 15\text{mm}$, $L_S = 30\text{mm}$ $W_S = 30\text{mm}$, $L_1 = 15$, $L_5 = 10$, $L_8 = 12$, $z_h = 1.6\text{mm}$, $\epsilon_r = 4.4$ (a) effect of L_2 (b) effect of L_3 (c) Effect of L_4

4.6.3.2 Effect of folded arm2

When the length of arm 2 is varied the matching condition for first resonance is affected. The second resonant frequency increases with decrease in arm 2 lengths. But when the arm 2 length is lower than quarter wavelength of the first resonance impedance matching is poor due to the increased capacitive coupling. Effect of arm 2 on the reflection characteristics of the dual band antenna is shown in Fig.4.35.

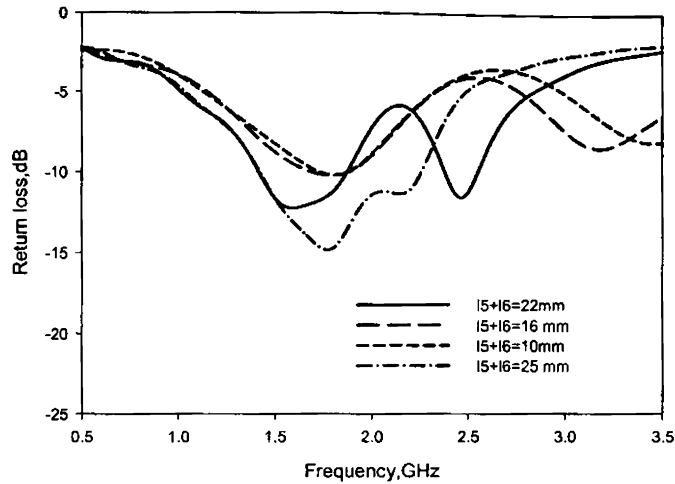
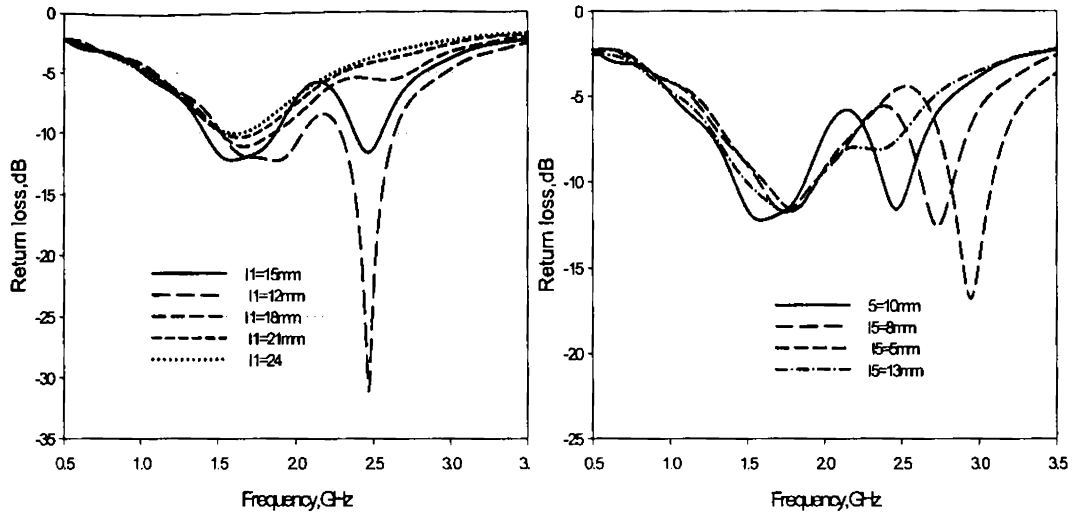


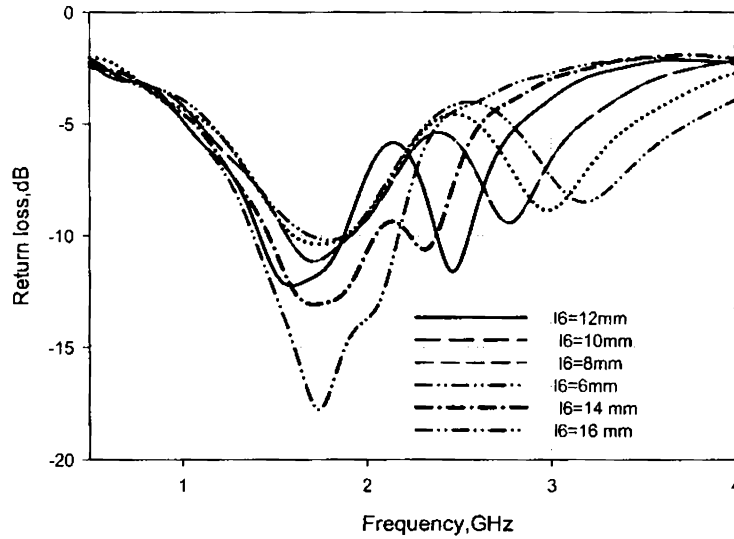
Fig.4.35 Influence of arm 2 length on the return loss characteristics of the dual folded monopole antenna. $L_G = 3\text{mm}$, $W_G = 15\text{mm}$, $L_S = 30\text{mm}$, $W_S = 30\text{mm}$, $L_2 = 5$, $L_3 = 13$, $L_4 = 16$, $h = 1.6\text{mm}$, $\epsilon_r = 4.4$

The individual strip lengths are varied to ascertain the effect of each of them on the reflection characteristics of the dual band folded monopole antenna. When the loading height L_1 is varied the impedance matching for the second mode becomes poor as shown in Fig.4.36 (a). This again confirms our earlier observation and inference that the arm must be loaded at a height of $\lambda_d/4$ corresponding to second resonant frequency. When the horizontal strip is varied the entire length of the arm 2 changes and there is shift in resonant frequency of the second mode as observed from Fig.4.36 (b). The effect of loaded parallel line of arm 2 on the reflection characteristics is the illustrated in Fig.4.36(c). When L_6 is varied the effective resonant path corresponding to second mode changes and the resonant frequency is varied in this case. But for higher variation of L_6 the two modes merge together to yield a wide bandwidth of 786MHz corresponding to 44%.



(a)

(b)



(c)

Fig.4.36 Influence of individual strip lengths of arm 2 lengths on the return loss characteristics of the dual folded monopole antenna. $L_6 = 3\text{mm}$ $W_6 = 15\text{mm}$, $L_5 = 30\text{mm}$ $W_5 = 30\text{mm}$, $L_2 = 5$, $L_3 = 13$, $L_4 = 16$, $2h = 1.6\text{mm}$, $\epsilon_r = 4.4$ (a) effect of L_2 (b) effect of L_3 (c) Effect of L_4

4.6.3.3 Effect of strip width 'w'

When the strip width of the folded strip monopole changes the characteristics impedance of the microstrip feed line varies which in turn affects the impedance matching and reflection characteristics. When the width of the monopole changes effective length of folded arm varies hence it can be observed a slight deviation in resonant frequency for the two modes as shown in Fig4.37. It is also observed that when the width is very small the radiation efficiency is very poor even though it can resonate at lower frequency. As a compromise the width is selected as the width of a microstrip transmission line in a substrate.

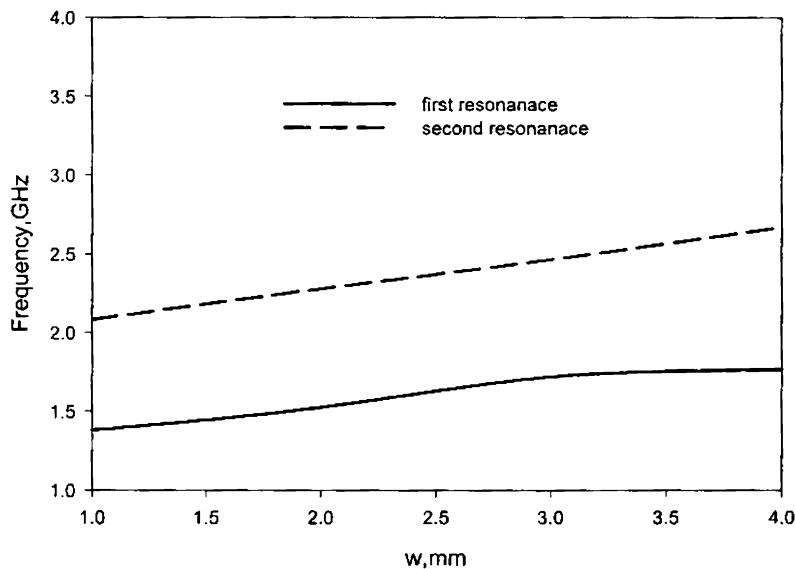


Fig.4.37 Influence of strip width 'w' on the return loss characteristics of the dual folded monopole antenna. $L_G = 3\text{mm}$, $W_G = 15\text{mm}$, $L_S = 30\text{mm}$, $W_S = 30\text{mm}$, $L_2 = 5$, $L_3 = 13$, $L_4 = 16$, $L_1 = 15$, $L_5 = 10$, $L_6 = 12$, $h = 1.6\text{mm}$, $\epsilon_r = 4.4$

4.6.3.4 Effect of dielectric constant of substrate

The dielectric constant of the substrate has influence on the two resonant frequencies. The dielectric constant variation changes the characteristic impedance of the feed line which modifies the reflection characteristics. The variation of resonant frequency of the two modes with dielectric substrates is shown in

Fig.4.38. When the dielectric constant of the substrate varies from 3 to 10 corresponding resonant frequency variation for the first and second modes are 600MHz and 625MHz respectively. The antenna efficiency varies with dielectric constant variation as the high dielectric constant substrates Q of the antenna is considerably high. The variation in radiation efficiency for different dielectric constant substrates is shown in Fig.4.38 (b). Moreover, when the dielectric constant increases the surface wave power increases which in turn decreases the efficiency of the antenna

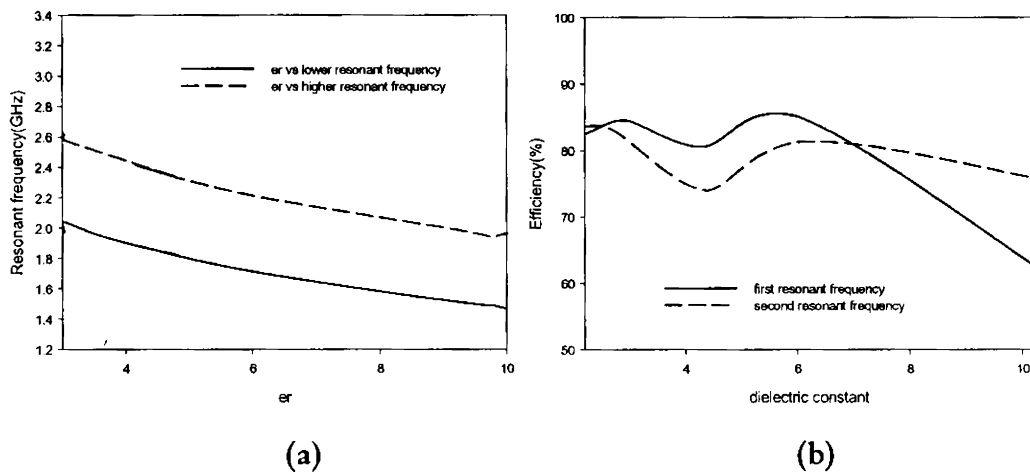


Fig.4.38 Effect of substrate dielectric constant

(a) Resonant frequency

(b) Radiation efficiency $L_6 = 3\text{mm}$ $W_6 = 15\text{mm}$, $L_S = 30\text{mm}$ $W_S = 30\text{mm}$, $L_2 = 5$,
 $L_3 = 13$, $L_4 = 16$, $L_1 = 15$, $L_5 = 10$, $L_6 = 12$ $h = 1.6\text{mm}$.

4.6.3.5 Effect of substrate height

From the previous investigations on folded monopole antenna the effect of substrate height on the resonant frequencies is investigated for single resonant case. In this section the effect of height variation in the two resonant frequencies are investigated. When the height of substrate varies from 1mm to 5mm corresponding frequency shift is 350MHz for first resonance and 460MHz for

second resonance. But for thick substrates the radiation efficiency is considerably reduced due to increased surface wave losses. The variations of resonant frequency and radiation efficiency of the two modes are shown in Fig.4.39 (a) and (b) respectively.

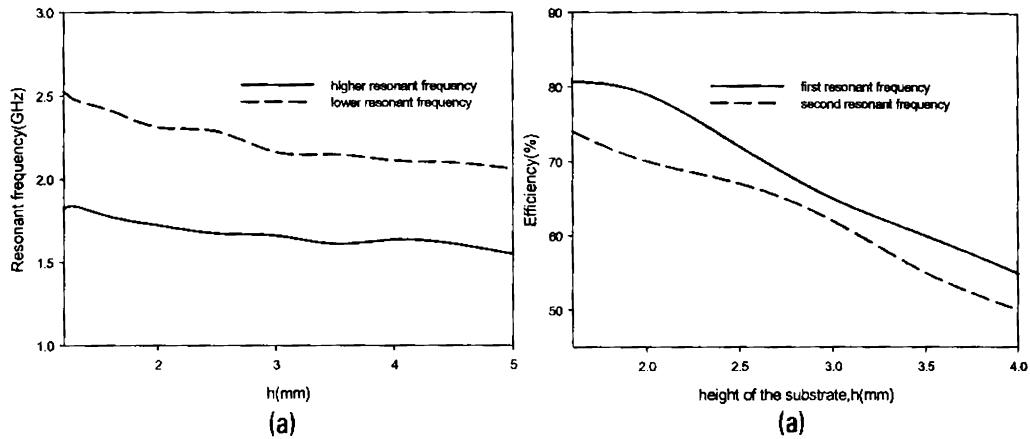


Fig.4.39 Effect of substrate height

(a) resonant frequency

(b) Radiation efficiency $L_0 = 3\text{mm}$, $W_0 = 15\text{mm}$, $L_2 = 5\text{mm}$, $L_3 = 13\text{mm}$, $L_4 = 16\text{mm}$, $L_1 = 15\text{mm}$, $L_5 = 10\text{mm}$, $L_6 = 12\text{mm}$.

4.5 Design procedure for compact dual band planar antenna

- Select any substrate with dielectric constant ϵ_r and height h . The width of the folded monopole is set as width of 50Ω microstrip feed line.
- Since the field components are not confined to the substrate alone effective dielectric constant has to be used in calculation.

$$\epsilon_{eff} = \frac{\epsilon_r + 1}{2} (1 + 0.3 * h) \dots\dots\dots (4.7)$$

Where h is the height of the substrate and ϵ_r is the dielectric constant of the substrate.

- Length of the loading height for the second resonant frequency

$$L_1 = \frac{0.25c}{f_{r2} * \sqrt{\epsilon_{eff}}} \dots\dots\dots(4.8)$$

- Length of the loading height for the first resonant frequency

$$L_2 = \frac{0.25c}{f_{r1} * \sqrt{\epsilon_{eff}}} - L_1 \dots\dots\dots(4.9)$$

- Horizontal strip of arm 1

$$L_3 = \frac{0.16c}{f_{r1} * \sqrt{\epsilon_{eff}}} \dots\dots\dots(4.10)$$

- Horizontal strip of arm 2

$$L_5 = \frac{0.17c}{f_{r2} * \sqrt{\epsilon_{eff}}} \dots\dots\dots(4.11)$$

- Length of the parallel strip of arm1

$$L_4 = \frac{0.2c}{f_{r1} * \sqrt{\epsilon_{eff}}} \dots\dots\dots(4.12)$$

- Length of the parallel strip of arm 2

$$L_6 = \frac{0.2c}{f_{r2} * \sqrt{\epsilon_{eff}}} \dots\dots\dots(4.13)$$

- Ground plane dimensions are then calculated using the following equations

$$L_G = \frac{0.0375c}{f_{r1} * \sqrt{\epsilon_{eff}}} \dots\dots\dots(4.14)$$

$$W_G = \frac{0.25c}{f_{r2} * \sqrt{\epsilon_{eff}}} \dots\dots\dots(4.15)$$

Where 'c' is the velocity of electromagnetic wave in free space. The constants in the above equations are derived from exhaustive parametric analysis.

4.6 Dual band designs in modern wireless communication bands

Design equations are confirmed by designing dual band antennas in various communication standards. This section describes features of such prototypes designed with the aid of design equations and operating in dual modes of various standard wireless communication bands. The experiments results the validity of the design equations in different bands.

Double folded monopole antenna for GSM 900/1.8GHz application

Low-profile planar monopole antennas capable of 900 and 1800 MHz dual-frequency operations are very attractive for GSM/DCS mobile phone applications. A dual band planar branched monopole antenna is designed on a substrate of dielectric constant 4.4 and height 1.6mm.. Photograph of the designed antenna is shown in Fig.4.40.

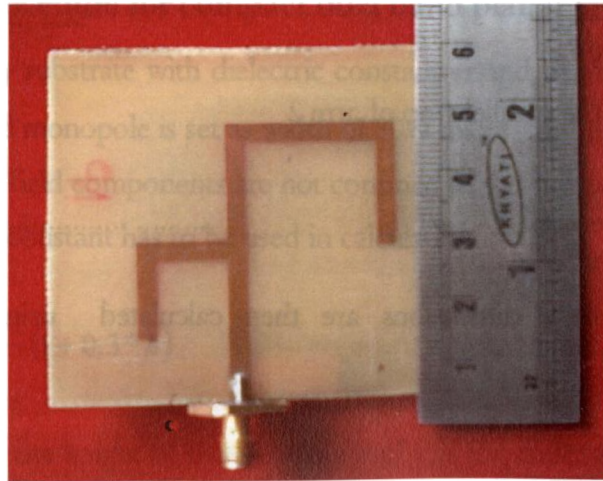


Fig.4.40. Photograph of Dual folded monopole antenna for GSM/DCS application

The proposed dual folded monopole antenna consists of two resonant paths of which the longer arm contributes the lower frequency 900 MHz and shorter contributes higher frequency of 1.8GHz. The designed antenna is fabricated and tested using E8362B PNA. The reflection characteristics of the prototype is shown in Fig.4.41

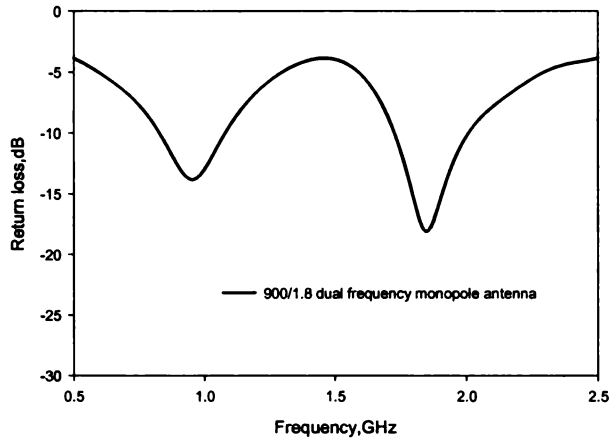


Fig.4.41 Dual folded monopole antenna for GSM/DCS application

$L_6 = 6\text{mm}$ $W_6 = 40\text{mm}$, $L_2 = 15\text{mm}$, $L_3 = 26\text{mm}$, $L_4 = 24\text{mm}$, $L_1 = 21\text{mm}$, $L_5 = 13\text{mm}$, $L_6 = 16\text{mm}$

The measured reflection characteristics exhibits two separate resonant modes with wide bandwidths as shown in the above figure. The bandwidth of the lower band, determined by 2.1 VSWR, reaches 252 MHz from 826MHz to 1.078GHz wide enough to cover the GSM band (890-960 MHz). The fractional bandwidth obtained in this case is 26.5% On the other hand; the upper band has a bandwidth as large as 278 MHz from 1.728GHz to 2.008GHz wide enough to cover the DCS (1710&1880 MHz) and PCS (1850-1990 MHz) bands. For the GSM band, a peak antenna gain of about 1.8 dBi is observed, with gain variations less than 0.5 dBi. For the DCS and PCS bands, the peak antenna gain observed is 2.0 and 2.2 dBi, respectively, and the gain variations are also less than 0.25 dBi. The proposed antenna is a potential candidate for triple frequency application with features like moderate gain, required bandwidth and nearly omni directional radiation coverage.

Double folded monopole antenna for 2.4GHz/5.2,5.8GHz WLAN applications

During the recent years there are rapid developments in wireless local area network (WLAN) applications. In order to satisfy the 2.4 GHz band of IEEE 802.11b and 5.2 GHz band of 802.11a WLAN standard, dual-band operations in the 2.4 GHz (2400-2484 MHz) and 5.2 GHz (5150-5350 MHz) bands are demanded in practical WLAN applications. For wireless communication, a dual frequency antenna is needed for simultaneously transmitting and receiving these two bands. . The antenna should be in the planar form, lightweight and compact, so that it can easily be embedded in the cover of communication devices. Planar branched monopole design is extended to study the effectiveness in the WLAN standards. A dual folded planar monopole antenna with the following parameters $L_G = 3\text{mm}$ $W_G = 15\text{mm}$, $L_2 = 8\text{mm}$, $L_3 = 10\text{mm}$, $L_4 = 12\text{mm}$, $L_1 = 7\text{mm}$, $L_5 = 5\text{mm}$, $L_6 = 5.4\text{mm}$ are printed on a substrate of dielectric constant 4.4 and thickness 1.6mm. Measured reflection characteristics of the proposed antenna are shown in Fig.4.42.

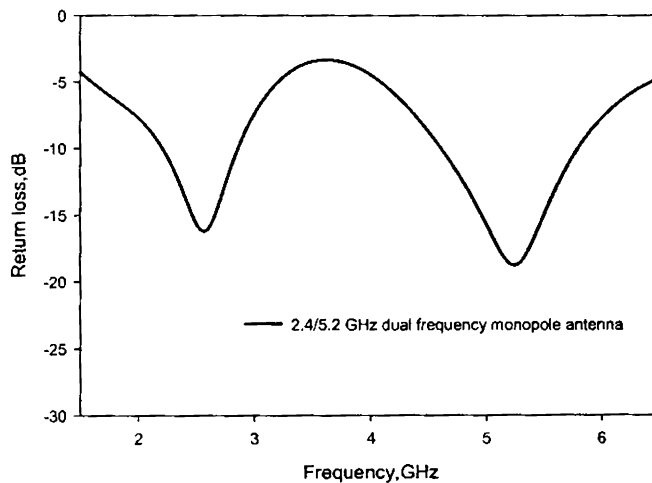


Fig.4.42 Dual folded monopole antenna for 2.4/5.2 GHz WLAN application $L_G = 3\text{mm}$ $W_G = 15\text{mm}$, $L_2 = 8\text{mm}$, $L_3 = 10\text{mm}$, $L_4 = 12\text{mm}$, $L_1 = 7\text{mm}$, $L_5 = 5\text{mm}$, $L_6 = 5.4\text{mm}$

Presented microstrip-fed dual frequency planar branched monopole antenna, with separate arms for the 2.4 and 5.2 GHz bands exhibits dual band behavior. The length of the antenna's larger strip controls the lower operating mode at 2.4GHz, while the length of the smaller strip is designed to generate a resonant mode for the upper operating mode at 5.2 GHz. The proposed antenna can easily be excited by a 50 Ω microstrip line, good impedance matching can be obtained for operating frequencies within both the WLAN and HIPERLAN bands. The lower resonant mode centered at 2.56GHz with a 2:1 VSWR bandwidth of 645MHz (2.21GHz-2.855GHz) corresponding to a fractional bandwidth of 25% which can easily cover the 2.4GHz WLAN band(2.4GHz-2.484GHz). The upper resonant mode centered at 5.24GHz exhibits a wide bandwidth from 4.61GHz to 5.79GHz corresponding to 22% bandwidth. The obtained bandwidths cover both the WLAN and HIPERLAN systems. The measured antenna gain at 2.45 and 5.25 GHz are 2.1dBi and 2.67dBi respectively.

4.7 Printed strip monopole designs in a nut shell.

In the chapter 3 a wide band printed monopole antenna is derived by suitably truncating the ground plane. The chapter concluded with the design of compact printed strip monopole antenna derived from the optimization of the ground plane. Further compactness can be achieved by folding the monopole at the cost of slight degradation in bandwidth. But suitably locating another arm the bandwidth degradation can be mitigated with supplementary advantage of additional resonance. The characteristics of different printed strip monopoles investigated in this thesis are summarized in the following table.

Antenna	Fr (GHz)	Band (GHz) Bandwidth (MHz) % bandwidth	Average Gain	Efficiency (%)	Area (mm ²)
Wide band printed strip monopole	2.4GHz	2.15-3.93 1780 60%	3.5dBi Vertical polarization	89.9%	95x65
Optimum ground plane compact printed strip monopole antenna	2.4GHz	2.19-2.768 575 23%	2.5dBi Vertical polarization	86%	32x35
Folded monopole antenna	2.44	2.28-2.68 400 16.4%	3dBi Vertical polarization	78%	20x20
Double folded printed monopole antenna	1.725 GHz	1.375-1.88 505 29%	2.53dBi Vertical polarization	80.1%	30x25
	2.45 GHz	2.33-2.55 220 8.9%	2.1dBi Vertical polarization	73.6%	

4.8 Conclusions

The important conclusions from the present investigations on folded monopole antenna are summarized below.

- When vertical strip is folded the optimum ground plane required for impedance matching is only quarter wavelength.
- The parallel arm must be loaded at height of about $\lambda d/4$ to ensure proper impedance matching and cross polar level.

- When a vertical strip monopole is folded there is strong capacitive coupling between the horizontal arm of the folded strip with ground. This coupling which accounts capacitive reactance at the input impedance and degrade in bandwidth performance.
- For the folded monopole the cross polar power level is high due to the horizontal current flowing along the horizontal strip.
- Capacitive coupling in folded monopole can be effectively reduced by adding an additional strip to account for inductive reactance at the input impedance of the folded monopole.
- A folded monopole with an inductive stub acts as combination of branched monopole to yield dual band with reasonable characteristics.
- Branched monopole is suitable concept for dual frequency operation in wireless gadgets where dual frequency with identical polarization is the demand.
- The mutual coupling between the branched arms affects the antenna reflection and radiation characteristics but these effects can be minimized by suitable design criteria.

Chapter 5

CONCLUSION AND FUTURE PERSPECTIVE

This chapter highlights the conclusions drawn from numerical and experimental investigations of truncated ground plane printed strip monopole antenna. The important inferences of the folding technique are also presented along with some of the future directions in this area.

5.1 Thesis highlights and Key contributions

This chapter brings the thesis to the closing stages by summarizing the important concepts drawn from the numerical and experimental analysis of printed strip monopole antenna. Aim of the work was to investigate the effect of ground plane on antenna characteristics and design of broadband printed strip monopole antenna suitable for use in wireless gadgets like PDAs, PCs, WLANs and mobile phones.

An overview of antenna research along with state of art technologies in planar antenna design are presented in chapter 1. The main attraction of this section is the itinerary toward the planar monopole antenna from conventional wire monopole antennas. A literature overview is presented in this chapter to highlight the present scenario in planar antenna design. Motivation of the present work in the context of today's technology advancement is the key part in the chapter 1.

The theoretical and experimental methodology for antenna characterization has been explained in the chapter 2. A detailed discussion on the FDTD technique used for antenna parameter extraction is illustrated with description different boundary conditions.

Investigations of the truncated ground plane printed strip monopole antenna are the main topic of chapter 3. Effect of ground plane truncation on antenna characteristics is explored. The key contributions in this chapter is the derivation of wide band printed strip monopole antenna suitable for laptop application and a printed strip monopole antenna with optimum ground plane suitable for compact wireless gadgets. Simple design equations, moderate gain, omni directional radiation characteristics portrays the aptness of the present design.

The folding technique applied to printed strip monopole for size reduction is the subject matter of the chapter 4. Technique to overcome the bandwidth degradation problem arising from meandering the radiating structure led to the design of compact dual band branched monopole antenna with broadband characteristics is the key contribution in this chapter.

5.2 Inferences from wideband printed strip monopole antenna

A conventional printed strip monopole excited by microstrip feed line exhibits resonance phenomenon whose impedance bandwidth can be controlled by suitable truncation of the ground plane of the microstrip feed line. A wide band printed strip monopole is thus derived by properly truncating the ground plane of the microstrip feed line. The salient features of this design are broadband width of the order of 60% with average gain of 3.5dBi with nearly omnidirectional characteristics. The antenna occupies an area $1.25 \lambda_d \times 0.85 \lambda_d$ when printed on dielectric substrate. The important conclusions drawn from the investigation of truncated ground plane printed strip monopole antenna are:

- By properly optimizing the ground plane, a new resonance can be generated in the printed strip monopole structure, occurring just after the fundamental resonance frequency of the monopole.
- A vertical strip monopole over a truncated ground plane can be explained as a parallel combination of two asymmetric dipoles of (L and reflected L shapes) excited at a common point at the centre of the microstrip line. In this configuration the radiating fields are contributed only by the fields radiated by the vertical monopole element. This asymmetric dipole is the cause of the second resonance occurring near the monopole mode.
- Due to the proximity of strip L_m , the current density becomes more dominant at the top edges on the ground plane along 'W_G'. The ground

plane currents are concentrated only at the edges, and not spreads all over the ground plane surface

- The horizontal part of the dipoles (ground plane edge) currents are always 180 degrees out of phase and cancels at the far field. This ensures the polarisation purity of the antenna.
- At the lower resonance the antenna behaves purely as a quarter wave monopole.
- We have effectively utilized the ground plane truncation to excite the second resonance, which has all radiation properties almost same as the first resonance, without the need of any additional balun, making the system more simple.
- Even though a current distribution on the edges along the width of the ground plane is essential for this mode; it is not at all contributing in the radiation. Thus the vertical strip is only contributing to radiation. Hence similar radiation characteristics are obtained through out the impedance bandwidth.

5.3 Conjecture from optimum ground plane compact printed strip monopole antenna

Investigations on ground plane truncation led to the derivation of an optimum ground plane required for printed strip monopole antenna design. A compact printed strip monopole antenna is thus derived with optimum ground plane with salient features of 23% bandwidth, average gain of 2.5dbi and omni directional radiation coverage with compact dimensions of the order of $0.5 \lambda_d \times \lambda_d$ suitable for application in compact wireless terminals. The key conjecture arrived from these investigations are:

- With optimum ground plane dimensions the impedance matching for the quarter wavelength fundamental mode is poor. But half wavelength mode exhibits proper impedance matching with truncated optimum ground plane. Hence taking compactness in to consideration, half wavelength monopole with truncated ground plane is suitable than quarter wavelength monopole with complicated balun structures.
- For a half wavelength monopole ground plane width should be at least of the order of half wavelength when the ground plane length is optimum.

5.4 Features of folded printed strip monopole antenna

The optimum ground plane printed strip monopole antenna can be further be dwindled in size by suitably folding the printed strip monopole antenna. The compact folded monopole antenna thus derived from optimum ground plane printed monopole antenna occupies only an area of $0.25 \lambda_d \times 0.25 \lambda_d$ when printed on a dielectric substrate with features of 16% bandwidth, average gain of 3dBi and omni directional radiation coverage suitable compact mobile phone terminals and WLANs. The conjectures obtained from folding technique are summarized as:

- When a vertical strip monopole is folded there is strong capacitive coupling between the horizontal folded strip with ground. This accounts capacitive reactance at the input impedance and degrades the bandwidth performance.
- The parallel arm must be loaded at position of about $\lambda_d/4$ to ensure proper impedance matching and better cross polar level.
- When vertical strip is folded the optimum ground plane required for impedance matching is only quarter wavelength.

- For the folded monopole the cross polar power level is high due to the horizontal current flowing along the horizontal strip.

5.5 Salient features of double folded printed strip monopole antenna

The bandwidth degradation problem in folded monopole antenna can be easily prevailed by judiciously placing another strip at appropriate location to nullify the capacitive reactance from the folded arm. A dual folded monopole antenna is thus derived from single folded monopole antenna with an additional arm to enhance the bandwidth of the first resonant mode. The novel approach increases the bandwidth of first mode and excites another mode due to the additional current paths excited in the radiating structure. Thus dual band folded monopole is resulted by modifying the single folded monopole antenna. The salient features of this dual branched antenna are the dual frequency operation with 29% and 9% bandwidths respectively in the two bands, moderate gains and omnidirectional radiation coverage. This dual band design is potential candidate for dual frequency applications in mobile communication applications like GSM900/1800 and wireless communication application like WLAN 2.4/5.2 GHz. The antenna occupies an area of $0.25 \lambda_d \times 0.25 \lambda_d$ corresponding to the fundamental mode. The important conclusions arrived from dual band branched monopole design are:

- Capacitive coupling in folded monopole can be effectively reduced by adding an additional strip to account for inductive reactance at the input impedance of the folded monopole.
- A folded monopole with an inductive stub acts as combination of branched monopole if the stub is placed at the apposite location to provide dual band operation.

- Branched monopole is suitable concept for dual frequency operation in wireless gadgets where dual frequency with identical polarization is the demand.
- The mutual coupling between the branched arms affects the antenna reflection and radiation characteristics but these effects can be minimized by suitable design criteria.

5.6 Suggestions for future work

The ground plane truncation edge currents can be utilized for design of dipole antennas and dual band dipole antennas. Hence the need of additional complicated balun structures can be avoided for printed dipole design. Ground plane modifications are one area that may be looked into to enhance the antenna properties. Meandering the ground plane resonant paths is another field of interest for size reduction. Printed monopole array is yet another subject of interest to modify the radiation pattern suitable for mobile phone application. By suitable array design the radiation pattern can be modified in such a way that the omnidirectional radiation pattern can be modified to cardioid radiation pattern forming a zone of silence in the user direction. Thus Specific Absorption Rate (SAR) distribution in the human head can be minimized. Metamaterial loading is yet another concept that can be looked into for size reduction to sub wavelength region. The metamaterial superstrate can further enhance the bandwidth of the antenna. Similarly the metamaterial ground plane can effectively reduce the antenna size. These may be an interesting problem to be carried out. Printed strip monopole antenna designs can be extended with parasitic strip radiators to design high gain planar Yagi antenna. Parasitic loading technique can be effectively utilized to design ultra wide band, dual band or multi band designs.

The folding technique can be used for the design of multiband or ultra wide band design with different branched arms to yield multiple resonant paths. The folding technique can be extended to uniplanar designs with excitation techniques like Coplanar Waveguide (CPW), slot line or asymmetric coplanar strip line (ACS) etc.

Appendix A

A Wideband Hybrid Printed Monopole/ Rectangular Patch Antenna

Experimental investigations on enhancing the bandwidth of printed strip monopole antenna with a parasitic radiator are highlighted in this section. A printed strip monopole acts as radiator as well excites the parasitic loaded rectangular patch antenna. Thus a hybrid antenna is developed with two independent radiators of identical radiation characteristics merged together to yield wide band performance. By the addition of parasitic radiator the gain of the hybrid antenna is considerably increased. This principle can be used for designing wide band high gain printed strip monopole antennas.

A.1 Introduction

The rapid developments of new multimedia communication bring along with it the need for wideband antenna for high speed transmission. The antenna should be wideband, compact, low profile with excellent reflection and radiation characteristics. Planar monopole antennas and microstrip antennas have attractive features of low profile, simple structure, ease of fabrication and are promising candidates for satisfying the miniaturization requirements of mobile terminals. However the primary barrier to implement microstrip antennas for many applications is its inherent narrow bandwidth. In addition, applications in present day mobile communication system usually require compact antenna in order to meet the miniaturization requirements. Size reduction and bandwidth enhancement are becoming major design consideration for practical application of microstrip antennas. Several techniques to broaden the bandwidth of conventional patch antennas were available in the literature. [1]. These techniques propose to use multilayer structures, employing reflector backed substrate, use chip resistor or chip capacitor loading etc. However using these techniques overall size and manufacturing cost of the antenna will increase. Monopole configurations such as circular, square, pentagonal and hexagonal [2] features wide impedance bandwidth, simple structure, ease of fabrication, and satisfactory radiation characteristics. But the practical applications of these broadband monopoles are limited due to high profile and cannot be easily integrated to present modular circuits. Recently, electromagnetic coupling technique has been used to enhance the impedance bandwidth of triangular [3-5] square planar, circular annular planar monopole antennas. In these design the radiating structure is perpendicular to the ground plane, which increases the complexity of the system as the entire system is not planar. Moreover these 3D monopoles occupy a volume of $320 \times 320 \times 40 \text{ mm}^3$ including the feed structure and ground plane. Printed monopole antennas [6], are

becoming important candidates due to their attractive features including wide impedance bandwidth, planar structures and monopole type radiation characteristics.

A novel design of hybrid antenna comprising of rectangular patch excited by backed printed monopole is addressed in this letter. A rectangular patch is electromagnetically coupled with microstrip fed printed monopole to yield broadband performance. The antenna has overall dimensions of 40.5x45x3.2 mm³ when printed on standard FR4 substrate. The greatest advantage of the proposed design when compared to many electromagnetically coupled planar monopoles available in the literature is its compact nature with broadband characteristics. The broadband and omni directional radiation characteristics of simple printed strip monopole antenna are incorporated with a rectangular patch to broaden the bandwidth of rectangular patch antenna. The reflection and radiation characteristics are extensively investigated using simulation and experiment. The uniqueness of the proposed hybrid antenna configuration is the ease of configuring the antenna for various wireless communications and mobile communication standards. The proposed design offers high gain, broad bandwidth and nearly omni directional radiation coverage with the same polarization in the entire band.

A.2 Antenna Structure and Design

The geometry of the two layer antenna is shown in Fig.A.1. The antenna comprises of rectangular patch electromagnetically excited by a printed strip monopole. A rectangular patch of dimensions $L \times W$ mm² is fabricated on a substrate of ϵ_{r2} and height h_2 . A microstrip fed strip monopole is fabricated on another substrate of ϵ_{r1} and height h_1 mm. L_G and W_G denotes the length and width of the truncated ground plane which covers only the section of microstrip feed line as shown in figure1. The microstrip 50 Ω line of length F_M and width W_M

excites the strip monopole of length F_L and width F_W . For the design convenience the width F_W of the strip monopole is set as the width of 50Ω microstrip feed line. Rectangular patch is electromagnetically coupled to the microstrip excited strip monopole. The advantage of the proposed antenna is that it can be easily configured for specific application by changing the parameters of the structure. Good reflection characteristics can be achieved by changing the position of the patch along the strip monopole. Frequency tuning can be achieved by adjusting the length F_L or width F_W of the strip monopole. The parameters of the proposed antenna are optimized experimentally to operate at 2.425 GHz with wide 2:1 VSWR bandwidth of 950MHz covering 2.4 GHz WLAN band.

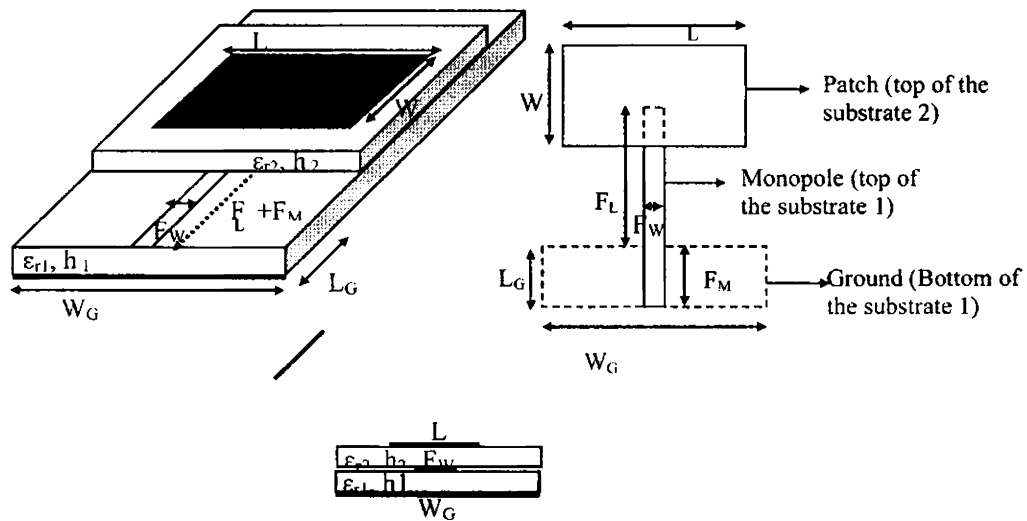


Fig. A. 1 Geometry of the proposed antenna

$L_G = 11\text{mm}$, $W_G = 40.5\text{mm}$, $L = 28.7\text{mm}$, $W = 22.08\text{mm}$, $F_W = 3\text{mm}$, $F_L = 25.5$, $h_1 = 1.6\text{mm}$, $h_2 = 1.6\text{mm}$, $\epsilon_{r1} = 4.36$, $\epsilon_{r2} = 4.36$

A.3. Experimental Results

The resonant frequency and bandwidth of the hybrid configuration extensively depends on the length of the strip monopole. The wide bandwidth of the hybrid antenna comes from the combined effect of the strip monopole and

loaded patch. For the parametric study of the hybrid antenna, a rectangular patch resonating at 2.4GHz is selected. When the patch is excited with conventional microstrip feed line, the antenna resonates at 2.4GHz with a 2:1 VSWR bandwidth of 250MHz. The resonant frequency of the printed strip monopole is mainly determined by the length of the strip monopole. A printed strip monopole is designed to resonate at frequency 2.4GHz. When the patch under test is loaded on the monopole the hybrid antenna is found to resonate at a lower frequency of 1.92GHz with a 2:1 VSWR bandwidth 520MHz and an average gain of 5 dBi. The resonant length of the strip monopole is varied to study the effect on the resonance of the hybrid antenna. The resonant length of the strip monopole is tuned so that the hybrid configuration resonates at the same resonant frequency of the loaded patch. The parameters of the proposed antenna are optimized to obtain maximum bandwidth at centre frequency 2.4GHz. A prototype of the antenna with the following parameters $L=28.7\text{mm}$, $W=22.08\text{mm}$, $L_G=11\text{mm}$, $W_G=40.5\text{mm}$, $F_W=3\text{mm}$, $F_L + F_M = 25.5\text{mm}$ $\epsilon_{r2}=4.36$, $h_2=1.6\text{mm}$, $\epsilon_{r1}=4.36$, $h_1=1.6\text{mm}$, is fabricated and its reflection and radiation characteristics are studied using 'HP8510C vector network analyzer. Simulations are performed using Zealand's fidelity software. Fig. 2 shows experimental results of variation of return loss with frequency for the proposed antenna. The simulated variation of return loss for the optimum bandwidth position is also included in Fig.A.2. The simulated and experimental results are in good agreement. At the optimum length of the strip monopole the hybrid configuration resonates at 2.425 GHz exhibiting a broad bandwidth of 975MHz (2.075GHz-3.05 GHz) with 40% bandwidth and an average gain of 7dBi. The simulated variation of return loss with strip monopole length is depicted in Fig. A.3

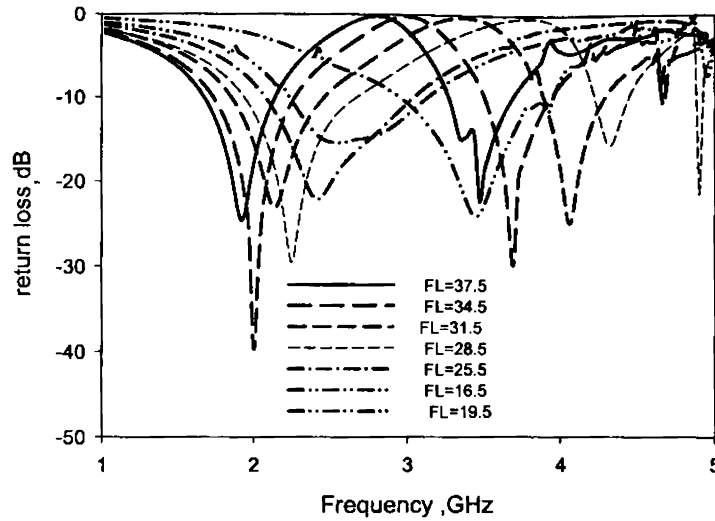


Fig.A 3. Variation of resonant frequency of the hybrid antenna with the strip monopole length, $L_s = 11\text{ mm}$, $W_6 = 40.5\text{ mm}$, $L = 28.7\text{ mm}$, $W = 22.08\text{ mm}$, $F_w = 3\text{ mm}$, $h_1 = 1.6\text{ mm}$, $h_2 = 1.6\text{ mm}$, $\epsilon_{r1} = 4.36$, $\epsilon_{r2} = 4.36$

A fine-tuning of the antenna resonant frequency can be achieved by varying the strip monopole width F_w . Typical results for the variation of resonant frequency with F_w are presented in fig.A.4. From the figure it can be observed that lowering of resonant frequency can be achieved by decreasing the width F_w .

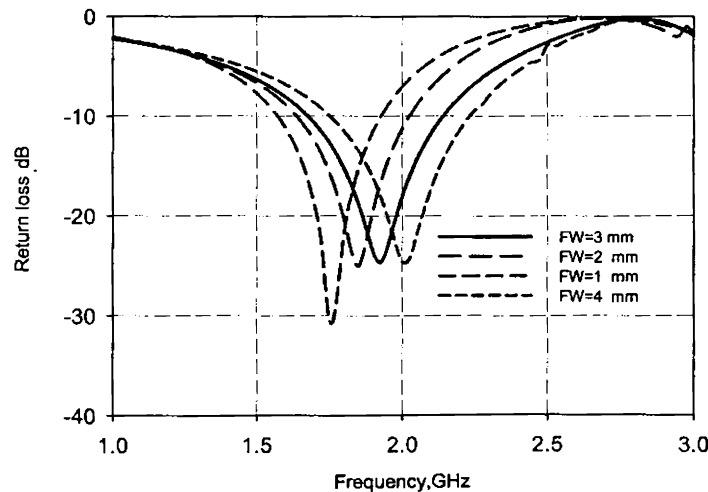


Fig. 4. Variation of resonant frequency with the width of the strip monopole, $L_s = 11\text{ mm}$, $W_6 = 40.5\text{ mm}$, $L = 28.7\text{ mm}$, $W = 22.08\text{ mm}$, $h_1 = 1.6\text{ mm}$, $h_2 = 1.6\text{ mm}$, $\epsilon_{r1} = 4.36$, $\epsilon_{r2} = 4.36$, $F_L = 37.5\text{ mm}$.

The antenna gain measured in the bore sight direction with in 2.4GHz WLAN band is shown in fig.A.5. The gain variation of the antenna is less than 1dBi with in the entire bandwidth.

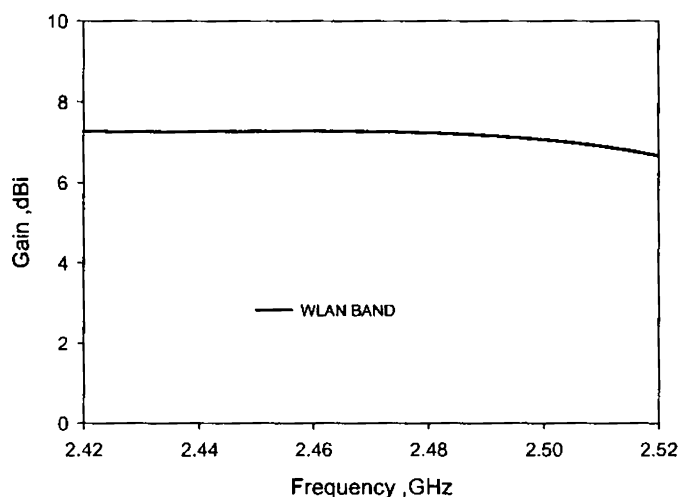


Fig. A.5. Gain of the proposed antenna at 2.4 GHz WLAN Band $L_G = 11\text{mm}$, $W_G = 40.5\text{mm}$, $L = 28.7\text{mm}$, $W = 22.08\text{mm}$, $F_w = 3\text{mm}$, $F_L = 25.5\text{mm}$ $h_1 = 1.6\text{mm}$, $h_2 = 1.6\text{mm}$, $\epsilon_{r1} = 4.36$, $\epsilon_{r2} = 4.36$

Fig. A.6 presents the radiation characteristics of the proposed antenna at 2.4 GHz in both the principal planes. Instead of unipolar radiation characteristics of conventional patch antennas, the present antenna offers nearly omni directional radiation coverage. The proposed design offers a cross polar discrimination better than 25dB. The design parameters of the printed strip monopole antenna are $W_G = 0.33 \lambda_0$, $L_G = 0.09 \lambda_0$, $F_L + F_M = 0.21 \lambda_0$, $L = 0.23 \lambda_0$, $W = 0.18 \lambda_0$, where λ_0 is the free space wavelength at operating frequency. The design parameters are confirmed by conducting experimental observations and simulations in various frequency bands. Good agreement is demonstrated between the simulations and experiment.

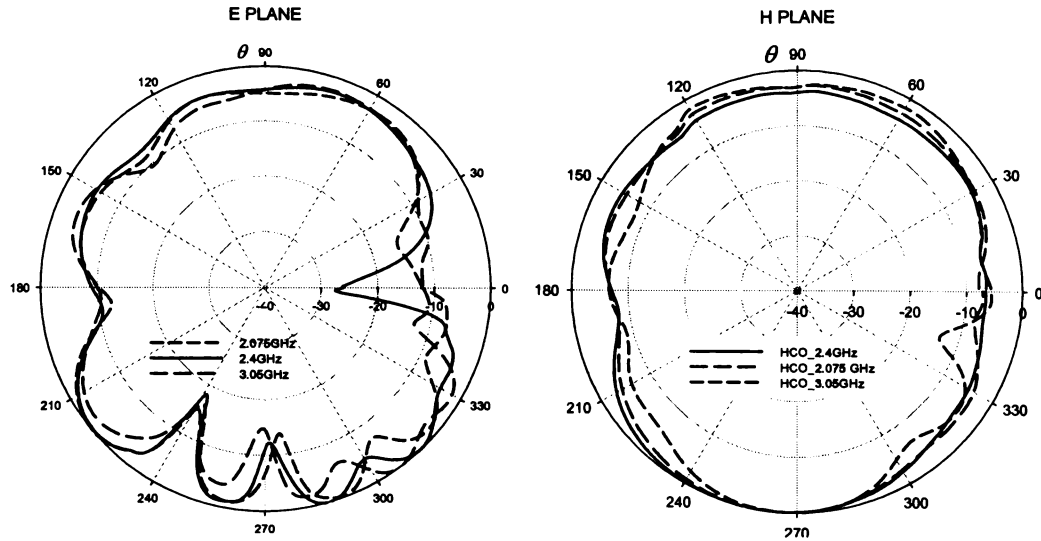


Fig. A.6. Radiation characteristics of the antenna, $L_6 = 11\text{mm}$, $W_6 = 40.5\text{mm}$, $L = 28.7\text{mm}$, $W = 22.08\text{mm}$, $F_w = 3\text{mm}$, $h_1 = 1.6\text{mm}$, $h_2 = 1.6\text{mm}$, $\epsilon_{r1} = 4.36$, $\epsilon_{r2} = 4.36$

A.4. Conclusion

A rectangular patch loaded microstrip excited strip monopole antenna for wideband application is proposed. The parameters affecting the antenna reflection and resonance performance are experimentally investigated and verified by simulation. The antenna design parameters are extracted from extensive simulation studies are also presented. The proposed wideband, high gain omnidirectional antenna is suitable for mobile and wireless communication systems where compact wideband antennas are in great demand

A.5 References

- [1] K.L Wong, Compact and Broadband Microstrip antennas, John Wiley & sons, New York, USA, 2002.
- [2] Agrawal N.P, Kumar G and Ray K.P.: 'Wide band planar monopole antennas' IEEE transactions on antennas and propagation 1998 46(2) pp 294-295.

- [3] Z.N Chen and M.Y.W Chia.: 'Impedance characteristics of EMC triangular monopoles' IEE Electronics letters, Vol. 37, No.21, October 2001, pp 1271-1272.
- [4] Z.N Chen. 'Broadband planar monopole antenna' IEE Proc. Microw. Antennas Propag. 2000, Vol. 147, No.6, pp 526-528.
- [5] Z.N Chen, M.J Ammann M.Y.W Chia and T.S.P See.: 'Circular annular planar monopole with EM coupling' IEE Proc. Microw. Antennas Propag. Vol. 150, No.4, August 2003, pp 269-273.
- [6] Hao-Chun Tung, Shyh-Ting Fang and Kin-Lu Wong.: 'Printed dual band monopole antenna for 2.4/5.2 GHz WLAN applications' Microwave and optical technology Letters, Vol 35, No.4, November 20, 2002, pp. 286-288.

Appendix B

A Compact Hybrid CPW Fed Planar Monopole/ Dielectric Resonator Antenna

The thesis presented a microstrip fed printed strip monopole antenna for wide band and dual band application. In this section the study is extended to a uniplanar printed strip monopole antenna excited by Coplanar Waveguide. The enhancement of bandwidth and gain of the printed strip monopole is achieved by parasitic radiator. In the present study low loss ceramic dielectric resonator is used as parasitic radiator. Thus design of hybrid antenna consisting of a Coplanar Waveguide (CPW) fed printed monopole and Cylindrical Dielectric resonator are the highlighted in this section. A CPW fed printed monopole acts as an effective radiator and excites the cylindrical dielectric resonator. A wide band width of the order of 50% is achieved with the hybrid antenna. The compact hybrid antenna with moderate gain and nearly omni directional radiation characteristics is highly suitable for wireless communication with broad bandwidth or multi band to support multiple services.

B.1 Introduction

Revolutionary progress in modern wireless communication has led to the invention of several low profile antennas. Dielectric resonator antennas are increasingly attractive for many applications in wireless communication due their attractive features like high efficiency, Compact size, compatibility with MMICs, ability to obtain different radiation patterns by exciting different modes with simple and efficient coupling to most of the transmission lines. When The Cylindrical dielectric resonator antenna (CDRA) is excited in the fundamental HE_{118} mode bandwidth is typically below 10%. Recently substantial efforts have been devoted to the bandwidth enhancement of dielectric resonator antennas by using geometry deforming¹, stacking DRA's², exciting two different modes with similar radiation characteristics³ etc. The concept of hybrid resonator antennas with two different radiators has attracted extensive interest with reference to dual band or wide band operations. An ultra wideband antenna proposed in⁴ uses such a hybrid combination of monopole and dielectric resonator antenna. But the monopole mounted on the large ground plane increases the system complexity as the entire system is not planar. CPW fed planar monopole antennas are increasingly popular due to their low profile, wide bandwidth and nearly omni directional radiation characteristics^{5,6}. This paper proposes a novel hybrid antenna configuration capable of achieving wide impedance bandwidth by combining the radiation properties of a CPW fed planar monopole and Cylindrical Dielectric Resonator Antenna (CDRA). The details of the antenna design and experimental results are presented and discussed.

B.2 Antenna Design

Fig. 1. shows the geometry of the hybrid antenna. The antenna consists of a CPW fed printed strip monopole and cylindrical dielectric resonator antenna. The planar monopole acts as an effective radiator as well as a feed for cylindrical

dielectric resonator. The CPW fed monopole antenna is printed on standard FR4 substrate of thickness $h=1.6\text{mm}$ and relative permittivity $\epsilon_r = 4.4$. A CPW transmission line with signal strip width $S=3\text{mm}$ and gap width between the ground plane and signal strip $G=0.3\text{mm}$ is used to feed the planar strip monopole antenna. Two finite ground planes with size $L_G \times W_G$ are situated symmetrically on each side of coplanar line. A cylindrical dielectric resonator of $\text{Ca}_3\text{Ta}_2\text{TiO}_{12}$ material synthesized by conventional solid state ceramic route with dimensions height $h_{dr}=3.83\text{mm}$, diameter $D_{dr}=16.4\text{mm}$ and dielectric constant $\epsilon_{dr}=38$ is loaded on the CPW fed planar monopole antenna.

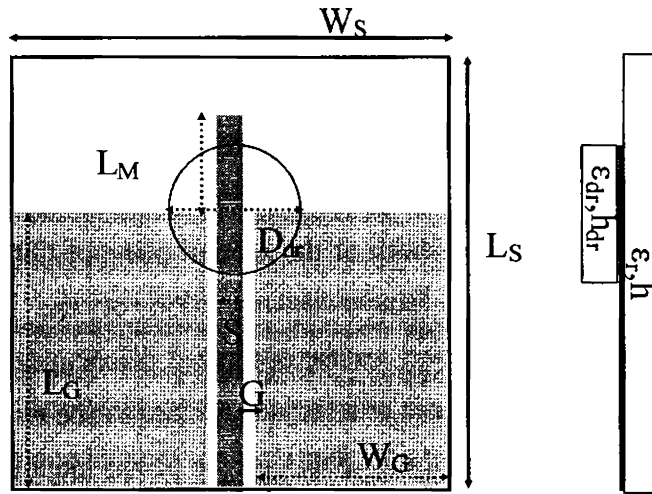


Fig.B.1. Geometry of the hybrid CPW fed planar monopole/Dielectric resonator antenna. $L_G = 25\text{mm}$, $W_G = 10\text{mm}$, $L_M = 18\text{mm}$, $\epsilon_r = 4.4$, $h = 1.6\text{mm}$, $L_S = 50\text{mm}$, $W_S = 30\text{mm}$, $S = 3\text{mm}$, $G = 0.3\text{mm}$, $\epsilon_{dr} = 38$, $h_{dr} = 3.83\text{mm}$, $D_{dr} = 16.4\text{mm}$

The arrangement is a cascaded resonant circuit with two different resonant frequencies. The resonant length L_M of the monopole is approximately $\lambda_d/4$ at the first resonant frequency. When the width W_G of the ground plane is increased the resonant frequency decreases but overall dimensions of the antenna increases. Increase in monopole length increases the resonant length which results in a decrease of the resonant frequency. The dimensions of the CPW fed monopole

are optimized for a maximum bandwidth with out affecting the compactness of the hybrid antenna configuration. The monopole is designed to resonate at the lower frequency and DRA at the higher resonant frequency. The fundamental HE_{118} resonant frequency of the cylindrical dielectric resonator is calculated using equation in⁷ as

$$F_r = \frac{18.972 \times 10^8}{\pi D_{dr} \sqrt{\epsilon_{dr}} + 2} \left[0.27 + 0.36 \left(\frac{D_{dr}}{4h_{dr}} \right) + 0.02 \left(\frac{D_{dr}}{4h_{dr}} \right)^2 \right] \dots\dots\dots[B.1]$$

The resonant frequency of the cylindrical DRA is selected approximately 1.5 times than that of planar monopole. The two frequencies are selected such as to maintain 10dB return loss over the entire band. If the two resonant frequencies are spaced further apart the dual band operation will result with the hybrid configuration. The parameters that affect the overall performance of the hybrid antenna include the length of the planar monopole, permittivity of the DRA and size of the ground plane. The length and width of the ground plane of CPW fed monopole is optimized for maximum bandwidth operation of the planar monopole antenna. When the DR is loaded on the optimized planar monopole the monopole excites the DR and it resonates at a frequency close to the resonant frequency of the monopole. The position of the CDRA on the planar monopole is adjusted to obtain maximum bandwidth.

B.3 Experimental Results

Typical proposed antenna is characterized using HP8510C vector network analyzer. The Dimensions of the planar monopole antenna is optimized numerically with the aid of IE3DTM. The return loss characteristics of non loaded and CDRA loaded CPW fed printed monopole is presented in Fig.B.2. Experimental results are confirmed using Ansoft HFSS.

The planar monopole resonating at 2.6 GHz offers a bandwidth of 375MHz (2.40GHz-2.775GHz).When Cylindrical Dielectric resonator is loaded on the planar monopole the hybrid antenna shows a wide band width with merging of two resonant frequencies. The first resonant frequency is due to the planar monopole and the second resonance is close to the calculated value of HE_{118} mode resonant frequency of the loaded cylindrical dielectric resonator. Using this cascaded arrangement a wide bandwidth of the order of 1650MHz (2.425 GHz-4.075 GHz) can be achieved.

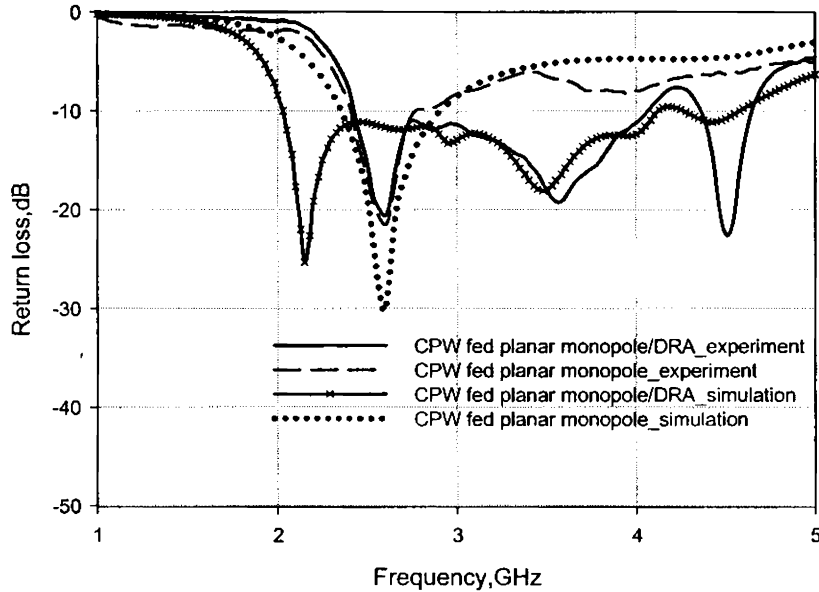


Fig.B.2. Return loss characteristics of the hybrid CPW fed planar monopole/Dielectric resonator antenna. $L_G = 25\text{mm}$, $W_G = 10\text{mm}$, $L_M = 18\text{mm}$, $\epsilon_r = 4.4$, $h = 1.6\text{mm}$, $L_S = 50\text{mm}$, $W_S = 30\text{mm}$, $S = 3\text{mm}$, $G = 0.3\text{mm}$, $\epsilon_{dr} = 38$, $h_{dr} = 3.83\text{mm}$, $D_{dr} = 16.4\text{mm}$

The position of DRA on the monopole plays a significant role in determining the bandwidth of operation. The variation of reflection characteristics for different position of DRA is summarized in Table 1. In the Table P1 corresponds to the position where the center of the CDRA is on the open end of the CPW feed line (refer Fig.3). At this position the resonant mode of planar monopole and

HE₁₁₈ mode of CDRA merge together resulting in wide impedance bandwidth. At position P2 the CDRA is on the monopole but with out touching the ground plane. At this position the CPW excited planar monopole energizes the CDRA resulting in two distinct resonant modes. Here the resonant frequency of the planar monopole is shifted to the low frequency regime due to the loading of CDRA. It can be inferred from the Table that position P3 and P4 where the CDRA is on the right or left side of the planar monopole the hybrid configuration yields dual frequency operation.

Position(x, y) in mm	Band	Bandwidth	%BW
P1(11.8,22.4)	3.425GHz- 4.075GHz	1650MHz	51%
Single frequency			
P2 (11.8,40.4)	2.1625GHz- 2.4125GHz	250MHz	10%
Dual frequency	4.3875GHz- 4.875GHz	487.5MHz	10.6%
P3(15.21,21.4)	2.4625GHz- 3.1125GHz	650MHz	22.7%
Dual frequency	4.2625GHz- 4.625GHz	362.5MHz	8%
P4 (15.21,38.4)	2.2375GHz- 2.4125GHz	175MHz	7.6%
Dual frequency	3.7125GHz- 4.2375GHz	525MHz	13%

Fig.B.3.illustrates the measured and simulated radiation patterns of the hybrid antenna at the centre and two edges of the matching band. The hybrid antenna is linearly polarized along Y direction in the entire band. With the proposed arrangement DRA is expected to resonate at the fundamental HE₁₁₈ mode that has broad side radiation patterns and planar monopole with similar radiation behavior.

Thus stable radiation characteristics are observed with in the entire operating band. Antenna exhibits nearly omni directional radiation characteristics. The cross polar radiation studies shows a cross polar discrimination better than 25dB in both the planes.

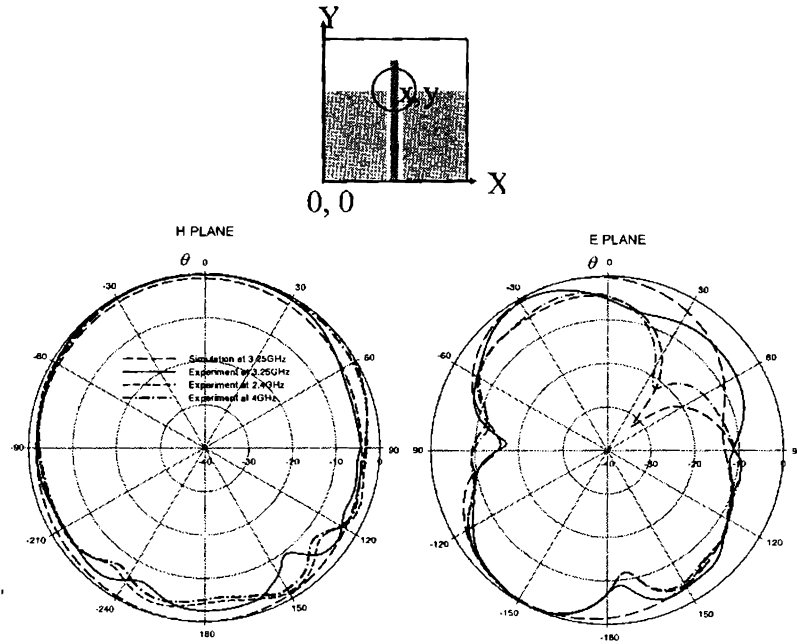


Fig. B.3. Radiation characteristics of the hybrid CPW fed planar monopole/Dielectric resonator antenna.

The conjecture made from experimental and simulated studies is further confirmed from the electric field pattern in the antenna structure at the resonant frequencies as shown in fig.4. The electric field distribution in the CDRA is very similar to that of HE_{116} occurring at its resonant frequency near 3.95GHz.

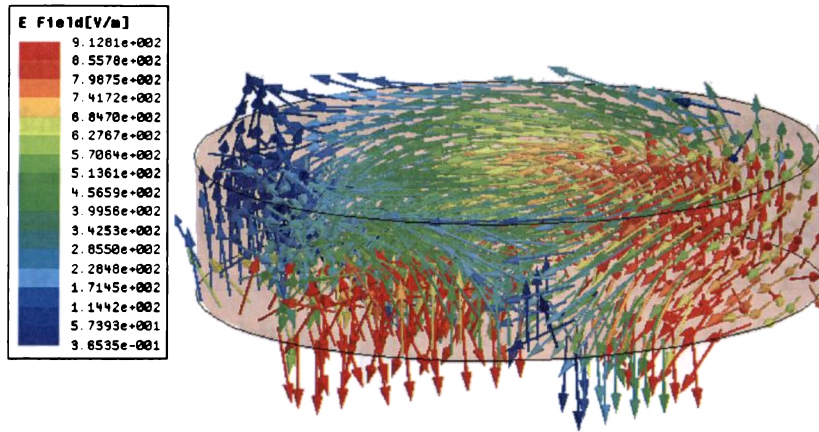


Fig.B.4. Simulated electric field distribution inside CDRA at 3.95GHz.

Fig.5. represents the gain of the antenna with in the operating bandwidth. Antenna exhibits an average gain of 5 dBi in the operating band. Gain variations are less than 1dBi with in the operating bandwidth.

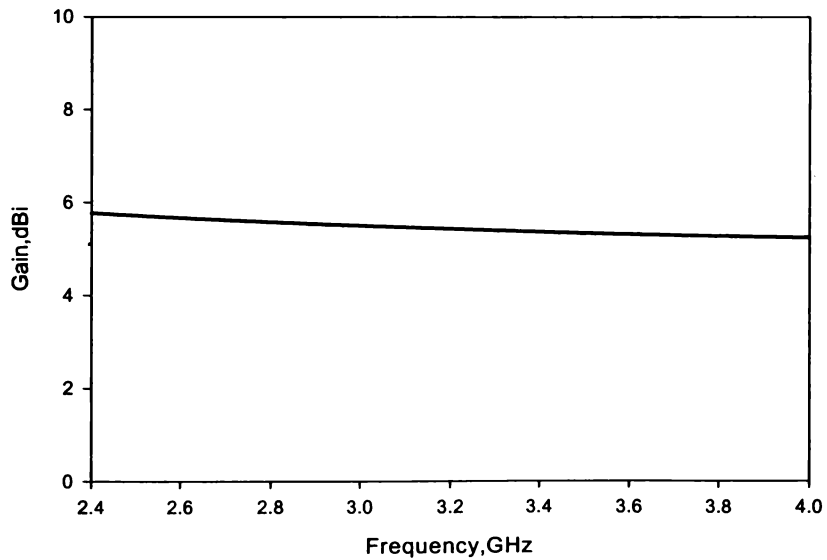


Fig.B.5. Gain characteristics of the hybrid CPW fed planar monopole/Dielectric resonator antenna.

B.4 Conclusion

A novel design of hybrid antenna with a CPW fed planar monopole and cylindrical dielectric resonator is proposed. CPW fed monopole is demonstrated as an effective radiator as well as feeding technique for cylindrical dielectric resonator antenna. The wide band planar hybrid antenna with moderate gain and nearly omni directional radiation characteristics reflects it as potential candidate for mobile and wireless communication applications.

B.5 References

- [1] A. A. Kishk, "Wideband dielectric resonator antenna in a truncated tetrahedron form excited by a coaxial probe," *IEEE Trans. Antennas Propag.*, vol. 51, no. 10, pp. 2907–2912, Oct. 2003.
- [2] A. A. Kishk, B. Ahn, and D. Kajfez, "Broadband stacked dielectric resonator antennas," *Electron. Lett.*, vol. 25, no. 18, pp. 1232–1233, Aug. 1989.
- [3] R. Chair, A.A Kishk, K.F Lee, "Wideband simple cylindrical dielectric resonator antennas", *IEEE Microwave and Wireless components letters.*, vol. 15, No. 4, pp. 241-243, April 2005.
- [4] M. Lapierre, Y.M.M Antar, A. Ittipiboon and A. Petosa, "Ultra wideband Monopole/ Dielectric resonator Antenna A CPW Fed Dual Frequency Monopole Antenna," *IEEE Microwave and Wireless components letters.*, vol.15, pp. 7-9, January 2005.
- [5] Chung, K., Yun, T., and Choi, J.: 'Wideband CPW-fed monopole antenna with parasitic elements and slots', *Electron. Lett.*, 2004, 40, (17), pp. 1038–1040
- [6] Liu, W.C., and Wu, C.M.: 'Broadband dual-frequency CPW-fed planar monopole antenna with rectangular notch', *Electron. Lett.*, 2004, 40, (11), pp. 642–643.
- [7] R.K. Mongia and P. Bhartia, 'Dielectric resonator antennas –A review and general design relations for resonant frequency and bandwidth', *Int. J. of Microwave and Millimeter-Wave Computer-Aided Engineering*, 1994, 4, pp. 230-247.

PUBLICATIONS RELEVANT TO THESIS

International Journals

1. Suma M.N, Rohith K.Raj, Manoj Joseph, Bybi P.C and P.Mohanan, “ A compact Dual Band Planar Branched Monopole Antenna for DCS/2.4GHz WLAN Applications” *IEEE Microwave and Wireless Components Letters* Vol.16, No.5, May 2006. pp 275-277.
2. Suma M.N, Bybi P.C and P.Mohanan, “A wide Band Printed Monopole antenna for 2.4GHz WLAN Applications” *Microwave and Optical Technology Letters* Vol.48, No.5, May 2006. pp 871-873.
3. Suma M.N, P.V Bijumon, M.T. Sebastain and P. Mohanan, “A Compact Hybrid CPW Fed Planar Monopole/Dielectric Resonator Antenna”, *Journal of the European Ceramic Society*, 27 (8), p.3001-3004, Jan 2007.
4. Suma M.N, Bybi P.C and P.Mohanan,” A Multiband Hybrid printed monopole-rectangular patch antenna for DCS/PCS/UMTS bands” *International Journal of Wireless and Optical Communications*, Volume 4, Issue 1, 2007, Pages: 53-59.

Citations

1. Reference to the paper “A compact Dual Band Planar Branched Monopole Antenna for DCS/2.4GHz WLAN Applications”, Suma M.N, Rohith K.Raj, Manoj Joseph, Bybi P.C and P.Mohanan, *IEEE Microwave and Wireless Components Letters* Vol.16, No.5, May 2006. pp 275-277.in the paper entitled “Dual Wideband Printed Monopole Antenna for WLAN/WiMAX Applications”. Chien-Yuan

Pan, Tzyy-Sheng Horng, Wen-Shan Chen and Chien-Hsiang Huang, *IEEE Antennas and Wireless Propagation Letters*, VOL. 6, 2007.

2. Reference to the paper "A wide Band Printed Monopole antenna for 2.4GHz WLAN Applications". Suma M.N, Bybi P.C and P.Mohanan, *Microwave and Optical Technology Letters* Vol.48, No.5, May 2006. pp 871-873 in the Master's Thesis entitled "Design and Application of Planar Dual-band S-shaped Monopole Antennas for WLAN" by Chuen-shian Yan, Electrical Engineering Department.
3. Reference to the paper " A compact Dual Band Planar Branched Monopole Antenna for DCS/2.4GHz WLAN Applications" Suma M.N, Rohith K.Raj, Manoj Joseph, Bybi P.C and P.Mohanan, *IEEE Microwave and Wireless Components Letters* Vol.16, No.5, May 2006. pp 275-277 in the Master's Thesis entitled "Design and Application of Planar Dual-band S-shaped Monopole Antennas for WLAN" by Chuen-shian Yan, Electrical Engineering Department.
4. Reference to the paper "A wide Band Printed Monopole antenna for 2.4GHz WLAN Applications". Suma M.N, Bybi P.C and P.Mohanan, *Microwave and Optical Technology Letters* Vol.48, No.5, May 2006. pp 871-873 in the paper entitled "Analysis and Application of an On-Package Planar Inverted-F Antenna" in *IEEE Transactions on Antennas And Propagation*, Vol. 55, No. 6, June 2007 authored by Ching-Wei Ling, Chia-Yu Lee, Chia-Lun Tang, and Shyh-Jong Chung.

LIST OF PUBLICATIONS

International/National Patent

1. “Novel wideband dielectric resonator loaded printed monopole antenna”, M.T. Sebastian, P.V. Bijumon, P. Mohanan and Suma M.N. NF - 0230/2005.

International Journals

1. Suma M.N, Rohith K.Raj, Manoj Joseph, Bybi P.C and P.Mohanan, “ A compact Dual Band Planar Branched Monopole Antenna for DCS/2.4GHz WLAN Applications” *IEEE Microwave and Wireless Components Letters* Vol.16, No.5, May 2006. pp 275-277.
2. Suma M.N, Bybi P.C and P.Mohanan, “A wide Band Printed Monopole antenna for 2.4GHz WLAN Applications” *Microwave and Optical Technology Letters* Vol.48, No.5, May 2006. pp 871-873.
3. Suma M.N , Sreedevi K Menon, P.V Bijumon, M.T Sebastain and P.Mohanan, “Rectangular Dielectric Resonator Antenna on Conductor Backed Coplanar Waveguide” *Microwave and Optical Technology Letters* .Vol.45, No.2, April 20 2005. pp 154-156.
4. Suma M.N, P.V Bijumon, M.T. Sebastain and P. Mohanan, “A Compact Hybrid CPW Fed Planar Monopole/Dielectric Resonator Antenna”, *Journal of the European Ceramic Society*, 27 (8), p.3001-3004, Jan 2007.
5. Suma M.N, Bybi P.C and P.Mohanan,” A Multiband Hybrid printed monopole-rectangular patch antenna for DCS/PCS/UMTS bands” *International Journal of Wireless and Optical Communications*, Volume 4, Issue 1, 2007, Pages: 53-59.

6. Shameena.V.A, Suma M.N, Rohith.K.Raj, Bybi P.C and P Mohanan "Compact Ultra wide Band Planar Serrated Antenna with Notch band ON/OFF Control" *IEE Electronic Letters*. Volume 42, Issue 23, November 9 2006 Page(s):1323 – 1324.
7. Deepu V, Rohith K. Raj, Manoj Joseph, Suma M.N and P. Mohanan "Compact Asymmetric Coplanar Strip Fed Monopole Antenna for Multiband Applications", *IEEE Transactions on Antennas and Propagations*. Vol. 55, No. 8, August 2007.
8. Deepu V, Rohith K. Raj, Manoj Joseph, Suma M.N and P. Mohanan, "A Compact uniplanar antenna for WLAN applications". *IEE Electronics Letters* Volume 43, Issue 2, January 18 2007 Page(s):70 – 72
9. Manoj Joseph, Rohith K.Raj, Suma M.N and P.Mohanan, "Compact Dual Band Antenna for DCS/2.4GHz WLAN Applications" *Microwave and Optical Technology Letters* .Vol.48, No.5, May 2006. pp 856-859.
10. P.V Bijumon, Sreedevi K Menon, Suma M.N, B.Lethakumari, MT Sebastain and P.Mohanan, "Broad band elliptical dielectric resonator antenna" *Microwave and Optical Technology Letters*. Vol.48, No.1, January 2006. pp 65-67.
11. P.V Bijumon, Sreedevi K Menon, Suma M.N, B.Lethakumari, MT Sebastain and P.Mohanan, " T Strip Fed High Permittivity rectangular dielectric resonator antenna for Broad band applications" *Microwave and Optical Technology Letters* Vol.47, No.3, Nov 2005. pp 226-227.
12. P.V Bijumon, Sreedevi K Menon, Suma M.N, MT Sebastain and P.Mohanan, "Broad band cylindrical dielectric resonator antenna excited by a modified microstrip feed line " *IEE Electronic letters* .Vol.41, March 2005. pp 385-387.

13. K. Francis Jacob, Suma M.N, Manoj Joseph and P.Mohanan, "Wide Band Dumbbell Shaped Patch Antenna" *Microwave and Optical Technology Letters*. Volume 48, Issue 11, Date: November 2006, Pages: 2295-2296.
14. Manoj Joseph, Rohith K.Raj, Suma M.N, C.K.Aanandan, K.Vasudevan And P.Mohanan, "Microstrip-fed dual band folded dipole antenna for DCS/PCS/2.4GHz WLAN applications" *International Journal On Wireless and Optical Communications*, Volume.4,No.1,pp 43-51,2007.
15. P.Mohanan, S.Mridula, Binu Paul, Suma M.N, P.V Bijumon, and M.T. Sebastain, "FDTD Analysis of Rectangular Dielectric Resonator Antenna", *Journal of the European Ceramic Society*, 27 (8), p.2753-2757, Jan 2007.
16. K. Francis Jacob, Suma M.N, Rohith K Raj , Manoj Joseph and P.Mohanan, "Planar Branched Ultra Wide Band Monopole Antenna" *Microwave and Optical Technology Letters*. Volume 49, Issue 1, January 2007, Pages: 45-47.

International and National Conferences

- 1 Suma M. N, Sreedevi K Menon, P.V Bijumon, MT Sebastian and P. Mohanan, "Experimental investigations on Rectangular Dielectric resonator antenna excited by a conductor backed coplanar waveguide". *IEEE Antennas and Propagation Society International Symposium, 2005*, Volume 4B, 3-8 July 2005 P.P 238 - 241
- 2 Suma M.N, Sreedevi K Menon, P.V.Bijumon, M.T.Sebastian and P.Mohanan, "A Broadband Cylindrical Dielectric Resonator Antenna Excited By Conductor Backed Coplanar Waveguide" *Proceedings of International Union of Radio Science (URSI 2005)*.

- 3 Sreedevi K Menon, Suma M.N, B.Lethakumari, C.K. Aanandan, P.Mohan K.Vasudevan and K.G Nair “ Rectangular microstrip antenna on EBG groundplane with unequal orthogonal periods” , *Proc. of the National Symposium on Microwave Antennas and Propagation, APSYM-04*, pp.68-70, Cochin, 2004
- 4 Suma M. N, Sreedevi K Menon, P.V Bijumon, M.T Sebastian and P. Mohanan. “Cylindrical Dielectric Resonator antenna excited by a conductor backed coplanar waveguide” *Proc. of the National Symposium on Microwave Antennas and Propagation, APSYM-04*, pp.219-221, Cochin, 2004.
- 5 Deepu V, Rohith K.Raj,Manoj Joseph, Suma M.N ,C.K.Aanandan,K. Vasudevan and P.Mohan “Compact asymmetric coplanar strip fed multiband antenna for wireless applications”, *Proc. of the National Symposium on Microwave Antennas and Propagation, (APSYM-06)*. pp 191-194,Cochin 2006.
- 6 Deepu V, Rohith K.Raj,Manoj Joseph, Suma M.N , and P.Mohan “Compact Dual band antenna for WLAN applications” Deepu V, Rohith K.Raj,Manoj Joseph, Suma MN , and P.Mohan *IEEE APS-2007,Honolulu,Hawaii,USA*.

Citations

1. Reference to the paper “A compact Dual Band Planar Branched Monopole Antenna for DCS/2.4GHz WLAN Applications”, Suma M.N, Rohith K.Raj, Manoj Joseph, Bybi P.C and P.Mohan, *IEEE Microwave and Wireless Components Letters* Vol.16, No.5, May 2006. pp 275-277.in the paper entitled “Dual Wideband Printed Monopole Antenna for WLAN/WiMAX Applications”. Chien-Yuan

- Pan, Tzyy-Sheng Horng, Wen-Shan Chen and Chien-Hsiang Huang, *IEEE Antennas and Wireless Propagation Letters*, VOL. 6, 2007.
2. Reference to the paper, "Planar Branched Monopole Antenna for UWB Applications," "K. F. Jacob, M. N. Suma, R. K. Raj, M. Joseph and P. Mohanan. *Microw. Opt. Technol.Letts.*, vol.49, no.1, pp45-47, Jan. 2007 in the paper entitled "Design of Ultra Wideband Coplanar Waveguide-Fed LI-shape Planar Monopole Antennas" Joon Il Kim, , and Yong Jee. *IEEE Antennas and Wireless propagation letters*.
 3. Reference to the paper "Broad band cylindrical dielectric resonator antenna excited by a modified microstrip feed line".P.V Bijumon, Sreedevi K Menon, Suma M.N, MT Sebastain and P.Mohanan," *IEE Electronic letters* .Vol.41, March 2005. pp 385-387 in the paper entitled "2.5ghz Batio3 Dielectric Resonator Antenna" *Progress In Electromagnetics Research*, PIER 76, 201–210, 2007.
 4. Reference to the paper "Broad band cylindrical dielectric resonator antenna excited by a modified microstrip feed line".P.V Bijumon, Sreedevi K Menon, Suma M.N, MT Sebastain and P.Mohanan," *IEE Electronic letters* .Vol.41, March 2005. pp 385-387 in the paper entitled "Microstripline-fed half-cylindrical dielectric resonator antenna for 2.4-GHz WLAN application "*Microwave and Optical Technology Letters* . Volume 48, Issue 4 , Pages 724 – 726.
 5. Reference to the paper"A wide Band Printed Monopole antenna for 2.4GHz WLAN Applications". Suma M.N, Bybi P.C and P.Mohanan, *Microwave and Optical Technology Letters* Vol.48, No.5, May 2006. pp 871-873 in the Master's Thesis entitled "Design and Application of Planar Dual-band S-shaped Monopole Antennas for WLAN" by Chuen-shian Yan, Electrical Engineering Department.

6. Reference to the paper “ A compact Dual Band Planar Branched Monopole Antenna for DCS/2.4GHz WLAN Applications” Suma M.N, Rohith K.Raj, Manoj Joseph, Bybi P.C and P.Mohanan, *IEEE Microwave and Wireless Components Letters* Vol.16, No.5, May 2006. pp 275-277 in the Master’s Thesis entitled “Design and Application of Planar Dual-band S-shaped Monopole Antennas for WLAN” by Chuen-shian Yan, Electrical Engineering Department.
7. Reference to the paper“A wide Band Printed Monopole antenna for 2.4GHz WLAN Applications”. Suma M.N, Bybi P.C and P.Mohanan, *Microwave and Optical Technology Letters* Vol.48, No.5, May 2006. pp 871-873 in the paper entitled “Analysis and Application of an On-Package Planar Inverted-F Antenna”in IEEE Transactions on Antennas And Propagation, Vol. 55, No. 6, June 2007 authored by Ching-Wei Ling, Chia-Yu Lee, Chia-Lun Tang, and Shyh-Jong Chung.

Resume of the Author

SUMA M.N

Senior Research Fellow
Centre for Research in Electromagnetics and Antennas
Department of Electronics
Cochin University of Science and Technology
Cochin-22, Kerala, India
Tel: +91-484-2576418, Mob: +91-98476 44627
Fax: +91-484-2575800
Email: sumabhat@cusat.ac.in

Objective:

To pursue research activities in the field of Computational Electromagnetics, Dielectric Resonator Antennas and printed antennas.

Education:

M.Sc Electronics
Specialization: Microwave Electronics
Cochin University of Science and Technology (2001)
Score: 81% First class
B.Sc Physics
Mahatma Gandhi University (1999)
Score: 92% First class with distinction

Awards Obtained:

Awarded with Senior Research Fellowship (SRF) by the Council for Scientific and Industrial Research (CSIR), Govt. of India.

Research Experience:

Worked as a Project Fellow in the Research Project entitled ‘Compact Dual Band Dielectric resonators for Mobile phone antenna with reduced radiation hazards’, funded by Kerala State Council for Science Technology Environment (KSCSTE), Govt. of Kerala from March 2005-March 2007.

Publications:

International Journal	: 16
International Conference	: 03
National Conference	: 03
Citation in international Journals	: 05

Computer Proficiency:

C, C++, MATLAB, Assembly Level Programming, VDSP, VHDL, Ansoft HFSS, Designer, Zeland IE3D, Zeland FIDELITY, Microwave Office, Microstripes, and CST Microwave Studio.

INDEX

A

ABC · 60, 62, 64, 109, 132
Active antennas · 11
Allen Taflove · 101
Antenna Bible · 7

B

Balanis · 103
Berenger · 60,64
Bose · 2,30
Broadband ·
 31,32,33,35,105,142,165,168

C

Capacitive coupling ·
 27,148,178,179,184,237
Compact ·
 6,34,35,36,38,163,242,243,248
CPW · 24, 25, 26, 32, 38, 39, 40,
 41, 251, 262, 263, 264, 265, 266

D

DCS · 5,169,201,226,227,240
Deschamps · 8,30
Design equations · 234
DFSMA · 2202,203
Double folded · 27,238
Dual band ·
 22,23,27,28,29,38,131,173,175,
 229,231
Dual folded ·
 175,202,204,208,211,214,217,
 219,220,221,222,226,238

E

Efficiency · 9,11,16,18,23, 43,76,
 89,91,97,98,103,118,126,127,1301
 31,145,146,151,152,154,160,161,
 162,163,167,167,169
Excitation techniques · 21,23
experimental ·
 28,29,34,41,91,92,93,95,96,

F

FDTD
 25,26,28,29,41,45,51,52,53,54,55
 ,58,59,,61,69,70,74,75,76,78,79,
 81,83,84,85,86,102,105,108,111,
 114,115,117,121,127,130,131,132,
 133,134,144,148,157,158,159,175,
 176,180,181,182,183,185,187,
 203,213,234
FEM · 42,45,47,49
FIT · 7,84,133
Fractal · 24,25,38

G

Gain
 3,6,7,9,17,18,23,28,85,89,94,96,
 97,109,118,124,126,127,130,131,
 145,146,147,151,152,154,159,
 161,162,163,164,167,169,170,172,
 174,191,193,194,201,204,206,212,
 216,217,218,220,227,229,230,234,
 235,236,237,238,239,
Garg · 31
Gaussian pulse · 3,78,79,81,82,86

H

HFSS · 98,103,117,157,184,204
HP8510C · 92,245
HPIB · 92,93

I

IE3D · 97,98,103
Impedance ·
43,50,60,65,67,77,80,82,84,89

K

Kraus · 30,103

L

Leubbers · 77

M

Marconi · 2,3,6,30
MATLAB · 75,83,93,108
Maxwell · 76
Metamaterial · 9,31
Microstrip antenna ·
15,16,17,31,43,100,170,208,248
Miniaturization · 38,174
MMIC · 8,17,97,170
MoM · 42,45
Monopole antenna ·
22,23,52,60,61,171,174,233,234

P

Parametric analysis ·
28,29,61,83,98,188,216,226
PIFA · 11,15,18,19,33
Planar branched monopole · 38

PML · 28,60,64,109,132
PNA · 203,227
Printed dipole · 35,141

R

Radiation pattern ·
7,18,23,34,76,86,116,117,184,
185
Resonance ·
10,27,97,105,108,110,111,112,
114,115,119,122,128,134,138,140,
142,147,173,175,203,208,211
Return loss ·
76,82,84,85,95,96,98,148,152,
154,163,166,183,217,254
RF stimulus · 93

S

Schneider · 51,101,102
Silver · 7,9,30
Single folded · 9,27,202,211,212

T

TEM · 142
THRU calibration · 96
TLM · 45,50,51,52,101
TRL · 95

U

UWB · 5,8,9,23

V

VNA · 92,95
VSWR · 84,85,95,97

W

Wheeler · 1,31,97,103,127,183,187

WLAN · 23,36,108,169,228

Wong · 36

Y

Yee ·

51,52,54,55,58,61,79,80,83,101,
108,176

YIG · 93

Z

Zimmerman · 88,103

